Fall 12-1-2015

Investigation of Pathways for Complex Sphingolipid Biosynthesis in *Arabidopsis thaliana* (L.) Heynh

Kyle Luttgeharm
University of Nebraska-Lincoln, kluttgeharm@gmail.com

Investigation of Pathways for Complex Sphingolipid Biosynthesis in *Arabidopsis thaliana* (L.) Heynh

By

Kyle D. Luttgeharm

A DISSERTATION

Presented to the Faculty of

The Graduate College at the University of Nebraska

In Partial Fulfillment of Requirements

For the Degree of Doctor of Philosophy

Major: Biochemistry

Under the Supervision of Professor Edgar B. Cahoon

December, 2015

ARABIDOPSIS THALIANA CONTAINS THREE CERAMIDE SYNTHASE ISOFORMS EACH WITH DISTINCT SUBSTRATE SPECIFICITY THAT MEDIATE SPHINGOLIPID COMPOSITION, PLANT GROWTH, AND MYCOTOXIN RESISTANCE

Kyle D. Luttgeharm, Ph.D.

University of Nebraska, 2015

Advisor: Edgar B. Cahoon

Sphingolipids are essential components of eukaryote membranes. The ceramide backbone of complex sphingolipids is composed of an 18 carbon Long Chain Base (LCB) bound to a 16-26 carbon fatty acid (FA) through an amide linkage. Ceramides are synthesized *de novo* from a free LCB and fatty acyl coA by ceramide synthase (sphingosine N-acyl transferase, EC 2.3.1.24) which can be inhibited by the fungal mycotoxin Fumonisin B_1. *Arabidopsis thaliana* contains three ceramide synthases denoted *LOH1*, *LOH2*, and *LOH3* that have previously been hypothesized to have unique substrate preferences that control the final sphingolipid composition, different susceptibilities to Fumonisin, and different influences plant growth/development. This dissertation works to answers to these questions as well as identify novel complex sphingolipid biosynthetic pathways. Through the use of *in vitro* assays it was found that LOH1 and LOH3 prefer LCBs witth hydroxyls at the C1, C2, and C4 positions (trihydroxy) and C20-24 saturated FA while LOH2 prefers LCBs with hydroxyls at the C1 and C2 positions (dihydroxy) and C16 saturated fatty acids. None of the isoforms

were able to use ω9 desaturated acyl CoAs which are abundant in the final sphingolipid profile. Surprisingly LOH2 showed the highest level of activity with C4 unsaturated LCBs which are not commonly found in leaf. Each isoform was also overexpressed *in planta* to determine the effects ceramide composition has on plant growth. Overexpression of *LOH1* or *LOH3* led to an increase in biomass while overexpression of *LOH2* resulted in a dwarf phenotype. Both the *in vitro* assays and *in planta* overexpression found LOH1 to the most susceptible to FB_1 inhibition. In addition to ceramide synthesis a novel Δ8 LCB desaturase from castor bean was identified which required the presence of a Δ4 double bond for activity. The presence of Δ4,8 unsaturated LCBs was found to result in increased glucoscylceramide levels as revealed by LCB feeding experiments and pollen sphingolipid profiling. Therefore, it is hypothesized that the presence of a Δ4 unsaturation targets LCBs through a LOH2-like ceramide synthase for subsequent Δ8 desaturation and glucosylceramide synthesis.

ACKNOWLEDGEMENTS

I would like to thank all members of the Cahoon Lab who have each helped me in some way complete this dissertation. In particular I would like to thank Edgar Cahoon for selecting me as an REU student many years ago and allowing me to continually come back to the lab, Becky Cahoon for providing me with my initial training in Sphingolipid quantitation and providing support to me in more ways than I can count, and Jonathan Markham for patiently working with me on the LCMS and my entire committee for guidance.

This work was funded in part by the National Science Foundation (MCB-11585000) awarded to Edgar B. Cahoon.

TABLE OF CONTENTS

LIST OF MULTIMEDIA OBJECTS

CHAPTER 1

INTRODUCTION

Note: This chapter is to be published and the text has been modified from the original.

The citation is: Luttgeharm, K.D., A.K. Kimberlin, and E.B. Cahoon (2015). Plant Sphingolipid Metabolism and Function. Springer, In Press.

1.1 INTRODUCTION

Sphingolipids were originally identified in the late 19th century by Johann Thudichum as an "enigmatic" major lipidic component of the brain (Thudichum 1884). Since this discovery, sphingolipids have been recognized as essential components of eukaryotic cells and have been extensively studied in humans due to their association with a number of lipid storage disorders, including Tay-Sachs disease and Niemann-Pick disease (Sandhoff 2013). Sphingolipids, however, were not identified in plants until the late 1950s (Carter et al. 1958) and for nearly four decades following this discovery, sphingolipid research in plants was limited mainly to structural and compositional analyses, including studies of sphingolipid compositional changes in response to abiotic stresses. Since the late 1990s, plant sphingolipids have become an increasing research focus. Driving this heightened interest is the realization that sphingolipids are among the most abundant endomembrane lipids in plant cells and that they contribute not only to membrane structure and function that underlies abiotic and biotic stress resistance, but also to the regulation of cellular processes (Dunn et al. 2004). Recent advances in plant sphingolipid research have been spurred by development and application of advanced mass spectrometry methods that enable the rapid and quantitative measurement of molecular species of specific sphingolipid classes (Markham and Jaworski 2007). Coupling of these methods with the characterization of Arabidopsis mutants and transgenics have resulted in advances in our fundamental understanding of plant sphingolipid metabolism.

The backbone of complex sphingolipids, the ceramide, is composed of a long chain base bound to a fatty acid through an amide linkage (Dunn et al. 2004). Ceramide

synthesis has been recognized as a key branching point in sphingolipid metabolism with the ceramide long chain base/fatty acid composition hypothesized to play a key role in determining the final complex sphingolipid formed (Markham et al. 2011; Chen et al. 2008). In mammals it has been found that different ceramide synthases have distinct substrate preferences allowing the organism to control ceramide composition (Venkataraman et al. 2002a; Laviad et al. 2008; Mizutani et al. 2006, 2005; Riebeling et al. 2003). Through the use of mutants, evidence suggests that plant ceramide synthases also have distinct substrate preferences (Markham et al. 2011; Ternes et al. 2011; Chen et al. 2008), though this has yet to be determined through the use of *in vitro* assays. This dissertation describes the characterization of the Arabidopsis ceramide synthases and the effects that ceramide composition has on plant growth/development, fungal mycotoxin resistance, and complex sphingolipid synthesis.

1.2 SPHINGOLIPID STRUCTURE

Sphingolipids consist of hydrophobic ceramide backbones that are typically linked to polar sugar residues to form amphipathic lipid components of membranes (Lynch and Dunn 2004; Chen et al. 2010). The ceramide backbone contains a long chain amino alcohol referred to as a sphingoid long-chain base (LCB) linked through an amide bond to a fatty acid. LCBs are unique to sphingolipids. In plants, LCBs typically have chain lengths of 18 carbon atoms and can contain double bonds in the Δ4 or Δ8 positions (Figure 1.1A). The Δ4 double bond is found only in the *trans* configuration, while the Δ8 double bond can be found in either the *trans* or *cis* configurations. Following its initial synthesis, a LCB has two hydroxyl groups at the C-1 and C-3 carbons (Lynch and Dunn 2004; Chen et al. 2010). These LCBs are referred to as dihydroxy LCBs. A third

hydroxyl group can be enzymatically added at the C-4 carbon to form a trihydroxy LCB. In the short-hand nomenclature, a dihydroxy LCB with 18 carbons and one double bond is referred to as “d18:1”, and a trihydroxy LCB with 18 carbons and one double bond is referred to as “t18:1”. LCBs can be phosphorylated at the C-1 position to form LCB-phosphates (LCB-P). Free LCBs and their phosphorylated forms are typically in low abundance in plant cells (Markham and Jaworski 2007; Markham et al. 2006). Instead, the majority of LCBs are found linked to fatty acids in ceramides (Figure 1.1B). The chain-lengths of plant ceramide fatty acids range from 16 to 26 carbon atoms, the majority of which contain an enzymatically added hydroxyl group at the C-2 or α-position (Lynch and Dunn 2004; Chen et al. 2010). vAnalogous to the diacylglycerol backbone of glycerolipids, ceramides serve as the hydrophobic component of complex sphingolipids. The polar head group of ceramides is attached at its C-1 position and can be a phosphate residue or a variety of sugar residues (Chen et al. 2010). The latter are referred to as glycosphingolipids. The simplest glycosphingolipid in plants is the glucosylceramide (GlcCer) with a single glucose residue and comprises approximately one-third of the glycosphingolipids of Arabidopsis leaves (Markham and Jaworski 2007; Markham et al. 2006) (Figure 1.1C). The most abundant glycosphingolipid in plants contains an inositol phosphate bound to the ceramide with up to seven additional hexose and pentose residues (Figure 1.1C) (Cacas et al. 2013). These molecules are referred to as glycosyl inositolphosphoceramides or GIPCs and comprise approximately two-thirds of the glycosphingolipids of Arabidopsis leaves (Markham and Jaworski 2007; Markham et al. 2006). The quantitative significance of GIPCs in plants was overlooked for many years due to the difficulty in their extraction using standard lipid analytical protocols

because of the high polarity of their glycosylated head groups. Between the different carbon chain-lengths and hydroxylation and unsaturation states of LCBs and fatty acids and the array of polar head groups, hundreds of potentially different sphingolipid species can occur in plants, the individual significance of which are only beginning to be elucidated (Markham et al. 2013; Bure et al. 2011).

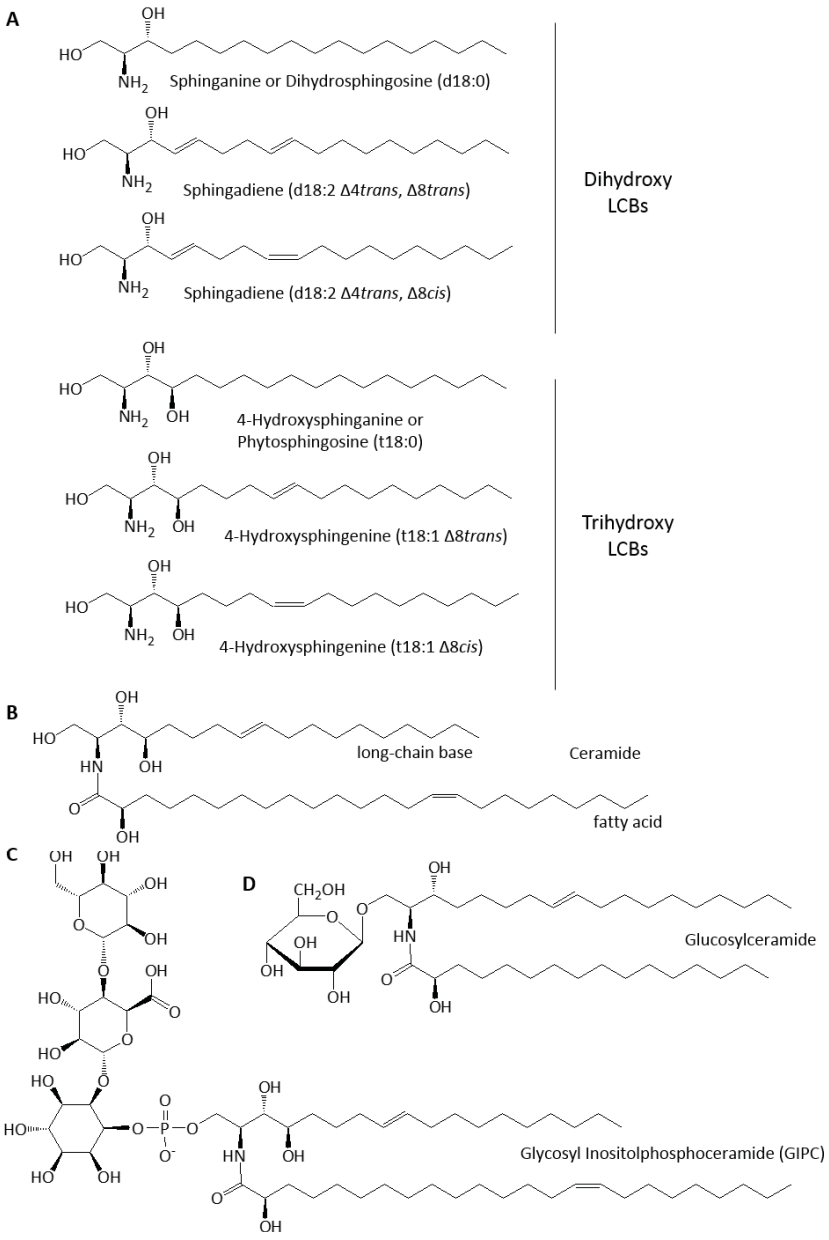

Figure 1.1 . *Examples of long-chain bases (LCB) and sphingolipids found in plants*. (A) Examples of LCB modifications found in plants. Shown are examples of dihydroxy and trihydroxy LCBs. The nomenclature "d18:0" indicates that the LCB has two hydroxyl groups (d) and 18 carbon atoms and no double bonds, and the nomenclature "t18:0" indicates that the LCB has three hydroxyl groups (t) and 18 carbon atoms and no double bonds. (B) Hydroxyceramide composed of the LCB t18:1 Δ8trans and the fatty acid 24:1 ω9cis that is hydroxylated at the C-2 position. (C) Most abundant glycosyl inositolphosphoceramide (GIPC) found in Arabidopsis leaves. (D) Glucosylceramide.

1.3 SPHINGOLIPID BIOSYNTHESIS

1.3.1 SYNTHESIS OF LONG CHAIN BASES: THE SERINE PALMITOYLTRANSFERASE COMPLEX AND 3-KETOSPHINGANINE REDUCTASE

The biosynthesis of LCBs is initiated through an endoplasmic reticulum- (ER-) localized reaction catalyzed by serine palmitoyltransferase (SPT) that condenses serine and palmitoyl-CoA to form the 18 carbon intermediate 3-ketosphinganine (Figs. 2 and 3) (Chen et al. 2006; Dietrich et al. 2008; Teng et al. 2008). The product of this reaction is then reduced by 3-ketosphinganine reductase (KSR) to form sphinganine or d18:0, the simplest long-chain base in plants and other eukaryotes (Chao et al. 2011). SPT is a member of the α-oxoamine synthase subfamily and is generally regarded as the main regulated step in sphingolipid biosynthesis (Hanada 2003). Similar to other eukaryotes, the Arabidopsis SPT functions as a heterodimer comprised of LCB1 and LCB2 subunits (Tamura et al. 2001; Chen et al. 2006; Dietrich et al. 2008; Teng et al. 2008). A third smaller subunit, termed the small subunit of SPT or ssSPT, also interacts with the LCB1/LCB2 subunits (Han et al. 2004; Kimberlin et al. 2013). Although SPT can function as a heterodimer (LCB1 and LCB2) with minimal enzymatic activity, ssSPT enhances SPT activity to levels that produce LCBs in amounts that are sufficient to support cell viability in Arabidopsis (Kimberlin et al. 2013).

In the second step of LCB synthesis, the SPT product 3-ketosphinganine is reduced by the enzyme 3-ketosphinganine reductase (KSR) to form sphinganine (d18:0), the simplest LCB found in plants (Figure 1.2). KSR is encoded by two genes in

Arabidopsis thaliana, *KSR-1* (At3g06060) and *KSR-2* (At5g19200). Both genes are essential and contribute to the reductase activity (Chao et al. 2011), although *KSR-1* is more highly expressed throughout the plant (Chao et al. 2011). *KSR-1* and *KSR-2* are functionally redundant, but *KSR-1* is the primary contributor to the reductase activity (Chao et al. 2011). The sphinganine (d18:0) produced from the combined activities of SPT and KSR can be used directly by ceramide synthase or modified by hydroxylation or desaturation at the C-4 position prior to use for ceramide synthesis.

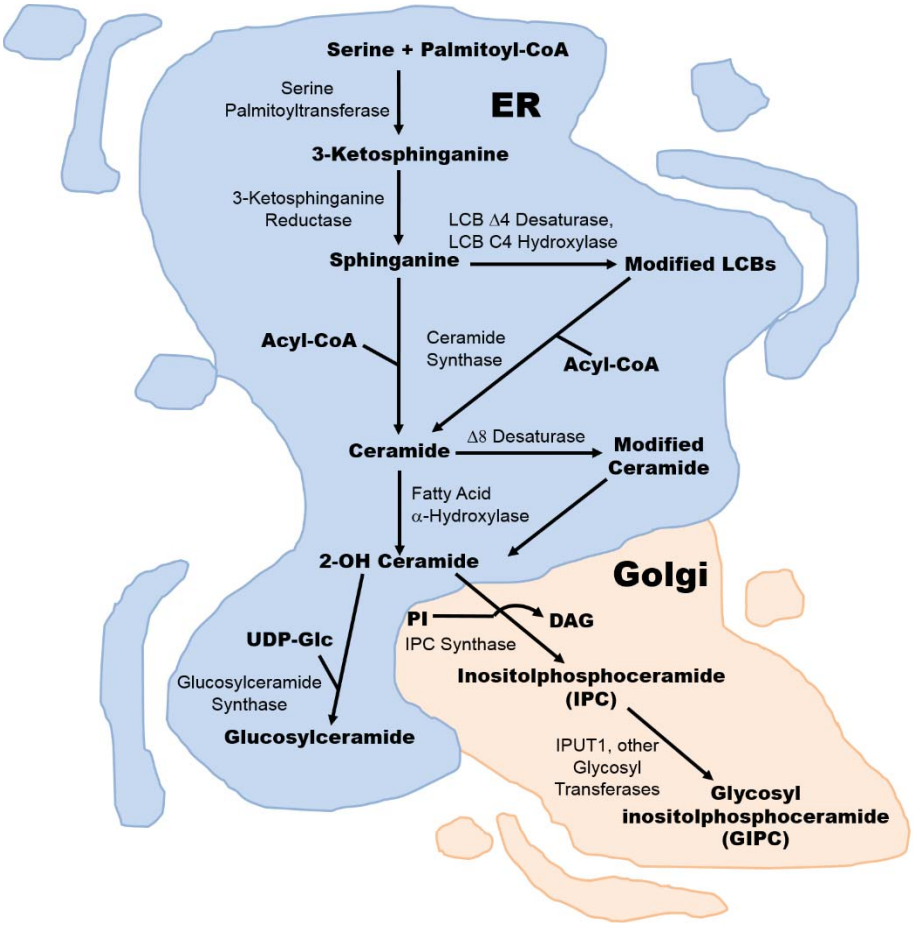

Figure 1.2 *Abbreviated plant sphingolipid biosynthetic pathway*. Abbreviations: LCB, long-chain base; Glc, glucose; PI, phosphatidylinositol; DAG, diacylglycerol; IP, inositolphosphate; GIPCase, glycosyl inositolphosphoceramidase; IPUT1, inositol phosphorylceramide glucuronosyltransferase 1.

1.3.2 LCB C-4 HYDROXYLATION

The d18:0 LCB resulting from the sequential activities of SPT and KSR can undergo combinations of three modification reactions to generate trihydroxylated and unsaturated LCBs (Figure 1.1A, Figure 1.2). In Arabidopsis leaves, ~90% of the total LCBs contain three hydroxyl groups and Δ8 unsaturation. The third hydroxyl group of these LCBs occurs at the C-4 position and is introduced by a LCB C-4 hydroxylase (Chen et al. 2008; Sperling et al. 2001). This enzyme is a di-iron oxo protein with homology to desaturases and hydroxylases (Sperling et al. 2001). The two genes that encode the LCB C-4 hydroxylase in Arabidopsis are designated *SPHINGOID BASE HYDROXYLASE* (*SBH*) *1* (At1g69640) and *2* (At1g14290). Expression of these genes in mutants of the *Saccharomyces cerevisiae SUR2* gene (Haak et al. 1997) that encodes a related LCB C-4 hydroxylase restores trihydroxy LCB synthesis (Chen et al. 2008; Sperling et al. 2001). It is presumed that the Arabidopsis LCB C-4 hydroxylase uses a free dihydroxy LCB as its substrate, in part, because of the prevalence of trihydroxy LCBs in the free LCB pool (Markham and Jaworski 2007).

1.3.3 LCB Δ8 DESATURATION

LCBs with Δ8 unsaturation, either in the dihydroxy or trihydroxy form, are also abundant in sphingolipids of most plant species (Lynch and Dunn 2004) (Figure 1.1A and 1.2). Like the LCB C-4 hydroxylase, LCB Δ8 desaturases are di-iron oxo enzymes (Shanklin and Cahoon 1998). The plant Δ8 LCB desaturase was originally identified in sunflower as a desaturase-like enzyme that also contains an N-terminal cytochrome b_5 domain and shown to confer production of Δ8 unsaturated LCBs when expressed in

Saccharomyces cerevisiae (Sperling et al. 1995). Notably, the LCB Δ8 desaturase is not found in mammals and *Saccharomyces cerevisiae*, but is present in plants and filamentous or dimorphic fungi such as *Pichia patoris* and *Yarrowia lipolytica*. Two homologs, *SLD1* (At3g61580) and *SLD2* (At2g46210), were identified in Arabidopsis and confirmed to be Δ8 desaturases through yeast and *in planta* studies (Sperling et al. 1998; Chen et al. 2012). To further add to the structural diversity found in LCBs, the Δ8 double bond can be introduced in either the *cis* or *trans* configuration (Markham et al. 2006), which likely results from presentation of LCB substrates in alternative conformations relative to the di-iron oxo atoms in the active site of these enzymes (Beckmann et al. 2002). Though evidence to date cannot preclude that at least a portion of LCB Δ8 desaturation uses free LCBs as substrates, it is presumed that these enzymes largely use LCBs bound in ceramides as substrates (Beckmann et al. 2002; Sperling et al. 1998).

1.3.4 LCB Δ4 DESATURATION

Long-chain bases (LCBs) with Δ4 unsaturation are also prevalent in sphingolipids in many plant species. LCB Δ4 unsaturation occurs almost entirely in combination with LCB Δ8 unsaturation in dihydroxy LCBs. These di-unsaturated, dihydroxy LCBs (d18:2) also are found almost exclusively in ceramides of GlcCer, but absent from ceramides of GIPCs (Markham and Jaworski 2007; Markham et al. 2006; Sperling et al. 2005) (Figure 1.1A and C, Figure 1.2). Arabidopsis contains one Δ4 desaturase gene (At4g049300) that was identified by homology to analogous genes in filamentous fungi and mammals (Ternes et al. 2002). In contrast to the LCB Δ8 desaturase, the Δ4 desaturase introduces double bonds exclusively in the *trans* configuration, most likely

using free LCBs as substrates (Ternes et al. 2002). As a result, two d18:2 isomers occur in plants: d18:2-*trans*Δ4, *trans*Δ8 and d18:2-*trans*Δ4, *cis*Δ8. It is notable that LCB C-4 hydroxylases and LCB Δ4 desaturase can both use d18:0 as substrates. As a result, C-4 hydroxylation precludes Δ4 desaturation, and conversely, Δ4 desaturation prevents C-4 hydroxylation. In Arabidopsis and likely other Brassicaceae, the LCB Δ4 desaturase gene has little or no expression in leaves (Michaelson et al. 2009). Instead, expression is limited almost entirely to flowers and, specifically, pollen, which is consistent with the occurrence of d18:2 in Arabidopsis reproductive organs (Michaelson et al. 2009). In most species outside of the Brassicaceae family, LCB Δ4 desaturation, as evidenced by d18:2 production, occurs throughout the plant, and in species such as tomato and soybean, d18:2 is the most abundant LCB in GlcCer (Markham et al. 2006; Sperling et al. 2005).

1.3.5 SPHINGOLIPID FATTY ACID SYNTHESIS AND STRUCTURAL MODIFICATIONS

Carbon chain-length, unsaturation, and hydroxylation of fatty acids contribute to the structural diversity of the ceramide backbone of sphingolipids. In plants, the fatty acid component ranges from 16-26 carbon atoms (Markham and Jaworski 2007), including small amounts of odd-chain fatty acids with 21, 23, and 25 carbon atoms (Cahoon and Lynch 1991). In Arabidopsis leaves, C16, C24, and C26 fatty acids predominate (Markham and Jaworski 2007; Markham et al. 2006). The C16 fatty acids of ceramides arise from palmitic acid formed by *de novo* fatty acid synthesis, whereas the very long-chain fatty acids or VLCFAs (i.e., fatty acids with ≥C20) of sphingolipids arise from the ER-localized reactions involving the two-carbon sequential elongation of fatty acids

produced *de novo* in plastids (Smith et al. 2013). Each two carbon elongation cycle involves the four successive reactions catalyzed by 3-ketoacyl-CoA synthase (KCS), 3-ketoacyl-CoA reductase (KCR), hydroxyacyl-CoA dehydrase (HAD), and enoyl-CoA reductase (ECR) (Smith et al. 2013). Arabidopsis mutants of the *PAS2* gene (At5g10480) encoding HAD are defective in VLCFA synthesis and have demonstrated the importance of sphingolipid VLCFAs for cellular function. Partial *PAS2* mutants are defective in growth and phragmoplast (or cell plate) formation resulting in impaired cell division, and null *PAS2* mutants display embryo lethality (Bach et al. 2011; Bach et al. 2008).

Sphingolipid VLCFAs are typically saturated in the plant kingdom, but monounsaturated VLCFAs occur in sphingolipids of Brassicaceae and some Poaceae species as well as selected species from other families (Cahoon and Lynch 1991; Lynch and Dunn 2004; Markham et al. 2006; Sperling et al. 2005). The double bond in sphingolipid VLCFAs of these species is at the ω-9 position (Imai et al. 2000). In Arabidopsis, this double bond is introduced by an enzyme encoded by *ADS2* (At2g31360) that has homology to acyl-CoA desaturases (Smith et al. 2013). The *ADS2* gene is induced by low temperatures and *ads2* null mutants display chilling sensitivity, indicating a link between sphingolipid structure and low temperature performance, as also shown for the LCB Δ8 desaturase (Chen and Thelen 2013). It is currently unknown if the fatty acid desaturase acts on the free acyl-CoA or the mature ceramide.

Fatty acids in ceramides of glycosphingolipids occur almost entirely with C-2 or α-hydroxylation (Lynch and Dunn 2004). The C-2 hydroxyl group is introduced by a di-iron-oxo enzyme related to the *Saccharomyces cerevisiae* fatty acid C-2 hydroxylase encoded by the *FAH1* or *SCS7* gene (Haak et al. 1997; Mitchell and Martin 1997). The

Arabidopsis homologs AtFAH1 (encoded by At2g34770) and AtFAH2 (encoded by At4g20870) notably lack the N-terminal cytochrome b_5 domain that is found in the *Saccharomyces cerevisiae* enzyme (Konig et al. 2012; Mitchell and Martin 1997; Nagano et al. 2012). Based on phenotypes in T-DNA insertion mutants and RNAi suppression lines, AtFAH1 appears to be primarily associated with hydroxylation of VLCFAs, and AtFAH2 appears to be primarily associated with hydroxylation of C16 fatty acids *in planta* (Nagano et al. 2012). It is presumed that AtFAH1 and AtFAH2 use fatty acids in ceramides rather than free or CoA esters of fatty acids as substrates, given that a substantial portion of fatty acids in the free ceramide pool lack C-2 hydroxylation, even though hydroxylated fatty acids predominate in glycosphingolipid ceramide backbones (Markham and Jaworski 2007). Double mutants of the At*FAH1* and At*FAH2* genes have elevated levels of ceramides but ~25% reduction in glucosylceramide level (Konig et al. 2012). These results suggest that ceramides with C-2 hydroxylated fatty acids are important for metabolic channeling of ceramides to form glycosphingolipids, due possibly to the substrate preference of enzymes such as glucosylceramide synthase. Suppression of PCD by ER-associated Bax inhibitor-1 protein in Arabidopsis has been shown to be dependent on functional fatty acid C-2 hydroxylases, and overexpression of the Bax inhibitor 1 gene increases fatty acid C-2 hydroxylation of ceramides through direct interaction with cytochrome b_5 (Nagano et al. 2009; Nagano et al. 2012). From these findings, it has been speculated that accumulation of ceramides with fatty acids lacking the C-2 hydroxyl group initiates PCD, whereas this response is reduced when the fatty acids of these ceramides are hydroxylated (Nagano et al. 2012).

1.3.6 CERAMIDE SYNTHESIS

Ceramides are synthesized by the linking of a long-chain base and fatty acyl-CoA through an acyltransferase-type reaction catalyzed by ceramide synthase (or sphinganine N-acyl transferase, 3.2.1.24) (Figure 1.2). Three ceramide synthases have been identified in Arabidopsis through homology with the yeast ceramide synthase encoded by *LAG1* (*LONGEVITY ASSURANCE GENE1*). These enzymes are designated Lag One Homolog (LOH)-1, -2, and -3 and correspond to genes encoded by *LOH1*, At3g25440; *LOH2*, At3g19260; and *LOH3*, At1g13580, respectively (Ternes et al. 2011; Markham et al. 2011). Homologs of these three enzymes are found throughout the plant kingdom and appear to form two distinct evolutionary branches, LOH1/LOH3-related isoforms and LOH2-related isoforms (Markham et al. 2011; Ternes et al. 2011). Arabidopsis LOH1 and LOH3 share approximately 80% amino acid sequence identity, while LOH2 shares approximately 60% identity with LOH1 and LOH3 (Ternes et al. 2011; Markham et al. 2011). Each of the ceramide synthases found in Arabidopsis contain the TRAM LAG1 domain that is characteristic of ceramide synthases. Sequences between the Arabidopsis isoforms and the *S. cerevisiae* LAG1 demonstrate a high degree of homology within the TRAM LAG1 domain. These alignments also predict six transmembrane domains (Markham et al. 2011).

Mammals contain multiple ceramide synthases each with a distinct specificity for fatty acyl-CoAs and/or long-chain bases (Venkataraman et al. 2002b; Laviad et al. 2008; Mizutani et al. 2006; Riebeling et al. 2003; Mizutani et al. 2005). Chimera studies with mammalian ceramide synthases CerS2 and CerS5 have demonstrated that less than 40% of the CerS sequence is responsible for determination of the Acyl CoA specificity and

that the loop between the predicted fifth and sixth transmembrane domains plays a significant role in both specificity and activity (Tidhar et al. 2012), however the exact catalytic residues and mechanism of any ceramide synthase has yet to be determined. To date no study has identified these domains in plants.

The ceramide synthases found in Arabidopsis appear to also have distinct substrate preferences. Studies of Arabidopsis LCB C-4 hydroxylase mutants initially pointed to the likelihood that two functional classes of ceramide synthases occur in plants (Chen et al. 2008). Loss of, or reduced, LCB C-4 hydroxylation has been shown to result in the aberrant accumulation of high levels of sphingolipids with ceramides containing C16 fatty acids bound to dihydroxy LCBs (Chen et al. 2008). Based on this observation, it was proposed that Arabidopsis has one class of ceramide synthase that links C16 fatty acyl-CoAs with dihydoxy LCBs (termed "Class I"), and a second class ("Class II") that primarily links very long-chain fatty acyl CoAs with trihydroxy LCBs (Chen et al. 2008) (Figure 1.3). This prediction was supported by the identification, biochemical and genetic characterization of LOH1, LOH2, and LOH3 in Arabidopsis. Studies using yeast complementation showed that LOH2 prefers C16 acyl-CoAs, similar to the predicted Class I ceramide synthase (Ternes et al. 2011). Similarly, Arabidopsis *LOH2* mutants were found to be deficient in sphingolipids with ceramide backbones containing C16 fatty acids and dihydroxy fatty acids (Markham et al. 2011). Consistent with the substrate properties of Class II ceramide synthase, partial knock-out mutants of *LOH1* and *LOH3* contained reduced amounts of ceramides with very long-chain fatty acids and trihydroxy LCBs (Markham et al. 2011). It is notable that under ideal growth conditions, null mutants of *LOH2* are viable, suggesting that the Class I ceramide synthase and hence

ceramides with C16 fatty acids and dihydroxy LCBs are not essential in Arabidopsis (Markham et al. 2011). Conversely, double null mutants of *LOH1* and *LOH3* were not recoverable, indicating that the Class II ceramide synthase and ceramides with very long-chain fatty acids and trihydroxy LCBs are essential (Markham et al. 2011).

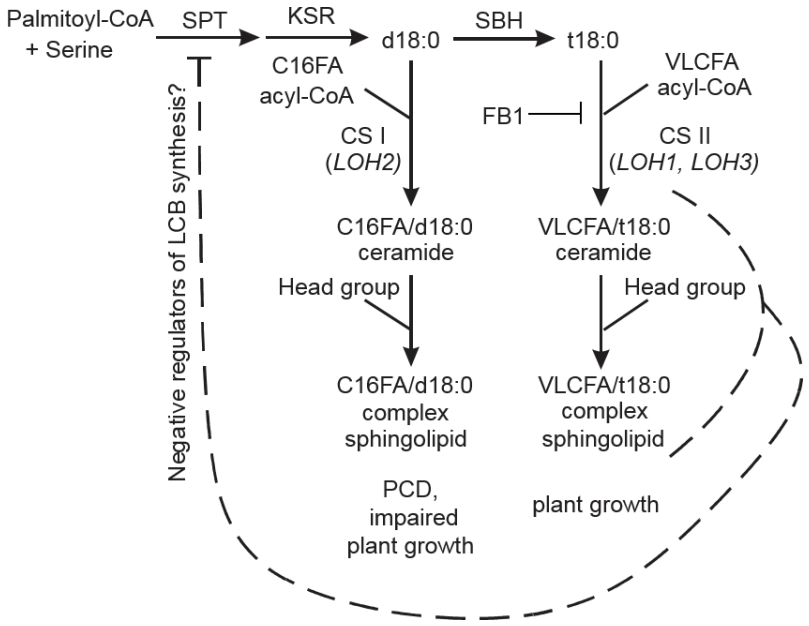

Figure 1.3 *Model of ceramide synthase mediated long-chain base (LCB) and fatty acid routing.* The Arabidopsis gene names are shown as reference. As indicated, Class I ceramide synthase (CSI) encoded by LOH2 displays strict substrate specificity of C16 fatty acid acyl-CoAs and dihydroxy LCBs, and Class II ceramide synthase (CSII) encoded by LOH1 or LOH3 display strict substrate specificity for very long-chain fatty acyl-CoAs and trihydroxy LCBs. One or more products of the CSII pathway appear to negatively regulate serine palmitoyltransferase (SPT) activity. In addition, sphingolipids with ceramides from the CSI pathway do not support growth, while those from the CSII pathway are essential for plant growth. The mycotoxin fumonisin B_1 (FB_1) appears to preferentially inhibit CSII enzymes. KSR, 3-ketosphinganine reductase; SBH, LCB C-4 hydroxylase.

Ceramide synthases are known targets for inhibition by sphinganine analog mycotoxins (SAMs) such as fumonisin B_1, or FB_1, produced by a variety of *Fusarium* species and AAL toxin produced by *Alternaria alternata* f. sp. *lycopersici* (Abbas et al. 1994). These compounds, particularly FB_1, have been widely used as tools for induction of programmed cell death (PCD) in plants, presumably due to the accumulation of cytotoxic LCBs from their inhibition of ceramide synthases (Stone et al. 2000). Recent evidence using FB_1 treatment of Arabidopsis ceramide synthase mutants has suggested that FB_1 is a more potent inhibitor of Class II ceramide synthases (i.e. LOH1 and LOH3 ceramide synthases) (Markham et al. 2011). Interestingly, in addition to accumulation of free LCBs, elevated levels of ceramides with C16 fatty acids and dihydroxy LCBs formed by Class I ceramide synthases (i.e. LOH2 ceramide synthases) are detectable following treatment of Arabidopsis with FB_1 (Markham et al. 2011). These results suggest that FB_1 cytotoxicity and PCD induction may be triggered by accumulated ceramides rather than or in addition to accumulated LCBs. FB_1 has also been used as a tool to study sphingolipid homeostasis in plants based on the observation that down-regulation of serine palmitoyltransferase (SPT) activity reduces FB_1 cytotoxicity and up-regulation of SPT activity enhances sensitivity of plants to FB_1 (Kimberlin et al. 2013; Shi et al. 2007).

1.3.7 GLUCOSYLCERAMIDE SYNTHESIS

Following its synthesis by Class I or Class II ceramide synthases, the ceramide backbone can be glycosylated at its C-1 OH to form either of two classes of glycosphingolipids: glucosylceramides (GlcCer) or glycosylinositolphosphoceramides (GIPCs) (Figure 1.2). GlcCer are the simplest glycosphingolipid and occur broadly in

eukaryotes, with the notable exception of *Saccharomyces cerevisiae* (Lynch and Dunn 2004). GlcCer consist of a glucose bound to the ceramide backbone by a 1,4-glycosidic linkage and are formed by the condensation of a ceramide substrate with UDP-glucose (Leipelt et al. 2001). This reaction is catalyzed by GlcCer synthase, an ER-localized enzyme in Arabidopsis that is encoded by At2g19980 (Melser et al. 2010). Compared to GIPCs, GlcCer are more enriched in ceramides with C16 fatty acids and dihydroxy LCBs (Markham et al. 2006; Sperling et al. 2005). In plants such as tomato and soybean, ceramides with C16 fatty acids and the LCB d18:2 predominate (Markham et al. 2006; Sperling et al. 2005). Based on this composition, it appears that a large portion of the GlcCer ceramide backbone is channeled from Class I-type ceramide synthases that have substrate preference for C16 fatty acids and dihydroxy LCBs (Markham et al. 2011). Although it is an abundant glycosphingolipid in plants, null mutants of the LCB Δ4 deasaturase in Arabidopsis have 30% reductions in GlcCer levels in flowers(Michaelson et al. 2009) without any apparent effect on flower physiology and function (Michaelson et al. 2009). The abundance of Δ4 unsaturated LCBs found in GlcCer and their subsequent decrease upon Δ4 LCB desaturase knockout seemingly indicates that the Δ4 desaturation targets LCBs for GlcCer synthesis, however this has yet to be confirmed. Arabidopsis GlcCer synthase mutants devoid of GlcCer are unable to undergo cell differentiation, but can be maintained in an undifferentiated callus state. Chemical complementation with psychosine (glycosylated LCB) is able to restore cell differentiation(Msanne et al. 2015). These findings are consistent with yeast GlcCer synthase mutants which are unable to transition from a yeast to filamentous state

(Michaelson et al. 2009; Rittenour et al. 2011) and are broadly consistent with GlcCer playing a role in cell differentiation.

1.3.8 INOSITOLPHOSPHOCERAMIDE SYNTHESIS

As an alternative fate to GlcCer synthesis, ceramides can be used for the production of GIPCs. GIPCs, which are approximately two-fold more abundant in Arabidopsis leaves than GlcCer, are typically enriched in ceramides with VLCFAs and trihydroxy LCBs that arise from Class II ceramide synthases (Markham et al. 2006). Although triple mutants of the three Arabidopsis IPC synthase genes have not been reported, it is presumed that IPC biosynthesis is essential, although the three genes are likely partially redundant. Following the synthesis of IPC, up to seven additional sugar residues can be added to the inositolphosphoryl head group to form an array of different GIPCs (Bure et al. 2011; Cacas et al. 2013), however the *in planta* functions of these complex GIPCs has yet to be determined.

1.4 SPHINGOLIPID FUNCTION - PROGRAMMED CELL DEATH AND THE HYPERSENSITIVE RESPONSE

Sphingolipids, primarily in the form of ceramides and LCBs, have been strongly implicated in mediation of programmed cell death (PCD) in plants. The Arabidopsis *acd5* mutant, which is defective in a proposed ceramide kinase (Greenberg et al. 2000; Liang et al. 2003) accumulates enhanced levels of free ceramides and displays early onset of PCD relative to wild-type controls (Greenberg et al. 2000; Liang et al. 2003). PCD induction in the *acd11* mutant has also been linked to ceramide accumulation associated with defects in ceramide-1-phosphate transport in this mutant (Simanshu et al. 2014).

Similar findings have been obtained by treatment of Arabidopsis cell cultures with C2 ceramide at a concentration of 50 μM (Townley et al. 2005). This treatment induces a transient increase in cytosolic $Ca^{2+}$and hydrogen peroxide production, followed by cell death, which was reversed by inhibition of Ca^{2+} release (Townley et al. 2005). These findings implicate Ca^{2+} as an essential component of ceramide induction of PCD. Notably, C2 ceramides containing 2- or α-hydroxylated fatty acids were not effective in PCD induction in Arabidopsis cell cultures (Townley et al. 2005). Consistent with this observation, the ability of Bax inhibitor-1 (BI-1) to suppress cell death in Arabidopsis is dependent of 2-hydroxylation of ceramide VLCFAs (Nagano et al. 2012).

Similar to results with ceramides, application of the free LCBs d18:1, d18:0, and t18:0 to Arabidopsis leaves also induces PCD, albeit at concentrations lower than that observed with ceramides (Shi et al. 2007). This induction of PCD was also dependent on ROS generation, but was suppressed by application of LCB-P along with free LCBs (Alden et al. 2011; Shi et al. 2007). These findings suggest that the ratio of free LCB to LCB-P, mediated by LCB kinases and LCB-P phosphatases, is an important "rheostat" for regulation of PCD (Figure 1.4) (Alden et al. 2011; Shi et al. 2007). This is analogous to the dependence of PCD induction on relative levels of ceramides and ceramide-1-phosphates (Greenberg et al. 2000; Liang et al. 2003). The transduction pathway for elicitation of PCD by free LCBs has been shown to be dependent in Arabidopsis on mitogen-activated protein kinase 6 (MPK6) (Saucedo-García et al. 2011) as well as 14-3-3 protein phosphorylation by calcium-dependent kinase 3 (CPK3) that is activated by LCB-triggered release of cytosolic Ca^{2+} (Lachaud et al. 2013).

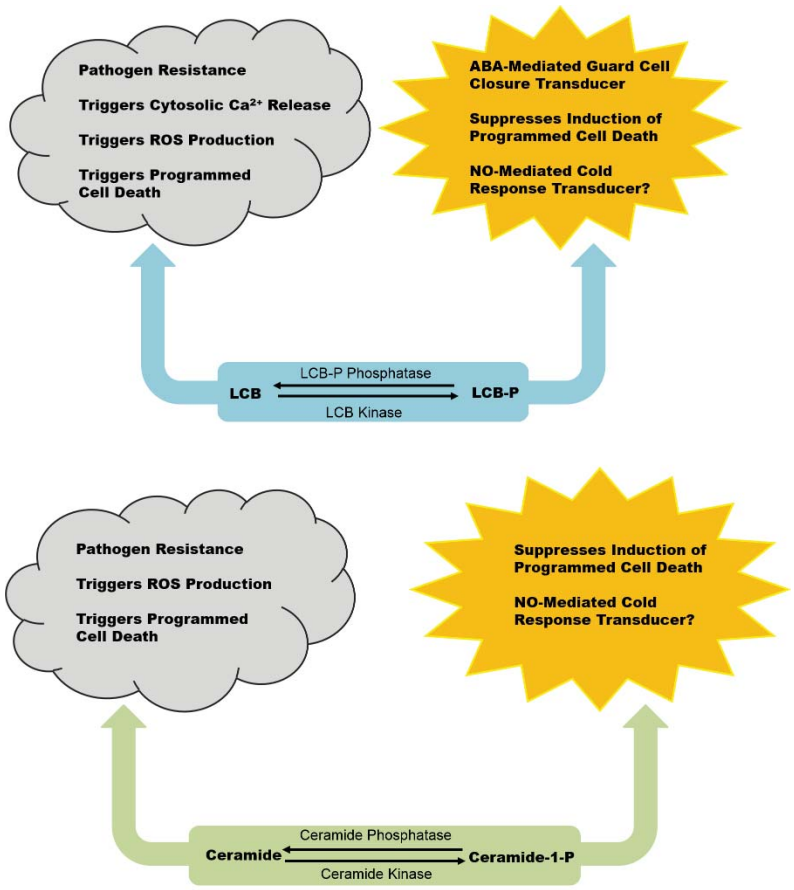

Figure 1.4 *Phosphorylated/dephosphorylated long-chain bases (LCBs) and ceramides serve as mediators of physiological processes in plants*. The interplay between LCBs and ceramides and their phosphorylated forms is regulates cellular process and responses to environmental stimuli. Abbreviations: LCB, long-chain base; LCB-P, long-chain base-1-phosphate; ABA, Abscisic acid; ROS, Reactive oxygen species; NO, nitric oxide.

The hypersensitive response (HR) is an important process for resistance to bacterial and fungal pathogens that is characterized by localized induction of PCD that reduces or prevents the spread of pathogens in plants. Given the importance of LCBs and ceramides to PCD induction, a considerable body of research has emerged linking sphingolipids to bacterial and fungal pathogen resistance as described in a recent review (Berkey et al. 2012). Notably, ceramide accumulation in *acd5* and *acd11* mutants has

been shown to be associated with salicylic acid (SA)-dependent upregulation of HR-type PCD and pathogen-resistance genes, including genes for PR1, ERD11, and chitinase (Brodersen et al. 2002; Greenberg et al. 2000). More recently, Arabidopsis mutants defective in 2-hydroxylation of ceramide fatty acids were found to have elevated LCB and ceramide levels, as well as, increased levels of free and glycosylated SA and constitutive induction of *PR1* and *PR2* genes (Konig et al. 2012). These mutants also displayed enhanced resistance to the biotrophic fungal pathogen *Golovinomyces cichoracearum* (Konig et al. 2012).

1.5 RATIONALE

The hypotheses addressed in this dissertation are as follows: 1, each ceramide synthase in Arabidopsis has a unique substrate specificity with LOH1 and LOH3 preferring trihydroxy LCBs/VLCFA and LOH2 preferring dihydroxy LCBs/C16 FAs; 2, each ceramide synthase is differentially inhibited by FB_1 with LOH2 being the most resistant to FB_1 inhibition; 3, ceramide synthesis and composition directly affects plant growth and development; 4, distinct complex sphingolipid biosynthesis pathways exist controlled in part by LCB identity and ceramide synthase specificity.

These hypotheses are based upon evidence that has emerged from sphingolipid compositional profiling of Arabidopsis mutants that hydroxylation and desaturation affect metabolic outcomes in sphingolipid biosynthesis. Since ceramide synthesis is a key branching point in sphingolipid metabolism the substrate preference and activity of each ceramide synthase is key to controlling the final complex sphingolipid formed (Chen et al. 2008; Dunn et al. 2004; Chen et al. 2012). For instance, the LCB C-4 hydroxylase

mutants accumulate high levels of sphingolipids with C16 fatty acid and dihydroxy LCB ceramide backbones, rather than the more typical ceramides composed of very long-chain fatty acids and trihydroxy LCBs (Chen et al. 2008). As discussed above, this metabolic phenotype arises from the proposed substrate preferences of ceramide synthases, but the exact specificity of each ceramide synthase isoform has yet to be determined. In order to address this question a mass spectrometry based ceramide synthase assay was developed (Chapter 2) and kinetic parameters were determined for the three ceramide synthase isoforms found in Arabidopsis using both d18:0 and t18:0 LCBs and varying lengths of acyl CoAs (Chapter 3). To confirm that the *in vitro* specificities found were consistent with *in planta* activity, each ceramide synthase isoform was individually overexpressed in Arabidopsis (Chapter 4). Using these two techniques the hypothesized specificities were not only confirmed but it was also determined that ceramides of different fatty acid/LCB combinations have profoundly different impacts on plant growth/development and induction of programmed cell death.

In addition to differences in substrate specificity previous research has indicated that ceramide synthases differ in their susceptibility to sphingoid base analog mycotoxins, such as Fumonisin B_1. Analysis of FB_1 treated wild-type Arabidopsis has revealed not only large increases in free LCB levels but a substantial increase in dihydroxy LCB/C16 FA ceramides thus indicating that LOH1 and LOH3 may be more susceptible to FB_1 inhibition than LOH2 (Markham et al. 2011). Using the *in vitro* ceramide synthase assay it was determined that both LOH2 and LOH3 are more resistant to FB_1 inhibition than LOH1 (Chapter 3) which was corroborated with *in planta* overexpression of LOH2 and

LOH3 imparting FB_1 resistance while overexpression of LOH1 resulted in no change from wild-type (Chapter 4).

Since ceramide is a key branching point in sphingolipid metabolism it has been thought that ceramide LCB/FA composition can influence the final complex sphingolipid formed. In particular it is believed that the presence of a d18:2(4,8) LCB targets ceramides to the GlcCer pool. This hypothesis is supported by both plant and fungi mutant studies. For instance, the Arabidopsis *sld1/sld2* double mutant lacks LCB Δ8 unsaturation and has a 50% reduction of GlcCers, perhaps due to the substrate specificity of ceramide synthases and/or GlcCer synthase (Chen et al. 2012). Similarly, Arabidopsis mutants for the LCB Δ4 desaturase, have an ~50% reduction in GlcCer in reproductive tissues (Michaelson et al. 2009). This phenotype is more extreme in LCB Δ4 desaturase mutants of the yeast *Pichia pastoris* where disruption of the LCB Δ4 desaturase results in a near complete loss of GlcCers (Michaelson et al. 2009). Ceramide synthase specificity and activity is hypothesized to play a significant role in which complex sphingolipid is formed, however the lack of data regarding ceramide synthase specificity toward Δ4 and Δ8 LCBs has left open questions about the influence these modifications have on ceramide formation. To answer this question *in vitro* assays where done using desaturated LCB substrates which found that LOH2 has a remarkable preference for d18:1(4) LCBs (Chapter 3). This preference helps explain the high level of d18:2(4,8)_c16:0 sphingolipids found in Arabidopsis pollen (Chapter 5). Furthermore, all of the d18:2(4,8)_c16:0 sphingolipids were found in the GlcCers demonstrating the presence of distinct complex sphingolipid synthesis pathways controlled, at least partially, by ceramide synthase specificity and activity. The presence of distinct

pathways was further supported by the discovery of a unique Δ8 LCB desaturase from castor bean that requires a Δ4 double bond for activity (Chapter 6) indicating that the Δ4 double bond acts as a marker for incorporation into GlcCers through a LOH2-like ceramide synthase. Through the use of publications units, the results presented in this dissertation demonstrate the importance that ceramide synthase specificity and activity have on complex sphingolipid composition, plant growth/development, and mycotoxin resistance.

1.6 REFERENCES

Abbas HK, Tanaka T, Duke SO, Porter JK, Wray EM, Hodges L, Sessions AE, Wang E, Merrill AH, Jr., Riley RT (1994) Fumonisin- and AAL-toxin-induced disruption of sphingolipid metabolism with accumulation of free sphingoid bases. Plant Physiol 106 (3):1085-1093.

Alden KP, Dhondt-Cordelier S, McDonald KL, Reape TJ, Ng CK, McCabe PF, Leaver CJ (2011) Sphingolipid long chain base phosphates can regulate apoptotic-like programmed cell death in plants. Biochem Bioph Res Commun 410 (3):574-580.

Bach L, Gissot L, Marion J, Tellier F, Moreau P, Satiat-Jeunemaitre B, Palauqui JC, Napier JA, Faure JD (2011) Very-long-chain fatty acids are required for cell plate formation during cytokinesis in Arabidopsis thaliana. J Cell Sci 124 (19):3223-3234.

Bach L, Michaelson LV, Haslam R, Bellec Y, Gissot L, Marion J, Da Costa M, Boutin JP, Miquel M, Tellier F, Domergue F, Markham JE, Beaudoin F, Napier JA, Faure JD (2008) The very-long-chain hydroxy fatty acyl-CoA dehydratase PASTICCINO2 is essential and limiting for plant development. Proc Natl Acad Sci USA 105 (38):14727-14731.

Beckmann C, Rattke J, Oldham NJ, Sperling P, Heinz E, Boland W (2002) Characterization of a Delta8-sphingolipid desaturase from higher plants: a stereochemical and mechanistic study on the origin of E,Z isomers. Angew Chem Int Ed 41 (13):2298-2300.

Berkey R, Bendigeri D, Xiao S (2012) Sphingolipids and plant defense/disease: the "death" connection and beyond. Front Plant Sci 3 (68).

Brodersen P, Petersen M, Pike H, Olszak B, Skov S, Odum N, Jørgensen L, Brown R, Mundy J (2002) Knockout of Arabidopsis accelerated-cell-death11 encoding a sphingosine transfer protein causes activation of programmed cell death and defense. Genes Dev 16 (4):490-502.

Bure C, Cacas JL, Wang F, Gaudin K, Domergue F, Mongrand S, Schmitter JM (2011) Fast screening of highly glycosylated plant sphingolipids by tandem mass spectrometry. Rapid Commun Mass Spectrom 25 (20):3131-3145.

Cacas JL, Bure C, Furt F, Maalouf JP, Badoc A, Cluzet S, Schmitter JM, Antajan E, Mongrand S (2013) Biochemical survey of the polar head of plant glycosylinositolphosphoceramides unravels broad diversity. Phytochem 96:191-200.

Cahoon EB, Lynch DV (1991) Analysis of Glucocerebrosides of Rye (Secale cereale L. cv Puma) Leaf and Plasma Membrane. Plant Physiol 95 (1):58-68.

Carter HE, Gigg RH, Law JH, Nakayama T, Weber E (1958) Biochemistry of the sphingolipides: structure of phytoglycolipide. J Biol Chem 233 (6):1309-1314.

Chao DY, Gable K, Chen M, Baxter I, Dietrich CR, Cahoon EB, Guerinot ML, Lahner B, Lu S, Markham JE, Morrissey J, Han G, Gupta SD, Harmon JM, Jaworski JG, Dunn TM, Salt DE (2011) Sphingolipids in the root play an important role in regulating the leaf ionome in Arabidopsis thaliana. Plant Cell 23 (3):1061-1081.

Chen M, Cahoon E, Saucedo-García M, Plasencia J, Gavilanes-Ruíz M (2010) Plant Sphingolipids: Structure, Synthesis and Function. In: Wada H, Murata N (eds) Lipids in Photosynthesis, vol 30. Advances in Photosynthesis and Respiration. Springer Netherlands, pp 77-115. doi:10.1007/978-90-481-2863-1_5

Chen M, Han G, Dietrich CR, Dunn TM, Cahoon EB (2006) The essential nature of sphingolipids in plants as revealed by the functional identification and characterization of the Arabidopsis LCB1 subunit of serine palmitoyltransferase. Plant Cell 18 (12):3576-3593.

Chen M, Markham JE, Cahoon EB (2012) Sphingolipid Delta8 unsaturation is important for glucosylceramide biosynthesis and low-temperature performance in Arabidopsis. Plant J 69 (5):769-781.

Chen M, Markham JE, Dietrich CR, Jaworski JG, Cahoon EB (2008) Sphingolipid long-chain base hydroxylation is important for growth and regulation of sphingolipid content and composition in Arabidopsis. Plant Cell 20 (7):1862-1878.
Chen M, Thelen JJ (2013) ACYL-LIPID DESATURASE2 is required for chilling and freezing tolerance in Arabidopsis. Plant Cell 25 (4):1430-1444.
Dietrich CR, Han G, Chen M, Berg RH, Dunn TM, Cahoon EB (2008) Loss-of-function mutations and inducible RNAi suppression of Arabidopsis LCB2 genes reveal the critical role of sphingolipids in gametophytic and sporophytic cell viability. Plant J 54 (2):284-298.
Dunn TM, Lynch DV, Michaelson LV, Napier JA (2004) A post-genomic approach to understanding sphingolipid metabolism in Arabidopsis thaliana. Ann Bot 93 (5):483-497.
Greenberg JT, Silverman FP, Liang H (2000) Uncoupling salicylic acid-dependent cell death and defense-related responses from disease resistance in the Arabidopsis mutant acd5. Genetics 156 (1):341-350.
Haak D, Gable K, Beeler T, Dunn T (1997) Hydroxylation of Saccharomyces cerevisiae ceramides requires Sur2p and Scs7p. J Biol Chem 272 (47):29704-29710.
Han G, Gable K, Yan L, Natarajan M, Krishnamurthy J, Gupta SD, Borovitskaya A, Harmon JM, Dunn TM (2004) The topology of the Lcb1p subunit of yeast serine palmitoyltransferase. J Biol Chem 279 (51):53707-53716.
Hanada K (2003) Serine palmitoyltransferase, a key enzyme of sphingolipid metabolism. Biochim Biophys Acta 1632 (1-3):16-30.
Imai H, Yamamoto K, Shibahara A, Miyatani S, Nakayama T (2000) Determining double-bond positions in monoenoic 2-hydroxy fatty acids of glucosylceramides by gas chromatography-mass spectrometry. Lipids 35 (2):233-236.
Kimberlin AN, Majumder S, Han G, Chen M, Cahoon RE, Stone JM, Dunn TM, Cahoon EB (2013) Arabidopsis 56-amino acid serine palmitoyltransferase-interacting proteins stimulate sphingolipid synthesis, are essential, and affect mycotoxin sensitivity. Plant Cell 25 (11):4627-4639.
Konig S, Feussner K, Schwarz M, Kaever A, Iven T, Landesfeind M, Ternes P, Karlovsky P, Lipka V, Feussner I (2012) Arabidopsis mutants of sphingolipid fatty acid alpha-hydroxylases accumulate ceramides and salicylates. New Phytol 196 (4):1086-1097.
Lachaud C, Prigent E, Thuleau P, Grat S, Da Silva D, Briere C, Mazars C, Cotelle V (2013) 14-3-3-Regulated Ca2+-dependent protein kinase CPK3 is required for sphingolipid-induced cell death in Arabidopsis. Cell Death Differ 20 (2):209-217.
Laviad EL, Albee L, Pankova-Kholmyansky I, Epstein S, Park H, Merrill AH, Jr., Futerman AH (2008) Characterization of ceramide synthase 2: tissue distribution, substrate specificity, and inhibition by sphingosine 1-phosphate. J Biol Chem 283 (9):5677-5684.
Leipelt M, Warnecke D, Zahringer U, Ott C, Muller F, Hube B, Heinz E (2001) Glucosylceramide synthases, a gene family responsible for the biosynthesis of glucosphingolipids in animals, plants, and fungi. J Biol Chem 276 (36):33621-33629.
Liang H, Yao N, Song JT, Luo S, Lu H, Greenberg JT (2003) Ceramides modulate programmed cell death in plants. Genes Dev 17 (21):2636-2641.
Lynch DV, Dunn TM (2004) An introduction to plant sphingolipids and a review of recent advances in understanding their metabolism and function. New Phytol 161 (3):677-702.
Markham JE, Jaworski JG (2007) Rapid measurement of sphingolipids from Arabidopsis thaliana by reversed-phase high-performance liquid chromatography coupled to electrospray ionization tandem mass spectrometry. Rapid Commun Mass Spectrom 21 (7):1304-1314.
Markham JE, Li J, Cahoon EB, Jaworski JG (2006) Separation and identification of major plant sphingolipid classes from leaves. J Biol Chem 281 (32):22684-22694.
Markham JE, Lynch DV, Napier JA, Dunn TM, Cahoon EB (2013) Plant sphingolipids: function follows form. Curr Opin Plant Biol 16 (3):350-357.

Markham JE, Molino D, Gissot L, Bellec Y, Hematy K, Marion J, Belcram K, Palauqui JC, Satiat-Jeunemaitre B, Faure JD (2011) Sphingolipids containing very-long-chain fatty acids define a secretory pathway for specific polar plasma membrane protein targeting in Arabidopsis. Plant Cell 23 (6):2362-2378.

Melser S, Batailler B, Peypelut M, Poujol C, Bellec Y, Wattelet-Boyer V, Maneta-Peyret L, Faure JD, Moreau P (2010) Glucosylceramide biosynthesis is involved in Golgi morphology and protein secretion in plant cells. Traffic 11 (4):479-490.

Michaelson LV, Zauner S, Markham JE, Haslam RP, Desikan R, Mugford S, Albrecht S, Warnecke D, Sperling P, Heinz E, Napier JA (2009) Functional characterization of a higher plant sphingolipid Delta4-desaturase: defining the role of sphingosine and sphingosine-1-phosphate in Arabidopsis. Plant Physiol 149 (1):487-498.

Mitchell AG, Martin CE (1997) Fah1p, a Saccharomyces cerevisiae cytochrome b5 fusion protein, and its Arabidopsis thaliana homolog that lacks the cytochrome b5 domain both function in the alpha-hydroxylation of sphingolipid-associated very long chain fatty acids. J Biol Chem 272 (45):28281-28288.

Mizutani Y, Kihara A, Igarashi Y (2005) Mammalian Lass6 and its related family members regulate synthesis of specific ceramides. Biochem J 390:263-271.

Mizutani Y, Kihara A, Igarashi Y (2006) LASS3 (longevity assurance homologue 3) is a mainly testis-specific (dihydro)ceramide synthase with relatively broad substrate specificity. Biochem J 398:531-538.

Msanne J, Chen M, Luttgeharm KD, Bradley AM, Mays ES, Paper JM, Boyle DL, Cahoon RE, Schrick K, Cahoon EB (2015) Glucosylceramide is Critical for Cell-Type Differentiation and Organogenesis, but not for Cell Viability in Arabidopsis. The Plant journal : for cell and molecular biology.

Nagano M, Ihara-Ohori Y, Imai H, Inada N, Fujimoto M, Tsutsumi N, Uchimiya H, Kawai-Yamada M (2009) Functional association of cell death suppressor, Arabidopsis Bax inhibitor-1, with fatty acid 2-hydroxylation through cytochrome b(5). Plant J 58 (1):122-134.

Nagano M, Takahara K, Fujimoto M, Tsutsumi N, Uchimiya H, Kawai-Yamada M (2012) Arabidopsis sphingolipid fatty acid 2-hydroxylases (AtFAH1 and AtFAH2) are functionally differentiated in fatty acid 2-hydroxylation and stress responses. Plant Physiol 159 (3):1138-1148.

Riebeling C, Allegood JC, Wang E, Merrill AH, Futerman AH (2003) Two mammalian longevity assurance gene (LAG1) family members, trh1 and trh4, regulate dihydroceramide synthesis using different fatty acyl-CoA donors. J Biol Chem 278 (44):43452-43459.

Rittenour WR, Chen M, Cahoon EB, Harris SD (2011) Control of glucosylceramide production and morphogenesis by the Bar1 ceramide synthase in Fusarium graminearum. PLoS One.

Sandhoff K (2013) Metabolic and cellular bases of sphingolipidoses. Biochem Soc Trans 41 (6):1562-1568.

Saucedo-García M, Guevara-García A, González-Solís A, Cruz-García F, Vázquez-Santana S, Markham J, Lozano-Rosas M, Dietrich C, Ramos-Vega M, Cahoon E, Gavilanes-Ruíz M (2011) MPK6, sphinganine and the LCB2a gene from serine palmitoyltransferase are required in the signaling pathway that mediates cell death induced by long chain bases in Arabidopsis. New Phytol 191 (4):943-957.

Shanklin J, Cahoon EB (1998) Desaturation and related modifications of fatty acids. Annu Rev Plant Physiol Plant Mol Biol 49:611-641.

Shi L, Bielawski J, Mu J, Dong H, Teng C, Zhang J, Yang X, Tomishige N, Hanada K, Hannun YA, Zuo J (2007) Involvement of sphingoid bases in mediating reactive oxygen intermediate production and programmed cell death in Arabidopsis. Cell Res 17 (12):1030-1040.

Simanshu DK, Zhai X, Munch D, Hofius D, Markham JE, Bielawski J, Bielawska A, Malinina L, Molotkovsky JG, Mundy JW, Patel DJ, Brown RE (2014) Arabidopsis accelerated cell death 11, ACD11, is a ceramide-1-phosphate transfer protein and intermediary regulator of phytoceramide levels. Cell Rep 6 (2):388-399.

Smith MA, Dauk M, Ramadan H, Yang H, Seamons LE, Haslam RP, Beaudoin F, Ramirez-Erosa I, Forseille L (2013) Involvement of Arabidopsis ACYL-COENZYME A DESATURASE-LIKE2 (At2g31360) in the biosynthesis of the very-long-chain monounsaturated fatty acid components of membrane lipids. Plant Physiol 161 (1):81-96.

Sperling P, Franke S, Luthje S, Heinz E (2005) Are glucocerebrosides the predominant sphingolipids in plant plasma membranes? Plant Physiol Biochem 43 (12):1031-1038.

Sperling P, Ternes P, Moll H, Franke S, Zahringer U, Heinz E (2001) Functional characterization of sphingolipid C4-hydroxylase genes from Arabidopsis thaliana. FEBs Lett 494 (1-2):90-94.

Sperling P, Zahringer U, Heinz E (1998) A sphingolipid desaturase from higher plants. Identification of a new cytochrome b5 fusion protein. J Biol Chem 273 (44):28590-28596.

Stone JM, Heard JE, Asai T, Ausubel FM (2000) Simulation of fungal-mediated cell death by fumonisin B1 and selection of *fumonisin B_1-resistant* (*fbr*) Arabidopsis mutants. Plant Cell 12 (10):1811-1822.

Tamura K, Mitsuhashi N, Hara-Nishimura I, Imai H (2001) Characterization of an Arabidopsis cDNA encoding a subunit of serine palmitoyltransferase, the initial enzyme in sphingolipid biosynthesis. Plant Cell Physiol 42 (11):1274-1281.

Teng C, Dong H, Shi L, Deng Y, Mu J, Zhang J, Yang X, Zuo J (2008) Serine palmitoyltransferase, a key enzyme for de novo synthesis of sphingolipids, is essential for male gametophyte development in Arabidopsis. Plant Physiol 146 (3):1322-1332.

Ternes P, Feussner K, Werner S, Lerche J, Iven T, Heilmann I, Riezman H, Feussner I (2011) Disruption of the ceramide synthase LOH1 causes spontaneous cell death in Arabidopsis thaliana. New Phytol 192 (4):841-854.

Ternes P, Franke S, Zahringer U, Sperling P, Heinz E (2002) Identification and characterization of a sphingolipid delta 4-desaturase family. J Biol Chem 277 (28):25512-25518.

Thudichum JLW (1884) A treatise on the chemical constitution of the brain. Baillière, Tindall and Cox, London

Tidhar R, Ben-Dor S, Wang E, Kelly S, Merrill AH, Futerman AH (2012) Acyl Chain Specificity of Ceramide Synthases Is Determined within a Region of 150 Residues in the Tram-Lag-CLN8 (TLC) Domain. J Biol Chem 287 (5):3197-3206.

Townley HE, McDonald K, Jenkins GI, Knight MR, Leaver CJ (2005) Ceramides induce programmed cell death in Arabidopsis cells in a calcium-dependent manner. Biol Chem 386 (2):161-166.

Venkataraman K, Riebeling C, Bodennec J, Riezman H, Allegood JC, Sullard MC, Merrill AH, Futerman AH (2002a) Upstream of growth and differentiation factor 1 (uog1), a mammalian homolog of the yeast longevity assurance gene 1 (LAG1), regulates N-stearoyl-sphinganine (C18-(dihydro)ceramide) synthesis in a fumonisin B-1-independent manner in mammalian cells. J Biol Chem 277 (38):35642-35649.

Venkataraman K, Riebeling C, Bodennec J, Riezman H, Allegood JC, Sullards MC, Merrill AH, Jr., Futerman AH (2002b) Upstream of growth and differentiation factor 1 (uog1), a mammalian homolog of the yeast longevity assurance gene 1 (LAG1), regulates N-stearoyl-sphinganine (C18-(dihydro)ceramide) synthesis in a fumonisin B1-independent manner in mammalian cells. J Biol Chem 277 (38):35642-35649.

CHAPTER 2

A MASS SPECTROMETRY-BASED METHOD FOR THE ASSAY OF CERAMIDE SYNTHASE SUBSTRATE SPECIFICITY

Note: The results described in this chapter have been previously published, no text has been changed.

The citation is: Luttgeharm, K. D., E. B. Cahoon, J.E. Markham (2015). "A mass-spectrometry based method for the assay of ceramide synthase substrate specificity." Analalytical Biochemistry **478**: 96-101.

2.1 INTRODUCTION

Sphingolipids are bioactive molecules that can enact profound outcomes on cell fate in the form of cell division or cell death (Townley et al. 2005; Hannun and Luberto 2000; Dickson et al. 1997; Wang et al. 1996). Ceramides are synthesized de novo from fatty acyl-coenzyme A (CoA) and long-chain base (LCB) that when phosphorylated may also affect cell fate decisions. Indeed, the ratio between longchain base phosphate and ceramide is proposed to function as a rheostat that regulates cell fate (Alden et al. 2011; Maceyka et al. 2002; Cuvillier et al. 1996). The synthesis of ceramide, therefore, is a critical reaction in sphingolipid metabolism that has the potential to coordinate LCB and ceramide levels (Kobayashi and Nagiec 2003; Aronova et al. 2008; Breslow and Weissman 2010). In addition, the LCB and fatty acid combinations of the ceramide, and thus the final complex sphingolipid, are important components in determining the ultimate role of the individual sphingolipids in the cell (Markham et al. 2011; Ali et al. 2013; Hartmann et al. 2013; Chen et al. 2008). Ceramide is synthesized by the enzyme sphingosine N-acyl transferase (EC 2.3.1.24), commonly referred to as ceramide synthase. In many organisms, ceramide synthase has multiple isoforms with different specificities for LCB and fatty acyl-CoA substrates that contribute significantly to the variation found in sphingolipid structure (Pewzner-Jung et al. 2006). For example, in plant ceramides up to 10 different LCBs are found combined with 14 or more different fatty acids to produce hundreds of theoretical species of ceramide (Markham and Jaworski 2007). Given the importance of the ceramide synthase reaction to the overall composition of the cell's sphingolipid profile, the enzymatic and regulatory properties of

the individual isoforms have been the subject of significant investigation (Levy and Futerman 2010).

A thorough enzymatic characterization of ceramide synthase is challenging due to the fact that ceramide synthase is an integral membrane protein and its substrates and products are not readily soluble in aqueous solutions (Wang and Merrill Jr 2000). Although ceramide synthase can be solubilized from the membrane using detergents such as octylglucoside (Shimeno et al. 1998) and digitonin (Vallée and Riezman 2005), most of the activity is lost; hence, the majority of reports have characterized the enzyme in isolated membranes (Lahiri et al. 2007). The most common method to assay ceramide synthase in vitro is through the use of radiolabeled 3,4-^{3}H dihydrosphingosine ([3,4-^{3}H]DHS) prepared by reduction of sphingosine. Subsequent to the reaction, radiolabeled substrates and reaction products are separated by normal-phase thin-layer chromatography and quantified. Using this approach, previous reports have detailed the substrate specificities for the mammalian ceramide synthases: CerS1 (C18 CoA) (Venkataraman et al. 2002), CerS2 (C22–C26 CoAs) (Laviad et al. 2008), CerS3 (C18–C20 CoAs) (Mizutani et al. 2006), CerS4 (C18–C20 CoAs) (Riebeling et al. 2003), CerS5 (C16 CoA) (Riebeling et al. 2003), and CerS6 (C14–C16 CoAs) (Mizutani et al. 2005). This methodology is eminently suitable for investigation of mammalian sphingolipid metabolism where the predominant LCB is DHS. However, in plants and certain fungi, the predominant LCB found in sphingolipids is 4-hydroxy-DHS or phytosphingosine along with a number of different unsaturated LCBs. None of these is readily available as a radiolabeled substrate, meaning that if it is to be used to measure ceramide synthase activity, a different method for detecting the products of the ceramide

synthase assay must be employed. Other methodologies to assay ceramide synthase activity are conducted using radiolabeled fatty acyl CoAs (Narimatsu et al. 1986), fluorescent LCB analogues (Kim et al. 2012), in vivo feeding experiments with radiolabeled substrate (Mizutani et al. 2006; Bauer et al. 2009), and mass spectrometry (Kim et al. 2012; Berdyshev et al. 2009) along with synthetic odd-chain substrates (Spassieva et al. 2006; Mullen et al. 2011). Although these methods work in detecting produced ceramide, they all have distinct limitations. In vivo assays are of only limited use in characterizing enzyme activity, whereas not all acyl-CoAs/fatty acids or LCBs are available as radiolabeled substrates and the cost of purchasing multiple radiolabeled CoA substrates is significant. To circumvent the difficulties with obtaining radiolabeled substrates, a method to assay ceramide synthase activity in vitro was developed that uses non-radiolabeled phytosphingosine (t18:0) or dihydrosphingosine (d18:0) and detection of the products of the ceramide synthase reaction by liquid chromatography coupled to mass spectrometry (LC–MS). This was applied to the assay of ceramide synthase in Saccharomyces cerevisiae using purified natural LCB and fatty acid substrates.

2.2. RESULTS

2.2.1 MEASUREMENT OF IN VITRO BACKGROUND ACTIVITY

Because purified membranes may contain endogenous ceramide, fatty acyl-CoAs, and LCBs, it was important to measure endogenous ceramide or ceramide synthase activity resulting from these sources. Measurement of activity without either LCB or acyl- CoA substrates showed that a small amount of ceramide is already present in purified membranes (Figure 2.1). The addition of LCB or acyl- CoA alone causes a minor increase in background ceramide, and because the microsomes plus acyl-CoA produced the highest level of background, this was used as the background activity for all further assays. For every assay completed, a no-LCB control was also performed to measure the background activity and was subtracted from the amount produced with added LCB and acyl- CoA combined.

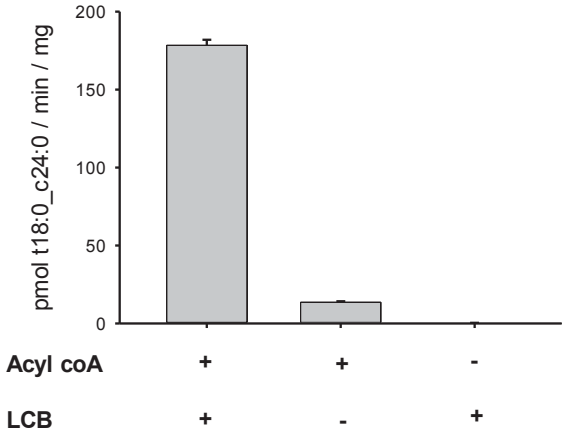

Figure 2.1 *Dependence of ceramide synthase activity on the addition of substrates*. Ceramide (t18:0c24:0) synthase activity in yeast microsomes in the presence of added LCB (t18:0) and acyl-CoA (24:0) substrate or with just acyl-CoA or LCB alone is shown. Data represent means ± standard errors (n = 3).

2.2.2 OPTIMIZATION OF ASSAY CONDITIONS

Initial attempts to establish an enzyme assay for ceramide synthase in the absence of BSA proved to be unsatisfactory because increased levels of either LCB or acyl-CoA substrate inhibited, rather than stimulated, enzyme activity (Figure 2.2).

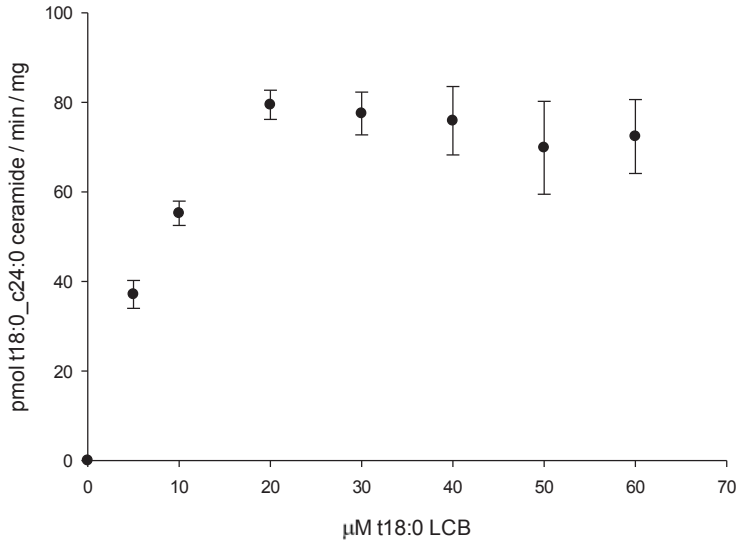

Figure 2.*2* *High concentrations of LCB result in deviation from Michaelis–Menten kinetics*. Ceramide synthase activity at increasing concentrations of t18:0 LCB. Zero activity represents the background activity present without added LCB. This same amount of activity was subtracted from all points. All assays were run with 10 µM protein, 15 µM t18:0 LCB, 50 µM Acyl coA and 10 µM BSA and run for 30 min. Data represented as the mean (n = 3) ± SE.

Consequently, alternative options were explored for delivery of LCB, including delivery in PC– LCB microsomes (Wang and Merrill Jr 2000) and as a complex with BSA. Due to significant background signal in the mass spectrometer from PC–LCB microsomes (see below), BSA was used as a vehicle for the delivery of LCB and acyl-CoA in solution as described previously (Wang and Merrill Jr 2000; Lahiri et al. 2007). At 10 µM BSA and 50 µM acyl-CoA, levels of LCB above 15 µM were found to be inhibitory rather than stimulatory; hence, 15 µM was the maximum LCB concentration used in subsequent

assays (Figure 2.2). At 15 μM LCB and 50 μM lignoceroyl-CoA, 10 μM BSA has a small but significant stimulatory effect on ceramide synthase activity and significantly improves the dependability of the assay (Figure 2.3A).

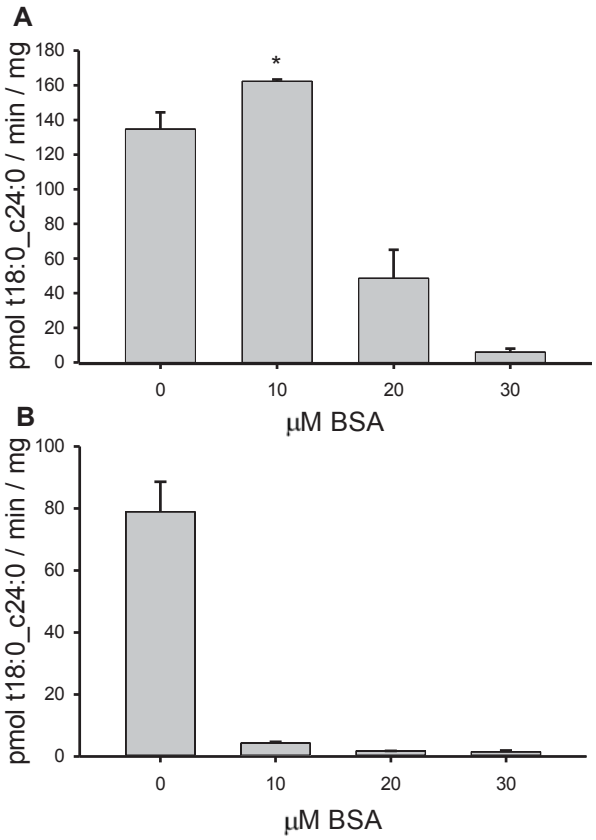

Figure 2.3 *Effect of BSA on ceramide synthase activity*. Ceramide synthase activity in yeast microsomes at varying concentrations of exogenous BSA and acyl-CoA is shown. (A) Ceramide synthase activity in the presence of 15 μM t18:0 LCB and 50 μM 24:0-CoA and varying amounts of BSA. (B) Ceramide synthase activity in the presence of 15 μM t18:0 LCB and 15 μM 24:0-CoA with varying amounts of BSA. All assays contained 10 μg of microsomal protein. Data represent means ± standard errors (n = 3).

Because higher concentrations of BSA inhibit ceramide synthase activity, BSA was used at 10 μM in all subsequent reactions. BSA has a complex interaction with lipids, binding and solubilizing a variety of lipids that may prevent them from engaging in biochemical reactions. When delivered as a complex with BSA, LCB has been

reported to rapidly transfer to the membrane phase (Hirschberg et al. 1993). Experiments using BSA–LCB complexes and microsomes showed that after 10 min more than 90% of the LCB was recovered in the microsome fraction (Figure 2.4). This indicates that solvation of the LCB by the membrane is preferred over LCB binding to BSA; hence, the stimulatory effect of BSA (Figure 2.3A) is due to its interaction with other components of the assay, most likely the acyl-CoA.

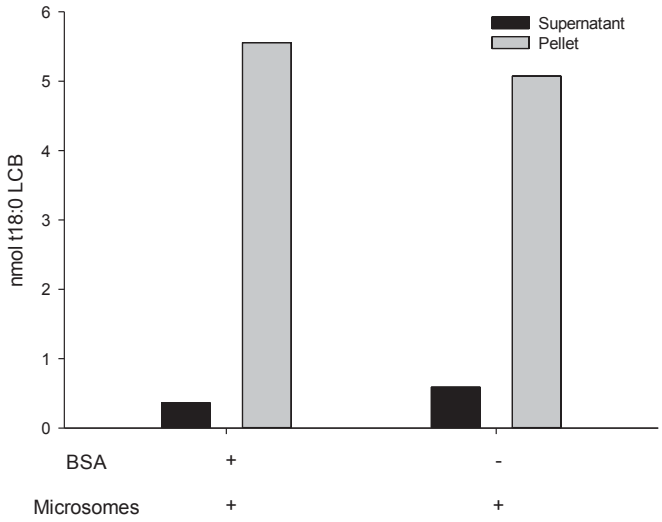

Figure 2.4 *LCBs quickly equilibrate with microsomes from BSA complexes.* Graph showing the amount of LCB detected in the aqueous phase (supernatant) and lipid phase (pellet) after ultracentrifugation in the presence or absence of BSA and microsomes.

To test the effect of BSA on the reaction at low acyl-CoA concentration, the amount of acyl-CoA in the assay was reduced to 15 μM. At this low concentration, the effect of BSA on the assay becomes inhibitory, presumably by reducing the availability of acyl-CoA (Figure 2.3B). Hence, there is an optimal acyl-CoA/BSA ratio for maximum ceramide synthase activity of approximately 5:1 (Lahiri et al. 2007).

In development of this assay, it was found that the method by which the reaction was terminated and the ceramide was extracted were critical to the overall sensitivity and accuracy of the assay. A standard method to stop many enzymatic assays involving lipid products is to phase separate the reaction mixture between chloroform and methanol/water, thereby denaturing the enzyme, stopping the reaction, and allowing extraction of the lipid products into the chloroform phase. In addition, for sphingolipid analysis, it is common to hydrolyze acyl–ester linkages by treatment with a mild base such as dilute sodium hydroxide. LC–MS analysis of reaction products processed in this way showed that treatment of the reaction mix with chloroform/methanol or a base such as sodium hydroxide resulted in the non-enzymatic production of ceramide. This was discovered initially when using a standard Bligh–Dyer lipid extraction to stop the reaction and extract the produced ceramide. Significant amounts of t18:0_C16:0 and t18:0_C18:0 ceramide were found that were not present in the original microsomes. To demonstrate that this is produced by a non-enzyme-catalyzed reaction, synthetic PC/LCB liposomes were made and subjected to both treatment with sodium hydroxide and the Bligh–Dyer total lipid extraction. When these samples were analyzed by LC–MS, ceramides containing both C16 and C18 fatty acids were identified (Figure 2.5). The C16 ceramide produced by this non-enzymatic reaction eluted with identical retention time to pure standard, suggesting that it is an authentic ceramide. To circumvent these problems, the reaction was stopped by the addition of MTBE/MeOH (1:1) without base hydrolysis of ester lipids and extraction of ceramides into the MTBE upper layer. Reactions stopped and extracted in this way do not generate ceramide by non-enzymatic catalysis; hence, this was the method of choice for further assays.

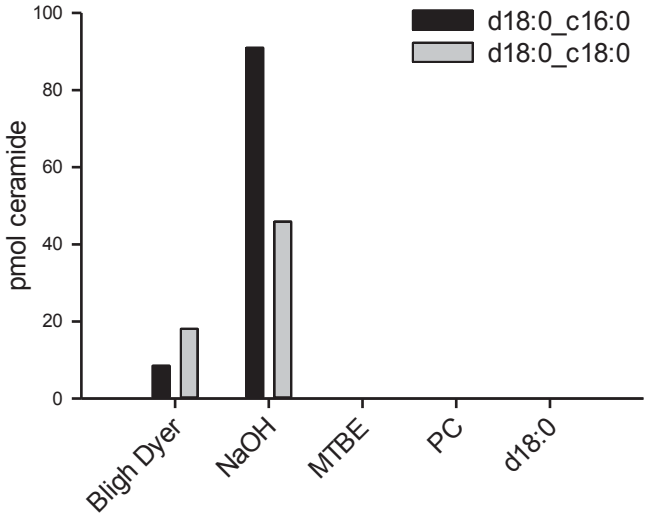

Figure 2.5 *Non-enzyme-catalyzed ceramide production*. Measurement of non-enzymatic ceramide production in synthetic liposomes of soybean PC and d18:0 LCB is shown. The graph shows ceramide levels detected in liposomes containing soybean PC and d18:0 after processing by Bligh–Dyer extraction into chloroform (Bligh–Dyer), treatment with dilute NaOH before extraction into chloroform (NaOH), or extraction into MTBE. The purified soybean PC (PC) and d18:0 standards (d18:0) used to make the liposomes were diluted straight into LC–MS sample buffer to demonstrate the lack of ceramide prior to processing.

2.2.3 ENZYME LINEARITY WITH RESPECT TO TIME AND PROTEIN CONCENTRATION

To assess the suitability of the optimized ceramide synthase assay, reactions were run with varying amounts of microsomal protein. For these assays, the substrates chosen were t18:0 LCB and 24:0 acyl-CoA (lignoceroyl-CoA). These substrates were chosen based on the presence of t18:0_C24:0 ceramide in S. cerevisiae and the solubility of the lignoceroyl-CoA substrate. The assay was linear with respect to microsomal protein up to a maximum of 10 µg (Figure 2.6A). In addition, the accumulation of ceramide was found

to be linear with respect to time up to the maximum tested time of 60 min (Figure 2.6B). All subsequent assays were run with 10 µg of protein for 30 min.

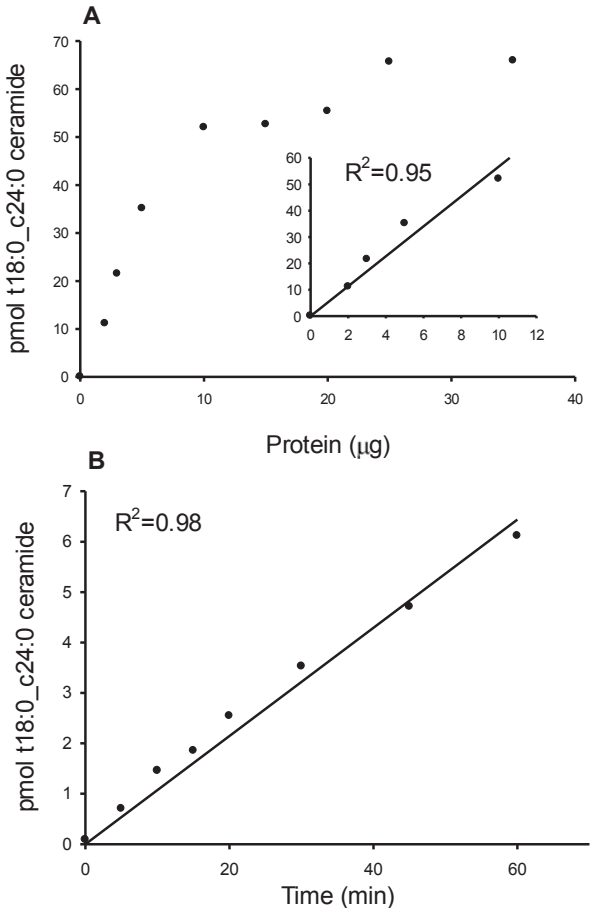

Figure 2.6 *Linearity of assay with respect to protein and time*. (A) To determine the range of proteins able to maintain linearity, assays were performed with 15 µM t18:0 LCB, 50 µM 24:0 CoA, and 10 µM BSA with increasing amounts of microsomal protein for 30 min. (B) On determination of protein concentration, assays were run for 0 to 60 min to determine linearity with respect to time. All assays were run with 10 µM protein, 15 µM t18:0 LCB, 50 µM 24:0 CoA, and 10 µM BSA.

2.2.4 ASSAY FLEXIBILITY WITH RESPECT TO SUBSTRATE

To demonstrate the flexibility of the assay with regard to substrate, different LCBs and acyl-CoAs were used to measure ceramide synthase activity. Because not all LCB substrates are commercially available, C20-phytosphingosine (t20:0) was purified from yeast. Ceramide synthase activity was measured using t20:0, C20-dihydrosphingosine (d20:0), t18:0, and d18:0 LCBs as well as 16:0, 18:0, 20:0, 22:0, 22:1, 24:0, 24:1, and 26:0 acyl- CoAs. A strong preference for t20:0 LCB and 20:0, 22:0, and 24:0 CoAs was observed (Figure 2.7), in agreement with previously published data on S. cerevisiae ceramide synthase activity that demonstrated a preference for very-long-chain acyl-CoAs with moderate activity toward long-chain acyl-CoAs (Vallée and Riezman 2005). It is also consistent with the large amount of t20:0 sphingolipids in the ceramide profile.

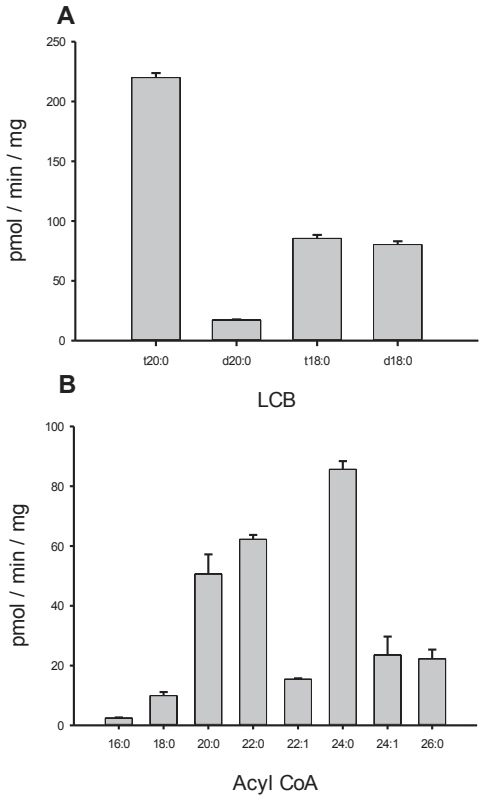

Figure 2.7 *Detection of ceramide synthase activity with a variety of LCB and acyl-CoA substrates*. Ceramide synthase activity in yeast microsomes using LCBs commonly found in yeast sphingolipids (A) and a variety of commercially available saturated and unsaturated acyl-CoAs (B) is shown. All assays contained 10 lM protein, 15 lM t18:0 LCB, 50 lM acyl-CoA, and 10 lM BSA and were incubated for 30 min. Data represent means ± standard errors (n = 3).

2.3. DISCUSSION

Sphingolipid metabolism and ceramide in particular have been the topic of intense research during recent years due to their recognized role in many cellular and pathological processes. Ceramide synthase is of particular interest because it is the enzyme responsible for the synthesis of ceramide and introduction of the acyl-chain diversity present in sphingolipid structure. Characterizing the biochemical properties of distinct ceramide synthase isoforms is a crucial step toward understanding the function of this diversity; however, most ceramide synthase assays developed to date have focused

on the use of the mammalian enzymes and substrates. This is a significant limitation for research in non-mammalian systems where there is substantial diversity of substrates for ceramide synthase, from 4-hydroxysphingosines (phytosphingosines) in plants and fungi to C17 branched-chain sphingosines in nematodes (Mosbech et al. 2013) and C14 and C16 sphingosines in flies (Acharya and Acharya 2005). This makes LC–MS the obvious choice for monitoring the products of the assay because it can be tuned to any combination of substrates.

The major disadvantage of using LC–MS to monitor reaction products is that it does not discriminate between ceramide generated during the reaction and ceramide present in membranes before the reaction has started. This can reduce the sensitivity of the detection method if significant amounts of free ceramide are already present in the microsomes. LC–MS will also detect ceramide produced by enzyme activity using endogenous LCBs, hence the need for a no-LCB control in measuring background levels of ceramide and ceramide synthase activity. Interestingly, LC–MS may also detect ceramide produced as a result of non-enzymatic synthesis (Ullman and Radin 1972). Using what are regarded as standard methods in the field, production of C16 and C18 ceramide was detected by non-enzyme-catalyzed reactions using either dilute sodium hydroxide or simple extraction into chloroform when performed in the presence of membrane lipids such as phosphatidylcholine. The compound produced in this way had the same retention time and mass transition as authentic ceramide, suggesting that it is bona fide ceramide produced by non-enzymatic acyl-migration from ester lipids (Van Overloop et al. 2005). Fortunately, this non-enzymatic contaminant is easily avoided by

extracting into an alternative solvent and skipping the base hydrolysis step, which is not needed for LC–MS analysis.

Using previously described optimal conditions for the assay of mammalian ceramide synthase as a starting point, criteria for the assay of ceramide synthase in yeast microsomes were established. These included parameters for the concentration of BSA, which has a critical and complex interaction with the LCB and acyl-CoA substrates. With too little BSA, the detergent effect of the acyl-CoA will inhibit the reaction (Richards et al. 1990). With too much BSA, the reaction will again be inhibited, potentially due to lower effective concentration of acyl-CoA in solution or due to competition for binding with the LCB substrate. Either way, the optimal concentrations of BSA and acyl-CoA in the reaction were found to be 10 and 50 μM, respectively, which are close to the 1:3 to 1:4 ratio described previously (Hirschberg et al. 1993).

The significant advantage and reason for creating the LC–MS method described here is that it can be tailored to any combination of LCB and fatty acid substrates. Plants, for example, synthesize up to 10 different LCBs in their sphingolipids, and this method should enable all of these to be used as substrates with any combination of acyl-CoAs to fully characterize the substrate specificity of plant ceramide synthases.

In summary, the assay described here is a rapid way to accurately measure ceramide synthase activity in vitro that has the potential to expand to different systems, including the use of complemented ceramide synthase yeast mutants and non-genetically modified microsomes from a variety of possible organisms. This will allow for the characterization of ceramide synthases from previously uncharacterized organisms,

which in turn may shed further light on the structural basis for ceramide synthase substrate specificity and enzyme regulation.

2.4 EXPERIMENTAL

All chemicals, unless otherwise indicated, were purchased from Sigma–Aldrich (St. Louis, MO, USA). Acyl-CoAs and lipid standards were purchased from Avanti Polar Lipids (Alabaster, AL, USA). LCBs were purchased from Matreya (Pleasant Gap, PA, USA). Solvents were OmniSolv grade from EMD Millipore (Billerica, MA, USA) unless otherwise noted. Chloroform (ethanol stabilized) was obtained from Thermo Fisher Scientific (Rockford, IL, USA).

2.4.1 PURIFICATION OF LCB SUBSTRATE FROM S. CEREVISIAE

LCBs were hydrolyzed from 1 g of lyophilized yeast as described previously (Markham et al. 2006). After hydrolysis, total LCBs were separated from fatty acids by weak cation exchange solid-phase extraction (Supelclean LC-WCX SPE, Sigma–Aldrich). The cartridge was equilibrated with 4 ml of 0.5 N acetic acid in methanol followed by 7 ml of methanol, and the LCB sample was applied in 4 ml of diethyl ether/acetic acid (98:5, v/v). The cartridge was washed with 10 ml of chloroform/methanol (3:1) to remove all traces of fatty acids, and the bound LCBs were eluted with 4 ml of 1 N acetic acid in methanol. Individual LCBs were purified by semi-preparative, reverse-phase high-performance liquid chromatography (HPLC) on a Zorbax XDB C18 column (9.4 250 mm; Agilent Technologies, Santa Clara, CA, USA) using a Shimadzu Prominence HPLC device and an FRC-10A fraction collector. LCBs were separated by a binary gradient of buffer A (10 mM ammonium acetate and 20% methanol, pH 7.0) and buffer B (methanol) at a flow rate of 1.5 ml/min and a column

temperature of 30 °C with a gradient as described previously (Markham and Jaworski 2007). Fractions containing the relevant LCBs were identified by mass spectrometry, pooled, dried under nitrogen, and quantified by *o*-phthalaldehyde derivatization as described previously (Markham et al. 2006).

2.4.2 MICROSOME ISOLATION

S. cerevisiae strain BY4741 was maintained on YPD Broth (RPI Y20090) agar plates. A liquid batch culture was grown to OD600 of 2, and the cells were harvested by centrifugation at 8000g for 10 min. The resulting pellet was washed once with 40 ml of sterile water and harvested by centrifugation as before. The washed cells were resuspended to a final concentration of OD600 = 200/ml in TNE buffer (50 mM Tris–HCl [pH 7.5], 150 mM NaCl, 5 mM ethylenediaminetetraacetic acid, and 1 mM phenylmethylsulfonyl fluoride) containing Protease Inhibitor Cocktail and 1 µl/ml TNE buffer. Cells were lysed at 4 °C by vortexing with 0.5 mm zirconia/ silica beads (BioSpec Products, Bartlesville, OK, USA) for 1 min followed by 1 min on ice, repeated 10 times. Cell debris was removed by centrifugation at 4 °C for 10 min at 8000g. The supernatant was removed and centrifuged a second time as before. The supernatant was removed and centrifuged at 100,000g for 1 h at 4 °C, and the pellet was resuspended by gentle pipetting in reaction buffer (20 mM potassium phosphate [pH 7.5] and 250 mM sorbitol). The microsomes were harvested again by centrifugation at 100,000g for 1 h at 4 °C, followed by final resuspension in reaction buffer using a Dounce homogenizer. Microsomes were snapfrozen in liquid nitrogen and stored at -80 °C. Protein concentration was measured using the Pierce BCA (bicinchoninic acid) Protein Assay (Thermo Fisher Scientific) with bovine serum albumin (BSA) used as a standard curve.

2.4.3 BSA/LCB COMPLEX FORMATION

Fatty acid-free BSA (Sigma–Aldrich A7030) and LCB were used to create BSA/LCB complexes. Stock solutions of BSA were made in reaction buffer (w/v), and the LCB was dissolved in 2:1 (v/v) ethanol/dimethyl sulfoxide (DMSO) to a final concentration of 2 mM. The complexes were made with a final BSA concentration of 100 μM and varying amounts of LCB not exceeding 150 μM. An additional 2:1 (v/v) ethanol/DMSO was added as necessary to standardize all solutions at 10% by volume 2:1 (v/v) ethanol/ DMSO. The final concentration of the BSA/LCB complex was a 10solution for direct addition to the ceramide synthase assay.

2.4.4 LCB EQUILIBRATION INTO MICROSOMES

First, 10LCB/BSA complexes were made as described above. In addition, a BSA-free 10LCB solution was made exactly as described above but omitting the BSA. Then, 10 μl of 15 μM LCB solution was added to an 8-ml glass tube with a Teflon-lined screw cap containing 20 mM potassium phosphate (pH 7.5), 250 mM sorbitol, and microsomes containing 10 μg of protein in a final volume of 100 μl and incubated in a digital heating block at 30 °C for 10 min. Reactions were then moved to an ultracentrifuge tube and spun at 100,000g for 1 h. The supernatant was removed, and LCBs were extracted by the addition of 750 μl 1:1 (v/v) methyltert- butyl-ether (MTBE)/methanol (MeOH) followed by the addition of 5 nmol of d17:1 LCB as an internal standard, 850 μl of MTBE, and 312 μl of 100 mM ammonium hydroxide. The MTBE layer was removed and dried under a stream of air at 60 °C. LCBs were resuspended in 100 μl of tetrahydrofuran/methanol/water (2:1:2, v/v/v) containing 0.1% formic acid and analyzed by LC–MS.

2.4.5 CERAMIDE SYNTHASE IN VITRO ASSAY

The assay was performed in an 8-ml glass tube with a Teflon lined screw cap and a final volume of 100 µl. The reaction mix contained a final concentration of 20 mM potassium phosphate (pH 7.5), 250 mM sorbitol, 50 µM acyl-CoA, 10 µM BSA, up to 15 µM LCB, and up to 10 µg microsomal protein. All components for the assay, except the microsomal protein, were mixed with a pipet tip and equilibrated for 10 min at 30 °C in a digital heating block. The reaction was started by the addition of the microsomal protein with gentle mixing using a pipet tip and incubated for 30 min. To stop the reaction, 750 µl of 1:1 (v/v) MTBE/MeOHwas added and mixed with a vortex mixer. Then, 50 pmol of C12 ceramide was added as an internal standard. Phase separation was induced by the addition of 850 µl of MTBE and 312 µl of water. The MTBE upper layer was removed to a clean tube and dried under a stream of air at 60 °C.

2.4.6 QUANTIFICATION BY LC–TANDEM MS

The sample was dissolved in 100 µl of tetrahydrofuran/methanol/ water (2:1:2, v/v/v) containing 0.1% formic acid. Sphingolipids were analyzed using a Shimadzu Prominence HPLC device coupled to a 4000 QTRAP mass spectrometer (ABSciex, Framingham, MA, USA) as described previously (Markham and Jaworski 2007). A reverse-phase 100-mm Acclaim C18 HPLC column (Thermo Scientific) was eluted by a binary gradient formed by buffer A (tetrahydrofuran/methanol/5 mM ammonium formate [3:2:5, v/v/v] + 0.1% formic acid) and buffer B (tetrahydrofuran/methanol/5 mM ammonium formate [7:2:1, v/v/ v] + 0.1% formic acid) with a flow rate of 1.00 ml/min and a column temperature of 40 °C. The starting concentrations were equilibrated for 1 min, with the gradient starting on inline switching of the sample in the sample loop with

an injection volume of 10 µl. The gradient started with 60% B and increased to 85% B by 5.00 min. At 5.01 min, the percentage B was increased to 100% and run until 6.00 min to ensure complete elution of any remaining compounds. Masses were monitored from 1.50 to 6.00 min. Data was analyzed using ABSciex MultiQuant software.

2.4.7 LCB/PC LIPOSOME FORMATION

A phosphatidylcholine (PC)/LCB liposome mixture was made using soybean phosphatidylcholine to contain 2 mM PC and 30 µM d18:0 LCB. The lipids were dried under nitrogen at 60 °C for 1 h, followed by resuspension in reaction buffer by gentle sonication using a sonicating water bath. The resuspended lipids were hydrated on ice for 1 h before liposome formation using a Mini- Extruder (Avanti Polar Lipids) by passage through a 0.1-µM Nuclepore Track-Etch membrane (GE Life Sciences, Pittsburgh, PA, USA). The liposome sample was pushed through the membrane a total of 15 times before being stored at 4 °C.

2.4.8 NON-ENZYME-CATALYZED CERAMIDE PRODUCTION

DHS/PC liposomes (100 µl) were treated in one of the following ways: (i) Bligh–Dyer total lipid extraction, 500 µl of 2:1 (v/v) methanol/chloroform followed by 50 pmol of internal standard, 166 µl of chloroform, and 300 µl of water, where the chloroform layer was removed and dried at 60 °C under a stream of air; (ii) 750 µl of 1:1 (v/v) MTBE/MeOH followed by 50 pmol of internal standard, 850 µl of MTBE, and 312 µl of water, where the MTBE layer was removed and dried at 60 °C under a stream of air; (iii) 1 ml of 1 M sodium hydroxide followed by 50 pmol of internal standard, with sample being incubated at room temperature for 30 min followed by extraction with 1 ml of chloroform, where the chloroform layer was removed and washed with 1 ml of water

followed by the chloroform layer being dried at 60 °C under a stream of air. All samples were dissolved in sample solvent and analyzed by LC–MS for the presence of ceramide as before. In addition to the above samples, 1 µl of 25 mg/ml soy PC was diluted into 1 ml of sample buffer and 1 µl of 2 mg/ml d18:0 was diluted into 1 ml of sample buffer and used as controls.

2.5 REFERENCES

Acharya U, Acharya JK (2005) Enzymes of sphingolipid metabolism in Drosophila melanogaster. Cell Mol Life Sci 62 (2):128-142.

Alden KP, Dhondt-Cordelier S, McDonald KL, Reape TJ, Ng CK, McCabe PF, Leaver CJ (2011) Sphingolipid long chain base phosphates can regulate apoptotic-like programmed cell death in plants. Biochem Bioph Res Commun 410 (3):574-580.

Ali M, Fritsch J, Zigdon H, Pewzner-Jung Y, Schutze S, Futerman AH (2013) Altering the sphingolipid acyl chain composition prevents LPS/GLN-mediated hepatic failure in mice by disrupting TNFR1 internalization. Cell Death Dis 4.

Aronova S, Wedaman K, Aronov PA, Fontes K, Ramos K, Hammock BD, Powers T (2008) Regulation of ceramide biosynthesis by TOR complex 2. Cell Metab 7 (2):148-158.

Bauer R, Voelzmann A, Breiden B, Schepers U, Farwanah H, Hahn I, Eckardt F, Sandhoff K, Hoch M (2009) Schlank, a member of the ceramide synthase family controls growth and body fat in Drosophila. Embo J 28 (23):3706-3716.

Berdyshev EV, Gorshkova I, Skobeleva A, Bittman R, Lu XQ, Dudek SM, Mirzapoiazova T, Garcia JGN, Natarajan V (2009) FTY720 Inhibits Ceramide Synthases and Up-regulates Dihydrosphingosine 1-Phosphate Formation in Human Lung Endothelial Cells. J Biol Chem 284 (9):5467-5477.

Breslow DK, Weissman JS (2010) Membranes in balance: mechanisms of sphingolipid homeostasis. Mol Cell 40 (2):267-279.

Chen M, Markham JE, Dietrich CR, Jaworski JG, Cahoon EB (2008) Sphingolipid long-chain base hydroxylation is important for growth and regulation of sphingolipid content and composition in Arabidopsis. Plant Cell 20 (7):1862-1878.

Cuvillier O, Pirianov G, Kleuser B, Vanek PG, Coso OA, Gutkind JS, Spiegel S (1996) Suppression of ceramide-mediated programmed cell death by sphingosine-1-phosphate. Nature 381 (6585):800-803.

Dickson RC, Nagiec EE, Skrzypek M, Tillman P, Wells GB, Lester RL (1997) Sphingolipids are potential heat stress signals in Saccharomyces. J Biol Chem 272 (48):30196-30200.

Hannun YA, Luberto C (2000) Ceramide in the eukaryotic stress response. Trends Cell Biol 10 (2):73-80.

Hartmann D, Wegner MS, Wanger RA, Ferreiros N, Schreiber Y, Lucks J, Schiffmann S, Geisslinger G, Grosch S (2013) The equilibrium between long and very long chain ceramides is important for the fate of the cell and can be influenced by co-expression of CerS. Int J Biochem Cell Biol 45 (7):1195-1203.

Hirschberg K, Rodger J, Futerman AH (1993) The Long-Chain Sphingoid Base of Sphingolipids Is Acylated at the Cytosolic Surface of the Endoplasmic-Reticulum in Rat-Liver. Biochem J 290:751-757.

Kim HJ, Qiao Q, Toop HD, Morris JC, Don AS (2012) A fluorescent assay for ceramide synthase activity. J Lipid Res 53 (8):1701-1707.

Kobayashi SD, Nagiec MM (2003) Ceramide/long-chain base phosphate rheostat in Saccharomyces cerevisiae: Regulation of ceramide synthesis by Elo3p and Cka2p. Eukaryot Cell 2 (2):284-294.

Lahiri S, Lee H, Mesicek J, Fuks Z, Haimovitz-Friedman A, Kolesnick RN, Futerman AH (2007) Kinetic characterization of mammalian ceramide synthases: Determination of K-m values towards sphinganine. FEBs Lett 581 (27):5289-5294.

Laviad EL, Albee L, Pankova-Kholmyansky I, Epstein S, Park H, Merrill AH, Jr., Futerman AH (2008) Characterization of ceramide synthase 2: tissue distribution, substrate specificity, and inhibition by sphingosine 1-phosphate. J Biol Chem 283 (9):5677-5684.

Levy M, Futerman AH (2010) Mammalian Ceramide Synthases. Iubmb Life 62 (5):347-356.

Maceyka M, Payne SG, Milstien S, Spiegel S (2002) Sphingosine kinase, sphingosine-1-phosphate, and apoptosis. Biochim Biophys Acta 1585 (2-3):193-201.

Markham JE, Jaworski JG (2007) Rapid measurement of sphingolipids from Arabidopsis thaliana by reversed-phase high-performance liquid chromatography coupled to electrospray ionization tandem mass spectrometry. Rapid Commun Mass Spectrom 21 (7):1304-1314.

Markham JE, Li J, Cahoon EB, Jaworski JG (2006) Separation and identification of major plant sphingolipid classes from leaves. J Biol Chem 281 (32):22684-22694.

Markham JE, Molino D, Gissot L, Bellec Y, Hematy K, Marion J, Belcram K, Palauqui JC, Satiat-Jeunemaitre B, Faure JD (2011) Sphingolipids containing very-long-chain fatty acids define a secretory pathway for specific polar plasma membrane protein targeting in Arabidopsis. Plant Cell 23 (6):2362-2378.

Mizutani Y, Kihara A, Igarashi Y (2005) Mammalian Lass6 and its related family members regulate synthesis of specific ceramides. Biochem J 390:263-271.

Mizutani Y, Kihara A, Igarashi Y (2006) LASS3 (longevity assurance homologue 3) is a mainly testis-specific (dihydro)ceramide synthase with relatively broad substrate specificity. Biochem J 398:531-538.

Mosbech MB, Kruse R, Harvald EB, Olsen ASB, Gallego SF, Hannibal-Bach HK, Ejsing CS, Faergeman NJ (2013) Functional Loss of Two Ceramide Synthases Elicits Autophagy-Dependent Lifespan Extension in C. elegans. PLoS One 8 (7).

Mullen TD, Spassieva S, Jenkins RW, Kitatani K, Bielawski J, Hannun YA, Obeid LM (2011) Selective knockdown of ceramide synthases reveals complex interregulation of sphingolipid metabolism. J Lipid Res 52 (1):68-77.

Narimatsu S, Soeda S, Tanaka T, Kishimoto Y (1986) Solubilization and Partial Characterization of Fatty Acyl-Coa-Sphingosine Acyltransferase (Ceramide Synthetase) from Rat-Liver and Brain. Biochim Biophys Acta 877 (3):334-341.

Pewzner-Jung Y, Ben-Dor S, Futerman AH (2006) When do lasses (longevity assurance genes) become CerS (ceramide synthases)? Insights into the regulation of ceramide synthesis. J Biol Chem 281 (35):25001-25005.

Richards EW, Hamm MW, Fletcher JE, Otto DA (1990) The Binding of Palmitoyl-Coa to Bovine Serum-Albumin. Biochim Biophys Acta 1044 (3):361-367.

Riebeling C, Allegood JC, Wang E, Merrill AH, Futerman AH (2003) Two mammalian longevity assurance gene (LAG1) family members, trh1 and trh4, regulate dihydroceramide synthesis using different fatty acyl-CoA donors. J Biol Chem 278 (44):43452-43459.

Shimeno H, Soeda S, Sakamoto M, Kouchi T, Kowakame T, Kihara T (1998) Partial purification and characterization of sphingosine N-acyltransferase (ceramide synthase) from bovine liver mitochondrion-rich fraction. Lipids 33 (6):601-605.
Spassieva S, Seo JG, Jiang JC, Bielawski J, Alvarez-Vasquez F, Jazwinski SM, Hannun YA, Obeid LM (2006) Necessary role for the Lag1p motif in (dihydro)ceramide synthase activity. J Biol Chem 281 (45):33931-33938.
Townley HE, McDonald K, Jenkins GI, Knight MR, Leaver CJ (2005) Ceramides induce programmed cell death in Arabidopsis cells in a calcium-dependent manner. Biol Chem 386 (2):161-166.
Ullman MD, Radin NS (1972) Enzymatic Formation of Hydroxy Ceramides and Comparison with Enzymes Forming Nonhydroxy Ceramides. Arch Biochem Biophys 152 (2):767-&.
Vallée B, Riezman H (2005) Lip1p: a novel subunit of acyl-CoA ceramide synthase. EMBO 24 (4):730-741.
Van Overloop H, Van der Hoeven G, Van Veldhoven PP (2005) N-Acyl migration in ceramides. J Lipid Res 46 (4):812-816.
Venkataraman K, Riebeling C, Bodennec J, Riezman H, Allegood JC, Sullards MC, Merrill AH, Jr., Futerman AH (2002) Upstream of growth and differentiation factor 1 (uog1), a mammalian homolog of the yeast longevity assurance gene 1 (LAG1), regulates N-stearoyl-sphinganine (C18-(dihydro)ceramide) synthesis in a fumonisin B1-independent manner in mammalian cells. J Biol Chem 277 (38):35642-35649.
Wang E, Merrill Jr AH (2000) Ceramide synthase. In: Alfred H. Merrill JYAH (ed) Methods in Enzymology, vol Volume 311. Academic Press, pp 15-21
Wang H, Li J, Bostock RM, Gilchrist DG (1996) Apoptosis: A functional paradigm for programmed plant cell death induced by a host-selective phytotoxin and invoked during development. Plant Cell 8 (3):375-391.

CHAPTER 3

SUBSTRATE SPECIFICITY, KINETIC PROPERTIES AND INHIBITION BY FUMONISIN B_1 OF CERAMIDE SYNTHASE ISOFORMS FROM ARABIDOPSIS

Note: This chapter is to be published. The authors will be Kyle D. Luttgeharm, Edgar B. Cahoon and Jonathan E. Markham

3.1 INTRODUCTION

Sphingolipids are a unique subset of membrane lipids that are synthesized in the ER by a pathway largely distinct from the rest of lipid metabolism (Li-Beisson et al. 2013). Sphingolipids consist of a sphingoid long-chain base (LCB) linked by an amide bond to a fatty acid of varying chain-length, thereby forming ceramide (Figure 3.1); more complex glyco- and phospho-sphingolipids are formed by O-linkage to the LCB of ceramide (Markham et al. 2013). In plants, a wide variety of LCB structures and fatty acids results in several hundred potential sphingolipid structures. The structure of the formed sphingolipids is critical to their function as both structural and signaling molecules (Townley et al. 2005; Hannun and Luberto 2000; Dickson et al. 1997; Wang et al. 1996), hence control over the synthesis of specific structures is essential to proper sphingolipid function. Ceramides and their derivatives can have a profound impact on the cell in both structural and signaling fashions. Sphingolipids have been hypothesized to play a major role in protein trafficking and the formation of lipid microdomains or lipid rafts (Carmona-Salazar et al. 2011; Cacas et al. 2012; Mongrand et al. 2004), as well as being known to control major cell events such as programmed cell death controlled by the ratio of phosphorylated LCBs to free ceramides (Maceyka et al. 2002; Alden et al. 2011; Cuvillier et al. 1996). Sphingolipids have also been shown to have roles in defense/disease resistance with ceramides acting to promote programed cell death (Bi et al. 2014; Wu et al. 2015; Liang et al. 2003).

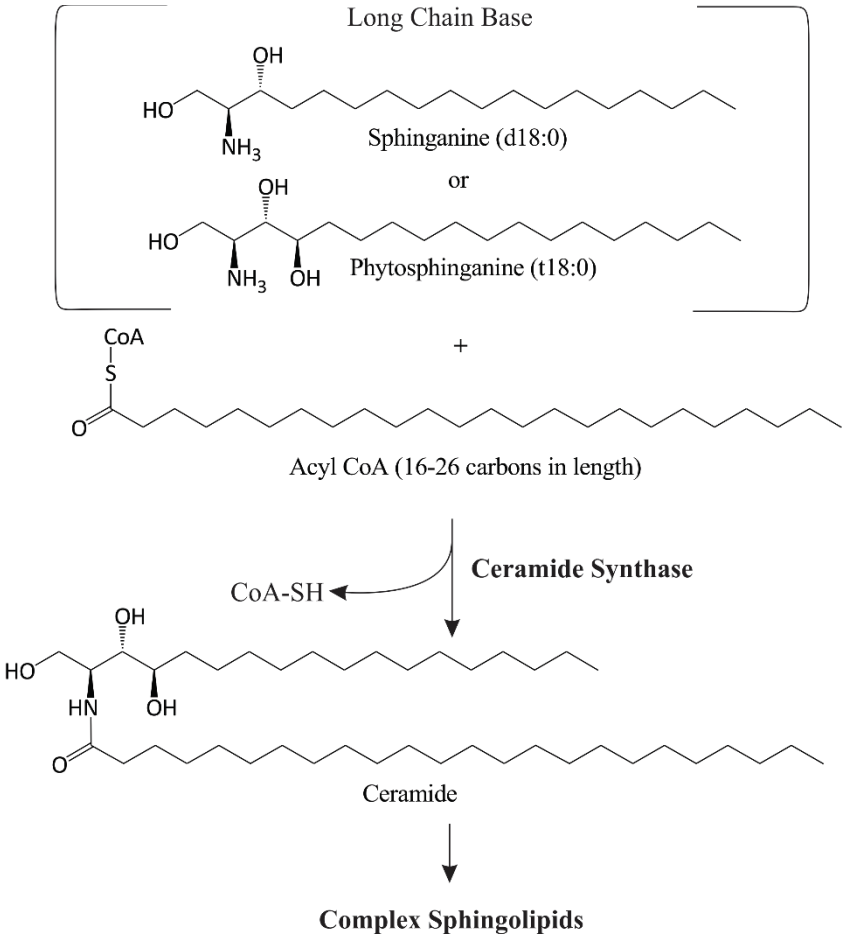

Figure 3.1 *Structural reaction for the synthesis of ceramide.* The synthesis of ceramide involves the formation of an amide bond between a LCB and an acyl-CoA substrates. The ceramide can undergo various modifications to the LCB and fatty acid as well as the addition of various head groups to at the C1 position on the LCB.

Ceramides are synthesized by the enzyme ceramide synthase (also known as sphingosine N-acyltransferase, E.C. 2.3.1.24) which forms the amide bond between the LCB and fatty acid. LCBs are usually 18 carbon acyl-chains with an amide group at C2, hydroxyl groups at C1, C3 and additionally in plants at C4 (Figure 3.1). Both these dihydroxy (d18) and trihydroxy (t18) carbon LCBs may be modified by desaturated at C8 to produce d18:1(8) or t18:1(8) while d18 LCBs may also be desaturated at C4 to make sphingosine d18:1(4). The fatty acid component of ceramide is 16-26 carbons in length (c16-c26) and is frequently hydroxylated at C2 to produce

hydroxyl-fatty acids (h16-h26). As the composition of ceramide greatly influences the identity of the final complex sphingolipid formed, the choice of LCB and fatty acid used to make ceramide is a key branching point in sphingolipid metabolism (Chen et al. 2008; Markham and Jaworski 2007). In *Arabidopsis thaliana*, three distinct ceramide synthases have been identified denoted *LOH1*, *LOH2*, and *LOH3* (Ternes et al. 2011; Markham et al. 2011). These ceramide synthases can be divided into two distinct groups based on sequence alignment and function that appears to be a conserved feature of ceramide synthases within the plant kingdom (Ternes et al. 2011). Studies with knockout mutants, *in planta* homologous overexpression, and heterologous expression in yeast led to the conclusion that LOH1 and LOH3 are responsible for the synthesis of ceramides with trihydroxy LCBs and very long chain fatty acids (VLCFA) while LOH2 is required for the synthesis of ceramides with dihydroxy LCB and C16 FAs (Ternes et al. 2011; Chen et al. 2008; Markham et al. 2011; Luttgeharm et al. 2015b). While the exact substrate preferences of the Arabidopsis ceramide synthases have not been definitely shown, a high degree of substrate specificity would be consistent with data from other organisms. For instance, humans contain six ceramide synthases (CerS) each with different preference for the acyl-CoA substrate (Venkataraman et al. 2002; Laviad et al. 2008; Mizutani et al. 2006; Riebeling et al. 2003; Mizutani et al. 2005).

Previously it has been shown that the VLCFA composition of sphingolipids is critical for plant growth and development (Markham et al. 2011; Bach et al. 2011; Zheng et al. 2005). Knockdown of *PAS2*, an acyl-CoA desaturase involved in fatty acid elongation, not only results in a significant decrease in the VLCFA content of sphingolipids, but also disrupts proper cell plate formation during cell division leading to malformed plant structures (Bach et al. 2011; Bach et al. 2008). The importance of VLCFA sphingolipids is further corroborated by knockouts of *PAS1* (required for VLCFA synthesis) and *PAS3* (acetyl-CoA carboxylase required for VLCFA synthesis) resulting in decreased levels of VLCFA sphingolipids and plant growth defects (Roudier et al. 2010; Baud et al. 2004). Indeed, complete removal of VLCFA-containing

sphingolipids by knockout of both *LOH1* and *LOH3* completely inhibits development past the embryo stage. (Markham et al. 2011). The LCB component of sphingolipids has also been shown to be critical for normal plant growth and development. In particular, knockout of the LCB hydroxylases *SBH1* and *SBH2* results in accumulation of sphingolipid, stunted growth and spontaneous cell death (Chen et al. 2008). The accumulated sphingolipid in these plants is made up entirely of compounds with C16 fatty acids (Chen et al. 2008). Since *loh1*/*loh3* mutant plants are only able to synthesize sphingolipids containing C16 fatty acids, it is hypothesized that LOH2 uses dihydroxy LCBs and C16 fatty acyl-CoAs exclusively (Markham et al. 2011). Certain LCB/FA combinations also seem to target newly synthesized ceramides for different complex sphingolipids. In particular, dihydroxy LCB/C16 FA ceramides have been proposed to be the preferred substrate for glucosylceramide synthesis (Markham et al. 2006). This is especially evident when the LCB contains double bonds in the Δ4 and Δ8 positions (d18:2) (Michaelson et al. 2009; Luttgeharm et al. 2015c). Having multiple ceramide synthase isoforms, each with a specific substrate preference, would allow plants to maintain greater control over the composition of synthesized ceramides and thus mature sphingolipids.

Ceramide synthase is also the target for a class of fungal toxins called sphinganine-analog mycotoxins (SAMs) such as fumonisin B_1 and AAL-toxin (Abbas et al. 1994; Stone et al. 2000). These refer to a class of compounds that are thought to inhibit ceramide synthases in a competitive manner by mimicking the structure of the LCB, however no enzymatic studies have been done to confirm this. This conclusion is based upon a large increase in free LCB levels observed after treatment with SAMs (Stone et al. 2000; Kimberlin et al. 2013; Luttgeharm et al. 2015b). Regardless of mode of inhibition, it has been repeatedly shown that treatment with SAMs induces programmed cell death (Wang et al. 1996; Abbas et al. 1994; Stone et al. 2000; Kimberlin et al. 2013). Disruption of ceramide synthase genes in tomato (Abbas et al. 1994) and Arabidopsis (Markham et al. 2011) increases sensitivity to SAMs while overexpression of LOH2 or LOH3 has been shown to impart resistance with LOH1 overexpression resulting in no change

(Luttgeharm et al. 2015b)(Chapter 4). The precise mechanism by which ceramide synthase mediates resistance to SAMs is unknown. Total sphingolipid profiling of fumonisin B_1 treated WT (Col-0) Arabidopsis revealed a significant increase in C16-ceramide containing sphingolipids (Markham et al. 2011; Luttgeharm et al. 2015b)(Chapter 4). This implies that LOH1 is the most sensitive to fumonisin B_1 with LOH2 being the most resistant *in planta.* In support of this, mutants of *LOH2* are more sensitive to the effect of SAMs (Markham et al. 2011). Although the precise mechanism of sensitivity towards SAMs remains to be discovered, changes in ceramide synthase expression positively correlate with SAMs resistance (Abbas et al. 1994; Markham et al. 2011; Luttgeharm et al. 2015b)(Chapter 4) suggesting that either particular enzymes are less sensitive to SAMs or that increased expression levels can overcome the effect of SAMs exposure.

In order to determine how each isoform of ceramide synthase contributes to the overall sphingolipid composition and resistance to SAMs, *in vitro* enzyme assays were conducted on LOH1, LOH2, and LOH3. As a result, for each isoform, distinct LCB and acyl-CoA substrate preferences were identified, as well as a binding constant and mode of fumonisin B_1 inhibition for each isoform. Through this study it was determined that LOH1, LOH2, and LOH3 each have unique substrate preferences in regards to LCB hydroxylation and desaturation status, fatty acid chain length and desaturation status, as well as different sensitivity to fumonisin B_1 inhibition.

3.2 RESULTS

3.2.1 FUNCTIONALITY OF ARABIDOPSIS CERAMIDE SYNTHASES EXPRESSED IN YEAST

Plant ceramide synthases are able to, at least partially, complement the growth defect associated with *Δlag1/Δlac1* deletion in yeast (Ternes et al. 2011; Spassieva et al. 2002). In order to characterize more fully the activity of plant ceramide synthases using this heterologous system, codon optimized versions of the Arabidopsis *LOH* cDNAs were introduced as GST-FLAG N-terminal fusions. All three constructs were expressed and complemented the growth defect in the yeast ceramide synthase mutants (Figure 3.2 A and B) indicating that the constructs produce active proteins *in vivo*. This was confirmed by analyzing sphingolipids from the three lines (Figure 3.2 C and D) which showed similar levels of inositolphosphoceramide (IPC) and ceramides to wild-type, unlike the Δ*lag1*Δ*lac1* mutant that shows reduced levels of IPC and an increase in C16 ceramides. Complementation with LOH2 led to the accumulation of C16-containing inositolphosphoceramides and ceramides indicating this isoforms preference for C16 fatty acids. Upon isolation of a microsomal membrane fraction from yeast expressing each of these constructs however, only LOH1 and LOH3 showed significant activity by an *in vitro* ceramide synthase assay (Figure 3.3A).

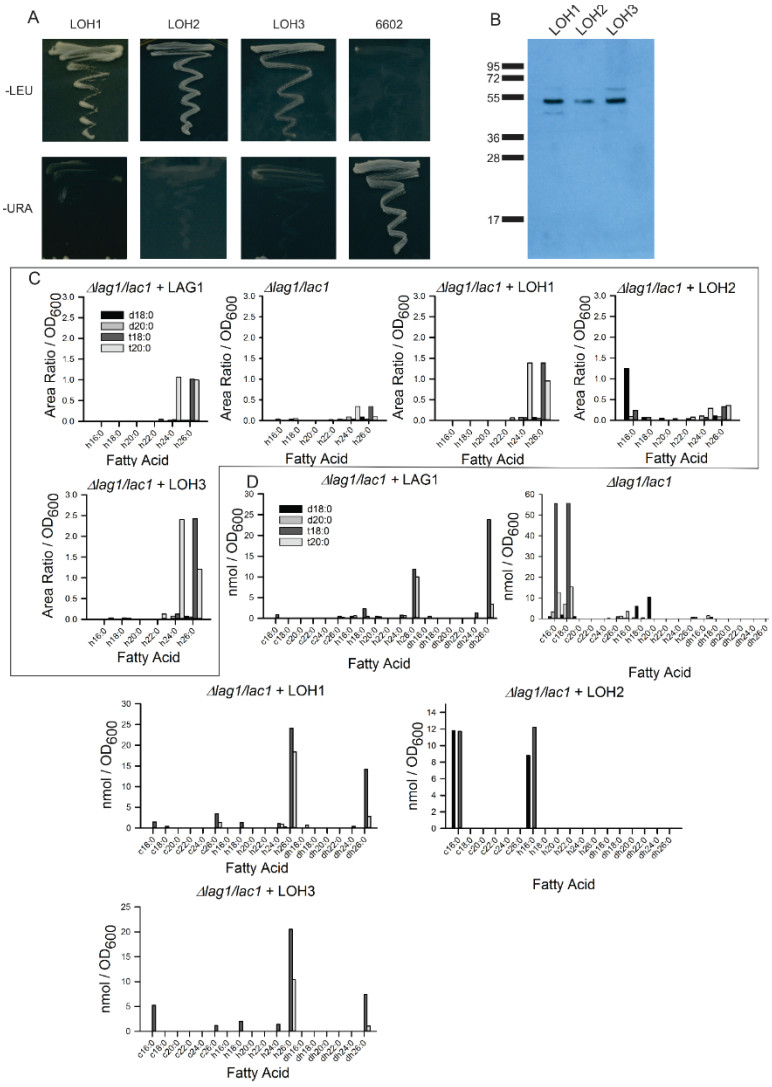

Figure 3.2 *Functional complementation of Δlag1/Δlac1 S. cerevisiae mutants with LOH1, LOH2, and LOH3.* (A) Growth of S.cerevisiae Δlag1/Δlac1 mutants containing p426GPD LOH1, 2 or 3 on minimal media. Strain 6602 contains LAG1 on a plasmid with a URA selectable marker permitting growth on CSM-uracil but not on CSM-leucine. p426GPD contains the LEU selectable marker allowing growth on media without leucine media but not on media without uracil demonstrating the loss of the LAG1-URA plasmid and complementation of the growth phenotype associated with loss of lag1 and lac1. (B) Western blot of microsomal proteins from the LOH expressing yeast strains. Heterologously expressed fusion proteins were detected with anti-FLAG antibodies. (C). Profile of Inositolphosphoceramides extracted from the LOH1, LOH2, and LOH3 complemented Δlag1/Δlac1mutant. Data shown as the ratio of the analyte peak area to Fucosylated monosialoganglioside GM1 internal standard area divided by the total number of OD_{600}

extracted. (D) Profile of ceramides extracted from the LOH1, LOH2, and LOH3 complemented Δlag1/Δlac1mutant with non-hydroxylated fatty acids denoted with a c, mono-hydroxylated fatty acids denoted with an h, and di-hydroxylated fatty acids denoted with a dh.

To overcome the inability to assay LOH2 when expressed in the heterologous yeast system, *LOH2* was over-expressed homologously in Arabidopsis plants (Figure 3.3B). Microsomes isolated from *LOH2* overexpressing plants showed high levels of C16-ceramide synthase activity compared to microsomes from wild-type plants (Figure 3.3C), indicating that *LOH2* overexpression results in accumulation of functional enzyme.

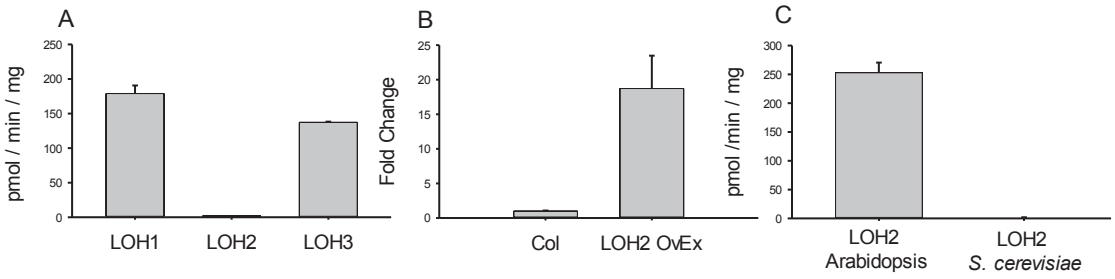

Figure 3.3 *Enzyme activity in yeast and Arabidopsis microsomes.* Results from in vitro ceramide synthase assays conducted with 15µM LCB (t18:0 for LOH1 and LOH3, d18:0 for LOH2), 50µM acyl-CoA (24:0 for LOH1 and LOH3, 16:0 for LOH2) and 10 µg yeast microsomal protein for 30 min showing; (A) activity of recombinant LOH proteins in yeast microsomes (mean ± S.E., n=3), (B) level of LOH2 overexpression in Arabidopsis thlailana and (C) activity of recombinant LOH2 protein in Arabidopsis leaf microsomes compared with yeast microsomes (mean ± S.E., n=3).

3.2.2 OPTIMIZATION OF ASSAY CONDITIONS

The assay conditions for ceramide synthase previously designed (Luttgeharm et al. 2015a)(Chapter 2) present the LCB and acyl-CoA substrates in solution, allowing for approximation to Michaelis-Menten kinetics. To identify conditions suitable for studies with the expressed LOH proteins, the assays were assessed for linearity with respect to both protein and

time. LOH1 and LOH3 microsomes were found to be linear through 25µg protein while LOH2 microsomes were found to linear through 20µg protein. (Figure 3.4). Additionally, the assay of LOH1 was linear over 60min while LOH2 and LOH3 were linear over 30min (Figure 3.4) indicating the assay provided a good estimate of initial velocity. For all future assays 10µg of microsomal protein was used and the activity was measured over a 30min period.

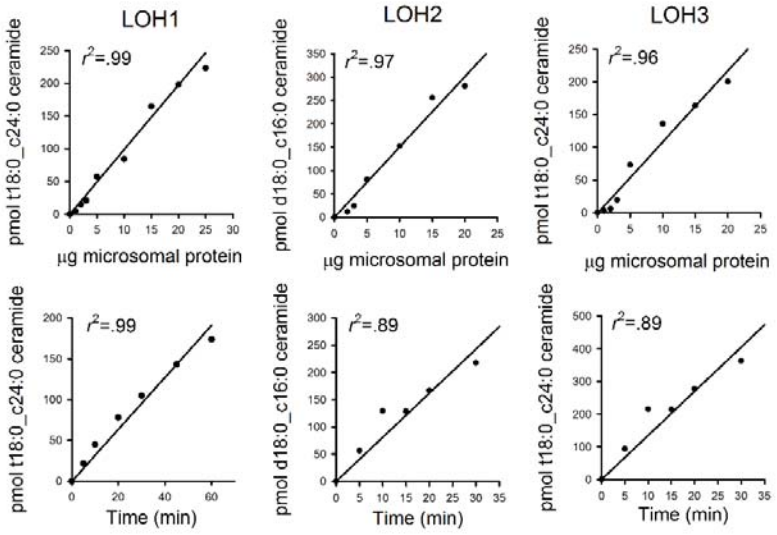

Figure 3.4 *Linearity with respect to protein and time.* Plots of ceramide synthase activity for LOH1, LOH2, and LOH3 measured after 30 min. using 15 µM LCB (t18:0 for LOH1 and LOH3, d18:0 for LOH2) and 50 µM acyl-CoA (24:0 for LOH1 and LOH3, 16:0 for LOH2), versus amount of microsomal protein added to the assay (Top). Plots of ceramide synthase activity for LOH1, LOH2, and LOH3 with 15 µM LCB (t18:0 for LOH1 and LOH3, d18:0 for LOH2), 50 µM acyl-CoA (24:0 for LOH1 and LOH3, 16:0 for LOH2), and 10 µg total microsomal protein vs assay time. A trend line was fitted to all plots by simple linear regression.

3.2.3 KINETIC PARAMETERS OF ARABIDOPSIS CERAMIDE SYNTHASES TOWARDS LCB SUBSTRATES

In plants, the primary LCB substrates for the synthesis of new sphingolipids are thought to be dihydrosphingosine (d18:0) and phytosphingosine (t18:0) (Figure 3.1). In order to identify

how these LCB substrates are used by the LOH ceramide synthase isoforms, enzyme assays were performed using increasing LCB concentrations up to a maximum of 15 µM LCB. It was found that, while LOH1 and LOH3 can use both t18:0 and d18:0 substrates (Figure 3.5A and C), they show a strong preference for the t18:0 substrate. Activity with the d18:0 substrate was minimal and insufficient to calculate any kinetic parameters. Kinetic constants for t18:0 (LOH1, V_{max}=273 ± 40 pmol/min/mg, K_m=6.9 ± 2.1 µM; LOH3, V_{max}=395 ± 120 pmol/min/mg, K_m=23 ± 10 µM) were extracted by curve fitting and parameter extraction. The opposite substrate preference was found for LOH2 which was able to use d18:0 (V_{max}=519 ± 90 pmol/min/mg, K_m=13 ± 4.0 µM) but showed almost no activity towards t18:0 (Figure 3.5B). These data already show quite clearly that the three ceramide synthase isoforms have distinct functionality. While LOH1 and LOH3 use t18:0 as their preferred substrate, the higher K_m and V_{max} of LOH3 suggest it may have a role under specific conditions of high substrates availability. LOH2 on the other hand, uses d18:0 as its preferred substrate with the highest V_{max} of any of the ceramide synthases. To verify that the different kinetic parameters extracted were not due to the different expression systems LOH1 and LOH3 were overexpressed *in planta* using previously characterized lines (Luttgeharm et al. 2015b)(Chapter 4). It was found that LOH1 could use t18:0 (V_{max}=146 ± 20 pmol/min/mg, K_m=4.0 ± 1.6 µM) but not d18:0 (Appendix A). The student's t-test was used to compare the K_m's from each system and was found to not be statically significant (P=0.54). LOH3 was unable to be assayed in plant overexpression microsomes for unknown reasons. All future assays were done using the preferred LCB.

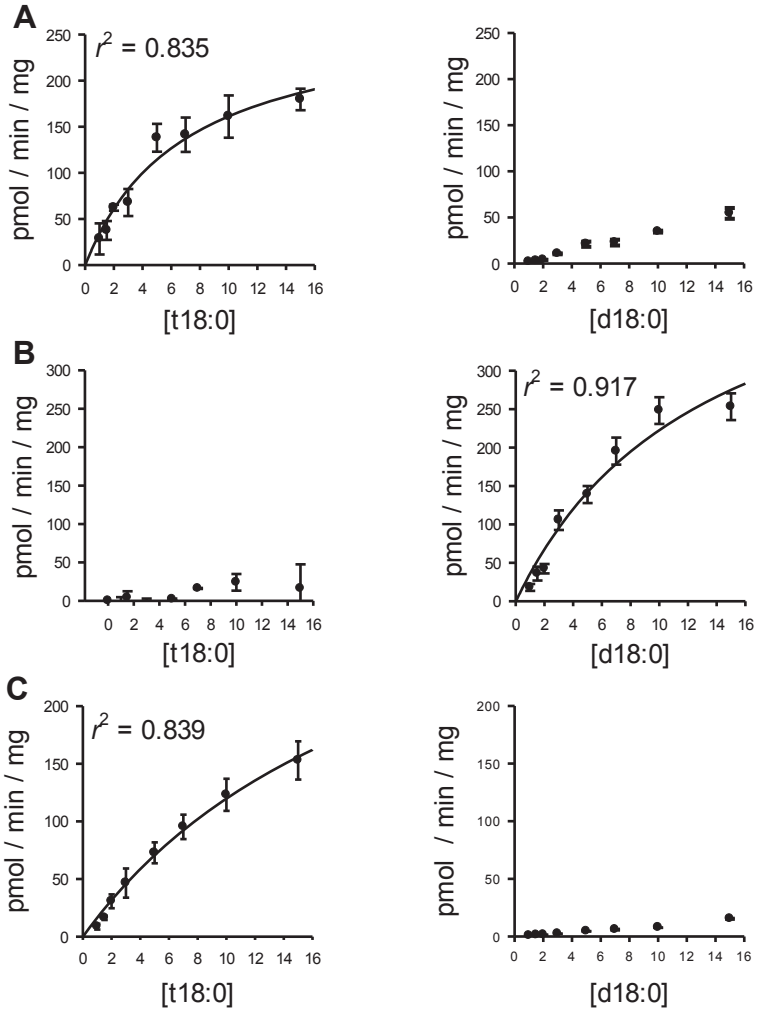

Figure 3.5 *Determination of kinetic constants in regards to trihydroxy and dihydroxy LCBs.* Plots of activity vs substrate concentration (t18:0 or d18:0 LCB) in assays containing 50µM acyl-CoA, 10µM BSA and 0-15 µM LCBs. The LOH1 **(A)** and LOH3 **(C)** enzyme assays contained 24:0-CoA, while the LOH2 assay **(B)** contained 16:0-CoA as acyl-CoA substrate. Data points represent the mean ± S.E. (*n*=3) for LOH1 and LOH2 while *n*=5 for LOH3. Kinetic parameters were estimated where possible by non-linear regression analysis using the Michaelis-Menten equation.

3.2.4 SPECIFICITY OF ARABIDOPSIS CERAMIDE SYNTHASES TOWARDS ACYL-COA SUBSTRATES

To determine the chain length specificity of the different ceramide synthase isoforms, acyl-CoA substrates of different chain lengths were supplied in separate reactions at a concentration of 50 μM acyl-CoA and the production of ceramide of the appropriate chain length measured. Measurements of activity were made using t18:0 LCB substrate for LOH1 and LOH3 and d18:0 LCB substrate for LOH2. Both LOH1 and LOH3 demonstrated a strong preference for very long chain acyl-CoAs (C>18) although LOH1 had the greatest activity toward 24 and 26 carbon acyl-CoAs, while LOH3 showed little preference for acyl-CoAs between 20 and 26 carbons in length. This specificity was conserved in LOH1 plant overexpression microsomes which preferred C24 acyl-CoAs over C16 acyl-CoAs (Appendix A). LOH2 was unable to use any acyl-CoA substrates greater than C18 and showed very strong preference for C16 acyl-CoA (Figure 3.6). Interestingly, unsaturated very long chain acyl-CoAs were poor substrates for all isoforms demonstrating a significant preference for saturated acyl-chains over their mono-unsaturated counterparts. All future assays were done using the preferred acyl-CoA substrate (24:0 for LOH1 and LOH3, 16:0 for LOH2). Kinetic parameters for acyl-CoAs could not be determined as modifying the level of BSA or Acyl-CoA in the assay leads to departure from Michaelis-Menten kinetics (Luttgeharm et al. 2015a)(Chapter 2).

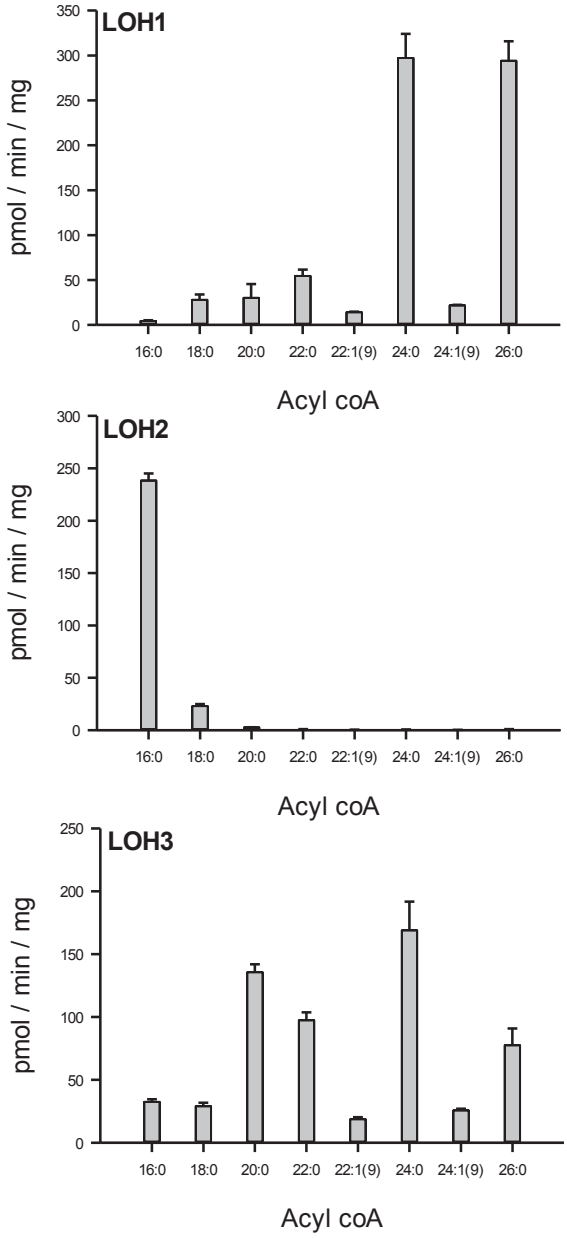

Figure 3.6 *Activity of the ceramide synthase isoforms with different acyl-CoA substrates.* Activity of the Arabidopsis ceramide synthases measured with a variety of different acyl-CoAs as substrates. Assays contained 15 μM LCB (t18:0 for LOH1 and LOH3, d18:0 for LOH2) with 50 μM of the indicated acyl-CoA. Data show the mean ± S.E. (*n*=3).

3.2.5 SPECIFICITY OF ARABIDOPSIS CERAMIDE SYNTHASES TOWARDS MODIFIED LCB SUBSTRATES

While ceramide is thought to be synthesized *de novo* from saturated LCB substrates, there is the potential for ceramide synthases to recycle LCBs released by the hydrolysis of complex sphingolipids. In plants, this would produce a variety of monosaturated and diunsaturated LCBs with different regio- and stereomeric configurations. LCBs not commercially available were purified from hydrolysates of plant material (Appendix B) producing LCB fractions enriched for the specific LCB substrates of interest. In order to understand how the different ceramide synthase isoforms might contribute towards LCB recycling, the activity of each LOH towards seven different unsaturated plant LCBs was measured (Figure 3.7).

LOH2 showed maximum activity with the d18:1(4*E*) LCB (Figure 3.7) about 6 times that with the d18:0 LCB, which was surprising as d18:1(4*E*) is not observed in Arabidopsis leaf. Rather d18:2(4*E*/8*Z*) or d18:2(4*E*/8*E*) is found only in select tissues such as pollen (Luttgeharm et al. 2015c). Assay of LOH2 using these diunsaturated LCBs showed levels of activity comparable to or greater than that found with d18:0 indicating that LOH2 shows enhanced activity towards Δ4 unsaturated LCB substrates.

In contrast, although LOH1 and LOH3 preferred the fully saturated, t18:0 LCB substrate (Figure 3.7), LOH3 had at least twice as much activity with t18:1 substrates as LOH1. Activity toward diunsaturated LCBs and d18:1(4*E*) was comparable between LOH1 and LOH3. However, none of the isoforms demonstrated a high level of activity with either d18:1(8*Z*) or d18:1(8*E*) suggesting this LCB cannot be recycled.

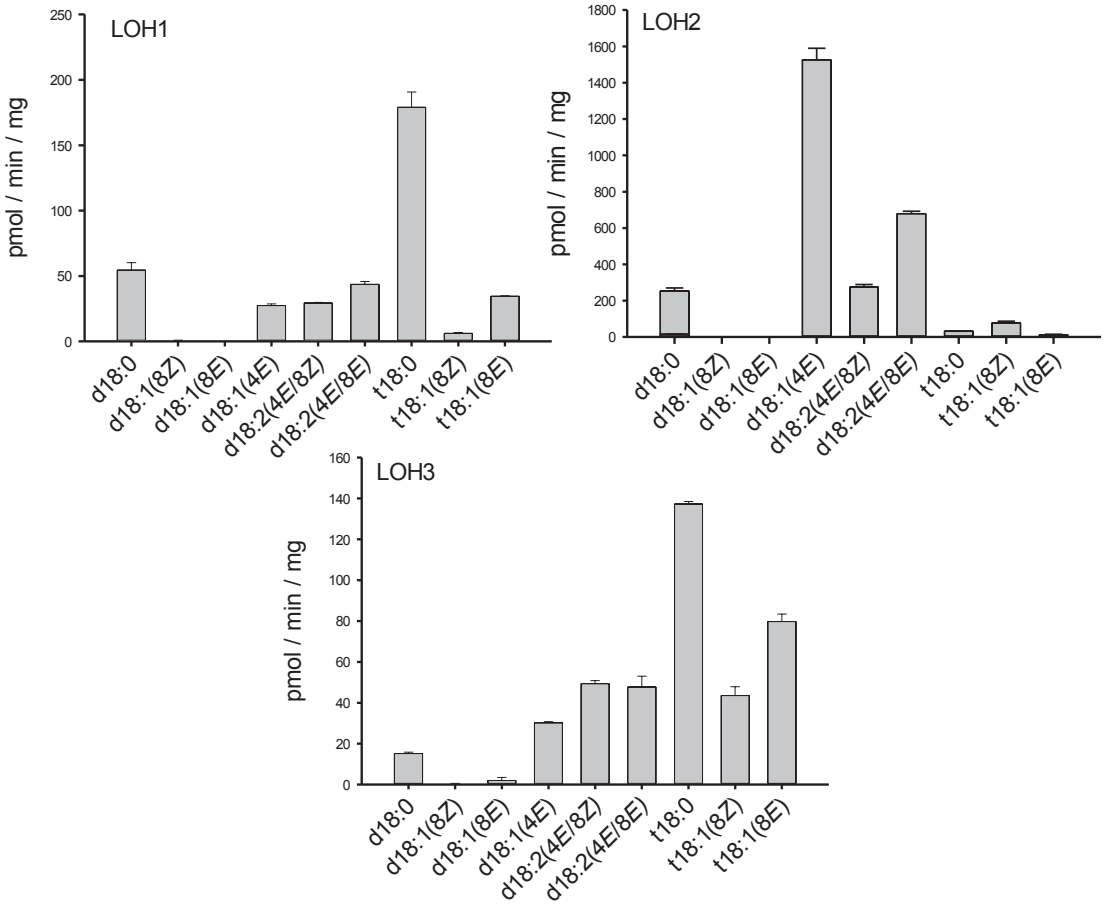

Figure 3.7 *Activity of the ceramide synthase isoforms with different LCB substrates*. Activity of the Arabidopsis ceramide synthases measured with a variety of different LCBs as substrates. Assays contained 15 μM of the indicated LCB (see Appendix B for composition of purified LCB fractions) and 50 μM acyl-CoA (24:0-CoA for LOH1 and LOH3, 16:0-CoA for LOH2). Data show the mean ± S.E. (*n*=3).

3.2.6 ARABIDOPSIS CERAMIDE SYNTHASES SHOW DIFFERENTIAL SENSITIVITY TO DIVALENT CATIONS

The response of ceramide synthase to divalent cations is potentially a complex one and may be involved in the regulation of this enzyme *in vivo*. While some ceramide synthases require divalent cations for maximum activity (Hirschberg et al. 1993; Sribney 1966), other studies have

demonstrated that certain divalent cations, such as Ca^{2+}, inhibit ceramide synthesis (Sribney 1966). The effect of a variety of divalent cations on Arabidopsis ceramide synthase activity was tested by measuring the activity of each isoform with its preferred LCB and acyl-CoA substrate in the presence of different divalent cations (Figure 3.8). Interestingly, both LOH1 and LOH3 were inhibited by most or all divalent cations tested, however LOH2 showed increased activity in the presence of 2mM Mg^{2+}, and 1µM Mn^{2+} and Ca^{2+}, with no affect observed by 1µM Cu^{2+}, Zn^{2+} or Co^{2+}. Additionally increased levels of Ca^{2+} resulted in inhibition of LOH1 while LOH2 maintained high level of activity.

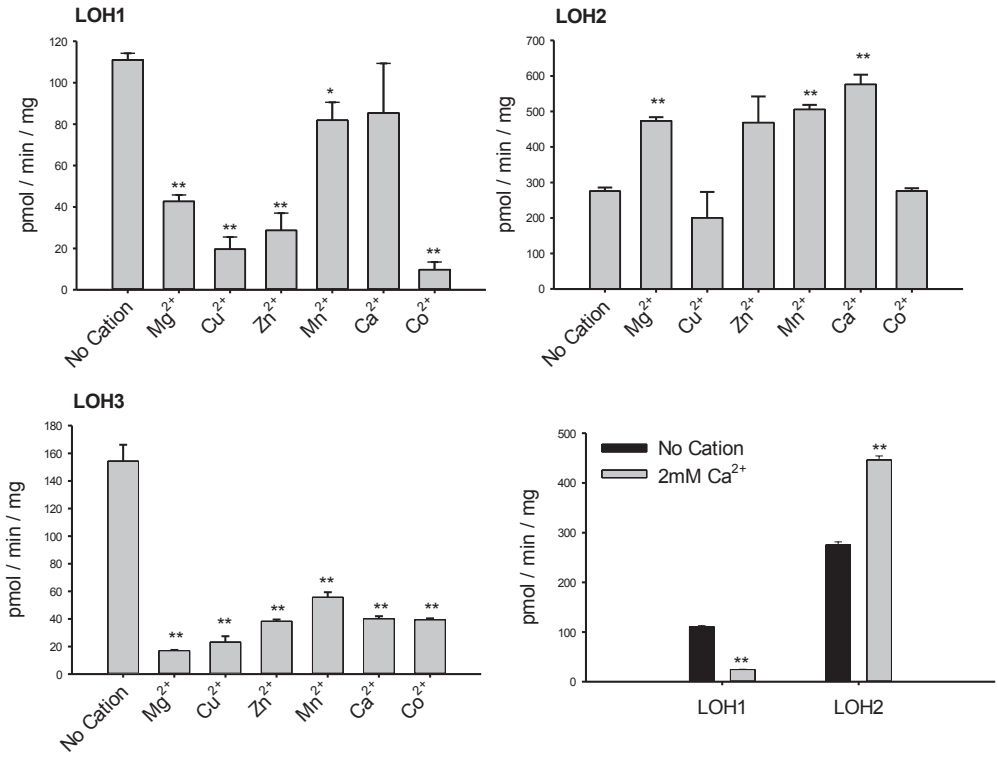

Figure 3.8 *Effect of divalent cations on the activity of Arabidopsis ceramide synthases*. Ceramide synthase activity for the three Arabidopsis isoforms measured with 0mM and 2mM of Mg^{2+} and 1µM of all other indicated divalent cation. LOH1 and LOH2 were also assayed in the presence of 2mM Ca^{2+}. Assays contained 15µM LCB and 50µM acyl-CoA (t18:0 LCB/24:0 CoA for LOH1 and LOH3, d18:0 LCB/16:0-CoA for LOH2). Graphs show the mean ± S.E. (n=3), * $P \leq 0.05$ and ** $P \leq 0.01$ compared to control (0 mM).

3.2.7 SENSITIVITY OF ARABIDOPSIS CERAMIDE SYNTHASE ISOFORMS TO INHIBITION BY FUMONISIN B_1 – In order to understand how different isoforms of ceramide synthase mediate resistance to SAMs, inhibition studies were conducted using fumonisin B_1 and the microsomes containing LOH1, LOH2, or LOH3. LCB-velocity curves were generated at different concentrations of fumonisin B_1 using the preferred LCB (t18:0 LCB for LOH1 and LOH3, d18:0 LCB for LOH2) and the acyl-CoA (C24:0-CoA for LOH1 and LOH3, C16:0-CoA for LOH2). By plotting all the data and fitting models of inhibition to the curves obtained, best estimates for K_i were obtained for each ceramide synthase isoform (Figure 3.9 and Table 3.1-3.3). LOH1 was most sensitive to inhibition by fumonisin B_1 with an estimated K_i of 0.003 ± 0.0008 μM (mixed partial model). The K_i for LOH2 and LOH3 were several magnitudes higher with a K_i of 0.970 ± 0.784 μM and 0.755 ± 0.423 μM (mixed partial model) for LOH2 and LOH3, respectively. While the data do not conclusively point to an inhibition model, they are broadly consistent with a mixed mode of inhibition with respect to LCB (Tabl 3.1). To confirm that the yeast microsomal data are consistent with *in planta* LOH1 overexpression microsomes were tested at 0.02 and 0.5 μM FB_1 Appendix A). A K_i of 0.027 ± 0.026 μM (mixed partial model) was found which was found to not be statistically different than the yeast microsomal data (P=0.10).

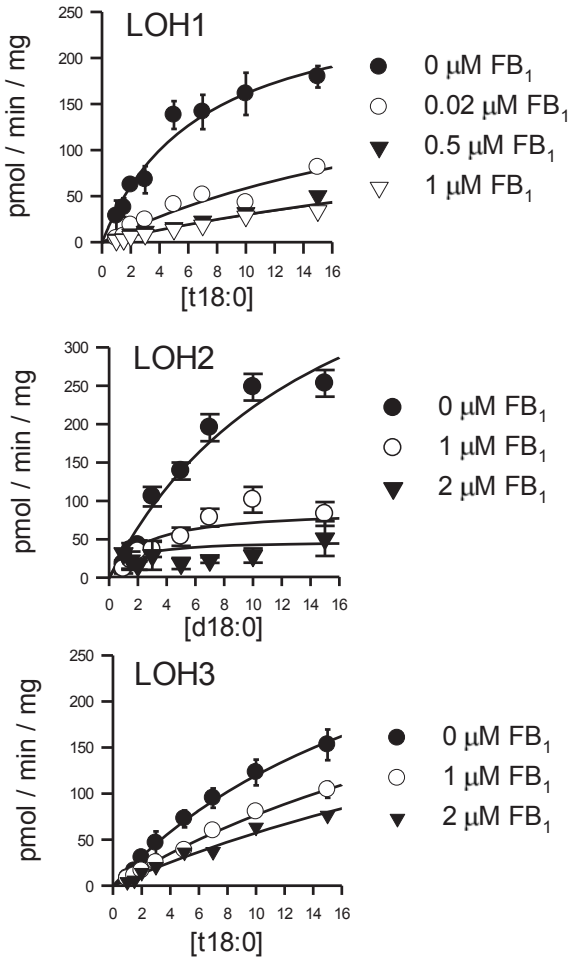

Figure 3.9 *Inhibition of Arabidopsis ceramide synthase activity by fumonsin B_1.* Plots of activity vs substrate concentration (t18:0 or d18:0 LCB) in assays containing 50 μM acyl-CoA (24:0-CoA for LOH1 and LOH3, 16:0-CoA for LOH2), 0-15μM LCB (t18:0 for LOH1 and LOH3, d18:0 for LOH2) in the presence of varying amounts of fumonisin B_1 (0.02-2 μM). Models of inhibition were fitted to the entire data set by non-linear regression analysis (statistical results for all inhibitions models shown in Table 3.1-3.3). The lines show the fit of the mixed partial inhibition model for LOH1, r^2=0.914; for LOH2, r^2=0.906; and for LOH3 r^2=0.902. Data points show the mean ± S.E. (n=3).

TABLE 3.1 *Enzyme Kinetics Model Comparison for LOH1*

Equation	R^2	AICc	Sy.x	V_{max}	±Std. Error	K_m	±Std. Error	K_i	±Std. Error
Competitive (Partial)	0.914	286	18.3	273	29.0	6.92	1.52	0.003	0.001
Noncompetitive (Partial)	0.911	288	18.6	281	30.7	7.37	1.63	0.006	0.003
Mixed (Partial)	0.914	289	18.5	273	29.5	6.93	1.55	0.003	0.002
Competitive (Full)	0.881	299	21.3	272	33.7	6.90	1.77	0.005	0.001
Uncompetitive (Partial)	0.886	300	21.0	281	35.7	7.40	1.90	0.004	0.002
Noncompetitive (Full)	0.879	300	21.4	278	34.8	7.20	1.83	0.012	0.003
Mixed (Full)	0.881	302	21.5	272	34.2	6.91	1.80	0.006	0.004
Uncompetitive (Full)	0.870	304	22.3	281	37.9	7.45	2.02	0.006	0.002

TABLE 3.2 *Enzyme Kinetics Model Comparison for LOH2*

Equation	R^2	AICc	Sy.x	V_{max}	±Std. Error	K_m	±Std. Error	K_i	±Std. Error
Noncompetitive (Full)	0.904	421	23.3	493	65.2	12.1	2.75	0.534	0.0629
Mixed (Full)	0.906	422	23.2	519	77.8	13.3	3.32	0.971	0.575
Noncompetitive (Partial)	0.904	424	23.5	493	65.9	12.1	2.77	0.534	0.242
Mixed (Partial)	0.906	424	23.4	519	78.4	13.3	3.35	0.970	0.784
Uncompetitive (Full)	0.899	425	23.9	554	90.6	14.9	3.91	0.191	0.0375
Uncompetitive (Partial)	0.899	427	24.1	554	92.1	14.9	3.98	0.191	0.0849
Competitive (Full)	0.893	429	24.6	500	76.1	12.5	3.23	0.289	0.0475
Competitive (Partial)	0.303	555	63.4	272	62.9	5.80	3.07	0.000	1.46

TABLE 3.3 *Enzyme Kinetics Model Comparison for LOH3*

Equation	R^2	AICc	Sy.x	V_{max}	±Std. Error	K_m	±Std. Error	K_i	±Std. Error
Competitive (Full)	0.902	389	14.4	384	73.7	19.1	5.51	0.963	0.144
Noncompetitive (Full)	0.899	391	14.6	454	92.5	24.5	6.98	1.49	0.172
Competitive (Partial)	0.902	391	14.5	384	74.0	19.1	5.52	0.74	0.380
Mixed (Full)	0.902	392	14.5	384	78.7	19.1	5.88	0.966	0.305
Noncompetitive (Partial)	0.900	393	14.6	455	93.1	24.4	7.01	1.09	0.637
Mixed (Partial)	0.902	394	14.6	385	79.4	19.1	5.92	0.755	0.423
Uncompetitive (Full)	0.868	411	16.7	781	371	51.5	29.3	0.271	0.133
Uncompetitive (Partial)	0.868	413	16.8	781	414	51.5	32.8	0.271	0.213

3.3 DISCUSSION

The eukaryotic cell has an absolute ~~requirement~~ for sphingolipids, moreover, these sphingolipids must contain fatty acids of a specific chain-length for sphingolipids to perform their function in membrane structure and organization. On top of this requirement for sphingolipids, ceramides and their substrates influence cell fate decisions making the ceramide synthase reaction a critical component of the cellular machinery. Not only must ceramides be synthesized with the correct chain length fatty acid, they must be synthesized in the right quantities and in response to the correct stimuli or risk unexpected outcomes for growth and development.

The results presented here demonstrate that Arabidopsis uses different ceramide synthases, each with unique properties that presumably enable different roles in maintaining sphingolipid homeostasis and function. This was determined by *in vitro* assays of LOH1 and LOH3 in a heterologous yeast microsome system and an *in vitro* assay of LOH2 in a homologous Arabidopsis leaf microsome system. LOH2 activity was not detected by *in vitro* assay in the heterologous yeast system despite the presence of C16 containing sphingolipids in the yeast

demonstrating that LOH2 is a C16-specific ceramide synthase *in vivo* and comparable level of LOH2 protein in the yeast microsomes. It is possible that for optimal activity LOH2 requires the presence of a protein complex not found in the yeast microsomal system similar to that previously described in humans (Laviad et al. 2012), or that LOH2 is subject to post-translational modification not present in *Saccharomyces*. Despite this difference, the biochemical properties of the over-expressed LOH proteins in each system are consistent with the known properties of Arabidopsis ceramide synthases identified to date and the kinetic properties of LOH1 were consistent between heterologous yeast and homologous plant microsomes, suggesting that each system provides a good estimate of the true biochemical properties of each of the ceramide synthase isoforms.

From work with knockout mutants of genes involved in sphingolipid biosynthesis and overexpression of ceramide synthases *in planta*, it has been hypothesized that LOH1 and LOH3 primarily use trihydroxy LCBs while LOH2 uses dihydroxy LCBs (Ternes et al. 2011; Chen et al. 2008; Markham et al. 2011; Luttgeharm et al. 2015b), but it has not been clear how the overall profile of sphingolipids is generated or maintained. The results of the kinetic analyses reported here make it evident that these isoforms have their own unique roles to play in generating and maintaining the sphingolipid profile and reveal important facts about the organization of sphingolipid metabolism. Given that neither LOH1 nor LOH3 will use d18:0 effectively as a substrate, it is clear that sphingoid base hydroxylation must occur on free LCB before the ceramide synthase reaction. Additionally, as LOH2 will not use t18:0 substrates, this makes the sphingoid base hydroxylase reaction a critical branch point between C16-containing ceramides and VLCFA-containing ceramides (Chen et al. 2008). Of the three ceramide synthase isoforms, LOH1 is known to have the highest transcript level, suggesting it is the most abundant enzyme *in planta* (Ternes et al. 2011). Given that LOH1 has the lowest K_m of the three isoforms and has a greater preference for 24 and 26 carbon VLCFA, which are predominant in the sphingolipid profile of Arabidopsis, it seems likely that LOH1 is the predominant ceramide synthase in

Arabidopsis. This may explain why knockout of LOH1 alone is able to generate a discernable, albeit subtle, phenotype (Ternes et al. 2011).

Surprisingly perhaps, given the abundance on monounsaturated fatty acids in the sphingolipids of Arabidopsis, none of the ceramide synthases tested was able to use unsaturated fatty acids as a substrate in the *in vitro* reaction. Arabidopsis contains approximately equimolar amounts of saturated and unsaturated C24 fatty acids but virtually no unsaturated C22 fatty acid. However, both C22:1-CoA and C24:1-CoA were poor substrates for ceramide synthesis by any of the LOH enzymes. This suggests that sphingolipids fatty acid unsaturation may occur post-ceramide synthesis and not on the acyl-CoA substrate.

Other details about the organization of sphingolipid metabolism arise from the studies on the substrate preference of the different LCB isoforms. In animals, LCBs contain a single double bond at the Δ4 position introduced by a desaturase after the synthesis of a saturated dihydroceramide (Michel et al. 1997). In plants, there are several more sphingolipid desaturases with unknown substrates. Interestingly, none of the Arabidopsis ceramide synthase isoforms showed appreciable activity when d18:1(8*E* or *Z*) was presented as a substrate, suggesting that the Δ8-desaturation is introduced after ceramide synthesis. This also means that d18:1(8*E* or *Z*) LCBs cannot be recycled and must be broken down. In contrast, the d18:1(4*E*) LCB, which is not abundant in Arabidopsis (Markham et al. 2006; Michaelson et al. 2009), was an excellent substrate for LOH2. One possible interpretation of this result is that, unlike animals, the C4-double bond is added prior to ceramide synthesis and acts as a structural feature to direct LCBs towards a LOH2-like ceramide synthase. As Δ4 unsaturation and 4-hydroxylation are chemically mutually exclusive, this would create a convenient system to balance flux through different ceramide synthase isoforms.

In contrast to the d18:1(8*E* or *Z*) LCBs, t18:1(8*E* or *Z*) were effective substrates for ceramide synthesis. Of the three isoforms, LOH3 was the most active with t18:1 substrates and demonstrated higher activity with the *E* isomer than the *Z*. If the LCB C8-desaturase works only

on ceramide, this suggests LOH3 may play an important role in the recycling of t18:1 from the breakdown of complex sphingolipids. Overall this assigns unique roles to the different ceramide synthase isoforms with LOH1 being primarily involved in VLCFA-containing ceramide synthesis, LOH2 being used for the synthesis of substrates for GlcCer synthesis and LOH3 either recycling LCBs and/ or providing alternative acyl profiles to LOH1. How these three isoforms work together to regulate overall sphingolipid metabolism will be an intriguing question.

One clue as to how this coordination could be achieved is through the differential sensitivity of the ceramide synthase isoforms to divalent cations. While all divalent cations tested inhibited LOH3 activity *in vitro*, LOH1 was only mildly inhibited Mn^{2+} and only inhibited by high concentrations of Ca^{2+}. LOH2 activity was substantially enhanced upon addition of Mg^{2+}, Mn^{2+}, and importantly, both low and high concentrations of Ca^{2+}. How these differential sensitivities might lead to regulation of ceramide synthase activity is unknown, but Ca^{2+} signaling during programmed cell death may result in a decrease in LOH1/LOH3 activity and an increase in LOH2 activity resulting in the upregulation of additional PCD related genes as seen upon LOH2 *in planta* overexpression (Luttgeharm et al. 2015b)(Chapter 4). The regulation of ceramide synthase is an important topic for future research.

Previously it has been shown that *in planta* levels of free LCBs increase upon treatment with fumonisin B_1 leading to the hypothesis that fumonisin B_1 competitively inhibits ceramide synthases (Kimberlin et al. 2013; Luttgeharm et al. 2015b)(Chapter 4). This study demonstrates that fumonisin B_1 most likely inhibits ceramide synthases by a mixed inhibition mechanism in relation to the LCB. Since the order of substrate binding and catalytic mechanism of ceramide synthesis is currently unknown, it cannot be concluded from these results exactly how fumonisin B_1 binds and inhibits ceramide synthases. Further complicating fumonisin B_1 inhibition are recent reports that mammalian ceramide synthases can catalyze the N-acylation of fumonisin B_1 producing a more potent ceramide analog inhibitor (Harrer et al. 2015; Harrer et al. 2013). What can be determined from the data presented here is that LOH1 is much more sensitive to fumonisin

B_1 than either LOH2 or LOH3. This was surprising given that LOH1 and LOH3 are ~90% identical (Ternes et al. 2011) but consistent with *in planta* overexpression of LOH3 imparting FB1 resistance while overexpression of LOH1 results in no change from wild type (Luttgeharm et al. 2015b)(Chapter 4).

In summary, the results reported here identify unique properties for each of the Arabidopsis ceramide synthases that may reflect their different roles in Arabidopsis sphingolipid metabolism (Figure 9). Each ceramide synthase isoform examined had a unique substrate preference profile suggesting they each contribute to overall sphingolipid metabolism in a slightly different way. For unknown reasons, certain ceramide synthases are much more susceptible to inhibition by SAMs than others, explaining the origin of SAM sensitivity in tomato and Arabidopsis. While regulation of ceramide synthase is an important topic that remains to be addressed, the differential response of the ceramide synthase isoforms to divalent cations suggests the balance between the synthesis of VLCFA-containing ceramides and C16-containing ceramides may be regulated by divalent cations such as calcium.

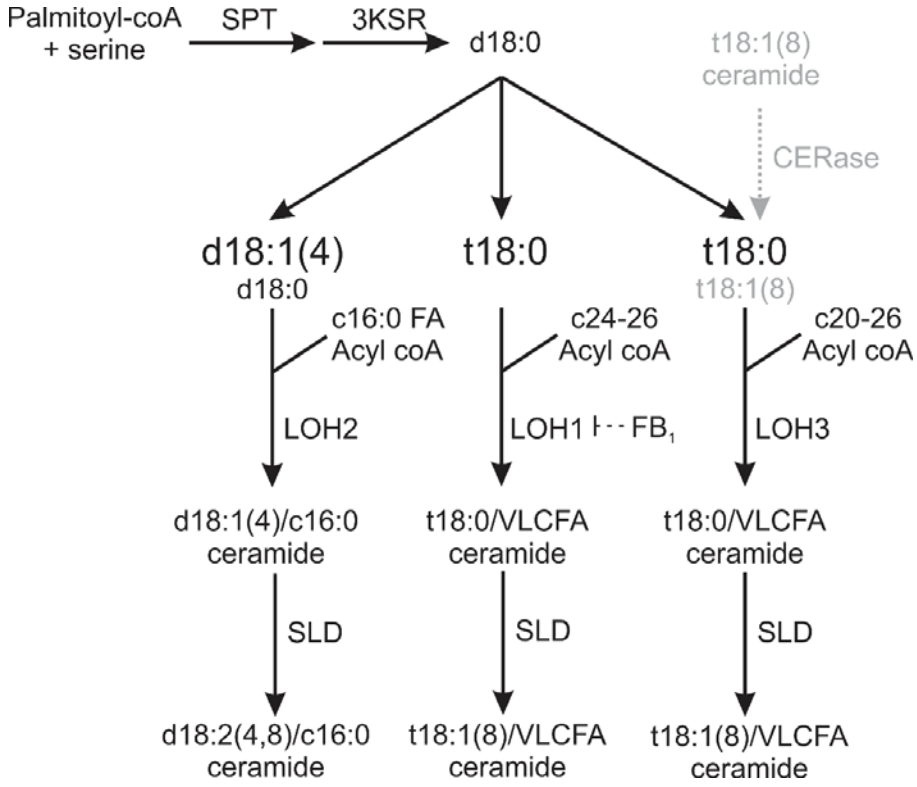

Figure 3.10 *Proposed model for the synthesis of Ceramide in Arabidopsis.* Each ceramide synthase in Arabidopsis has a unique specificity that contributes to the overall sphingolipidome. The *de novo* synthesis pathway is shown in black with LCBs originating from sphingolipid recycling shown in grey. The primary substrates are shown with minor substrates omitted. LOH1 and LOH3 primarily use saturated trihydroxy LCBs and saturated VLCFA. LOH3 can also use t18:1(8) allowing it to potential be involved in LCB recycling from sphingolipid degradation. Fumonison B_1 (FB_1) preferentially inhibits LOH1 over LOH2 and LOH3. LOH2 primarily uses dihydroxy LCBs and C16 FAs. In leaf, the primary LCB used is d18:0 due to a lack of Δ4 desaturated LCBs, however it was found that LOH2 shows a strong preference for the d18:1(4) LCB and is the primary substrate in the reproductive tissues where the Δ4 LCB DES is expressed (Luttgeharm et al. 2015c; Michaelson et al. 2009). After synthesis the dihydroxy LCB can also be desaturated at the Δ8 position.

3.4 EXPERIMENTAL PROCEDURES

All chemicals, unless otherwise indicated, were purchased from Sigma–Aldrich (St. Louis, MO). Acyl-CoA and lipid standards were purchased from Avanti Polar Lipids (Alabaster, AL). LCBs were purchased from Matreya (Pleasant Gap, PA). Solvents were OmniSolv grade from EMD Millipore (Billerica, MA) unless otherwise noted.

3.4.1 HETEROLOGOUS EXPRESSION OF LOH GENES IN SACCHAROMYCES CEREVISIAE

Synthetic, codon optimized, gene constructs were custom synthesized (Genscript, Piscataway, NJ) for each LOH gene. Constructs consisted of the GST and PreScission Protease sequence from pGEX-6P-1 (bases 228to 944) (Life Technologies) fused to the LOH open reading frame with an N-terminal FLAG tag sequence and Pst1 restriction site. A C-terminal Sbf1 sequence allowed for cloning into p426GDP (Mumberg et al. 1995) at the SpeI and PstI cloning sites. Verified constructs were transformed (Frozen-EZ Yeast Transformation II; Zymo Research, Orange, CA) into yeast strain 6602 (Kageyama-Yahara and Riezman 2006) (*Δlag1/Δlac1* + pRS416-lag1) and plated on complete supplement mixture (CSM)-Leu media. After growth at 28°C for 3 days, colonies were transferred onto CSM-Leu media containing 1 mg/mL 5-fluoroorotic acid (FOA, Gold Biotechnology, St Louis, MO) and allowed to grow for 1 week at 28°C. Colonies that grew on FOA were then regrown in duplicate on CSM-Leu and CSM-Ura plates to confirm the absence of the *URA3* containing plasmid pRS416-lag1.

3.4.2 WESTERN BLOT OF HETEROLOGOUS EXPRESSED LOH GENES IN SACCHAROMYCES CEREVISIAE

Microsomal protein was incubated in 1x SDS Sample buffer (.06M Tris Base pH 6.8, 5% glycerol, 2% SDS, 0.05% bromophenol blue) at 50°C for 30 min. 10µg microsomal protein was loaded onto a 2% SDS gel (4% stacking, 12% running) and run at 160V for 1.5 hours. The gel was equilibrated with Western Transfer buffer (192mM glycine, 25mM Tris Base, 0.019% SDS, 20% methanol) at room temperature for 30 min followed by transfer onto a PVDF membrane at

160mA for 3h at 4°C. The membrane was blocked with 5% non-fat dry milk in Tris buffered saline (TBS) for 1h at room temperature followed by hybridization with primary antibody (Rabbit anti-FLAG, Sigma, diluted 1:1000 in 5% non-fat dry milk in TBS) for 1h at room temperature. The membrane was washed 3x 10 with 5% non-fat milk in TBS followed by hybridization with the secondary antibody (Goat anti-Rabbit HRP, diluted 1:2000 in 5% non-fat dry milk in TBS) at room temperature for 1h. The membrane was washed 3x 10 min with TBS followed by incubation in luminol solution (0.1M Tris pH 8.5, 1.25mM comaric acid (MP Biomedicals), 0.198mM luminol (Thermo Fisher Scientific), 0.034% hydrogen peroxide) for 1 min at room temperature. Membrane was exposed to X-ray film for 10 min before developing.

3.4.3 YEAST CERAMIDE AND INOSITOLPHOSPHOCERAMIDE ANALYSIS

Yeast sphingolipids were extracted (Hanson and Lester 1980) followed by de-esterification as previously described (Markham and Jaworski 2007). Ceramides were analyzed using the same LC conditions as previously described (Markham and Jaworski 2007) using MRMs found in Appendix C. Inositolphosphoceramide (IPC) sphingolipids were analyzed by LC-MS/MS as previously described (Markham and Jaworski 2007) using MRMs for yeast sphingolipids including species with shorter fatty acids (Guan and Wenk 2006).

3.4.4 HOMOLOGOUS OVEREXPRESSION OF LOH -1, -2, AND -3

Homologous overexpression plants used in this study where previously characterized and corresponds to LOH1 C, LOH2 C, and LOH3 B (Luttgeharm et al. 2015b)(Chapter 4).

3.4.5 PREPARATION OF MICROSOMES

Yeast microsomes were prepared as previously described (Luttgeharm et al. 2015a)(Chapter 2). Plant microsomes were prepared by homogenization of Arabidopsis leaf tissue for ~30s in 0.5M sucrose, 50mM HEPES (pH 7.8), 5mM EDTA, 2mM DTT, and 0.5% polyvinylpyrolidone in a chilled (4°C) Waring blender followed by homogenization for 30s at 10,000rpm using an IKA ULTRA TURRAX fitted with a T25 probe. Homogenized tissue was filtered through cheese cloth and spun at 12,000 x g for 30 min at 4°C to remove cellular debris.

The supernatant was removed and spun at 135,000 x g for 30min at 4°C. The membrane pellet was resuspended by pipetting in reaction buffer (20mM potassium phosphate pH 7.5, 250mM Sorbitol) and spun at 100,000 x g for 1h at 4°C. The resulting pellet was resuspended in reaction buffer using the pestle from a Dounce homogenizer, flash frozen with liquid N_2, and stored at -80°C. Protein concentration was measured using Pierce BCA Protein Assay (Thermo Fisher Scientific) using bovine serum albumin (BSA) as a reference.

3.4.6 CERAMIDE SYNTHASE ASSAY

Assays were performed as previously described (Luttgeharm et al. 2015a)(Chapter 2). Briefly LCB/BSA complexes containing 100µM BSA and varying amounts of LCB (dissolved in 2:1 ethanol/DMSO) not exceeding 150µM were prepared. 2:1 ethanol/DMSO was added to standardize all solutions at 10% by volume with the LCB/BSA complexes representing a 10x solution for addition to the assay. The assay was run in a 100µl volume containing 20 mM potassium phosphate (pH 7.5), 250 mM sorbitol, 50 µM acyl-CoA, 10 µM BSA, up to 15 µM LCB, and up to 10 µg microsomal protein. The reaction mixture (lacking microsomal protein) was incubated for 10min at 30°C followed by addition of microsomal protein and gentle mixing using a pipet tip. The reaction was run for 30min and stopped by addition of 750 µl of 1:1 (v/v) MTBE/MeOH and mixing with a vortex mixer. 50 pmol of C12 ceramide standard was added followed by phase separation induced by the addition of 850 µl of MTBE and 312 µl of water. The MTBE upper layer was removed to a clean tube and dried under a stream of air at 60 °C. Ceramide composition was analyzed on an ABSciex QTrapp4000 as previously described (Markham and Jaworski 2007). Kinetic data was determined by the use of SigmaPlot 13 (Systat Software, San Jose, CA) using the single substrate option of the Enzyme Kinetics Module. For assays using divalent cations a 10x solution was made from the chloride salt with 10µl added to the reaction mix.

3.4.7 PURIFICATION OF LCB SUBSTRATES

LCBs not commercially available were purified using preparatory HPLC as previously described (Luttgeharm et al. 2015a)(Chapter 2). Briefly, t18:1(8*Z*), t18:1(8*E*), and d18:2(4*E*/8*Z*) were purified from *Ravenea rivularis* by hydrolyzing ~1g of fresh tissue as previously described (Markham et al. 2006) followed by separation of total LCBs from fatty acids by weak cation exchange solid-phase extraction (Supelcelan LC-WCX SPE, Sigma-Aldrich and isolation by semi-preparative HPLC exactly as previously described (Luttgeharm et al. 2015a)(Chapter 2). The d18:1(8*Z*) and d18:1(8*E*) LCBs were purified from the glucoscylceramide fraction of *Vaccinium corymbosum*. Briefly, ~1g fresh tissue was homogenized with an Omni THQ digital tissue homogenizer (Omni Internation, Kennesaw GA) at 24,000 rpm in 2:1 MeOH/Chloroform followed by a Bligh Dyer total lipid extraction (Bligh and Dyer 1959). Glucosyceramides were isolated from the total lipid extract as previously described (Cahoon and Lynch 1991) using a 3mL Supleclean LC-Si SPE column. Briefly, the column was equilibrated with 5mL of chloroform/acetic acid (100:1. v/v) and the LCB sample was applied in 2mL of the same solvent. The cartridge was washed with of the same solvent followed by 10mL chloroform/acetone (4:1, v/v) and 15mL chloroform/acetone (1:1, v/v). Glucosylceramide were eluted by addition of 8mL acetone followed by 6mL acetone/acetic acid (100:1, v/v). The glucosylceramide fraction was dried under nitrogen at 60°C and LCBs were hydrolyzed overnight as previously described (Markham et al. 2006) followed by semi-preparative, reverse-phase HPLC exactly as previously described (Luttgeharm et al. 2015a)(Chapter 2). The d18:2(4*E*/8*E*) LCB was purified from commercially available plant glucosylceramide (Matreya). Briefly, 1mg plant glucosylceramide was hydrolyzed overnight as previously described (Markham et al. 2006) followed by semi-preparative HPLC exactly as previously described (Luttgeharm et al. 2015a)(Chapter 2). The isolated LCBs were assessed for purity and quantity by fluorescent derivitization and comparison to an internal standard after separation by HPLC (Markham et al. 2006).

3.4.8 FORMATION OF SUBSTRATE-INHIBITOR COMPLEXES WITH BSA AND INHIBITOR STUDIES

For fumonisin B_1 inhibition studies fumonisin B_1 (Sigma-Aldrich) was dissolved in 2:1 (v/v) ethanol/DMSO at concentrations of 1 mM and 0.5 mM. Fumonsin B_1 was added directly to BSA/LCB complexes as previously described (Luttgeharm et al. 2015a)(Chapter 2). The initial fumonisin B_1 concentration used was selected in order to keep the final amount of 2:1 (v/v) ethanol/DMSO to 10% total reaction volume. K_i and modes of inhibition were calculated by selecting the best fit model from SigmaPlot 13 using the single substrate, single inhibitor option of the Enzyme Kinetics Module.

3.5 ACKNOWLEDGEMENTS

We thank Howard Reizman for providing the yeast strain used in this study and Ming Chen for construction of *LOH2* overexpressing plants. This study was supported in part by funding from the U.S. National Science Foundation (MCB-1158500) to EBC.

3.6 REFERENCES

Abbas HK, Tanaka T, Duke SO, Porter JK, Wray EM, Hodges L, Sessions AE, Wang E, Merrill AH, Jr., Riley RT (1994) Fumonisin- and AAL-toxin-induced disruption of sphingolipid metabolism with accumulation of free sphingoid bases. Plant Physiol 106 (3):1085-1093.

Alden KP, Dhondt-Cordelier S, McDonald KL, Reape TJ, Ng CK, McCabe PF, Leaver CJ (2011) Sphingolipid long chain base phosphates can regulate apoptotic-like programmed cell death in plants. Biochem Bioph Res Commun 410 (3):574-580.

Bach L, Gissot L, Marion J, Tellier F, Moreau P, Satiat-Jeunemaitre B, Palauqui JC, Napier JA, Faure JD (2011) Very-long-chain fatty acids are required for cell plate formation during cytokinesis in Arabidopsis thaliana. Journal of Cell Science 124 (19):3223-3234.

Bach L, Michaelson LV, Haslam R, Bellec Y, Gissot L, Marion J, Da Costa M, Boutin JP, Miquel M, Tellier F, Domergue F, Markham JE, Beaudoin F, Napier JA, Faure JD (2008) The very-long-chain hydroxy fatty acyl-CoA dehydratase PASTICCINO2 is essential and limiting for plant development. Proc Natl Acad Sci USA 105 (38):14727-14731.

Baud S, Bellec Y, Miquel M, Bellini C, Caboche M, Lepiniec L, Faure JD, Rochat C (2004) gurke and pasticcino3 mutants affected in embryo development are impaired in acetyl-CoA carboxylase. EMBO Rep 5 (5):515-520.

Bi FC, Liu Z, Wu JX, Liang H, Xi XL, Fang C, Sun TJ, Yin J, Dai GY, Rong C, Greenberg JT, Su WW, Yao N (2014) Loss of ceramide kinase in Arabidopsis impairs defenses and

promotes ceramide accumulation and mitochondrial H2O2 bursts. Plant Cell 26 (8):3449-3467.
Bligh EG, Dyer WJ (1959) A rapid method of total lipid extraction and purification. Canadian journal of biochemistry and physiology 37 (8):911-917.
Cacas J-L, Furt F, Le Guédard M, Schmitter J-M, Buré C, Gerbeau-Pissot P, Moreau P, Bessoule J-J, Simon-Plas F, Mongrand S (2012) Lipids of plant membrane rafts. Progress in Lipid Research 51 (3):272-299.
Cahoon EB, Lynch DV (1991) Analysis of Glucocerebrosides of Rye (Secale cereale L. cv Puma) Leaf and Plasma Membrane. Plant Physiol 95 (1):58-68.
Carmona-Salazar L, El Hafidi M, Enriquez-Arredondo C, Vazquez-Vazquez C, Gonzalez de la Vara LE, Gavilanes-Ruiz M (2011) Isolation of detergent-resistant membranes from plant photosynthetic and non-photosynthetic tissues. Anal Biochem 417 (2):220-227.
Chen M, Markham JE, Dietrich CR, Jaworski JG, Cahoon EB (2008) Sphingolipid long-chain base hydroxylation is important for growth and regulation of sphingolipid content and composition in Arabidopsis. Plant Cell 20 (7):1862-1878.
Cuvillier O, Pirianov G, Kleuser B, Vanek PG, Coso OA, Gutkind JS, Spiegel S (1996) Suppression of ceramide-mediated programmed cell death by sphingosine-1-phosphate. Nature 381 (6585):800-803.
Dickson RC, Nagiec EE, Skrzypek M, Tillman P, Wells GB, Lester RL (1997) Sphingolipids are potential heat stress signals in Saccharomyces. J Biol Chem 272 (48):30196-30200.
Guan XL, Wenk MR (2006) Mass spectrometry-based profiling of phospholipids and sphingolipids in extracts from Saccharomyces cerevisiae. Yeast 23 (6):465-477.
Hannun YA, Luberto C (2000) Ceramide in the eukaryotic stress response. Trends in Cell Biology 10 (2):73-80.
Hanson BA, Lester RL (1980) The Extraction of Inositol-Containing Phospholipids and Phosphatidylcholine from Saccharomyces-Cerevisiae and Neurospora-Crassa. J Lipid Res 21 (3):309-315.
Harrer H, Humpf HU, Voss KA (2015) In vivo formation of N-acyl-fumonisin B1. Mycotoxin research 31 (1):33-40.
Harrer H, Laviad EL, Humpf HU, Futerman AH (2013) Identification of N-acyl-fumonisin B1 as new cytotoxic metabolites of fumonisin mycotoxins. Mol Nutr Food Res 57 (3):516-522.
Hirschberg K, Rodger J, Futerman AH (1993) The Long-Chain Sphingoid Base of Sphingolipids Is Acylated at the Cytosolic Surface of the Endoplasmic-Reticulum in Rat-Liver. Biochem J 290:751-757.
Kageyama-Yahara N, Riezman H (2006) Transmembrane topology of ceramide synthase in yeast. Biochem J 398:585-593.
Kimberlin AN, Majumder S, Han G, Chen M, Cahoon RE, Stone JM, Dunn TM, Cahoon EB (2013) Arabidopsis 56-amino acid serine palmitoyltransferase-interacting proteins stimulate sphingolipid synthesis, are essential, and affect mycotoxin sensitivity. Plant Cell 25 (11):4627-4639.
Laviad EL, Albee L, Pankova-Kholmyansky I, Epstein S, Park H, Merrill AH, Jr., Futerman AH (2008) Characterization of ceramide synthase 2: tissue distribution, substrate specificity, and inhibition by sphingosine 1-phosphate. J Biol Chem 283 (9):5677-5684.
Laviad EL, Kelly S, Merrill AH, Futerman AH (2012) Modulation of Ceramide Synthase Activity via Dimerization. J Biol Chem 287 (25):21025-21033.
Li-Beisson Y, Shorrosh B, Beisson F, Andersson MX, Arondel V, Bates PD, Baud S, Bird D, Debono A, Durrett TP, Franke RB, Graham IA, Katayama K, Kelly AA, Larson T, Markham JE, Miquel M, Molina I, Nishida I, Rowland O, Samuels L, Schmid KM, Wada H, Welti R, Xu C, Zallot R, Ohlrogge J (2013) Acyl-lipid metabolism. The Arabidopsis Book 11:e0161.

Liang H, Yao N, Song JT, Luo S, Lu H, Greenberg JT (2003) Ceramides modulate programmed cell death in plants. Genes Dev 17 (21):2636-2641.
Luttgeharm KD, Cahoon EB, Markham JE (2015a) A mass-spectrometry based method for the assay of ceramide synthase substrate specificity. Anal Biochem 478:96-101.
Luttgeharm KD, Chen M, Mehra A, Cahoon RE, Markham JE, Cahoon EB (2015b) Overexpression of Arabidopsis Ceramide Synthases Differentially Affects Growth, Sphingolipid Metabolism, Programmed Cell Death, and Mycotoxin Resistance. Plant Physiol.
Luttgeharm KD, Kimberlin AN, Cahoon RE, Cerny RL, Napier JA, Markham JE, Cahoon EB (2015c) Sphingolipid metabolism is strikingly different between pollen and leaf in Arabidopsis as revealed by compositional and gene expression profiling. Phytochem 115:121-129.
Maceyka M, Payne SG, Milstien S, Spiegel S (2002) Sphingosine kinase, sphingosine-1-phosphate, and apoptosis. Biochim Biophys Acta 1585 (2-3):193-201.
Markham JE, Jaworski JG (2007) Rapid measurement of sphingolipids from Arabidopsis thaliana by reversed-phase high-performance liquid chromatography coupled to electrospray ionization tandem mass spectrometry. Rapid Communications in Mass Spectrometry 21 (7):1304-1314.
Markham JE, Li J, Cahoon EB, Jaworski JG (2006) Separation and identification of major plant sphingolipid classes from leaves. J Biol Chem 281 (32):22684-22694.
Markham JE, Lynch DV, Napier JA, Dunn TM, Cahoon EB (2013) Plant sphingolipids: function follows form. Curr Opin Plant Biol 16 (3):350-357.
Markham JE, Molino D, Gissot L, Bellec Y, Hematy K, Marion J, Belcram K, Palauqui JC, Satiat-Jeunemaitre B, Faure JD (2011) Sphingolipids containing very-long-chain fatty acids define a secretory pathway for specific polar plasma membrane protein targeting in Arabidopsis. Plant Cell 23 (6):2362-2378.
Michaelson LV, Zauner S, Markham JE, Haslam RP, Desikan R, Mugford S, Albrecht S, Warnecke D, Sperling P, Heinz E, Napier JA (2009) Functional characterization of a higher plant sphingolipid Delta4-desaturase: defining the role of sphingosine and sphingosine-1-phosphate in Arabidopsis. Plant Physiol 149 (1):487-498.
Michel C, vanEchtenDeckert G, Rother J, Sandhoff K, Wang E, Merrill AH (1997) Characterization of ceramide synthesis - A dihydroceramide desaturase introduces the 4,5-trans-double bond of sphingosine at the level of dihydroceramide. J Biol Chem 272 (36):22432-22437.
Mizutani Y, Kihara A, Igarashi Y (2005) Mammalian Lass6 and its related family members regulate synthesis of specific ceramides. Biochem J 390:263-271.
Mizutani Y, Kihara A, Igarashi Y (2006) LASS3 (longevity assurance homologue 3) is a mainly testis-specific (dihydro)ceramide synthase with relatively broad substrate specificity. Biochem J 398:531-538.
Mongrand S, Morel J, Laroche J, Claverol S, Carde JP, Hartmann MA, Bonneu M, Simon-Plas F, Lessire R, Bessoule JJ (2004) Lipid rafts in higher plant cells: purification and characterization of Triton X-100-insoluble microdomains from tobacco plasma membrane. J Biol Chem 279 (35):36277-36286.
Mumberg D, Muller R, Funk M (1995) Yeast vectors for the controlled expression of heterologous proteins in different genetic backgrounds. Gene 156 (1):119-122.
Riebeling C, Allegood JC, Wang E, Merrill AH, Futerman AH (2003) Two mammalian longevity assurance gene (LAG1) family members, trh1 and trh4, regulate dihydroceramide synthesis using different fatty acyl-CoA donors. J Biol Chem 278 (44):43452-43459.
Roudier F, Gissot L, Beaudoin F, Haslam R, Michaelson L, Marion J, Molino D, Lima A, Bach L, Morin H, Tellier F, Palauqui JC, Bellec Y, Renne C, Miquel M, Dacosta M, Vignard J, Rochat C, Markham JE, Moreau P, Napier J, Faure JD (2010) Very-long-chain fatty acids

are involved in polar auxin transport and developmental patterning in Arabidopsis. Plant Cell 22 (2):364-375.
Spassieva SD, Markham JE, Hille J (2002) The plant disease resistance gene Asc-1 prevents disruption of sphingolipid metabolism during AAL-toxin-induced programmed cell death. Plant J 32 (4):561-572.
Sribney M (1966) Enzymatic synthesis of ceramide. Biochim Biophys Acta 125 (3):542-547.
Stone JM, Heard JE, Asai T, Ausubel FM (2000) Simulation of fungal-mediated cell death by fumonisin B1 and selection of *fumonisin B_1-resistant* (*fbr*) Arabidopsis mutants. Plant Cell 12 (10):1811-1822.
Ternes P, Feussner K, Werner S, Lerche J, Iven T, Heilmann I, Riezman H, Feussner I (2011) Disruption of the ceramide synthase LOH1 causes spontaneous cell death in Arabidopsis thaliana. New Phytol 192 (4):841-854.
Townley HE, McDonald K, Jenkins GI, Knight MR, Leaver CJ (2005) Ceramides induce programmed cell death in Arabidopsis cells in a calcium-dependent manner. Biol Chem 386 (2):161-166.
Venkataraman K, Riebeling C, Bodennec J, Riezman H, Allegood JC, Sullards MC, Merrill AH, Jr., Futerman AH (2002) Upstream of growth and differentiation factor 1 (uog1), a mammalian homolog of the yeast longevity assurance gene 1 (LAG1), regulates N-stearoyl-sphinganine (C18-(dihydro)ceramide) synthesis in a fumonisin B1-independent manner in mammalian cells. J Biol Chem 277 (38):35642-35649.
Wang H, Li J, Bostock RM, Gilchrist DG (1996) Apoptosis: A functional paradigm for programmed plant cell death induced by a host-selective phytotoxin and invoked during development. Plant Cell 8 (3):375-391.
Wu JX, Li J, Liu Z, Yin J, Chang ZY, Rong C, Wu JL, Bi FC, Yao N (2015) The Arabidopsis ceramidase AtACER functions in disease resistance and salt tolerance. The Plant journal : for cell and molecular biology 81 (5):767-780.
Zheng H, Rowland O, Kunst L (2005) Disruptions of the Arabidopsis Enoyl-CoA reductase gene reveal an essential role for very-long-chain fatty acid synthesis in cell expansion during plant morphogenesis. Plant Cell 17 (5):1467-1481.

CHAPTER 4

OVEREXPRESSION OF ARABIDOPSIS CERAMIDE SYNTHASES DIFFERENTIALLY AFFECTS GROWTH, SPHINGOLIPID METABOLISM, PROGRAMMED CELL DEATH, AND MYCOTOXIN RESISTANCE

Note: The results described here have been previously published, no text has been changed.

The citation is: Luttgeharm, K.D., M. Chen, A. Mehra, R.E. Cahoon, J.E. Markham, E.B. Cahoon (2015). "Overexpression of Arabidopsis ceramide synthases differentialy affects growth sphingolipid metabolism, programmed cell death, and mycotoxin resistance." Plant Physiology

4.1 INTRODUCTION

Ceramides are central intermediates in sphingolipid biosynthesis and mediators of programmed cell death in plants (Dunn et al. 2004; Saucedo-García et al. 2011; Ternes et al. 2011a). Ceramides are synthesized by ceramide synthase (or sphingosine N-acyl transferase; E.C. 2.3.1.24), which catalyzes the formation of an amide linkage between a sphingoid long chain base (LCB) and a fatty acid using LCB and fatty acyl-CoA substrates (Mullen et al. 2012).The LCB substrate can have two or three hydroxyl groups that are referred to as dihydroxy or trihydroxy LCBs, respectively (Chen et al. 2010). The fatty acyl-CoA substrates typically have chain lengths of C16 or C22 to C26 (Dunn et al. 2004). The latter are referred to as very long-chain fatty acids (VLCFA). The ceramide product of ceramide synthase is used primarily as a substrate for synthesis of either of the two major glycosphingolipids found in plants: glucosylceramides (GlcCer) and glycosyl inositolphosphoceramides (GIPC) (Chen et al. 2010). These glycosphingolipids are major structural components of the plasma membrane and other endomembranes of plant cells (Sperling et al. 2005; Verhoek et al. 1983). In this role, they contribute to membrane physical properties that are important for the ability of plant cells to adjust to environmental extremes and to Golgi-mediated protein trafficking of proteins, including cell wall metabolic enzymes and auxin transporters that underlie plant growth (Markham et al. 2011; Mortimer et al. 2013; Yang et al. 2012; Borner et al. 2005). Alternatively, ceramides can be converted to ceramide-1-phosphates by ceramide kinase activity (Liang et al. 2003). The interchange of ceramides between their free and phosphorylated forms has been linked to regulation of PCD and PCD-associated

resistance to pathogens via the hypersensitive response (Liang et al. 2003; Bi et al. 2014; Simanshu et al. 2014).

The *Arabidopsis thaliana* genome contains three ceramide synthase genes denoted *LOH1* (At3g25540), *LOH2* (At3g19260), and *LOH3* (At1g13580) (Markham et al. 2011; Ternes et al. 2011a). These studies suggest that LOH1 and LOH3 polypeptides are structurally related and catalyze primarily the amidation reaction of trihydroxy LCBs and CoA esters of VLCFA. The LOH2 polypeptide is more distantly related to LOH1 and LOH3 and catalyzes primarily the condensation of dihydroxy LCBs and C16 fatty acyl-CoAs (Chen et al. 2008; Markham et al. 2011; Ternes et al. 2011a). The ceramide products of LOH1 and LOH3 are most prevalent in GIPC, whereas the ceramide products of LOH2 are more enriched in GlcCer (Ternes et al. 2011b; Markham and Jaworski 2007; Chen et al. 2008). Similar to plants, the six ceramide synthase isoforms found in humans and mice have distinct specificities for their LCB and acyl-CoA substrates, and these specificities contribute to the formation of complex sphingolipids with differing structures and functions (Laviad et al. 2008; Mizutani et al. 2006; Venkataraman et al. 2002; Riebeling et al. 2003; Mizutani et al. 2005).

In Arabidopsis, *LOH1* and *LOH3* are partially redundant, but the combined activities of the corresponding polypeptides are essential for plant cell viability, as null double mutants of these genes are lethal (Markham et al. 2011). In contrast, mutants of *LOH2* are viable and display no apparent growth phenotype, which brings into question the role of LOH2 in plant performance (Markham et al. 2011; Ternes et al. 2011a). Overall, these observations indicate that sphingolipids with LOH1-/LOH3-derived trihydroxy LCBs and VLCFA ceramides are essential, but LOH2-derived dihydroxy

LCBs and C16-fatty acid ceramides are not required by plant cells. Related to this, LCB C-4 hydroxylase mutants that are deficient in trihydroxy LCBs accumulate elevated amounts of sphingolipids with dihydroxy LCB- and C16 fatty acid-containing ceramides via LOH2 activity (Chen et al. 2008). These mutants are severely impaired in growth and do not transition from vegetative to reproductive growth (Chen et al. 2008).

Ceramide synthases are known targets for competitive inhibition by sphingosine analog mycotoxins, including fumonisin B_1 (FB_1) and AAL toxin, produced by pathogenic fungi such as various *Fusarium* species and *Alternaria alternata* f. sp. Lycopersici (Abbas et al. 1994). Inhibition of ceramide synthase results in the accumulation of LCBs that are believed to trigger PCD and result in cytotoxicity (Abbas et al. 1994). In studies of *LOH* mutants, treatment of Arabidopsis seedlings with FB_1 resulted in not only increases in LCBs but also increases in C16 FA-containing sphingolipids and decreases in VLCFA-containing sphingolipids (Abbas et al. 1994; Markham et al. 2011; Saucedo-García et al. 2011; Ternes et al. 2011a). The interpretation of this observation was that FB_1 preferentially inhibits LOH1 and LOH3 ceramide synthases, but inhibits LOH2 ceramide synthase to a lesser extent (Markham et al. 2011; Ternes et al. 2011a).

Given the findings from Arabidopsis mutants that LOH1 and LOH3 ceramide synthases have distinct substrate specificities and sensitivity to FB_1 relative to LOH2, we hypothesized that overexpression of each of these ceramide synthases would lead to the production of different sphingolipid compositions as well as different growth phenotypes. This report details experiments designed to test this hypothesis. Among the results presented is a large divergence in the effects of overexpression of *LOH1* and *LOH3*

versus *LOH2* on the growth of Arabidopsis. *LOH2* overexpression was also shown to result in sphingolipid compositional, growth, and physiological phenotypes that closely mimic those previously observed in LCB C-4 hydroxylase mutants (Chen et al., 2008).

4.2 RESULTS

4.2.1 OVEREXPRESSION OF LOH1, LOH2, AND LOH3 IN ARABIDOPSIS RESULTS IN DIFFERENTIALLY ALTERED GROWTH

LOH1, *LOH2*, or *LOH3* cDNAs were expressed under control of the CaMV35S promoter in wild-type (Col-0) Arabidopsis. From up to ten independent transgenic lines generated for each cDNA, three lines were selected for further characterization based on confirmed overexpression of the cDNAs as determined by qRT-PCR or Northern blot analysis (Figure 4.1). These lines were taken to homozygosity prior to quantitative measurement of growth and sphingolipid profiles.

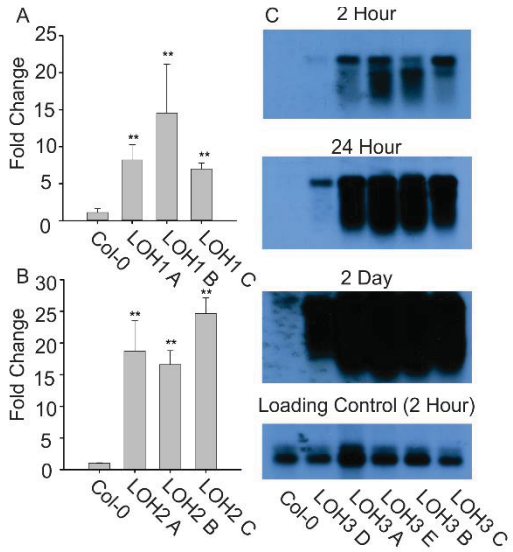

Figure 4.1 *Expression level of LOH1, LOH2, and LOH3 in leaves of independent overexpression lines.* qPCR results for LOH1 (A) and LOH2 (B) overexpression lines are shown. Col-0 expression set to 1 with *LOH1* and *LOH2* expression shown as the fold change in relation to Col-0. All data shown as the average of three independent plants ± SD (** $P < 0.01$; LOH1 A, $P = 0.00$; LOH1 B, $P = 0.00$, LOH1 C $P = 0.00$; LOH2 A, $P = 0.00$; LOH2 B, $P = 0.00$; LOH2 C, $P = 0.00$). Northern blot shown for the overexpression of LOH3 (C) for 3 different exposure times with UBC shown as a loading control.

Overexpression of *LOH1* and *LOH3* resulted in a significant increase in plant size as determined by measurement of total dry weight of soil-grown rosettes and hydroponically-grown roots at one month post germination. These results contrasted with *LOH2* overexpression which resulted in severe dwarfing and reduced root mass compared to wild-type plants (Figure 4.2A and B). To determine if the difference in plant size was caused by an increase in the number of cells, root meristem cell numbers were determined for 10 day old representative *LOH1*-, *LOH2-,* and *LOH3*-overexpressing lines. *LOH1* and *LOH3* overexpression resulted in a significant increase in cell number of root meristems, while *LOH2* overexpression resulted in a significant decrease in cell

number of root meristems (Average number of cells ± S.E., n = 10, Col-0 = 33.9 ± 1.9, LOH1 B = 39.4 ± 1.7, LOH2 A = 24.6 ± 1.4, LOH3 C = 47 ± 2.8, Figure 4.3A). Representative root meristems are shown in Figure 4.4A-D. These results indicate that differences in growth can be attributed, at least in part, to increased cell division in *LOH1*- and *LOH3*-ovexpression lines, and decreased cell division in *LOH2*-overexpression lines.

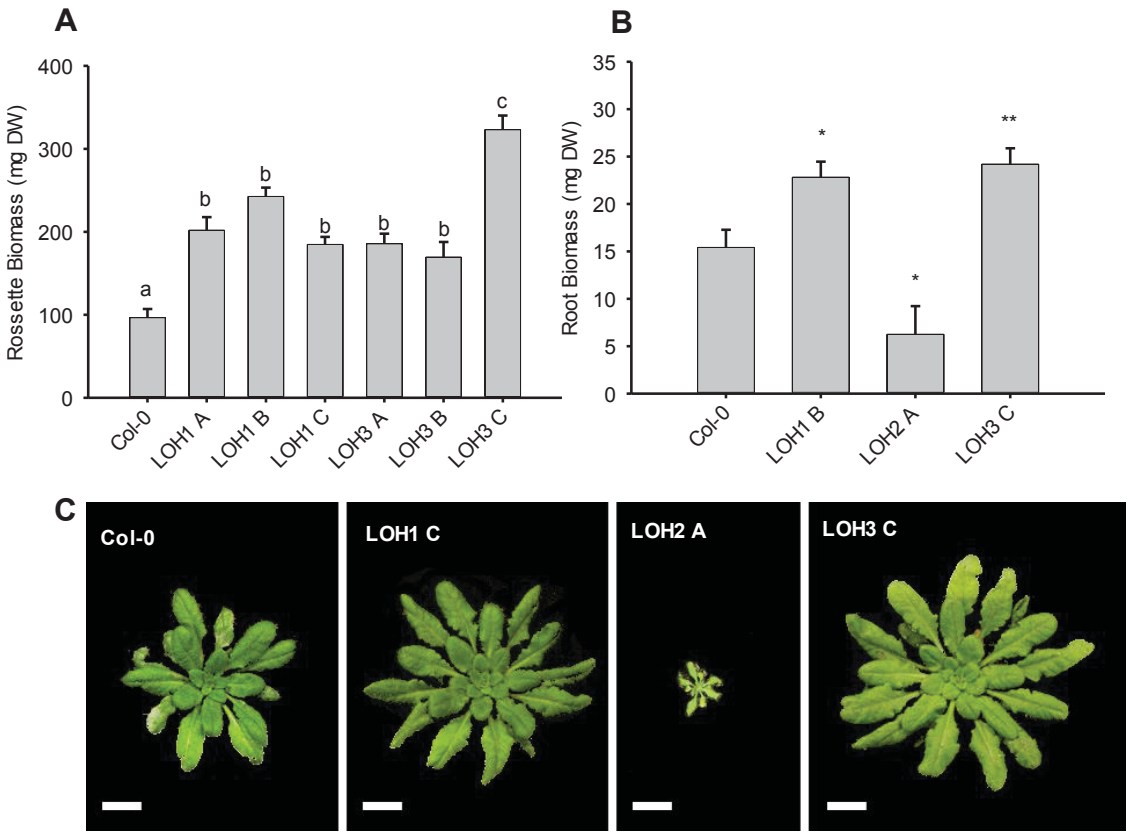

Figure 4.2 *Comparison of rosette and root biomasses in ceramide synthase overexpression lines.* (A) Dry weights of rosettes from four-week old plants are presented as the average of independent plants [n= 23 for wild-type (Col-0) and n = 12 for all overexpression lines, lines with the same letter are not significantly different at $P < 0.05$ by Tukey's test] ± SE ($P = 0.00$, $P = 0.00$, $P = 0.00$, $P = 0.00$, $P = 0.00$, $P = 0.00$ for LOH1 A, LOH1 B, LOH1 C, LOH3 A, LOH3 B, LOH3 C respectively compared to Col-0). (B) Dry weights of roots from hydroponically grown plants are presented as the average of independent plants [n = 6 for wild-type (Col-0), n = 3 for LOH1 B, n = 3 LOH2 A, n = 7 for LOH3 C; * $P < 0.05$, ** $P < 0.01$; LOH1 B, $P = 0.04$; LOH2 A, $P = 0.03$; LOH3 C, $P = 0.005$)]. Data presented in A and B were obtained from independent transgenic events as indicated in the line nomenclature. (C) Representative rosettes from overexpression lines of LOH1, LOH2, and LOH3. Scale bar represents 2 cm.

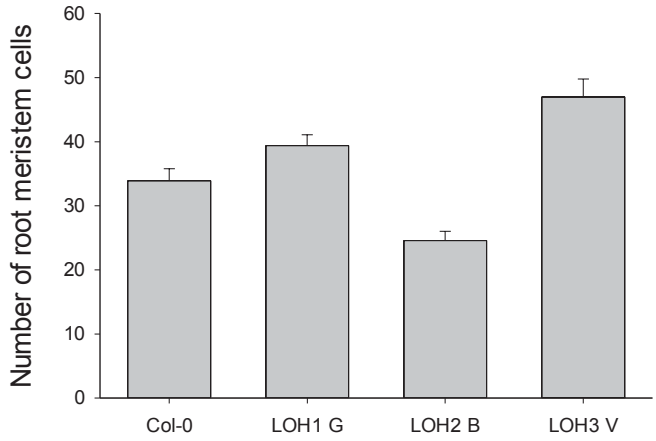

Figure 4.3 *Comparison of epidermal cell numbers in root meristematic region of ceramide synthase overexpression lines*. Epidermal cell numbers were counted in the root meristems of ten plants from wild-type (Col-0) and representative overexpression lines. Data shown is the average (n=10) ± SE (* $P < 0.05$, ** $P < 0.01$; $P = 0.044$, LOH1 B; $P = 0.00$ LOH2 A; $P = 0.0011$, LOH3 C)

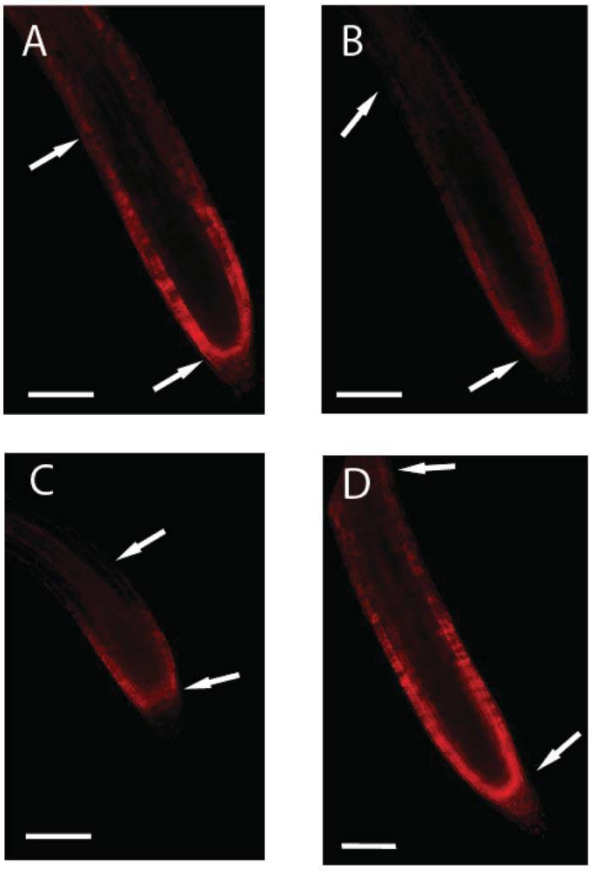

Figure 4.*4* *Representative root meristem region for measurement of cell numbers* in wild-type (Col-0) (A) and LOH1 B (B), LOH2 A (C), and LOH3 C (D) overexpression lines. Arrows indicate the meristematic region used for counting of cell numbers. Scale bar represents 100 μm.

4.2.2 LOH1, LOH2, AND LOH3 OVEREXPRESSION IN ARABIDOPSIS DIFFERENTIALLY ALTERS SPHINGOLIPID PROFILES

Sphingolipid profile analyses of *LOH2* overexpression lines revealed ~2.5-3.5 fold increase in overall total sphingolipids, almost exclusively comprised of molecular species with ceramide backbones containing dihydroxy LCBs and C16 fatty acids (Figure 4.5A). In addition, ~90% of sphingolipids contained C16 fatty acids in *LOH2*-

overexpression plants. By comparison, ~20% of sphingolipids contained C16 fatty acids in wild-type Arabidopsis (Figure 4.5B). The increase in dihydroxy/C16 fatty acid sphingolipids was not limited to any single class but found in the Cer, hCer, GlcCer, and GIPC fractions (Figure 4.6). The amount of trihydroxy LCB-containing sphingolipids did not change in any of LOH2 overexpression lines. In contrast to results from *LOH2*-overexpresion lines, *LOH1* and *LOH3* overexpression resulted in little change in total sphingolipid content and composition of plants relative to wild-type controls, although small, but significant reductions in C16 fatty acid-containing sphingolipids were detected as a result of minor changes throughout the sphingolipidome (Figure 4.5; Figure 4.7).

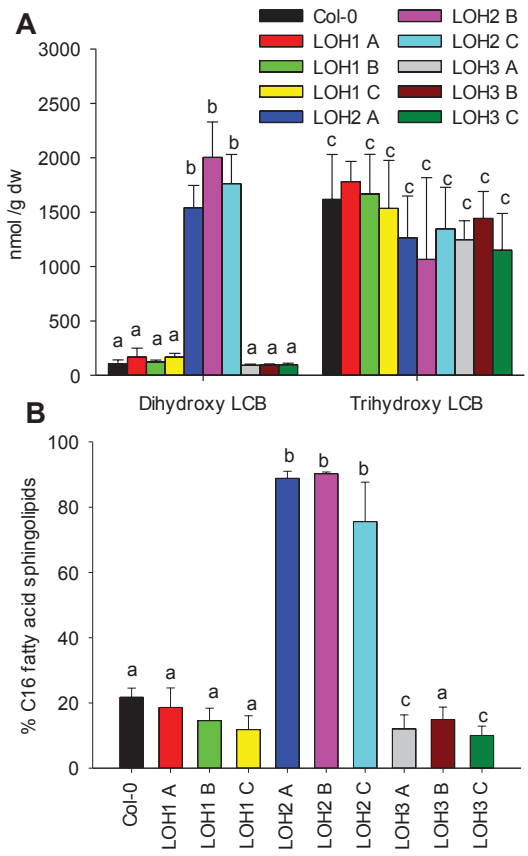

Figure 4.5 *Comparison of concentrations of long-chain bases (LCBs) and C16 fatty acids (FA) in total sphingolipids from four week old rosettes of wild-type plants (Col-0) and LOH1, LOH2, and LOH3 overexpression lines*. Shown in A is a comparison of concentrations of total dihydroxy and trihydroxy LCBs in Col-0 and plants from independent transgenic lines, as indicated by the line nomenclature. Data presented are from measurements of total LCBs measured by HPLC following hydrolysis of sphingolipids in rosettes. Only LOH2 overexpression lines showed any differences in LCB levels. Data shown are the average of measurements of three independent plants ± SD and lines with the same letter are not significantly different at $P < 0.05$ by Tukey's test ($P = 0.00$ for all LOH2 lines compared to Col-0 by Tukey's Test). (B) Percentage of total sphingolipids containing a C16 FA in ceramide backbones as determined by LC-ESI-MS/MS. Measurements presented are the average from three individual plants ± SD from independent LOH1, LOH2, and LOH3 overexpression lines, lines with the same letter are not significantly different at $P < 0.05$ by Tukey's test ($P = 0.00$ for all LOH2 lines, $P = 0.038$, LOH3 A; $P = 0.014$, LOH3 C compared to Col-0 by Tukey's Test)

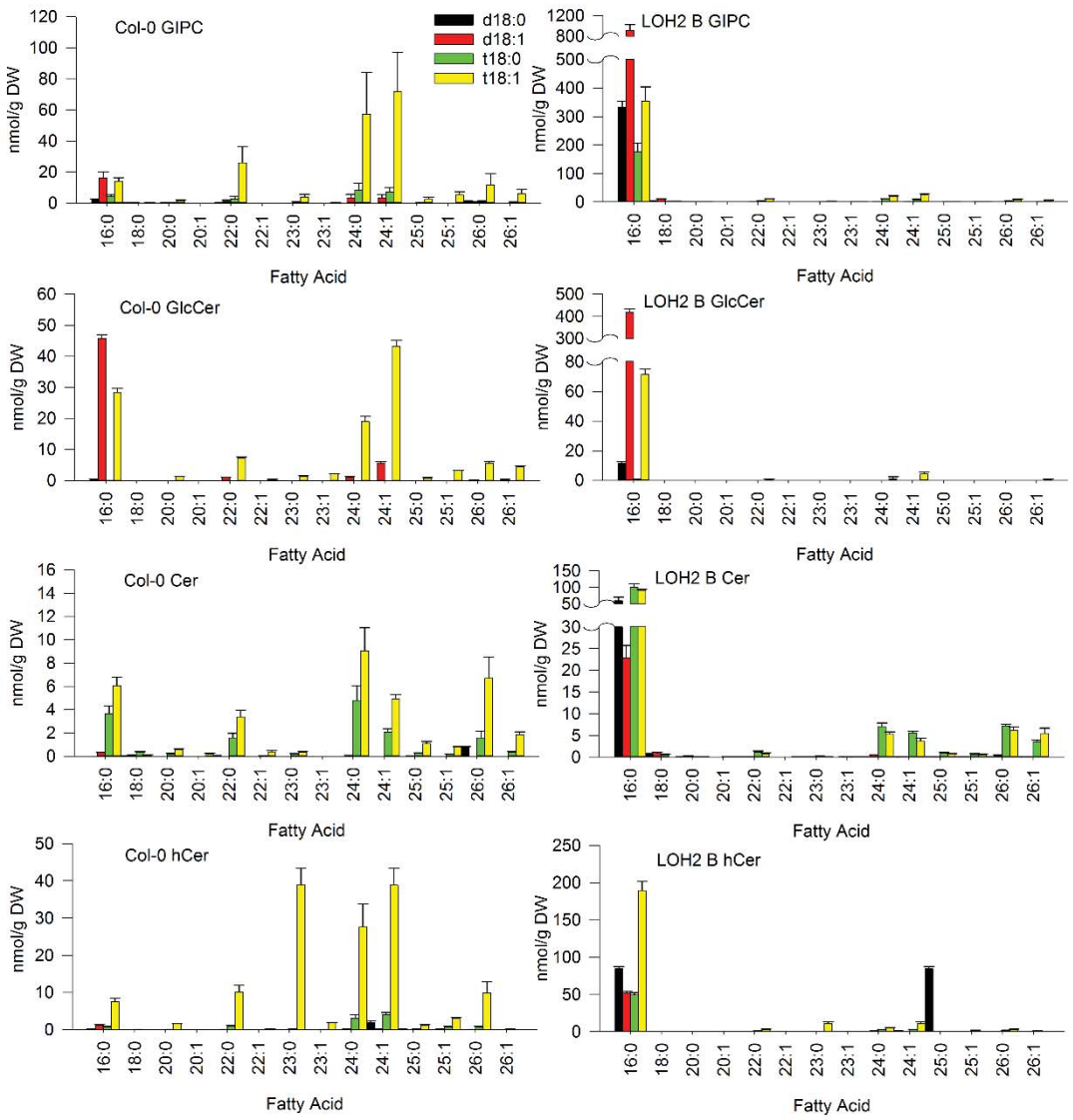

Figure 4.6 *Sphingolipidome of wild-type (Col-0) and LOH2 overexpression lines.* The content of molecular species of GIPC, GlcCer, Cer, and hCer for Col-0 and a representative LOH2 line are shown. The data presented are the LCB (y-axis) and fatty acid (x-axis) concentrations of molecular species as determined by LC-ESI-MS/MS analyses Data shown as the average of measurements of rosettes from four week-old plants (n=3 biological replicates ± SD).

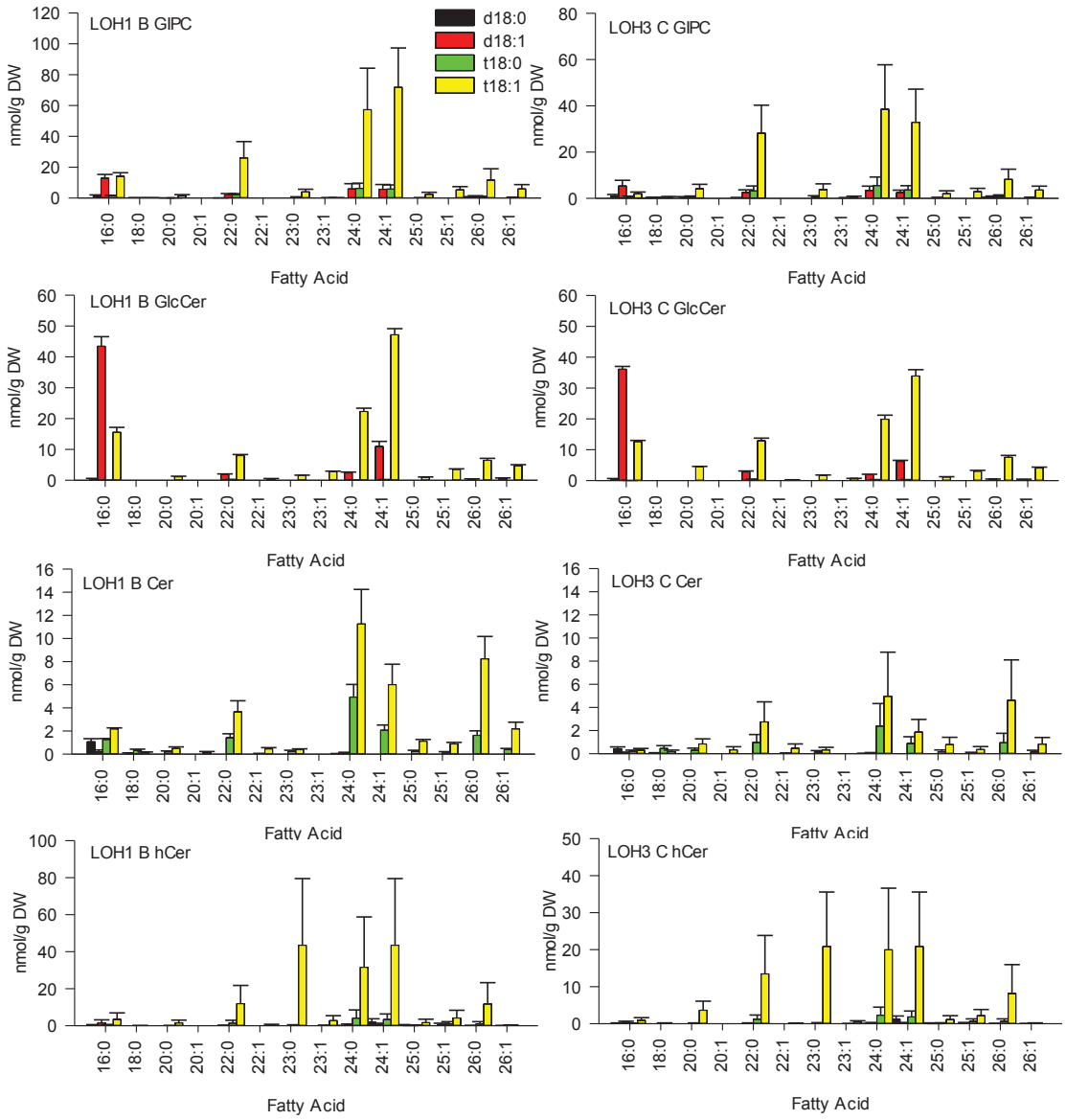

Figure 4.7 *Sphingolipidome of LOH1 and LOH3 overexpression lines.* The content of molecular species of GIPC, GlcCer, Cer, and hCer for representative LOH1 and LOH3 lines are shown. The data presented are the LCB (y-axis) and fatty acid (x-axis) concentrations of molecular species as determined by LC-ESI-MS/MS analyses Data shown as the average of measurements of rosettes from four week-old plants (n=3 biological replicates ± SD).

4.2.3 LOH2 OVEREXPRESSION ENHANCES SALICYLIC ACID PRODUCTION AND INDUCES HYPERSENSITIVE RESPONSE-TYPE PROGRAMMED CELL DEATH-RELATED GENES

The phenotypes described above for *LOH2*-overexpression lines, including reduced plant size and enhanced accumulation of sphingolipids, closely resemble those previously reported in mutants and RNAi suppression lines of the LCB C-4 hydroxylase genes (Chen et al. 2008). Another notable feature of the LCB C-4 hydroxylase *sbh-1sbh-2* mutant was the detection of constitutive upregulation of a number of genes associated with hypersensitive response (HR)-type programmed cell death (PCD) (Chen et al. 2008). RT-PCR was conducted to determine if constitutive upregulation of HR-type PCD marker genes is also detectable in *LOH2*-overexpression lines. Similar to patterns observed in the *sbh-1sbh-2* mutant (Chen et al. 2008), HR-type PCD marker genes displayed constitutive upregulation in the *LOH2*-overexpression lines. Upregulation of the expression of these PCD marker genes, however, was not detected in wild-type, *LOH1*- or *LOH3*-overexpression lines (Figure 4.8A and Figure 4.9). Accumulation of salicylic acid (SA) in *LOH-2* overexpression lines was also indicative of HR-type PCD. Consistent with this, a 16-fold increase in SA levels was detected in the *LOH2*-overexpression line (Figure 4.8B). Notably, *LOH1*- and *LOH3*-overexpression lines had SA concentrations three-fold higher for LOH1 B and LOH3 C, respectively ($P = 0.007$, LOH1 B; $P = 0.000$ LOH3 C) compared to those detected in wild-type plants.

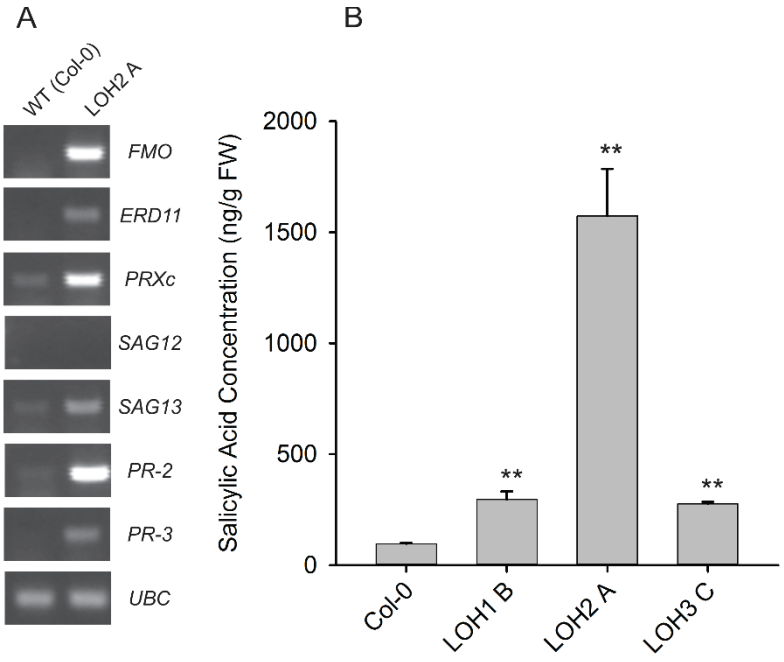

Figure 4.8 *Expression of marker genes for hypersensitive response programmed cell death (PCD) in wild-type (Col-0) and LOH2 overexpression lines and comparison of salicylic acid concentrations in wild-type (Col-0) and LOH1, LOH2, and LOH3 overexpression lines.* (A) RT-PCR was conducted to assess expression of PCD marker genes in leaves of four week-old Col-0 and a representative *LOH2* overexpression line. The PCD marker genes analyzed are *FMO* (At1g19250), *ERD11* (At1g02930), *PRXc* (At3g49120), *SAG13* (At2g29350), *SAG12* (At5g45890), *PR2* (At3g57260), and *PR3* (At3g12500). The gene for ubiquitin conjugating enzyme *UBC* (At5g25760) was used as a positive control. (B) Salicylic acid concentrations were measured in leaves of four week old *LOH1*, *LOH2*, and *LOH3* overexpression lines. Data presented are the average of measurements from three independent plants for each line ± SE (** $P < 0.01$; $P = 0.002$, LOH2 A).

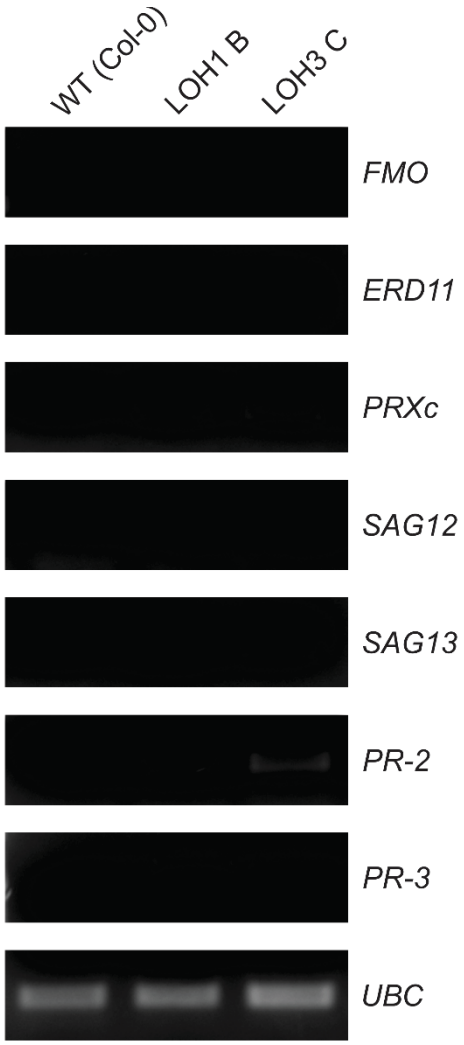

Figure 4.9 *Expression of marker genes for hypersensitive response programmed cell death (PCD) in wild-type (Col-0), LOH1- and LOH3-overexpression lines.* RT-PCR was conducted to measure expression of PCD marker genes in leaves of four week-old Col-0, representative *LOH1*- and *LOH3*-overexpression lines. The PCD marker genes analyzed are *FMO* (At1g19250), *ERD11* (At1g02930), *PRXc* (At3g49120), *SAG13* (At2g29350), *SAG12* (At5g45890), *PR2* (At3g57260), and *PR3* (At3g12500). The gene for ubiquitin conjugating enzyme *UBC* (At5g25760) was used as a positive control.

4.2.4 LOH1, LOH2, AND LOH3 OVEREXPRESSING PLANTS DISPLAYED DIFFERENT PHENOTYPES WHEN GROWN ON FUMONISIN B_1 (FB_1)

Ceramide synthases are known targets for inhibition by the PCD-inducing mycotoxin. It is generally believed that FB_1 cytotoxicity is associated with the accumulation of free long-chain bases (Abbas et al. 1994). Given that FB_1 is regarded as being a competitive inhibitor of ceramide synthases, we hypothesized that ceramide synthase overexpression would reduce the cytotoxicity of FB_1. To test this, seedlings of wild-type Arabidopsis (Col-0) and overexpression lines of *LOH1*, *LOH2*, or *LOH3* were germinated on media containing 0.5 μM FB_1 and grown for one month. In contrast to wild-type controls, plants expressing *LOH2* and *LOH3* were viable on 0.5 μM of FB_1, whereas *LOH1*-overexpressing plants displayed severely reduced viability similar to wild-type control plants on 0.5 μM of FB_1 (Figure 4.10A). Consistent with these observations, *LOH2* and *LOH3*-overexpressing plants accumulated ~25% of the free and phosphorylated long-chain base concentrations of wild-type plants grown on 0.5 μM of FB_1 (Figure 4.10B). Total free and phosphorylated long-chain base concentrations in *LOH1*-overexpressing plants were ~50% of those of wild-type plants in the FB_1 treatment (Figure 4.10B). These results suggest that LOH1 ceramide synthase is more sensitive to inhibition by FB_1 than LOH2 and LOH3 ceramide synthases. Sphingolipid compositional analysis of wild-type seedlings grown on plates supplied with FB_1 showed increases primarily in C16 fatty acid-containing sphingolipids, including C16 fatty acid-containing ceramides, indicating a preferential inhibition of LOH1 and/or LOH3 ceramide synthases by FB_1 (Figure 4.11). Notably, accumulation of ceramide with C16 fatty acids was strongly suppressed in *LOH3*-overexpressing plants relative to wild-type and *LOH1*- and

LOH2-overexpressing plants. Instead, ceramides in *LOH3*-overexpression lines were primarily enriched in VLCFA (Figure 4.11).

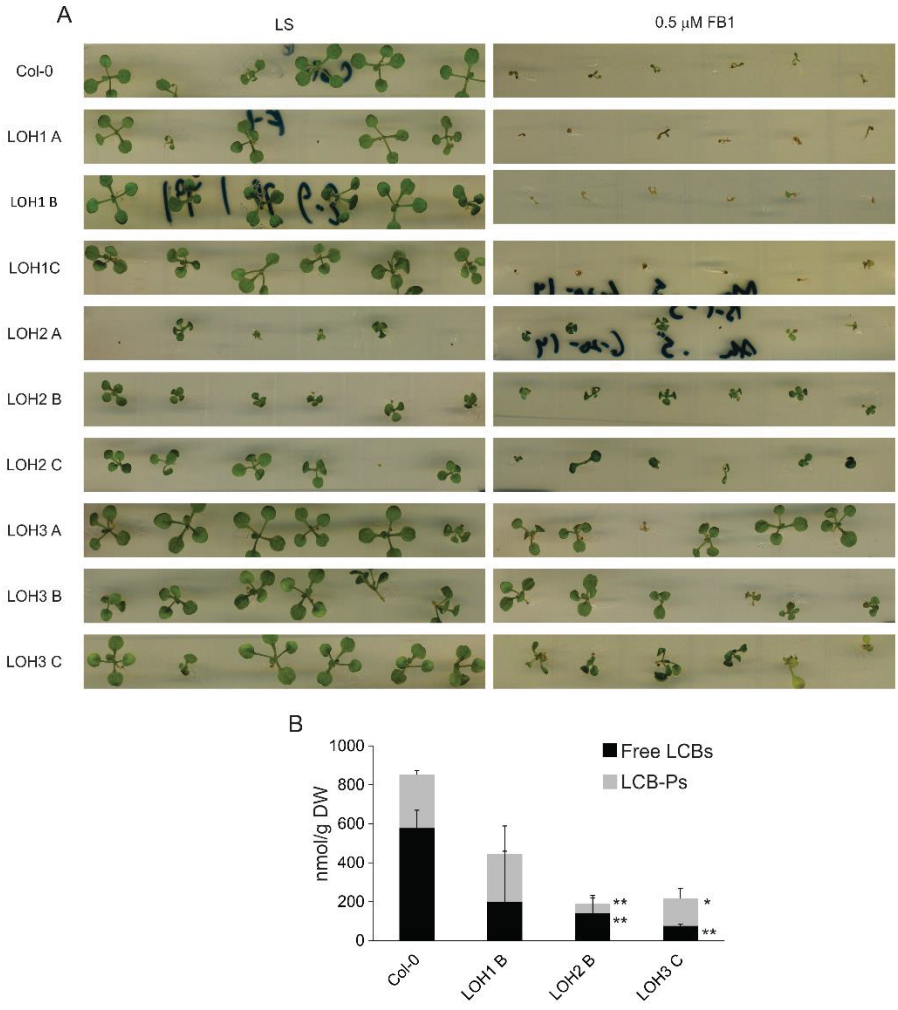

Figure 4.10 *Comparison of responses of wild-type and ceramide synthase overexpression lines to the mycotoxin fumonisin B_1 (FB_1).* (A) Comparison of sensitivities of wild-type (Col-0) and selected *LOH1*, *LOH2*, and *LOH3* overexpression lines to FB_1. As shown, plants were grown for four weeks on LS media ± 0.5 µM FB_1. (B) Free long-chain bases (LCBs) and LCB-phosphates (LCB-Ps) were measured in four week-old plants harvested from FB_1-containing plates. Data shown are the average of three biological replicates ± SD for Col-0 and *LOH1*, *LOH2*, and *LOH3* overexpression lines. (* $P < 0.05$, ** $P < 0.01$; Free LCBs—LOH2 B $P = 0.00$, LOH3 C $P = 0.00$; LCB-Ps—LOH2 B $P = 0.00$, LOH3 C $P = 0.01$).

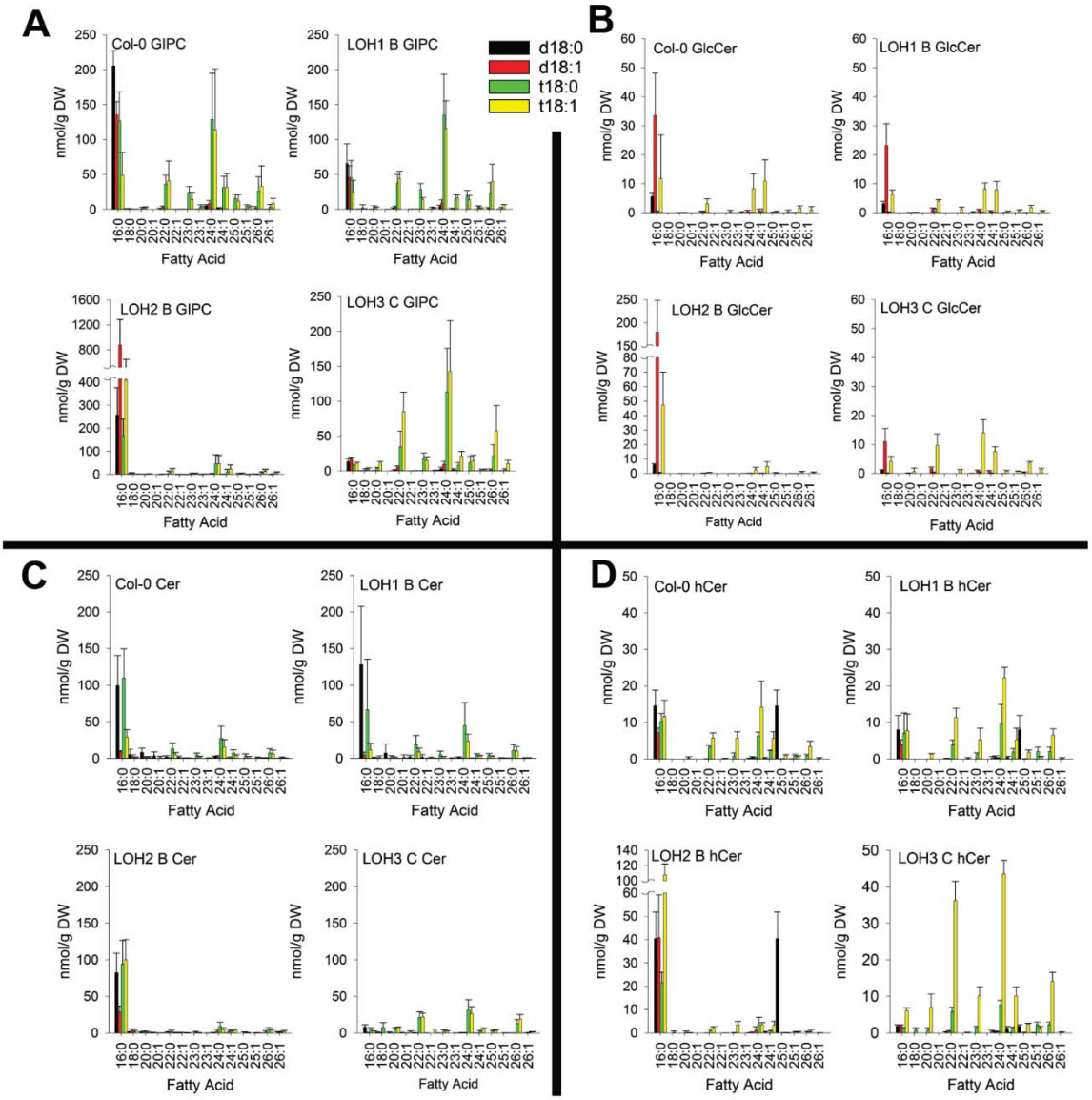

Figure 4.11 *Sphingolipidome of fumonisin B_1 (FB_1)-treated wild-type and ceramide synthase overexpression lines*. The content of molecular species of GIPC, GlcCer, Cer, and hCer for wild-type Col-0 and representative *LOH1*, *LOH2*, and *LOH3* lines are shown. The data presented are the LCB (*y-axis*) and fatty acid (*x-axis*) concentrations of molecular species as determined by LC-ESI-MS/MS analyses Data shown as the average of measurements of rosettes from four week-old FB_1-treated plants (n=3 biological replicates ± SD).

4.3 DISCUSSION

The results presented here demonstrate that enhanced expression of each of the three Arabidopsis ceramide synthase genes has widely differing effects on growth, sphingolipid metabolism, and response to the PCD-inducing mycotoxin FB_1. Most strikingly, *LOH2* overexpression resulted in severe dwarfing and accumulation of sphingolipids enriched in C16 fatty acids and dihydroxy LCBs (Figure 4.12). Conversely, overexpression of *LOH1* and *LOH3*, in particular, resulted in plants with significantly increased biomass relative to wild-type control plants, but little, if any, alteration in sphingolipid composition or content on a tissue mass basis (Figure 4.12). In addition, *LOH2* overexpression was accompanied by constitutive upregulation of HR-type PCD marker genes and strongly enhanced accumulation of salicylic acid. Furthermore, plants overexpressing *LOH2* and *LOH3* displayed resistance to FB_1 and had reduced accumulation of free LCBs and LCB-Ps in response to FB_1 compared to wild-type controls. *LOH1* overexpressing plants, in contrast, displayed sensitivity to FB_1 and although, these lines accumulated ~50% lower amounts of free LCBs and LCB-Ps compared to the wild-type plants, levels of these metabolites were ≥two-fold higher than those in *LOH2*- and *LOH3*-overexpression plants grown on FB_1-containing media.

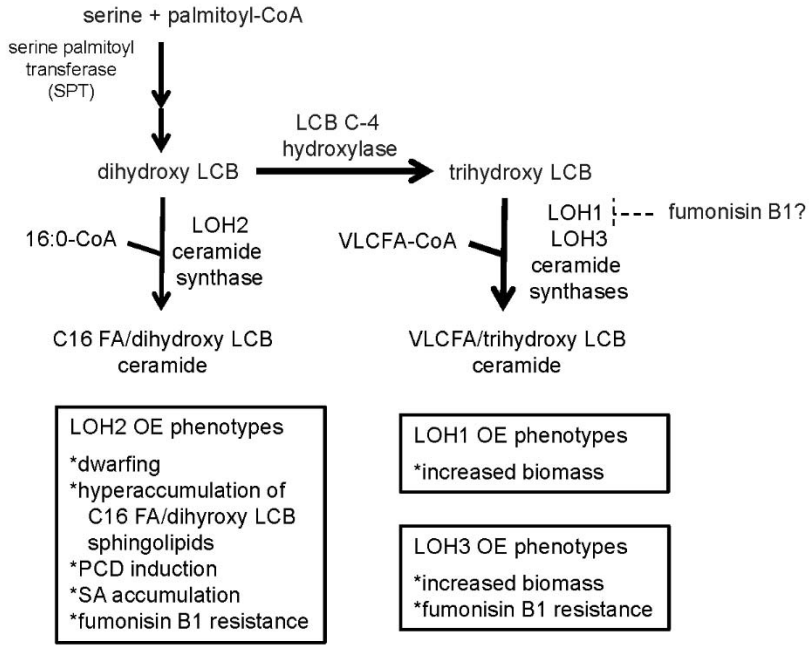

Figure 4.12 *Model of ceramide synthesis and biochemical and physiological outcomes from overexpression of LOH1-, LOH2-, and LOH3-encoded ceramide synthases*. Dihydroxy long-chain baes (LCBs) originating from serine palmitoyltransferase (SPT) activity can be linked to C16-fatty acyl-CoA substrates via LOH2 ceramide synthase activity. Alternatively, dihydroxy LCBs can be hydroxylated by LCB C-4 hydroxylase. The resulting trihydroxy LCBs can then be used as a substrates for LOH1 and LOH3 ceramide synthases for linkage with very long-chain fatty acyl (VLCFA)-CoA substrates.

The nearly identical phenotypes for LCB C-4 hydroxylase suppression, described previously (Chen et al. 2008), and LOH2 ceramide synthase overexpression, described here, are consistent with these enzymes catalyzing competing reactions for the metabolism of dihydroxy LCBs (Figure 4.12). Based on these findings, functional LCB C-4 hydroxylation combined with activities of LOH1 and LOH3 ceramide synthases are sufficient for channeling LCBs into ceramides enriched in VLCFA and trihydroxy LCBs

that are capable of supporting growth. It is likely that the high accumulation of ceramides with C16 fatty acids and dihydroxy LCBs in the *LOH2*-overexpression lines disrupts the growth-supporting roles of LOH1 and LOH3 ceramide synthase-derived sphingolipids in processes such as Golgi trafficking. Given that LOH2 ceramide synthase products do not support growth and their accumulation induces PCD, it is unclear what the physiological significance of this enzyme is. Consistent with this, *LOH2* mutants do not display phenotypic defects when maintained under typical growth conditions (Markham et al. 2011; Ternes et al. 2011a). Ultimately, the composition of ceramides in Arabidopsis reflects the combined activities of LOH1, LOH2, and LOH3 ceramide synthases. Publically available data from microarray studies, indicate that *LOH2* is expressed in vegetative organs at similar levels as *LOH1* (Figure 4.13). *LOH3* is also expressed in vegetative organs but at levels lower than *LOH1* and *LOH2* (Figure 4.13). Despite the nearly equal expression of *LOH1* and *LOH2*, sphingolipids containing C16 fatty acids arising from LOH2 ceramide synthase activity account for only 20% of total sphingolipid content in rosettes of wild-type plants (Figure 4.5B). One possibility to explain this apparent discrepancy in the production of *LOH2*-derived ceramides versus the expression levels of this gene is the competition between the LOH2 ceramide synthase and the LCB C-4 hydroxylase for dihydroxy LCBs. Under normal conditions, greater activity of LCB C-4 hydroxylase may favor the biosynthesis of trihydroxy LCBs that are subsequently incorporated into ceramides by LOH1 and LOH3 ceramide synthases. In such a metabolic scenario, LOH2 ceramide synthase activity may serve as a "safety valve" to sequester excess LCBs into ceramides as a less cytotoxic form than free LCBs. Supportive of this idea, *LOH2* overexpression resulted in the accumulation of

C16 fatty acid/dihydroxy LCB-containing ceramides, but it reduced LCB accumulation that was associated with enhanced resistance to FB_1 (Figure 4.10B; Figure 4.11C). These findings also suggest that FB_1 toxicity is due primarily to accumulation of free LCBs rather than the accumulation of C16 fatty acid/dihydroxy LCB ceramides. Also consistent with the "safety valve" function of the LOH2 ceramide synthase is the apparent relative resistance of this enzyme to FB_1 inhibition, relative to the LOH1 ceramide synthase (Figure 4.10A).

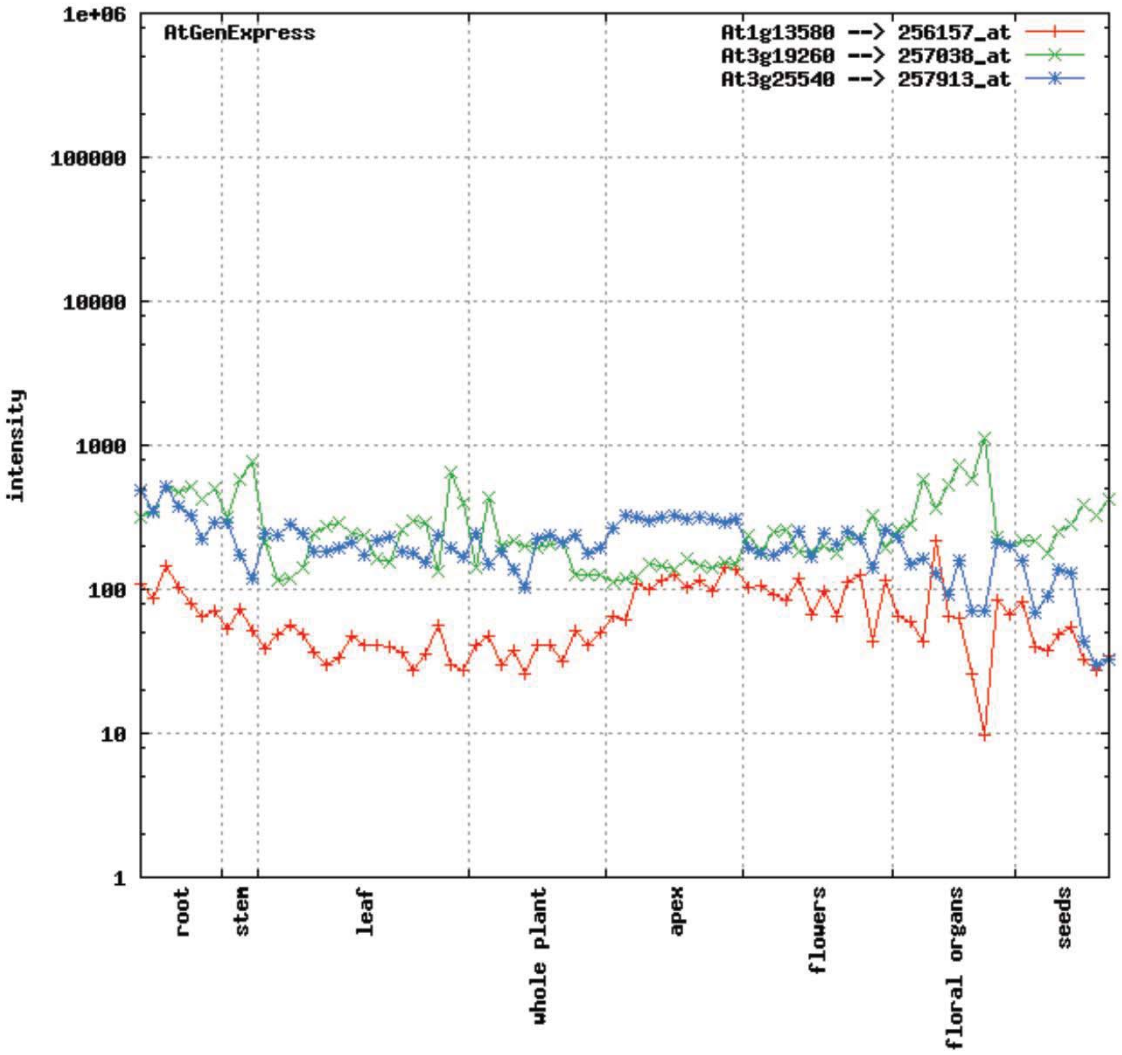

Figure 4.13 *Gene expression levels for LOH1 (At3g25540), LOH2 (At3g19260), and LOH3 (At1g13580) in various tissues.* *LOH1* and *LOH2* are expressed at relatively the same levels throughout most tissues with the exception of reproductive tissues where *LOH2* is expressed at much higher levels. *LOH3* is consistently expressed at the lowest level of the three. Gene expression analysis from (Schmid et al. 2005).

Another notable finding from these studies is the ability of *LOH1* and *LOH3* overexpression to promote increased biomass of Arabidopsis plants (Figure 4.2). Despite upregulation of *LOH1* and *LOH3* expression, the plants did not have significantly increased levels of sphingolipids on a mass basis (Figure 4.7). Similarly, it was previously shown that plants with partial suppression of sphingolipid synthesis are dwarfed, but did not have reduced amounts of sphingolipids on a mass basis (Chen et al. 2006). From these findings, it was proposed that sphingolipid production limits growth (Chen et al. 2006). Our current findings suggest that the converse is also true: enhanced production of ceramides with VLCFA and trihydroxy LCBs can promote growth. An understanding of the mechanism for this growth promotion and possible translation of these finding for engineering of crops with increased biomass requires further study. It is known that sphingolipids with VLCFA are important for Golgi trafficking of proteins to the plasma membrane that are associated with plant growth, including cell wall biosynthetic enzymes and auxin influx and efflux carriers (Bach et al. 2011; Markham et al. 2011). One possibility is that enhanced production of sphingolipids with VLCFA drives increased rates of Golgi trafficking in Arabidopsis cells. Sphingolipids with VLCFA resulting from LOH1 and LOH3 ceramide synthase activities also contribute to cell plate or phragmoplast formation during cell division (Bach et al. 2011; Molino et al. 2014). Consistent with this, our findings show that enhanced growth of *LOH1* and *LOH3* overexpression plants is due in part to increased cell division. It is also possible that enhanced growth results, in part, from increased cell expansion due to targeting of sphingolipids with LOH1 and LOH3 ceramide synthase-derived ceramides to membranes, such as tonoplast and plasma membrane, that contribute directly to cell

expansion. Clarification of this possibility awaits reports of sphingolipid compositional profiling of specific membrane fractions in plant cells.

An additional observation from these studies is that the structural distinction of GlcCer and GIPC ceramides typically found in plants can be altered by *LOH2* overexpression. In Arabidopsis and other plants, Glcer are enriched in C16 fatty acid/dihydroxy LCB ceramides derived from LOH2 ceramide synthase and GIPC are enriched in VLCFA/trihydroxy LCB ceramides derived from LOH1 and LOH3 ceramide synthases (Markham et al. 2006). However, ceramides of both GlcCer and GIPC contain predominantly C16 fatty acids and dihydroxy LCBs upon *LOH2* overexpression, a phenotype also observed in LCB C-4 hydroxylase mutants (Chen et al. 2008). This observation may reflect broad ceramide substrate specificity of inositol phosphorylceramide (IPC) synthases, the enzymes that catalyze the initial reaction in GIPC synthesis (Mina et al. 2010; Wang et al. 2008), or impaired sorting of specific ceramides between ER and Golgi bodies, the primary site of IPC and GIPC synthesis (Rennie et al. 2014; Wang et al. 2008), in response to *LOH2* overexpression. This point cannot be currently addressed due to lack of published information on substrate specificities of IPC synthases and ER-Golgi ceramide sorting mechanisms.

Although LOH1 and LOH3 ceramide synthases share nearly 80% amino acid sequence identity, *LOH1* and *LOH3* expression resulted in distinct differences in FB_1 sensitivity. In three *LOH1* and *LOH3* independent overexpression lines, *LOH1* overexpression resulted in sensitivity to 0.5 μM FB_1, but *LOH3* overexpression resulted in resistance to 0.5 μM FB_1 (Figure 4.10). In addition, accumulation of LCBs and LCB-Ps was more strongly suppressed in the LOH3 C line versus the LOH1 B line, and in

contrast to the LOH1 B line, little accumulation of C16 fatty acid-containing ceramides was detected in the LOH3 C line (Figure 4.10; Figure 4.11). Based on these findings, one possibility is that the LOH3 ceramide synthase, like the LOH2 ceramide synthase, is considerably less sensitive to FB_1 inhibition than the LOH1 ceramide synthase. Differential sensitivity to FB_1 among the LOH1, 2, and 3 ceramide synthases may also explain why GIPC levels are increased following FB_1 treatment of wild-type plants (Figure 4.11A). In this case, the predominant GIPC species accumulated were from LOH2 ceramide synthase-type activity. We are currently examining the hypothesis that LOH1, LOH2, and LOH3 ceramide synthases are differentially inhibited by FB_1 through *in vitro* assay of recombinant forms of each enzyme, in the absence or presence of FB_1.

Overall, these findings complement those from previous characterizations of LOH1, LOH2, and LOH3 ceramide synthase knock-out mutants (Markham et al. 2011; Ternes et al. 2011a) and show that increased expression of the corresponding enzymes can have profound effects on growth, sphingolipid metabolism, PCD induction, and sensitivity to sphinganine-analog mycotoxins. These findings also provide insights into potential targets for crop improvement by tailoring of sphingolipid biosynthesis.

4.4 MATERIALS AND METHODS

All chemicals, unless otherwise stated, were purchased from Sigma-Aldrich (Saint Louis, MO). All statistical analyses, unless otherwise stated, are represented as the P value of the Student's t-test. ANOVA and Tukey's Test were performed using the SigmaStat function of SigmaPlot 13.0.

4.4.1 PLANT GROWTH CONDITIONS

Plants were grown on Farfard soil mix (Hummert International, Saint Louis, MO) or surface sterilized in 1:1 (v/v) bleach/water for 10 min followed by washing three times with sterile water and grown on Linsmaier Skoog (LS; Phytotechnology Laboratories, Shawnee Mission, KS) agar plates. Plates were vernalized at 4°C for 48 h after seeds were sowed. Soil-grown plants were maintained at 22°C and 50% humidity with a 16 h-light (100 $\mu mol/m^{-2}/s^{-1}$)/8-h-dark cycle. Plants sown on LS agar plates were maintained at room temperature under 24 h light (100 $\mu mol/m^{-2}/s^{-1}$).

Hydroponic plants for root mass were grown essentially as previously described (Conn et al. 2013). Briefly, seeds were sown onto germination media (1.2 mM K^{1+}, 1 mM Ca^{2+}, 1 mM Mg^{2+}, 2.51 mM Cl^{1-}, 0.5 mM NO_3^-, 1.0105 mM SO_4^{2-}, 0.2 mM PO_4^{2-}, 0.101 mM Na^+, 0.01 mM Fe^{3+}, 0.005 mM Mn^{2+}, 0.01 mM Zn^{2+}, 0.0005 mM Cu^{2+}, 0.0001 mM Mo^{4+}) + 0.7% agar and vernalized at 4°C for two days. Plants were transferred to 22°C and 50% humidity with a 16 h-light (100 $\mu mol/m^{-2}/s^{-1}$)/8-h-dark cycle with the germination media as the hydroponic solution. After 1 week of growth plants were transferred to a hydroponic solution consisting of 1:1 germination media and basal media (5.6 mM K^{1+}, 2.1 mM Ca^{2+}, 2 mM Mg^{2+}, 2 mM NH_4^+, 3.71 mM Cl^{1-}, 9 mM NO_3^-, 2.0105 mM SO_4^{2-}, 0.6 mM PO_4^{2-}, 1.5502 mM Na^+, 0.01 mM Fe^{3+}, 0.005 mM Mn^{2+}, 0.01 mM Zn^{2+}, 0.0005 mM Cu^{2+}, 0.0001 mM Mo^{4+}). After one week in a 1:1 germination media/basal media solution, plants were moved to 100% basal media with the hydroponic solution changed weekly.

Overexpression and Col-0 plants were plated as described above onto LS plants with and without FB_1 (5 μM). Four-week post germination plants were harvested and lyophilized overnight for sphingolipidomic analyses.

4.4.2 PLANT TRANSFORMATIONS

LOH1 and *LOH3* cDNAs were amplified by PCR using oligonucleotide primer sets P1 and P3 (Appendix D) and Phusion polymerase (New England Biolabs, Ipswich, MA) from an Arabidopsis cDNA library prepared from flowers (Paul et al. 2006). *LOH1* and *LOH3* PCR products were cloned into the *Eco*RI-*Xba*I restriction sites of the binary vector pBinRed35S downstream of the CaMV35S promotor. The *LOH2* cDNA was amplified by PCR using the oligonucleotides primer set P2 (Appendix D) and cloned into pENTR/D-TOPO (Invitrogen, Waltham, MA) vector. The vector was linearized using *Apa*I, gel purified, and used to conduct a LR reaction with the binary vector pCD3-724-Red (pEarlyGate100 modified to contain the DsRed selection) (Earley et al. 2006). The binary vectors harboring each cDNA under control of the CaMV35 promoter were introduced in *Agrobacterium tumefaciens* C58 by electroporation. Transgenic plants were created by floral dip of *Arabidopsis* (Col-0) (Clough and Bent 1998). Seeds were screened with a green LED and a Red2 camera filter to identify transformed seeds based on DsRed fluorescence (Jach et al. 2001). Seeds were planted in soil and maintained under 22°C and 50% humidity with a 16 h-light (100 $\mu mol/m^{-2}/s^{-1}$)/8-h-dark cycle conditions through ≥3 generations to obtain homozygous lines for phenotypic characterizations.

4.4.3 TRANSGENE EXPRESSION ANALYSES

For analyses of *LOH1* and *LOH2* overexpression levels, total RNA was extracted from leaves of four-week-old *Arabidopsis* wild-type (Col-0) and overexpression plants. RNA extraction was performed using the RNeasy Plant Kit (Qiagen, Valencia, CA) according to the manufacturer's protocol. Total RNA (1 μg) was treated with DNaseI (Invitrogen, Waltham, MA) according to the manufacturer's protocol. Treated RNA was then reverse transcribed to cDNA with the iScript cDNA synthesis kit (Bio-Rad, Hercules, CA) according to the manufacturer's protocol. qPCR was performed on the cDNA using the Bio-Rad MyiQ iCycler qPCR instrument. SYBR green was used as the fluorophore in a qPCR supermix (Qiagen, Valencia, CA). QuantiTect (Qiagen, Valencia, CA) primer sets for *LOH1* (QT00779331) and *LOH2* (QT00774949) were used for relative quantification with *PP2AA3* (At1g13320) used as an internal reference gene.

Because of difficulties obtaining qPCR signals for *LOH3* using the QuantiTect primer set, Northern blot analysis of *LOH3* expression was carried out as previously described (Buhr et al. 2002). Briefly, RNA was isolated using the RNeasy Plant Kit (Qiagen, Valencia, CA) according to the manufacturer's protocol. A total of 8.5 μg of RNA was separated on a 1% formaldehyde agarose gel. The separated RNA was subsequently transferred to a nylon membrane (Zeta Probe GT; Bio-Rad, Hercules, CA) and fixed by UV cross-linking. Probes, approximately 50 ng, were made by digesting LOH3 cDNA out of the plant transformation construct and were labelled with ^{32}P-dCTP by random primer synthesis (Prime-It II Random Synthesis Kit; Agilent Technologies, La Jolla, CA). The membrane was hybridized in a solution of 1 mM EDTA, 0.5 M Na_2HPO_4 (pH 7.2), 7% SDS and 1% BSA at 65°C overnight. The membrane was washed twice

with 5% SDS, 40 mM Na_2HPO_4 solution for 30 min at 65 °C, with a subsequent third wash with 1% SDS, 40 mM Na_2HPO_4 solution for 30 min at 65 °C after hybridization. The membrane was exposed on X-ray film for 2 hours to 2 days at -80°C. After development, the membrane was stripped by incubating 2 x in 0.1 x SSC/0.5% SDS at 95°C for 20 min and re-probed for expression of ubiquitin conjugating enzyme gene (At5g25760) as a loading control. The probe was made as described above with the cDNA source coming from PCR amplification from an Arabidopsis flower cDNA library using oligonucleotide primer set P4 (Appendix D).

4.4.4 SPHINGOLIPIDOMIC ANALYSIS

Sphingolipids were extracted from 2 to 30 mg of ~4-week-old plants as previously described (Markham and Jaworski 2007). Sphingolipid profiling by liquid chromatography/electrospray ionization-tandem mass spectrometry was performed as described (Markham and Jaworski 2007). Binary gradients were generated as described (Markham and Jaworski 2007) using tetrahydrofuran/methanol/5 mM ammonium formate (3:2:5) + 0.1% formic acid (solvent A) and tetrahydrofuran/methanol/5 mM ammonium formate (7:2:1) + 0.1% formic acid (solvent B). Sphingolipids were detected using a 4000 QTRAP mass spectrometer (AB SCIEX, Redwood City, CA) with instrument settings as previously described (Markham and Jaworski 2007). Multiple reaction monitoring (MRM) transitions and data analysis using Analyst 1.5 and Multiquant 2.1 software (AB SCIEX, Redwood City, CA) were performed as described by Markham and Jaworski (2007).

4.4.5 TOTAL LCB ANALYSIS

Total LCB content was analyzed by HPLC as previously described (Markham et al. 2006). Briefly, ~10 mg lyophilized plant material was hydrolyzed for 14 h at 110°C in 10% (w/v) barium hydroxide/dioxane (1:1 v/v). Following hydrolysis samples treated with two volumes 2% (w/v) ammonium sulfate to remove barium ions and two volumes diethyl ether to extract the released LCBs. The upper layer was transferred to a 13 mm x 100 mm glass screw-capped tube and dried under N_2 at 60°C, derivatized with *ortho*-phthalaldehyde, and analyzed as previously described by Markham et al. (2006).

4.4.6 TOTAL DRY WEIGHT ANALYSIS

Four week old plants soil grown plants were harvested by cutting the tap root just below the rosette and removing any flower bolts, if present. The harvested tissue was frozen in liquid N_2 and lyophilized overnight. For root mass, hydroponically grown plants were cut just under the rosette, and roots frozen in liquid N_2 and lyophilized overnight.

4.4.7 ROOT MERISTEM IMAGING AND CELL NUMBER MEASUREMENT

Plants were sown onto LS media as described above and grown vertically under 24 h light (100 $\mu mol/m^{-2}/s^{-1}$). Roots at ten days post germination were harvested and fixed in 4% paraformaldehyde in 1X phosphate buffered saline (PBS) and stored at 4°C. Roots were stained with propidium iodide (10 µg/mL) for ~2 min and washed with 1x PBS. Images were taken using the Nikon A1 confocal using the NIS-Elements 4.20.01 acquisition software. Propidium iodide images were acquired with a 561.4 nm excitation and an emission of 570-620 nm. Images were taken at 20X magnification. Cells located in the first continuous root epidermal layer were counted from the cell plate just above

the quiescent center to the first fully differentiated cell (identified by the first cell that is approximately double the size of the previous cell) using the cell counter function of Fiji ImageJ.

4.4.8 RT-PCR OF PROGRAMED CELL DEATH RELATED GENES

Total RNA was extracted from four-week-old Col-0, *LOH1, LOH2,* and *LOH3* overexpression plants, and first-strand cDNA was prepared as described above. Semi-quantitative RT-PCR analysis was conducted with equal amounts of first-strand cDNA as template. Oligonucleotide primer sets and the numbers of PCR cycles used for each target gene are provided in Appendix D (P5-11). Gene expression was analyzed for *FMO* (At1g19250), *ERD11* (At1g02930), *PRXc* (At3g49120), *SAG13* (At2g29350), *SAG12* (At5g45890), *PR2* (At3g57260), and *PR3* (At3g12500). *UBC* (P4, At5g25760) expression was measured as an internal positive control as described previously (Brodersen et al. 2002; Chen et al. 2008).

4.4.9 SALICYLIC ACID MEASUREMENTS

Free salicylic acid was quantitated by ESI-MS/MS using the method of Pan et al, 2010 with modifications. Five ng of 2-hydroxybenzoic acid-[$^2H_6$] (d_6-SA) per 50 mg tissue was added as an internal standard. Extracts were re-suspended in 100 µl of methanol and 500 µl of column buffer A [H_2O/0.1% (v/v) formic acid/0.3 mM ammonium formate], injected onto a 100 mm x 2.1 mm Agilent Eclipse Plus C18 column (3.5 µm particle size), holding at 25% B [water:acetonitrile 10:90 containing 0.1% (v/v) formic acid and 0.3 mM ammonium formate] for 1 min, and eluted with a 5 min gradient formed by 45-95 % B at a flow rate of 0.25 ml/min. In this system, free salicylic acid and

the deuterated standard elute at 3.8 minutes. Ions were detected using previously published MRMs (Pan et al. 2010) by a QTRAP 4000 triple quadrupole mass spectrometer operated in negative mode, with instrument settings optimized first using standards. Quantitation based on comparison of analyte to standard peak area was done using Multiquant 2.1 software (ABSciEX, Redwood City, CA).

4.5 REFERENCES

Abbas HK, Tanaka T, Duke SO, Porter JK, Wray EM, Hodges L, Sessions AE, Wang E, Merrill AH, Jr., Riley RT (1994) Fumonisin- and AAL-toxin-induced disruption of sphingolipid metabolism with accumulation of free sphingoid bases. Plant Physiol 106 (3):1085-1093.

Bach L, Gissot L, Marion J, Tellier F, Moreau P, Satiat-Jeunemaitre B, Palauqui JC, Napier JA, Faure JD (2011) Very-long-chain fatty acids are required for cell plate formation during cytokinesis in Arabidopsis thaliana. J Cell Sci 124 (Pt 19):3223-3234.

Bi FC, Liu Z, Wu JX, Liang H, Xi XL, Fang C, Sun TJ, Yin J, Dai GY, Rong C, Greenberg JT, Su WW, Yao N (2014) Loss of ceramide kinase in Arabidopsis impairs defenses and promotes ceramide accumulation and mitochondrial H2O2 bursts. Plant Cell 26 (8):3449-3467.

Borner GH, Sherrier D, Weimar T, Michaelson L, Hawkins N, Macaskill A, Napier J, Beale M, Lilley K, Dupree P (2005) Analysis of detergent-resistant membranes in Arabidopsis. Evidence for plasma membrane lipid rafts. Plant Physiol 137 (1):104-116.

Brodersen P, Petersen M, Pike H, Olszak B, Skov S, Odum N, Jørgensen L, Brown R, Mundy J (2002) Knockout of Arabidopsis accelerated-cell-death11 encoding a sphingosine transfer protein causes activation of programmed cell death and defense. Genes Dev 16 (4):490-502.

Buhr T, Sato S, Ebrahim F, Xing A, Zhou Y, Mathiesen M, Schweiger B, Kinney A, Staswick P, Tom C (2002) Ribozyme termination of RNA transcripts down-regulate seed fatty acid genes in transgenic soybean. Plant J 30 (2):155-163.

Chen M, Cahoon E, Saucedo-García M, Plasencia J, Gavilanes-Ruíz M (2010) Plant Sphingolipids: Structure, Synthesis and Function. In: Wada H, Murata N (eds) Lipids in Photosynthesis, vol 30. Advances in Photosynthesis and Respiration. Springer Netherlands, pp 77-115. doi:10.1007/978-90-481-2863-1_5

Chen M, Han G, Dietrich CR, Dunn TM, Cahoon EB (2006) The essential nature of sphingolipids in plants as revealed by the functional identification and characterization of the Arabidopsis LCB1 subunit of serine palmitoyltransferase. Plant Cell 18 (12):3576-3593.

Chen M, Markham JE, Dietrich CR, Jaworski JG, Cahoon EB (2008) Sphingolipid long-chain base hydroxylation is important for growth and regulation of sphingolipid content and composition in Arabidopsis. Plant Cell 20 (7):1862-1878.

Clough SJ, Bent AF (1998) Floral dip: a simplified method for Agrobacterium-mediated transformation of Arabidopsis thaliana. The Plant journal : for cell and molecular biology 16 (6):735-743.

Conn SJ, Hocking B, Dayod M, Xu B, Athman A, Henderson S, Aukett L, Conn V, Shearer MK, Fuentes S, Tyerman SD, Gilliham M (2013) Protocol: optimising hydroponic growth systems for nutritional and physiological analysis of Arabidopsis thaliana and other plants. Plant Methods 9 (1):4.

Dunn T, Lynch D, Michaelson L, Napier J (2004) A post-genomic approach to understanding sphingolipid metabolism in Arabidopsis thaliana. Ann Bot 93 (5):483-497.

Earley KW, Haag JR, Pontes O, Opper K, Juehne T, Song K, Pikaard CS (2006) Gateway-compatible vectors for plant functional genomics and proteomics. The Plant journal : for cell and molecular biology 45 (4):616-629.

Jach G, Binot E, Frings S, Luxa K, Schell J (2001) Use of red fluorescent protein from Discosoma sp (dsRED) as a reporter for plant gene expression. Plant J 28 (4):483-491.

Laviad EL, Albee L, Pankova-Kholmyansky I, Epstein S, Park H, Merrill AH, Futerman AH (2008) Characterization of ceramide synthase 2 - Tissue distribution, substrate specificity, and inhibition by sphingosine 1-phosphate. J Biol Chem 283 (9):5677-5684.

Liang H, Yao N, Song JT, Luo S, Lu H, Greenberg JT (2003) Ceramides modulate programmed cell death in plants. Genes Dev 17 (21):2636-2641.

Markham J, Jaworski J (2007) Rapid measurement of sphingolipids from Arabidopsis thaliana by reversed-phase high-performance liquid chromatography coupled to electrospray ionization tandem mass spectrometry. Rapid Commun Mass Spectrom 21 (7):1304-1314.

Markham J, Molino D, Gissot L, Bellec Y, Hématy K, Marion J, Belcram K, Palauqui J-C, Satiat-Jeunemaître B, Faure J-D (2011) Sphingolipids containing very-long-chain fatty acids define a secretory pathway for specific polar plasma membrane protein targeting in Arabidopsis. Plant Cell 23 (6):2362-2378.

Markham JE, Li J, Cahoon EB, Jaworski JG (2006) Separation and identification of major plant sphingolipid classes from leaves. J Biol Chem 281 (32):22684-22694.

Mina JG, Okada Y, Wansadhipathi-Kannangara NK, Pratt S, Shams-Eldin H, Schwarz RT, Steel PG, Fawcett T, Denny PW (2010) Functional analyses of differentially expressed isoforms of the Arabidopsis inositol phosphorylceramide synthase. Plant Mol Biol 73 (4-5):399-407.

Mizutani Y, Kihara A, Igarashi Y (2005) Mammalian Lass6 and its related family members regulate synthesis of specific ceramides. The Biochemical journal 390 (Pt 1):263-271.

Mizutani Y, Kihara A, Igarashi Y (2006) LASS3 (longevity assurance homologue 3) is a mainly testis-specific (dihydro) ceramide synthase with relatively broad substrate specificity. The Biochemical journal 398:531-538.

Molino D, Van der Giessen E, Gissot L, Hematy K, Marion J, Barthelemy J, Bellec Y, Vernhettes S, Satiat-Jeunemaitre B, Galli T, Tareste D, Faure JD (2014) Inhibition of very long acyl chain sphingolipid synthesis modifies membrane dynamics during plant cytokinesis. Biochim Biophys Acta 1842 (10):1422-1430.

Mortimer J, Yu X, Albrecht S, Sicilia F, Huichalaf M, Ampuero D, Michaelson L, Murphy A, Matsunaga T, Kurz S, Stephens E, Baldwin T, Ishii T, Napier J, Weber A, Handford M, Dupree P (2013) Abnormal glycosphingolipid mannosylation triggers salicylic acid-mediated responses in Arabidopsis. Plant Cell 25 (5):1881-1894.

Mullen TD, Hannun YA, Obeid LM (2012) Ceramide synthases at the centre of sphingolipid metabolism and biology. Biochem J 441 (3):789-802.

Pan XQ, Welti R, Wang XM (2010) Quantitative analysis of major plant hormones in crude plant extracts by high-performance liquid chromatography-mass spectrometry. Nature Protocols 5 (6):986-992.

Paul S, Gable K, Beaudoin F, Cahoon E, Jaworski J, Napier J, Dunn T (2006) Members of the Arabidopsis FAE1-like 3-ketoacyl-CoA synthase gene family substitute for the Elop proteins of Saccharomyces cerevisiae. J Biol Chem 281 (14):9018-9029.

Rennie EA, Ebert B, Miles GP, Cahoon RE, Christiansen KM, Stonebloom S, Khatab H, Twell D, Petzold CJ, Adams PD, Dupree P, Heazlewood JL, Cahoon EB, Scheller HV (2014) Identification of a sphingolipid alpha-glucuronosyltransferase that is essential for pollen function in Arabidopsis. Plant Cell 26 (8):3314-3325.

Riebeling C, Allegood JC, Wang E, Merrill AH, Futerman AH (2003) Two mammalian longevity assurance gene (LAG1) family members, trh1 and trh4, regulate dihydroceramide synthesis using different fatty acyl-CoA donors. J Biol Chem 278 (44):43452-43459.

Saucedo-García M, Guevara-García A, González-Solís A, Cruz-García F, Vázquez-Santana S, Markham J, Lozano-Rosas M, Dietrich C, Ramos-Vega M, Cahoon E, Gavilanes-Ruíz M (2011) MPK6, sphinganine and the LCB2a gene from serine palmitoyltransferase are required in the signaling pathway that mediates cell death induced by long chain bases in Arabidopsis. New Phytol 191 (4):943-957.

Schmid M, Davison TS, Henz SR, Pape UJ, Demar M, Vingron M, Scholkopf B, Weigel D, Lohmann JU (2005) A gene expression map of Arabidopsis thaliana development. Nature Genetics 37 (5):501-506.

Simanshu DK, Zhai XH, Munch D, Hofius D, Markham JE, Bielawski J, Bielawska A, Malinina L, Molotkovsky JG, Mundy JW, Patel DJ, Brown RE (2014) Arabidopsis Accelerated Cell Death 11, ACD11, Is a Ceramide-1-Phosphate Transfer Protein and Intermediary Regulator of Phytoceramide Levels. Cell Reports 6 (2):388-399.

Sperling P, Franke S, Luthje S, Heinz E (2005) Are glucocerebrosides the predominant sphingolipids in plant plasma membranes? Plant Physiol Biochem 43 (12):1031-1038.

Ternes P, Feussner K, Werner S, Lerche J, Iven T, Heilmann I, Riezman H, Feussner I (2011a) Disruption of the ceramide synthase LOH1 causes spontaneous cell death in Arabidopsis thaliana. New Phytol 192 (4):841-854.

Ternes P, Wobbe T, Schwarz M, Albrecht S, Feussner K, Riezman I, Cregg J, Heinz E, Riezman H, Feussner I, Warnecke D (2011b) Two pathways of sphingolipid

biosynthesis are separated in the yeast Pichia pastoris. J Biol Chem 286 (13):11401-11414.
Venkataraman K, Riebeling C, Bodennec J, Riezman H, Allegood JC, Sullard MC, Merrill AH, Futerman AH (2002) Upstream of growth and differentiation factor 1 (uog1), a mammalian homolog of the yeast longevity assurance gene 1 (LAG1), regulates N-stearoyl-sphinganine (C18-(dihydro)ceramide) synthesis in a fumonisin B-1-independent manner in mammalian cells. J Biol Chem 277 (38):35642-35649.
Verhoek B, Haas R, Wrage K, Linscheid M, Heinz E (1983) Lipids and Enzymatic-Activities in Vacuolar Membranes Isolated Via Protoplasts from Oat Primary Leaves. Zeitschrift Fur Naturforschung C-a Journal of Biosciences 38 (9-10):770-777.
Wang WM, Yang XH, Tangchaiburana S, Ndeh R, Markham JE, Tsegaye Y, Dunn TM, Wang GL, Bellizzi M, Parsons JF, Morrissey D, Bravo JE, Lynch DV, Xiao SY (2008) An Inositolphosphorylceramide Synthase Is Involved in Regulation of Plant Programmed Cell Death Associated with Defense in Arabidopsis. Plant Cell 20 (11):3163-3179.
Yang H, Richter GL, Wang X, Mlodzinska E, Carraro N, Ma G, Jenness M, Chao DY, Peer WA, Murphy AS (2012) Sterols and sphingolipids differentially function in trafficking of the Arabidopsis ABCB19 auxin transporter. Plant J.

CHAPTER 5

SPHINGOLIPID METABOLISM IS STRIKINGLY DIFFERENT BETWEEN POLLEN AND LEAF IN ARABIDOPSIS AS REVEALED BY COMPOSITIONAL AND GENE EXPRESSION PROFILING

Note: The results described in this chapter have been published, no text has been modified.

The citation is: Luttgeharm, K.D., A.K. Kimberlin, R.E. Cahoon, R.L. Cerny, J.A. Napier, J.E. Markham, E.B. Cahoon (2015). "Sphingolipid metabolism is strikingly different between pollen and leaf in Arabidopsis as revealed by compositional and gene expression profiling." Phytochemistry **115**:121-129.

5.1 INTRODUCTION

Sphingolipids are major structural components of the plasma membrane, tonoplast, and endomembranes and are enriched in detergent-resistant plasma membrane microdomains or lipid rafts in plant cells (Borner et al. 2005; Mongrand et al. 2004; Sperling et al. 2005) Desaturation of sphingolipid long-chain bases (LCBs) as well as total sphingolipid levels have been demonstrated to con- tribute to cold-tolerance (Chen et al. 2008; Guillas et al. 2012; Nagano et al. 2014) Sphingolipid metabolites also function in non-structural roles in plants. The accumulation of ceramides and free long-chain bases (LCBs), for example, has been shown to trigger programmed cell death (PCD) through a MAP kinase 6 transduction pathway, which is important for hypersensitive response resistance to pathogens (Brodersen et al. 2002; Saucedo-Garcia et al. 2011). Phosphorylated long-chain bases have also been shown to participate in ABA signaling for guard cell closure (Coursol et al. 2003; Ng et al. 2001) and cold-responsive nitric oxide production has been linked to reductions in phosphorylated ceramides and LCBs levels (Cantrel et al. 2011).

Sphingolipids are defined by the presence of long-chain bases (LCBs), which are linked through an amide bond to fatty acids to form ceramides, the backbones of complex sphingolipids. Ceramides can be modified by addition of polar head groups consisting of phosphates, carbohydrates, or combinations of the two (Chen et al. 2010; Lynch and Dunn 2004; Markham and Jaworski 2007). Additionally LCBs can be modified by hydroxylation at their C-4 positions to yield trihydroxy LCBs and/or desaturation at the C-4 (Δ4) and C-8 (Δ8) positions (Lynch and Dunn 2004). Further structural diversity in sphingolipids is generated by hydroxylation of the C-2 (or α) position of the constituent

fatty acids, which typically range in chain-lengths from 16 to 26 carbon atoms (Chen et al. 2010; Markham et al. 2011). Moreover, fatty acids in sphingolipids of Arabidopsis, other Brassicaceae and many Poaceae can contain ω-9 unsaturation (Imai et al. 2000).

Contributing to the large structural complexity of plant sphingolipids is an array of possible polar head groups linked to the C-1 hydroxyl group of ceramides. In Arabidopsis, two major classes of complex sphingolipids occur: glucosylceramides (GlcCer) and glycosylinositolphosphoceramides (GIPCs). In contrast to the simple glucose head group of GlcCer, GIPCs can contain an array of sugar residues linked to inositol phosphate that is present in all GIPCs. Recently Buré et al. (2011) developed a provisional form of GIPC nomenclature based on the numbers and composition of the head group sugars: Hex-HexA-IPC (Series A), Hex-Hex-HexA- IPC (Series B), Pent-Hex-Hex-HexA-IPC (Series C), $(Pent)_2$-Hex- Hex-HexA-IPC (Series D), $(Pent)_3$-Hex-Hex-HexA-IPC (Series E), $(Pent)_4$-Hex-Hex-HexA-IPC (Series F). In this nomenclature scheme, Hex corresponds to a hexose sugar, Pent corresponds to a pentose sugar, HexA corresponds to hexuronic acid, and IPC corresponds to inositolphosphoceramide. The primary GIPC head group identified to date in Arabidopsis leaves contains a single hexose (Hex) with hydroxylation (OH) bound to a hexuronic acid (HexA) linked to IPC and corresponds to that of Series A (Bure et al. 2011; Cacas et al. 2013; Markham and Jaworski 2007). Other plants, such as tobacco and tomato, contain large amounts of Hex with N-acetylation (NAc)-HexA-IPCs with up to seven sugar residues bound to IPC (Bure et al. 2011; Hsieh et al. 1981; Kaul and Lester 1978; Markham et al. 2006; Tellier et al. 2014). For example, GIPCs in tobacco BY2 cells contain up to four Pent and three Hex residues (including glucuronic acid, HexA) linked to IPC (Bure et al. 2011).

Although Hex(OH)-HexA (Series A) is the primary glycosylation of GIPCs in Arabidopsis leaves, additional GIPC structures including Hex-Hex(OH)-HexA- IPC (Series B), $(Pent)_2$-Hex-Hex(OH)-HexA-IPC (Series D), $(Pent)_3$- Hex-Hex(OH)-HexA-IPC (Series E), and $(Pent)_4$-Hex-Hex(OH)- HexA-IPC (Series F) have been identified in Arabidopsis cell cultures (Bure et al. 2011; Mortimer et al. 2013). A recent study also found Hex(NAc)-HexA-IPCs (Series A) in Arabidopsis seeds and seedlings (Tellier et al. 2014), not previously found in Arabidopsis cell cultures (Bure et al. 2011). The GIPCs of Arabidopsis seeds and seedlings, however, lacked the complex sugar head groups previously found in Arabidopsis cell culture (Bure et al. 2011; Tellier et al. 2014). The functional significance of the different GIPC sugar structures and numbers is currently unknown, as is the reason for their occurrence in only certain cell types.

Sphingolipids are essential for pollen development in Arabidopsis. In this regard, null mutants for the LCB2 subunit of serine palmitoyltransferase (SPT), which catalyzes the first step in sphingolipid LCB synthesis, have non-viable pollen (Dietrich et al. 2008; Teng et al. 2008). In addition, double mutants of the redundant LCB2a and LCB2b genes in Arabidopsis were unable to transmit mutant loci through pollen, and pollen lacking LCB biosynthetic ability displayed aberrant endomembranes and lacked the Golgi-derived intine layer (Dietrich et al. 2008). In addition, a T-DNA insertion mutant of ssSPTa encoding the major stimulatory small subunit of SPT results in defective pollen development (Kimberlin et al. 2013).

Arabidopsis differs from most plant species in that expression of the gene for LCB Δ4 desaturase (At4g04930) is limited almost exclusively to pollen (Islam et al. 2012; Michaelson et al. 2009). As a result, LCBs with Δ4 unsaturation are enriched in

pollen and flowers, but are nearly absent in leaves of Arabidopsis (Michaelson et al. 2009). Mutants defective in LCB Δ4 desaturation, however, lack detectable defects in pollen development (Michaelson et al. 2009). LCB Δ4 unsaturation is found exclusively in the *trans* configuration, and typically in combination with either *cis* or *trans* Δ8 unsaturation in the C18 dihydroxy LCB sphingadiene (d18:2) (Sperling et al. 1998). In addition, Δ4 unsaturated LCBs are found in GlcCers, but largely absent from GIPCs (Michaelson et al. 2009; Sperling et al. 2005).

Despite the fact that sphingolipids are essential for pollen and that the occurrence of the LCB d18:2 is limited primarily to pollen in Arabidopsis, a comprehensive profiling of pollen sphingolipids has not been previously described. This report provides a comprehensive description of the sphingolipid composition of Arabidopsis pollen and compares it to that of Arabidopsis leaves from numerous prior reports (Chen et al. 2012; Chen et al. 2008; Kimberlin et al. 2013; Markham and Jaworski 2007; Markham et al. 2011). In addition to characterization of pollen from wild-type Col-0, pollen from a T-DNA mutant of the single LCB Δ4 desaturase gene (At4g04930) was also examined (Michaelson et al. 2009) to gain further insights into the importance of Δ4 unsaturated LCBs in pollen sphingolipid metabolism. In addition, RNA-Seq and microarray data for expression of key sphingolipid biosynthetic genes in Arabidopsis pollen and leaves was compiled, highlighting the differences in sphingolipid metabolism between the two tissue types. Collectively, these data show large differences in sphingolipid composition and biosynthetic gene expression between pollen and leaves, including the identification of an array of abundant novel GIPC structures in pollen indicating that sphingolipids may play a unique role in pollen.

5.2. RESULTS

5.2.1. POLLEN ISOLATION

Two methods for pollen isolation were compared: a vacuum- based method and a buffered mannitol-based method (Honys and Twell 2003; Johnson-Brousseau and McCormick 2004). The latter method resulted in higher yields and more rapid recovery of pollen. Given the need for significant amounts of pollen with minimal lipolytic degradation for sphingolipid profiling, the buffered-mannitol method was chosen for use in these studies. Using this method, highly enriched, intact pollen was isolated that contained only small amounts of lysed pollen (as determined by viability staining) and floral tissue (Figure 5.1A and B). RT-PCR of the enriched pollen also revealed expression of the LCB Δ4 desaturase (Δ4 DES) gene, a pollen-specific gene in Arabidopsis (Figure 5.1C and D). Lyophilized pollen isolated from the Arabidopsis Col-0 and a mutant of the LCB Δ4 DES mutant plants were subsequently used for ESI–MS/MS profiling of sphingolipid content and composition.

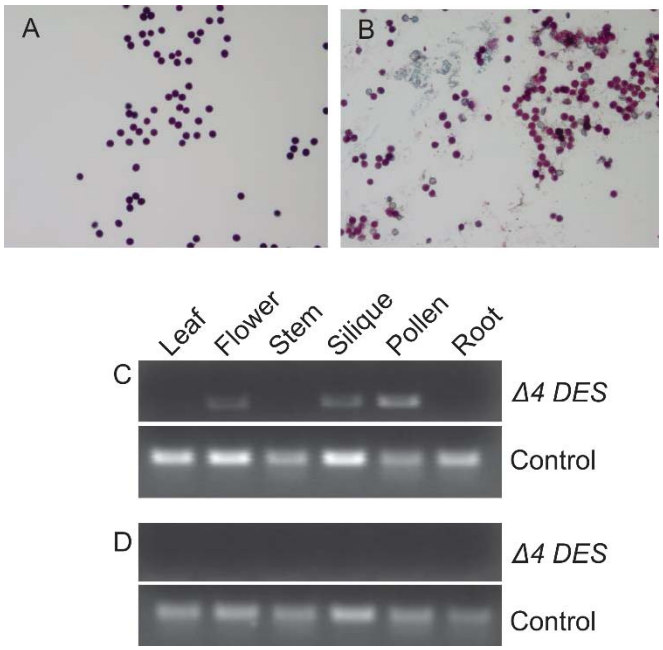

Figure 5.1: *Viability staining of Col-0 pollen* collected (A) directly from anther and (B) after isolation in 0.3 M mannitol. The presence of round, dark purple pollen in A indicates that pollen was viable prior to extraction in mannitol. As shown in B, the mannitol-extract is highly enriched in viable pollen but also contains minor amounts of unstained lysed pollen and anther debris. RT-PCR of the pollen specific D4 DES and loading control gene (At5g25760) on (C) Col-0 and (D) D4 DES mutant plants.

5.2.2. ARABIDOPSIS COL-0 POLLEN SPHINGOLIPIDOME

As has been previously reported (Markham and Jaworski, 2007) and confirmed in other studies (Chen et al., 2012, 2008; Markham et al., 2011), the sphingolipidome of Arabidopsis Col-0 leaves consists primarily of provisionally identified Hex(OH)-HexA-IPC (Series A) and glucosylceramide (GlcCer), which occur at a molar ratio of approximately 2:1. In addition, ceramides, hydroxyceramides (i.e., ceramides containing 2-OH fatty acids), free LCB, and LCB-phosphates account for ≤10% of the sphingolipids of Arabidopsis leaves (Markham and Jaworski 2007). In addition, the LCBs in Arabidopsis leaves consist almost entirely of t18:1, t18:0, d18:1, and d18:0 (Chen et al.

2006; Markham et al. 2006). The sphingolipid profile of Arabidopsis Col-0 pollen determined in this study was strikingly different than that of Arabidopsis leaves (Figure 5.2). Among these differences, GlcCer content was nearly 8-fold higher than that reported in Arabidopsis leaves (~1377 nmol/g in pollen vs. 160 nmol/g in leaves) (Markham and Jaworski 2007). Consistent with this, nearly 50% of the LCBs in pollen GlcCer were d18:2, which was not detectable in Arabidopsis Col-0 leaf as reported previously (Markham and Jaworski 2007). In addition, free ceramides, hydroxyceramides, and free LCBs were found to be more abundant in pollen on a per gram dry weight basis than in leaf (Markham and Jaworski 2007)

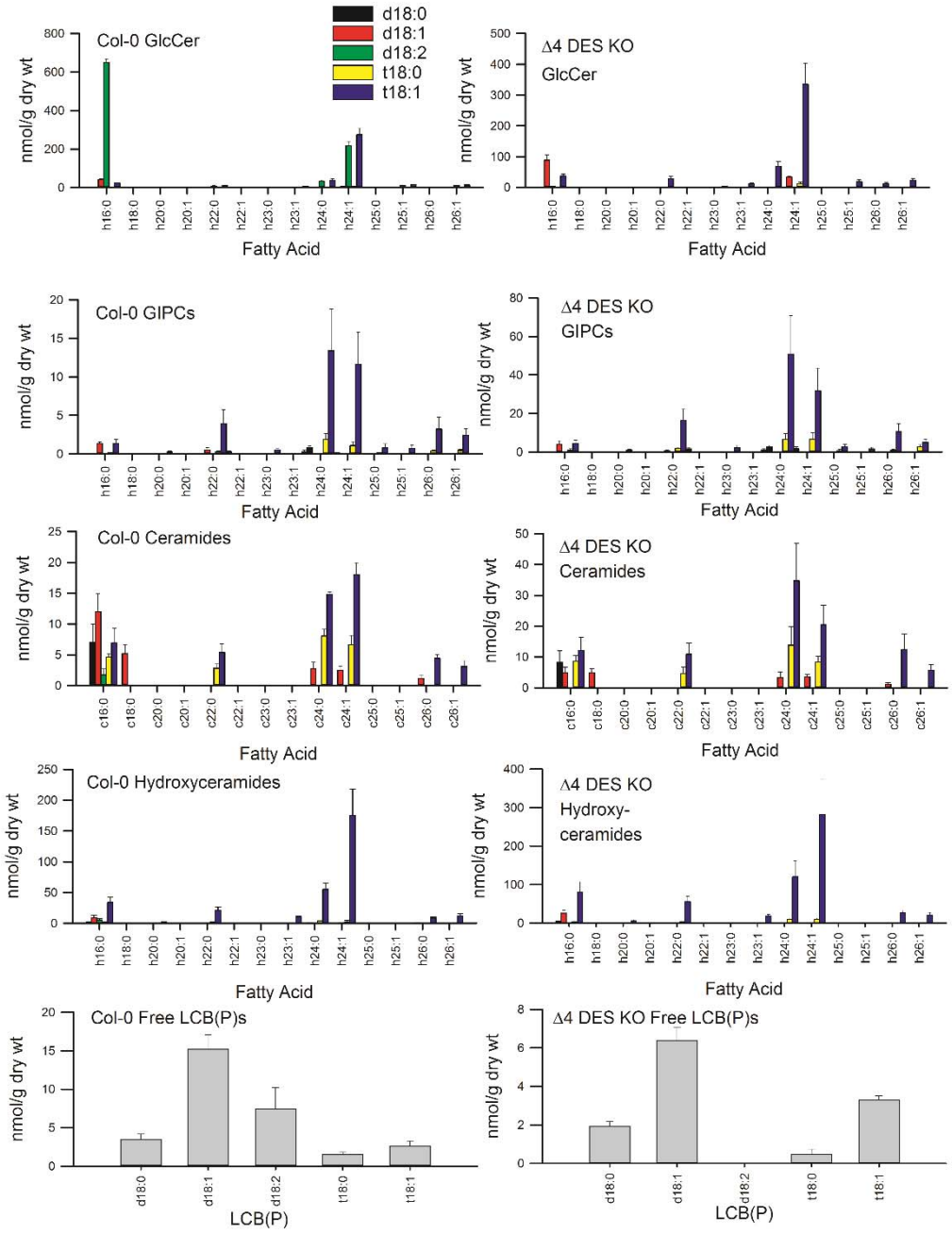

Figure 5.2. *Sphingolipid profiles of glucosylceramides (GlcCer), provisionally identified glycosylinositolphosphoceramides (Hex(OH)-HexA-IPCs, Series A), ceramides, hydroxyceramides, and free LCBs for enriched pollen from Col-0 and LCB D4 desaturase knockout mutant* (D4 DES KO) obtained by ESI-LC MS/MS analyzes. All values shown as the average of measurements of three independent pollen isolations ± SD.

The only sphingolipid found to be less abundant in pollen relative to leaf was GIPC, specifically the provisionally identified Hex(OH)-HexA-IPC GIPC (Series A) found in leaf. All previous studies of Arabidopsis leaf sphingolipids have found GIPCs as the most abundant sphingolipid class (Chen et al. 2012; Chen et al. 2008; Markham and Jaworski 2007; Markham et al. 2011) so it was surprising to find that Hex(OH)-HexA-IPC GIPC (Series A) was fivefold lower in pollen. One hypothesis to explain this apparent reduction in GIPC levels is that pollen synthesizes other GIPC types with alternative glycosylation patterns. In order to test this hypothesis, a precursor scan using product ion 662.60 *m/*z (corresponding to the t18:1_h24:1 ceramide fragment) was performed. This identified ions indicative of Hex(NAc)-HexA-IPCs (Series A) with the addition of multiple sugar residues (Figure 5.3), as well as the provisionally identified leaf-type Hex(OH)-HexA-IPC (Series A), predicted and observed mass for detected species can be found in Appendix E. To further confirm the identities of these ions, MRMs were developed for complex GIPCs not previously reported in Arabidopsis. These analyses confirmed the presence of provisionally identified $(Pent)_3$-Hex-Hex(NAc)-HexA-(Series E), $(Pent)_2$- Hex-Hex(NAc)-HexA-(Series D), and Hex-Hex(OH)-HexA-IPCs (Series B) (Figure 5.4A–D) in sphingolipid extracts from pollen. Only the Hex-Hex(OH)-HexA-IPC form was found in both leaf and pollen. Notably, the Hex(NAc) GIPCs were found in pollen but were absent from leaves. By using relative quantitation of Hex- Hex(OH)-HexA-IPC, it was found that this species is ~six fold more abundant in leaf than in pollen. The lack of standards precluded absolute quantification and full identification of the novel GIPC forms, however, it is possible that their inclusion would result in total GIPC abundance in pollen equivalent to that of leaf.

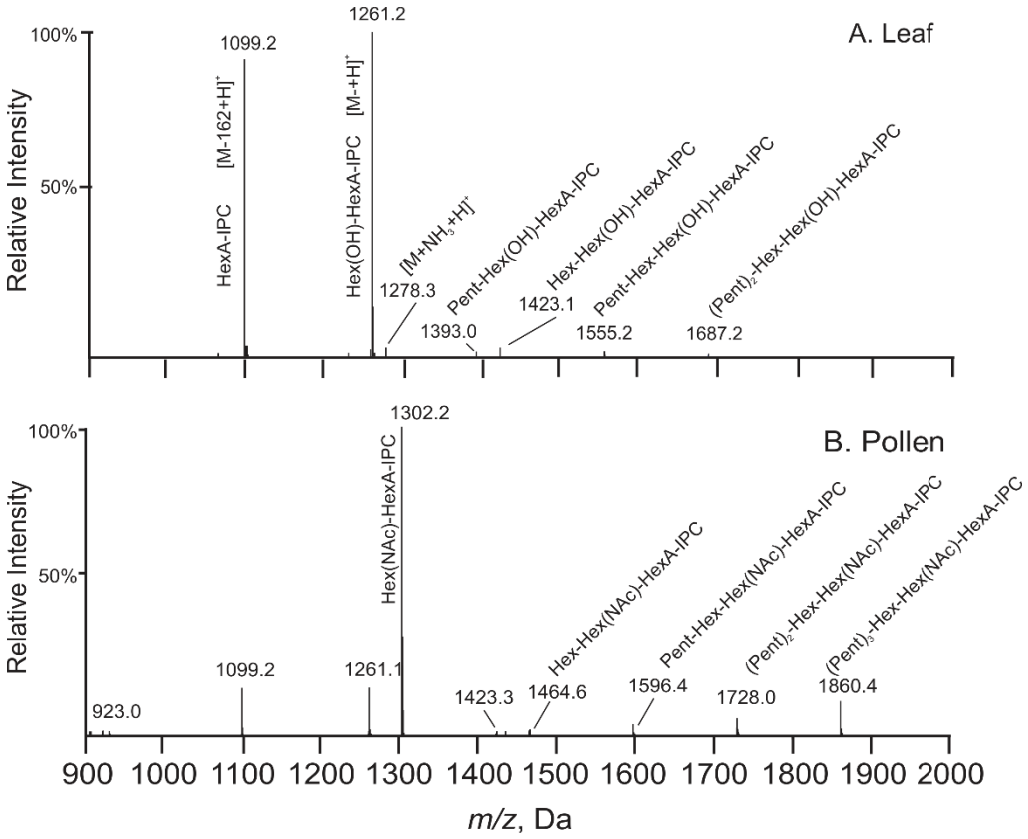

Figure 5.3. *ESI–MS/MS spectrum of ions detected by precursor m/z 662.6 scanning of GIPC species eluted between 5 and 10 min during chromatography* as described in Kimberlin et al. (2013). These spectra depict GIPC species built upon a t18:1_h24:1 ceramide backbone and show differences in pollen and leaf GIPC glycosylation patterns. (A) Abundant ions detected in leaf were *m/z* 1099.2 (HexA-IPC), *m/z* 1261.2 (Hex(OH)-HexA-IPC, Series A). Further glycosylation by addition of a pentose sugar adds 132 mass units, while addition of a hexose sugar adds 162 mass units. Relatively small amounts of *m/z* 1393.0 (Pent-Hex(OH)-HexA-IPC), *m/z* 1423.1 (Hex-Hex(OH)-HexA-IPC, Series B), *m/z* 1555.2 (Pent-Hex-Hex(OH)-HexA-IPC, Series C) and *m/z* 1687.2 ($Pent_2$-Hex-Hex(OH)-HexA-IPC, Series D) were also detected in leaf. (B) GIPC species detected in pollen contain Hex(OH) species found in leaf as well as Hex(NAc) species: *m/z* 1302.2 (Hex(NAc)-HexA-IPC, Series A), *m/z* 1464.6 (Hex-Hex(NAc)-HexA-IPC, Series B), *m/z* 1596.4 (Pent-Hex-Hex(NAc)-HexA-IPC, Series C), *m/z* 1728.0 ($Pent_2$-Hex-Hex(NAc)-HexA-IPC, Series D) and *m/z* 1860.4 ($Pent_3$-Hex-Hex(NAc)-HexA-IPC, Series E). Hex, hexose; Pent, pentose; HexA, hexuronic acid; Hex(OH), hexose lacking N-acetylation; Hex(NAc), hexose with N-acetylation; IPC, inositolphosphoceramide.

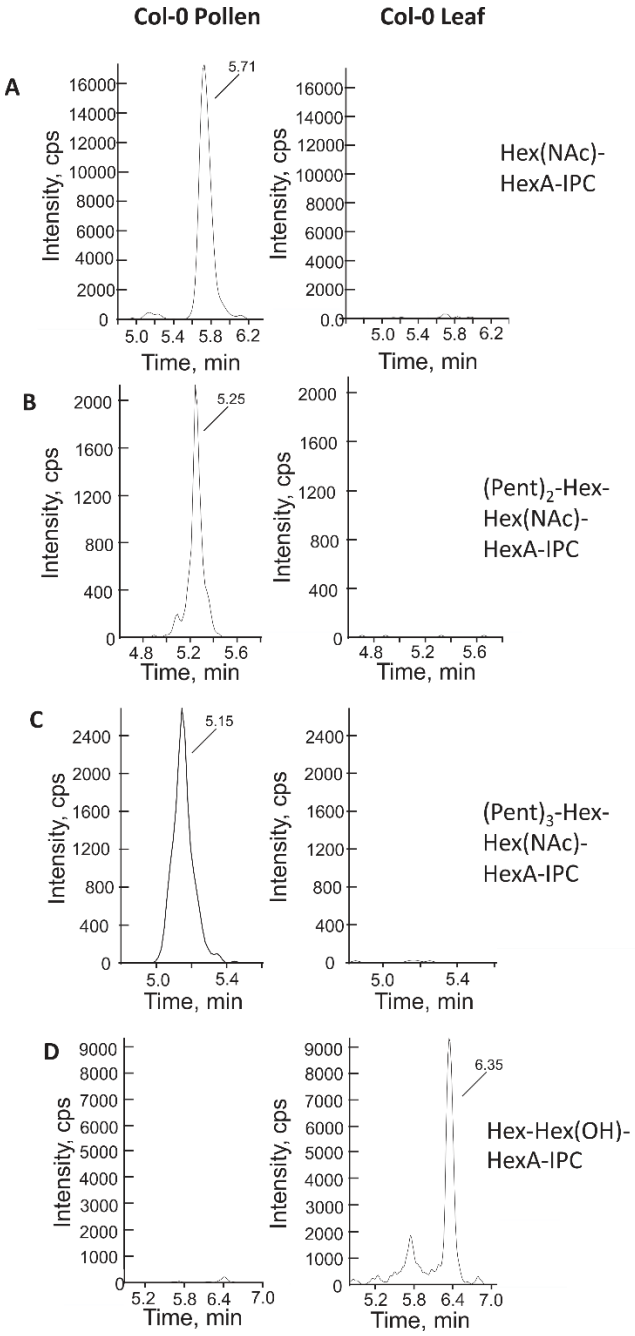

Figure 5.4. *Detection of provisionally identified complex GIPC species in Arabidopsis Col-0*. LC–MSMS traces are shown for different complex GIPC species (A) Hex(NAc)-HexA-IPC (Series A), (B) $(Pent)_2$-Hex-Hex(NAc)-HexA-IPC (Series D), (C) $(Pent)_3$-Hex-Hex(NAc)-HexA-IPC (Series E), (D) Hex-Hex(OH)-HexA-IPC (Series B) and their relative amounts in pollen and leaf. All head groups shown are bound to a t18:1_h24:1 ceramide backbone except for the Hex-Hex(OH)-HexA-IPC (Series B) which is built upon the t18:1_h24:0 ceramide backbone.

5.2.3. SPHINGOLIPIDOME OF POLLEN FROM A LCB Δ4 DESATURASE MUTANT

While T-DNA disruption of the LCB Δ4 DES gene does not result in observable phenotypic alterations in plant growth or pollen viability (Michaelson et al. 2009), significant changes in the sphingolipidome of pollen from this mutant were found. The most striking change was an approximately 50% decrease in GlcCer levels relative to pollen from Col-0. However, aside from a lack of the Δ4 unsaturated LCB d18:2, GlcCer molecular species in pollen of the Δ4 DES mutant were similar to those in pollen from Col-0 plants (Table 5.1).

Table 5.1: Total amounts of each sphingolipid class in pollen from Col-0 and LCB Δ4 desaturase mutant (Δ4 DES KO) plants. Data shown are the average of three independent pollen isolations (± SD).

Sphingolipid Class	**Col-0 (nmol/g dry wt)**	**Δ4 DES KO (nmol/g dry wt)**
Ceramide	107 ± 18	158 ± 49
Hydroxyceramide	345 ± 79	665 ± 192
Glucosylceramide	1377 ± 85	678 ± 128
GIPCs	48 ± 18	168 ± 66
LCB(P)s	30 ± 6	12 ± 0
Total	1906 ± 81	1672 ± 407

Although the detectable differences in GlcCer compositions were small, there were significant increases in the amounts of d18:1_h16:0 ($p = 0.0092$), d18:1_24:1 ($p = 0.00060$) t18:1_h16 ($p = 0.021$), and t18:1_26:0 ($p = 0.013$). The other major difference between pollen from the Δ4 DES mutant and Col-0 was an increased amount of the Hex(OH)-HexA-IPC (Series A), which was detected in pollen from Δ4 DES mutant ($p =$

0.039), resulting from an increased amount of ceramides containing the d18:0, t18:0, and t18:1 LCBs (Figure 5.5B). In addition, free LCB levels were significantly decreased in pollen from the Δ4 DES mutant ($p < 0.001$), derived, not only from a lack of d18:2 species, but also a significant ($p = 0.011$) decrease in d18:1. Overall amounts of sphingolipids were not significantly different in pollen from Col-0 and Δ4 DES mutant plants (Figure 5.5C).

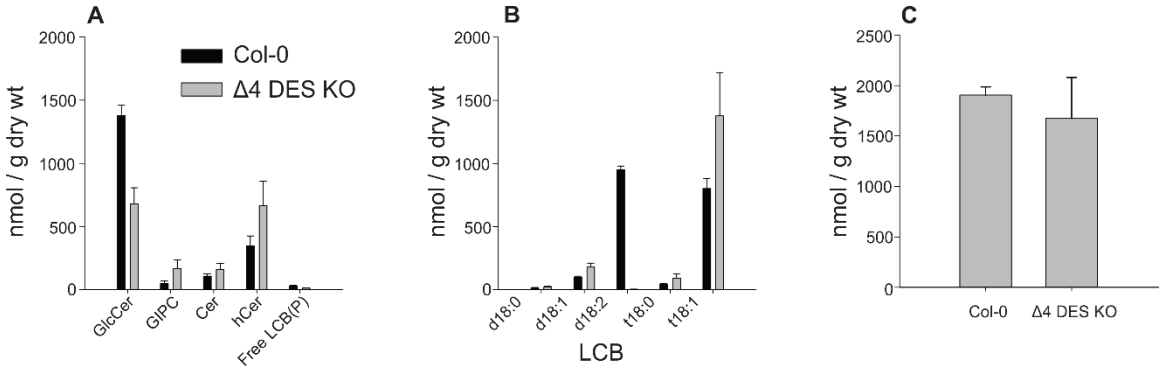

Figure 5.5 *Col-0 and Δ4 DES mutant pollen sphingolipid concentrations* (A) Total sphingolipid per class in pollen identified by LC–MS/MS. Data represented as the average of three independent pollen isolations ± SD. (B) Total amounts of each LCB found in both Col-0 and Δ4 DES mutant pollen. Data represents the average of the sum of all LCB levels from three independent pollen isolations with standard deviation. (C) Total sphingolipid identified by LC–MS/MS. Data represents the average of the sum of all sphingolipid species ± SD.

5.2.4. GENE EXPRESSION DATA MINING OF SPHINGOLIPID BIOSYNTHETIC GENES IN POLLEN RELATIVE TO SEEDLING AND LEAF

Previously published RNA-Seq data (Loraine et al. 2013) and the microarray-based Arabidopsis EFP Browser (Winter et al. 2007) were mined for sphingolipid biosynthesis-related genes. Expression levels were obtained for genes encoding the serine palmitoyltransferase (SPT) subunits LCB1 (At4g36480), LCB2a (At5g23670), LCB2b (At3g48780), the two 3-ketosphinganine reductases TSC10A (At5g19200) and TSC10B

(At3g06060), the two sphingoid base C-4 hydroxylases SBH1 (At1g69640) and SBH2 (At1g14290), the ceramide synthases LOH1 (At3g25540), LOH2 (At3g19260), and LOH3 (At1g13580), LCB Δ4 desaturase (At4g04930), the two LCB Δ8 desaturases SLD1 (At3g61580) and SLD2 (At2g46210), glucosylceramide synthase (GCS; At2g19880), the three IPC synthases (IPS) IPS1 (At3g54020), IPS2 (At2g37940), and IPS3 (At2g29525). RNA-Seq data were also compiled for the recently identified small subunits of SPT (ssSPT) ssSPTa (At1g06515) and ssSPTb (At2g30942) as well as the recently identified UDP-glucose IPC transferase (IPUT1; At5g18480) (Rennie et al., 2014), which were not present in microarray data in the EFP Browser. The RNA-Seq study contained data for Arabidopsis pollen versus seedling (Loraine et al. 2013), while data for pollen versus leaf was mined from the EFP Browser. Data from RNA-Seq (Figure 5.6) and microarray data (Figure 5.7) indicated expression of selected genes at higher levels in pollen compared to seedling or leaf. These included LCB2a LCB2b, SLD1, SLD2, and SBH2 as well as genes associated with d18:2 and GlcCer synthesis Δ4 DES and GCS. Microarray data also indicated higher pollen expression of the gene for the LOH2 ceramide synthase that generates ceramides with C16 fatty acids found primarily in GlcCer. Quantitative PCR (qPCR) conducted to confirm this, revealed 14-fold higher expression of LOH2 in pollen relative to leaf of Col-0 plants (Figure 5.8). Overall, these data are consistent with an increased GlcCer biosynthetic capacity in pollen, as indicated by sphingolipid profiling.

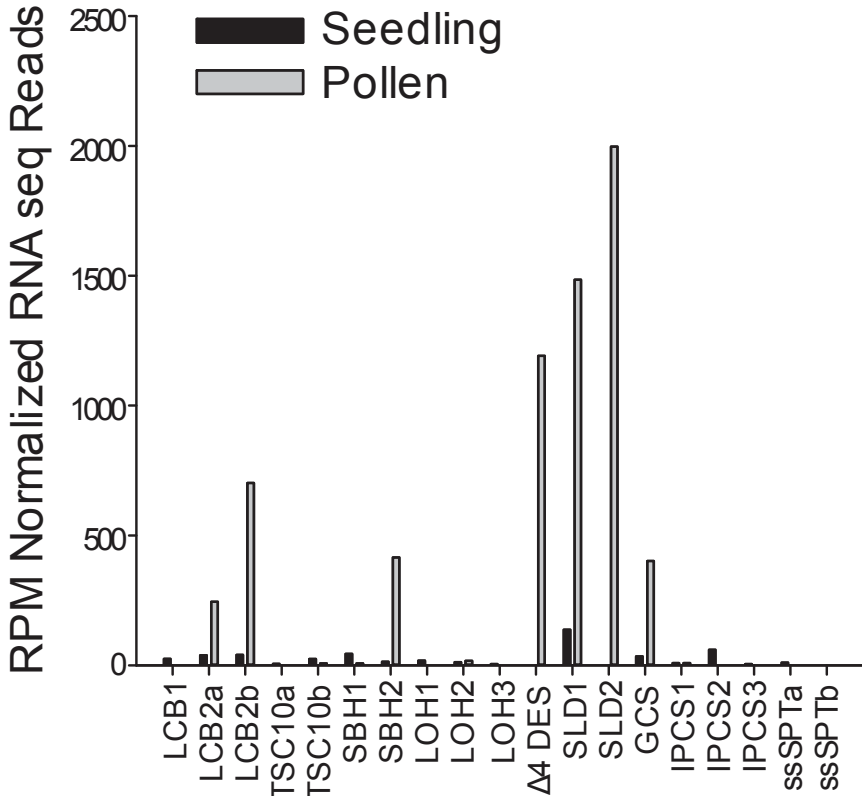

Figure 5.6. *Arabidopsis RNA-Seq gene expression levels for different genes involved with sphingolipid synthesis in pollen and seedling*. Data were compiled from RPM normalized data (Loraine et al. 2013) for genes encoding the following polypeptides: SPT subunits LCB1 (At4g36480), LCB2a (At5g23670), LCB2b (At3g48780), the two small subunits of SPT (ssSPT) ssSPTa (At1g06515) and ssSPTb (At2g30942), the two 3-ketosphinganine reductases TSC10A (At5g19200) and TSC10B (At3g06060), the two sphingoid base C-4 hydroxylases SBH1 (At1g69640) and SBH2 (At1g14290), the ceramide synthases LOH1 (At3g25540), LOH2 (At3g19260), and LOH3 (At1g13580), LCB D4 desaturase (At4g04930), the two LCB D8 desaturases SLD1 (At3g61580) and SLD2 (At2g46210), glucosylceramide synthase (GCS; At2g19880), the three IPC synthases (IPS) IPS1 (At3g54020), IPS2 (At2g37940), and IPS3 (At2g29525), the UDP-glucose IPC transferase IPUT1 (At5g18480).

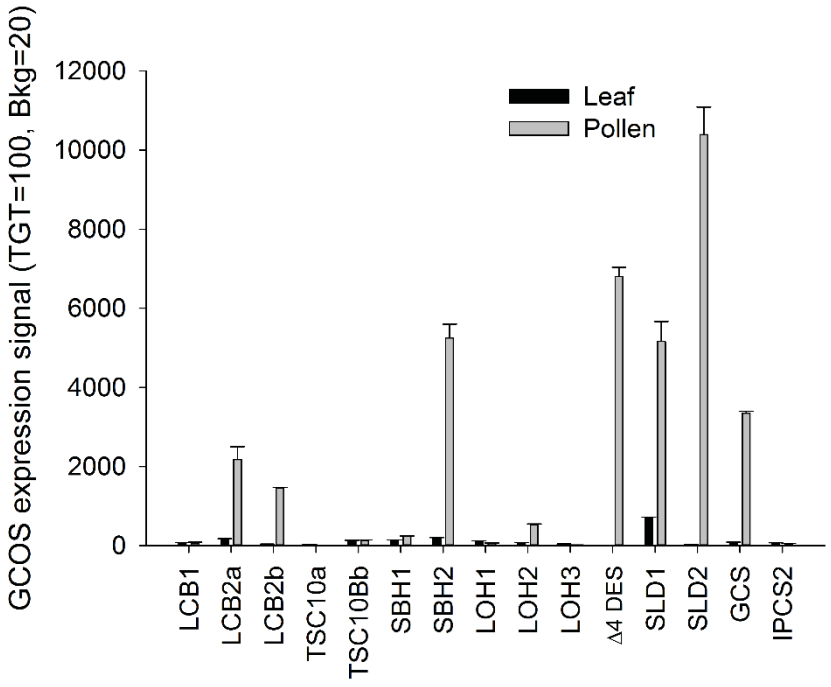

Figure 5.7 *Arabidopsis eFP browser expression levels for different genes involved with sphingolipid biosynthesis.* Data represents the average of three independent experiments ± SD.

5.3. DISCUSSION

Sphingolipids are essential for Arabidopsis pollen development, based on studies of serine palmitoyltransferase (SPT) that catalyzes the first step in long-chain base (LCB) synthesis (Dietrich et al. 2008; Kimberlin et al. 2013). Despite this, sphingolipid composition of Arabidopsis pollen has not been previously been examined, nor have expression profiles of sphingolipid biosynthetic genes in Arabidopsis pollen been cataloged. As part of an effort to under- stand the function of sphingolipids in Arabidopsis pollen, ESI– MS/MS methodology (Markham and Jaworski 2007) was applied to characterize sphingolipids in Arabidopsis pollen. In addition, extracted data from publicly available RNA-Seq and microarray studies on expression levels of genes for key sphingolipid biosynthetic and LCB modification enzymes were also examined.

One of the most striking findings was the high content of GlcCer in Arabidopsis Col-0 pollen. GlcCer content was approximately 8-fold higher in pollen than previously reported in leaves of Arabidopsis rosettes, and Δ4-unsaturated d18:2 isomers composed >50% of the GlcCer LCBs. These LCBs were not detectable in GlcCer from pollen of the LCB Δ4 DES mutant, and GlcCer concentrations were twofold lower than those in wild-type pollen. This is consistent with the 25% lower GlcCer levels reported in flowers of the LCB Δ4 DES mutant relative to flowers of wild-type Col-0 (Michaelson et al. 2009). Given that pollen from the Δ4 DES mutant were shown to be unaffected in germination and morphology (Michaelson et al. 2009), the functional significance of the relative enrichment of GlcCer in Arabidopsis pollen is not clear. It is possible that any selective advantage of GlcCer enrichment in pollen may not be apparent under optimized growth conditions but is instead important for pollen performance, for example, under environmental extremes or for extended viability.

Another distinctive feature of Arabidopsis pollen sphingolipid composition was the unexpected complexity of GIPCs. Initially, complex but incompletely identified GIPCs containing up to six sugar residues were identified by LC–MS precursor scans monitoring for all GIPCs with the t18:1_h24:1 ceramide backbone. This method is limited in its ability to accurately determine the GIPC profile, since in source fragmentation during desolvation and ionization of GIPCs can give the appearance for more possible species than are actually present. To further characterize complex GIPCs, a MRM method was developed to identify different iterations of sugars. This allowed for identification of sugar composition by both mass and retention time. Using this method, two unique complex GIPCs, $(Pent)_3$-Hex-Hex(NAc)-HexA-IPC (Series E) and $(Pent)_2$-

Hex- Hex(NAc)-HexA-IPC (Series D) were identified. Neither of these species was found in leaf, though both forms of GIPC (lacking the N-acetyl or NAc substitution) were previously reported in Arabidopsis cell culture (Bure et al. 2011). The differences in observed retention times indicate that both of these species are found in planta and are not formed as a result of in source frag- mentation. The presence of N-acetylated hexose or Hex(NAc) containing-GIPCs has recently been reported in small amounts in Arabidopsis seedlings and seeds (Tellier et al. 2014), and GIPCs containing complex sugars have been reported in Arabidopsis cell culture (Bure et al. 2011). Our results for pollen differ from those in that Hex(NAc) containing-GIPCs were detected on the pentose- containing GIPCs, but not in Arabidopsis cell cultures (Bure et al. 2011), and no pentose-containing GIPCs were found in Arabidopsis seedlings and seeds (Tellier et al. 2014). Provisionally identified Hex-Hex(OH)-HexA-IPCs (Series B) were also found in leaf tissue, but not in pollen, which contrasts with the previous detection of Hex-Hex(OH)-HexA-IPCs (Series B) in Arabidopsis cell culture but not in leaf (Bure et al. 2011). This finding builds upon recent work by Tellier et al., 2014, in profiling different organs to identify unique Arabidopsis sphingolipids. The implication of these findings is that different sphingolipid structures may be required for optimal function in different tissues, suggesting that either the tissue environment requires a modified sphingolipid structure to perform the same function carried out in other tissues, or that a modified function is demanded of the different sphingolipid structure. Future studies to modify GIPC structure may help shed light on the role of GIPC structure in different tissue types.

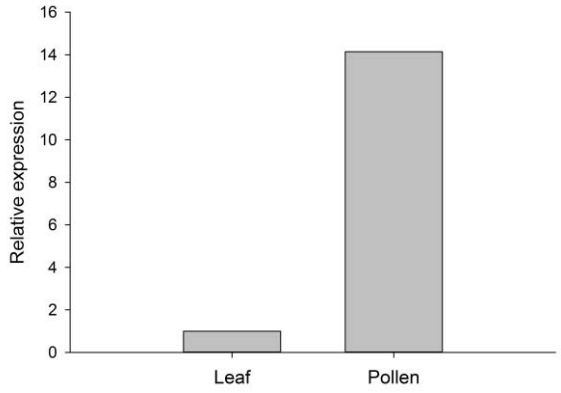

Figure 5.8 *qPCR of LOH2 in leaf and pollen tissues.* The leaf expression level was set to 1 with pollen representing a fold change in relation to leaf.

Publicly available RNA-Seq (Loraine et al. 2013) and microarray (Winter et al. 2007) data also pointed to distinct sphingolipid-related gene expression profiles. Consistent with the high GlcCer content, the GCS gene encoding the GlcCer synthase, which catalyzes the final step in GlcCer synthesis, was at least 100-fold more highly expressed in pollen than in seedlings and leaves. In addition, the LOH2 gene for the Type I ceramide synthase, which generates C16 fatty acid-containing ceramides for GlcCer synthesis, was more highly expressed in pollen based on microarray data and confirmed by qPCR analyses (Figure 5.8). Furthermore, in addition to the expected nearly exclusive expression of the Δ4 DES gene in pollen relative to seedlings and leaves, genes for other LCB modification enzymes were more highly expressed in pollen. Among these genes are SLD1 and SLD2, encoding the LCB Δ8 desaturase, and SBH1 and SBH2, encoding the LCB C-4 hydroxylase. Interestingly, the SLD2 and SBH2 genes were more highly expressed in pollen than SLD1 and SBH1, respectively. By contrast, SLD1 and SBH1 are more highly expressed than SLD2 and SBH2 in leaves and seedlings, based on data from

RNA-Seq and microarrays and from published northern blot analyses (Chen et al. 2012; Chen et al. 2008). These findings suggest that the SLD2 and SBH2 may have distinct and important roles in sphingolipid biosynthesis in pollen, including supporting biosynthetic pathways for GlcCer.

The primary goal of this study was to detect differences in sphingolipid metabolism between Arabidopsis pollen and leaf using lipidomic profiling and gene expression data. Although the analytical methods used are incapable of determining the exact identities of GIPC sugar residues and their linkages, they do provide an intriguing documentation of the specialized localization of novel GIPC species in Arabidopsis pollen that warrants further phytochemical investigation. Indeed, two of the major questions left in plant sphingolipid research are the function and identity of the variety of GIPC structures in plant physiology. The use of ESI–MS/MS and the application of multiple reaction monitoring (MRM) offer unprecedented sensitivity for identifying and reproducibly profiling the general classes of sugar residues in GIPCs with as little as three mg of tissue (Markham and Jaworski 2007). In addition, with internal standards, ESI–MS/MS coupled with MRM enable quantification of GIPCs as now routinely done for the major Arabidopsis leaf GIPC (Markham and Jaworski 2007). Notably, the only GIPC head group structures that have been completely characterized are those from tobacco leaf based on research from Lester and coworkers (Hsieh et al. 1978; Hsieh et al. 1981; Kaul and Lester 1978, 1975). These characterizations were conducted using extracts from three kg of tobacco leaf and established that glucosamine (±N-acetylation; α 1→4) glucuronic acid (α 1→2) myo-inositol-1-O-phosphorylceramide are the major GIPC forms in tobacco leaves. From these studies, it can be inferred that the major GIPC

of Arabidopsis pollen is possibly N-acetylated-glucosamine (α 1→4) glucuronic acid (α 1→2) myo-inositol-1-Ophosphoceramide (Figure 5.9), and the other Arabidopsis pollen GIPCs likely arise from additional and alternative glycosylation of the glucuronic acid (α 1→2) myo-inositol-1-O-phosphoceramide core structure. However, detailed structural characterization of Arabidopsis GIPCs awaits further purification and structural characterization. Given that these analyses require considerable amounts of plant material, complete structural elucidation of the distinct GIPCs of Arabidopsis pollen will be especially challenging using current approaches.

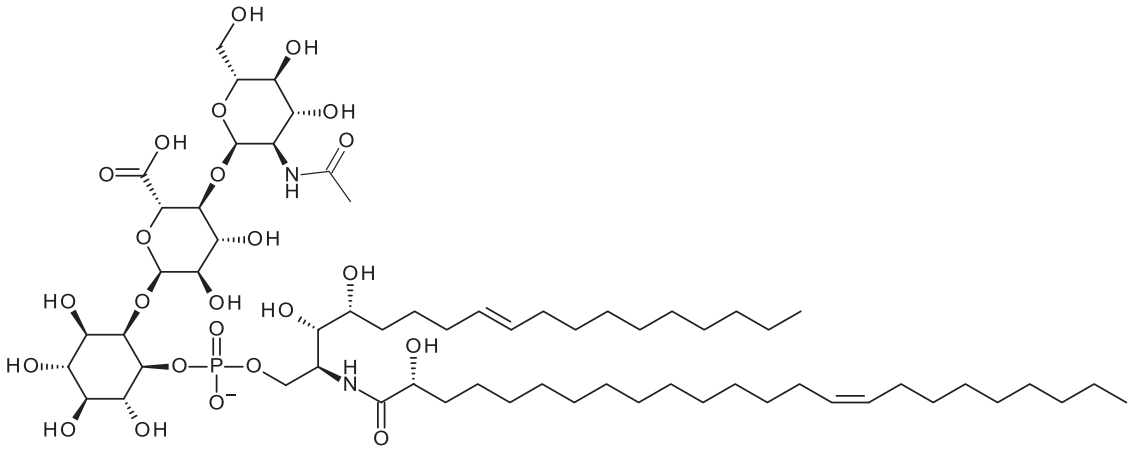

Figure 5.9. *Inferred structure of the major GIPC species in Arabidopsis pollen*. The structure shown is N-acetylated-glucosamine (α 1→4) glucuronic acid (α 1→2) myo-inositol-1-O-phosphoceramide, based on tobacco GIPC structural characterizations conducted by Lester and coworkers (Hsieh et al. 1978; Hsieh et al. 1981; Kaul and Lester 1975, 1978). The other Arabidopsis pollen GIPCs likely arise from additional and alternative glycosylation of the glucuronic acid (α 1→2) myo-inositol-1-O-phosphorylceramide core structure.

5.4. CONCLUDING REMARKS

The findings herein suggest that sphingolipid metabolism is strikingly different in Arabidopsis pollen than in leaves. In fact, based on compositional similarities, sphingolipid metabolism in Arabidopsis pollen is more similar to that found in leaves of plants such as tomato, soybean and tobacco (Bure et al. 2011; Hsieh et al. 1981; Kaul and Lester 1978; Markham et al. 2006). Similar to Arabidopsis pollen, previous studies, for example, have shown that GlcCer of tomato and soybean leaves is not only enriched in d18:2 LCBs, but also GlcCer concentrations are equal or greater than GIPC concentrations, suggesting a correlation between d18:2 and GlcCer concentrations in plant tissues (Markham et al. 2006). In addition, the large complexity of GIPC head groups in Arabidopsis pollen, in contrast to leaves, is similar to that reported for tobacco leaves (Hsieh et al. 1981; Kaul and Lester 1978). Given the GIPC structural dichotomy between Arabidopsis pollen and leaves, it is possible that a comparison of glycosyltransferase gene expression levels between these organs may reveal novel pollen-specific genes associated with complex GIPC head group assembly. Overall, our findings point to specialization in sphingolipid metabolism in pollen leading to distinct sphingolipid composition, the functional significance of which remains to be elucidated.

5.5. EXPERIMENTAL

5.5.1. POLLEN ISOLATION

Pollen was isolated from Arabidopsis Col-0 and Δ4 desaturase mutant (Salk_107761.42.15.x) plants grown in 16 h days at 22 °C. Flowers were harvested from 5 weeks old plants and incubated with shaking for 2 min in 0.3 M mannitol as previously described (Honys and Twell, 2003). Pollen was collected by centrifugation at 3780 x g for 10 min in 50 mL aliquots. Pollen pellets were then pooled in a microcentrifuge tube and collected by centrifugation at 16.3 x 1000g for 5 min. Isolated pollen was flash frozen in liquid N_2 and stored at -80 °C.

5.5.2. SPHINGOLIPIDOMIC ANALYSIS

Sphingolipids were extracted from 1 to 2 mg of lyophilized pollen using the lower phase of isopropanol/hexane/water (55:20:25 v/v/v) followed by Me3N:H2O (33:67, v/v) treatment described previously (Markham and Jaworski, 2007). Samples were dissolved in tetrahydrofuran (THF)/MeOH/H2O (2:1:2 v/v/v) containing 0.1% HCO2H. Sphingolipids were analyzed using a Shimadzu Prominence UPLC coupled with a QTRAP4000 mass spectrometer (ABSciex) as previously described (Kimberlin et al. 2013). MRMs to initially detect N-acetyl-sugar-containing GIPCs were calculated by adding 41 mass units to the Q1 ion of previously described GIPC MRMs (Markham and Jaworski, 2007). Instrument potentials and chromatography conditions for the initial detection of N-acetyl-sugar containing GIPCs were as for Hex-HexA-GIPCs described previously (Kimberlin et al. 2013). Precursor ion scanning to assess GIPC modifications was performed by monitoring for the t18:1_h24:1 backbone (precursors of *m/z* 662.6)

combined with chromatographic separation of GIPCs as described (Kimberlin et al. 2013).

5.5.3. COMPLEX GIPC MULTIPLE REACTION MONITORING METHOD

Pollen sphingolipid extracts were injected onto a reversed phase 75 mm Kinetex C18 HPLC column and eluted with a binary gradient with a flow rate of 0.60 mL/min with a column temperature of 40°C. The specific source and gradient conditions used can be found in Appendix E. The mass spectrometer was set to record starting at minute 2 and continued to minute 14. The mass spectrometer was operated in positive electrospray ionization using multiple reaction monitoring (MRM). GIPC structures monitored and their corresponding MRMs can be found in Appendix E along with the declustering potentials and collision energies used.

5.5.4. EXPANDED LC-ESI/MS/MS PROFILING METHOD MODIFICATIONS

Sphingolipid profiling to monitor an expanded set of sphingolipid structures was done using modifications of chromatography conditions and instrument settings, building on those described previously by Markham and Jaworski (2007). The QTRAP4000 ion spray voltage, entrance potential, and collision exit potential were set to 5000, 10, and 14 V respectively. For free LCB analysis, the collision exit potential was set at 17 V. Curtain gas, gas 1, and gas 2 were set to 20, 60, and 50 psi respectively for all classes except for hydroxyceramide analysis, which used curtain gas at 10 psi, gas1 at 40 psi and gas 2 at 50 psi. A reversed phase 100 mm Acclaim C-18 HPLC column (ThermoScientific, Waltham, MA USA) was eluted by a binary gradient formed by buffers A and B described above with a flow rate of 1.00 mL/min with a column temperature of 40 °C for ceramide, hydroxyceramide and GlcCer elution gradients. For provisionally identified

Hex(OH)-HexA GIPCs and free LCB gradients, the flow rate was set at 0.8 ml/min Source temperatures used were 550 °C (ceramides), 300 °C (hydroxyceramides), 350 °C (GlcCer), 350 °C (Hex(OH)-HexA GIPC), and 400 °C (free LCB). A summary of these conditions can be found in Appendix E. Binary gradient percentages and time monitored can be found in Appendix E. MRMs along with the corresponding collision energies and declustering potentials can be found in Appendix E.

5.5.5. RNA-SEQ AND MICROARRAY DATA MINING

Previously published RNA-Seq data (Loraine et al. 2013) comparing pollen and seedling was mined for sphingolipid synthesis genes. Data were compiled from RPM normalized data for genes encoding the following polypeptides: SPT subunits LCB1 (At4g36480), LCB2a (At5g23670), LCB2b (At3g48780), the two small subunits of SPT (ssSPT) ssSPTa (At1g06515) and ssSPTb (At2g30942), the two 3-ketosphinganine reductases TSC10A (At5g19200) and TSC10B (At3g06060), the two sphingoid base C-4 hydroxylases SBH1 (At1g69640) and SBH2 (At1g14290), the ceramide synthases LOH1 (At3g25540), LOH2 (At3g19260), and LOH3 (At1g13580), LCB Δ4 desaturase (At4g04930), the two LCB Δ8 desaturases SLD1 (At3g61580) and SLD2 (At2g46210), glucosylceramide synthase (GCS;At2g19880), the three inositolphosphoceramide synthases (IPS) IPS1 (At3g54020), IPS2 (At2g37940), and IPS3 (At2g29525) and the UDP-glucose IPC transferase IPUT1 (At5g18480). Microarray data for Arabidopsis sphingolipid genes were obtained from the Arabidopsis eFP Browser 2.0 (Winter et al. 2007). Gene numbers, names, and probe sets can be found in Appendix F. Vegetative rosette and mature pollen tissues were compared using total expression values. Error is represented by the reported standard deviation of three experiments.

5.5.6. RT-PCR AND qPCR

For analyses of organ-specific expression of 4, 6- to 8-week old Col-0 plants were used as sources of plant material. Pollen was harvested as described previously (Johnson-Brousseau and McCormick, 2004). RNA extraction was performed using the RNeasy Plant Kit (Qiagen) according to the manufacturer's protocol. RNA (1 μg) was treated with DNase I (Invitrogen) according to the manufacturer's protocol. Treated RNA was then reverse transcribed to cDNA with the iScript cDNA synthesis kit (Bio-Rad) according to the manufacturer's protocol. RT-PCR was conducted with an annealing temperature of 56 °C for 40 cycles. Forward and reverse primers used for Δ4 DES were 5-GAGGACGTGAGAAGATATCATC- 3 and 5-GCAAGGTTGTGACTTAGCTCATG-3. Forward and reverse primers used for the control ubiquitin-conjugating enzyme At5g25760 were 5-ATGCAGGCATCAAGAGCGCGACTGT-3 and 5-CACCGCCTTCGTAAGGAGTCTCCGA-3. qPCR was performed on the cDNA using the Bio-Rad MyiQ iCycler qPCR instrument. SYBR green was used as the fluorophore in a qPCR supermix (Qiagen). QuantiTect (Qiagen) primer sets for LOH2 (QT00774949) were used for relative quantification with PP2AA3 (At1g13320) used as an internal reference gene.

5.5.7. POLLEN IMAGING

Pollen imaging was performed using an Olympus AX70 optical microscope. Anthers and siliques of mature plants were isolated using a Nikon SMZ745T dissection microscope. Anthers were smeared on a glass slide and incubated with Alexander stain (Alexander 1969) at 4 °C for 45 min before viewing. Pollen viability was assessed by shape and color.

5.6 ACKNOWLEDGEMENT

The research was supported by funding from the U.S. National Science Foundation (MCB-1158500) to EBC.

5.7 REFERENCES

Alexander MP (1969) Differential Staining of Aborted and Nonaborted Pollen. Biotech Histochem 44 (3):117-122.

Borner GH, Sherrier DJ, Weimar T, Michaelson LV, Hawkins ND, Macaskill A, Napier JA, Beale MH, Lilley KS, Dupree P (2005) Analysis of detergent-resistant membranes in Arabidopsis. Evidence for plasma membrane lipid rafts. Plant Physiol 137 (1):104-116.

Brodersen P, Petersen M, Pike HM, Olszak B, Skov S, Odum N, Jorgensen LB, Brown RE, Mundy J (2002) Knockout of Arabidopsis accelerated-cell-death11 encoding a sphingosine transfer protein causes activation of programmed cell death and defense. Genes Dev 16 (4):490-502.

Bure C, Cacas JL, Wang F, Gaudin K, Domergue F, Mongrand S, Schmitter JM (2011) Fast screening of highly glycosylated plant sphingolipids by tandem mass spectrometry. Rapid Commun Mass Spectrom 25 (20):3131-3145.

Cacas JL, Bure C, Furt F, Maalouf JP, Badoc A, Cluzet S, Schmitter JM, Antajan E, Mongrand S (2013) Biochemical survey of the polar head of plant glycosylinositolphosphoceramides unravels broad diversity. Phytochem 96:191-200.

Cantrel C, Vazquez T, Puyaubert J, Reze N, Lesch M, Kaiser WM, Dutilleul C, Guillas I, Zachowski A, Baudouin E (2011) Nitric oxide participates in cold-responsive phosphosphingolipid formation and gene expression in Arabidopsis thaliana. New Phytol 189 (2):415-427.

Chen M, Cahoon E, Saucedo-García M, Plasencia J, Gavilanes-Ruíz M (2010) Plant Sphingolipids: Structure, Synthesis and Function. In: Wada H, Murata N (eds) Lipids in Photosynthesis, vol 30. Advances in Photosynthesis and Respiration. Springer Netherlands, pp 77-115. doi:10.1007/978-90-481-2863-1_5

Chen M, Han G, Dietrich CR, Dunn TM, Cahoon EB (2006) The essential nature of sphingolipids in plants as revealed by the functional identification and characterization of the Arabidopsis LCB1 subunit of serine palmitoyltransferase. Plant Cell 18 (12):3576-3593.

Chen M, Markham JE, Cahoon EB (2012) Sphingolipid Delta8 unsaturation is important for glucosylceramide biosynthesis and low-temperature performance in Arabidopsis. Plant J 69 (5):769-781.

Chen M, Markham JE, Dietrich CR, Jaworski JG, Cahoon EB (2008) Sphingolipid long-chain base hydroxylation is important for growth and regulation of sphingolipid content and composition in Arabidopsis. Plant Cell 20 (7):1862-1878.

Coursol S, Fan LM, Le Stunff H, Spiegel S, Gilroy S, Assmann SM (2003) Sphingolipid signalling in Arabidopsis guard cells involves heterotrimeric G proteins. Nature 423 (6940):651-654.

Dietrich CR, Han G, Chen M, Berg RH, Dunn TM, Cahoon EB (2008) Loss-of-function mutations and inducible RNAi suppression of Arabidopsis LCB2 genes reveal the critical role of sphingolipids in gametophytic and sporophytic cell viability. Plant J 54 (2):284-298.

Guillas I, Guellim A, Reze N, Baudouin E (2012) Long chain base changes triggered by a short exposure of Arabidopsis to low temperature are altered by AHb1 non-symbiotic haemoglobin overexpression. Plant Physiol Biochem 63C:191-195.

Honys D, Twell D (2003) Comparative Analysis of the Arabidopsis Pollen Transcriptome. Plant Physiol 132 (2):640-652.

Hsieh TC, Kaul K, Laine RA, Lester RL (1978) Structure of a major glycophosphoceramide from tobacco leaves, PSL-I: 2-deoxy-2-acetamido-D-glucopyranosyl(alpha1 leads to 4)-D-glucuronopyranosyl(alpha1 leads to 2)myoinositol-1-O-phosphoceramide. Biochem 17 (17):3575-3581.

Hsieh TC, Lester RL, Laine RA (1981) Glycophosphoceramides from plants. Purification and characterization of a novel tetrasaccharide derived from tobacco leaf glycolipids. J Biol Chem 256 (15):7747-7755.

Imai H, Yamamoto K, Shibahara A, Miyatani S, Nakayama T (2000) Determining double-bond positions in monoenoic 2-hydroxy fatty acids of glucosylceramides by gas chromatography-mass spectrometry. Lipids 35 (2):233-236.

Islam MN, Jacquemot MP, Coursol S, Ng CK (2012) Sphingosine in plants--more riddles from the Sphinx? New Phytol 193 (1):51-57.

Johnson-Brousseau SA, McCormick S (2004) A compendium of methods useful for characterizing Arabidopsis pollen mutants and gametophytically- expressed genes. Plant J 39 (5):761-775.

Kaul K, Lester RL (1975) Characterization of Inositol-containing Phosphosphingolipids from Tobacco Leaves: Isolation and Identification of Two Novel, Major Lipids: N-Acetylglucosamidoglucuronidoinositol Phosphorylceramide and Glucosamidoglucuronidoinositol Phosphorylceramide. Plant Physiol 55 (1):120-129.

Kaul K, Lester RL (1978) Isolation of six novel phosphoinositol-containing sphingolipids from tobacco leaves. Biochem 17 (17):3569-3575.

Kimberlin AN, Majumder S, Han G, Chen M, Cahoon RE, Stone JM, Dunn TM, Cahoon EB (2013) Arabidopsis 56-Amino Acid Serine Palmitoyltransferase-Interacting Proteins Stimulate Sphingolipid Synthesis, Are Essential, and Affect Mycotoxin Sensitivity. Plant Cell 25 (11):4627-4639.

Loraine AE, McCormick S, Estrada A, Patel K, Qin P (2013) RNA-Seq of Arabidopsis Pollen Uncovers Novel Transcription and Alternative Splicing. Plant Physiol 162 (2):1092-1109.

Lynch DV, Dunn TM (2004) An introduction to plant sphingolipids and a review of recent advances in understanding their metabolism and function. New Phytol 161 (3):677-702.

Markham JE, Jaworski JG (2007) Rapid measurement of sphingolipids from Arabidopsis thaliana by reversed-phase high-performance liquid chromatography coupled to electrospray ionization tandem mass spectrometry. Rapid Commun Mass Spectrom 21 (7):1304-1314.

Markham JE, Li J, Cahoon EB, Jaworski JG (2006) Separation and identification of major plant sphingolipid classes from leaves. J Biol Chem 281 (32):22684-22694.
Markham JE, Molino D, Gissot L, Bellec Y, Hematy K, Marion J, Belcram K, Palauqui JC, Satiat-Jeunemaitre B, Faure JD (2011) Sphingolipids containing very-long-chain fatty acids define a secretory pathway for specific polar plasma membrane protein targeting in Arabidopsis. Plant Cell 23 (6):2362-2378.
Michaelson LV, Zauner S, Markham JE, Haslam RP, Desikan R, Mugford S, Albrecht S, Warnecke D, Sperling P, Heinz E, Napier JA (2009) Functional characterization of a higher plant sphingolipid Delta4-desaturase: defining the role of sphingosine and sphingosine-1-phosphate in Arabidopsis. Plant Physiol 149 (1):487-498.
Mongrand S, Morel J, Laroche J, Claverol S, Carde JP, Hartmann MA, Bonneu M, Simon-Plas F, Lessire R, Bessoule JJ (2004) Lipid rafts in higher plant cells: purification and characterization of Triton X-100-insoluble microdomains from tobacco plasma membrane. J Biol Chem 279 (35):36277-36286.
Mortimer JC, Yu XL, Albrecht S, Sicilia F, Huichalaf M, Ampuero D, Michaelson LV, Murphy AM, Matsunaga T, Kurz S, Stephens E, Baldwin TC, Ishii T, Napier JA, Weber APM, Handford MG, Dupree P (2013) Abnormal Glycosphingolipid Mannosylation Triggers Salicylic Acid-Mediated Responses in Arabidopsis. Plant Cell 25 (5):1881-1894.
Nagano M, Ishikawa T, Ogawa Y, Iwabuchi M, Nakasone A, Shimamoto K, Uchimiya H, Kawai-Yamada M (2014) Arabidopsis Bax inhibitor-1 promotes sphingolipid synthesis during cold stress by interacting with ceramide-modifying enzymes. Planta 240 (1):77-89.
Ng CKY, Carr K, McAinsh MR, Powell B, Hetherington AM (2001) Drought-induced guard cell signal transduction involves sphingosine-1-phosphate (vol 410, pg 596, 2001). Nature 411 (6834):219-219.
Saucedo-Garcia M, Gonzalez-Solis A, Rodriguez-Mejia P, Olivera-Flores Tde J, Vazquez-Santana S, Cahoon EB, Gavilanes-Ruiz M (2011) Reactive oxygen species as transducers of sphinganine-mediated cell death pathway. Plant Signal Behav 6 (10):1616-1619.
Sperling P, Franke S, Luthje S, Heinz E (2005) Are glucocerebrosides the predominant sphingolipids in plant plasma membranes? Plant Physiol Biochem 43 (12):1031-1038.
Sperling P, Zahringer U, Heinz E (1998) A sphingolipid desaturase from higher plants. Identification of a new cytochrome b5 fusion protein. J Biol Chem 273 (44):28590-28596.
Tellier F, Maia-Grondard A, Schmitz-Afonso I, Faure JD (2014) Comparative plant sphingolipidomic reveals specific lipids in seeds and oil. Phytochem 103:50-58.
Teng C, Dong H, Shi L, Deng Y, Mu J, Zhang J, Yang X, Zuo J (2008) Serine palmitoyltransferase, a key enzyme for de novo synthesis of sphingolipids, is essential for male gametophyte development in Arabidopsis. Plant Physiol 146 (3):1322-1332.
Winter D, Vinegar B, Nahal H, Ammar R, Wilson GV, Provart NJ (2007) An "Electronic Fluorescent Pictograph" browser for exploring and analyzing large-scale biological data sets. PLoS One 2 (8):e718.

CHAPTER 6

IDENTIFICATION AND CHARACTERIZATION OF A Δ8 LONG CHAIN BASE DESATURASE THAT IS HIGHLY SPECIFIC FOR Δ4 UNSATURATED LONG CHAIN BASES

Note: The results described here are to be published.

The authors of this work are: Luttgeharm K.D., A. Mehra, A. Kamigaki, J.A. Napier, J.E. Markham, E.B. Cahoon

6.1 INTRODUCTION

Sphingolipid modifications vary between plant species. For instance tomato and soybean contain large amounts of d18:2(4,8) LCBs in leaf while other species, such as Arabidopsis, contain primarily d18:1(8) and t18:1(8) (Markham et al. 2006). Sphingolipid profiles can also vary between different tissues within the same plant; indeed Arabidopsis reproductive tissues have been found to contain large amounts of d18:2(4,8) LCBs (Michaelson et al. 2009; Luttgeharm et al. 2015) (Chapter 5). In all plants examined to date, the d18:2(4,8) LCB is almost exclusively found in glucosylceramides (GlcCer) indicating the presence of distinct complex sphingolipid synthesis pathways which has been proposed in multiple reports (Chen et al. 2008; Garcia-Maroto et al. 2007). In support of this hypothesis knockout of the Δ4 LCB DES in Arabidopsis significantly reduces the amount of GlcCers found in pollen and flower but does not result in drastic changes in other complex sphingolipid levels (Luttgeharm et al. 2015; Michaelson et al. 2009) (Chapter 5). Seemingly minor sphingolipid modifications could serve to direct LCBs through specific ceramide synthases for eventual synthesis into specific complex sphingolipids. For instance, *in vitro* study of the Arabidopsis ceramide synthases found that the Arabidopsis ceramide synthase isoform LOH2 is most active with the d18:1(4) LCB not usually found in leaf (Chapter 3) which could explain the high GlcCer levels found in pollen where the Δ4 LCB DES is expressed.

The Δ8 LCB DES was originally discovered in sunflower and found to contain an N-terminal cytochrome b_5 domain and a domain similar to membrane-bound acyl lipid desaturases. Homologs identified in *Brassica napus* and Arabidopsis were confirmed to

be sphingolipid Δ8 LCB desaturases by expression in *Saccaromyces cerevisiae* (Sperling et al. 1998). Since the discovery and characterization of the Δ8 desaturase little work has been done on the substrate specificity of these enzymes. Previous research has identified three *Nicotiana tabacum* Δ8 LCB DES denoated *NTD8DES1*, *NTD8DES2*, and *NTDXDES* with *NTD8DES1*/2 being closely related to confirmed Δ8 LCB DESes while *NTDXDES* is more closely related to Δ6 fatty acid desaturases. Further study revealed that *NTDXDES* is a bona fide Δ8 LCB DES with RNAi knockdown indicating that *NTDXDES* prefers to desaturate t18:0 to t18:1(8). Knockdown of *NTDXDES* did not affect d18:2(4,8) LCB levels further demonstrating its preference for t18:0 (Garcia-Maroto et al. 2007) indicating that different Δ8 LCB DES classes may exist. Indeed Garcia-Maroto (2007) hypothesized that two different classes of Δ8 LCB DES exists: one for the synthesis of GlcCer (i.e. d18:2(4,8) LCBs) and one for the synthesis of glucosylinositolphosphoceramides (GIPCs, i.e. t18:1(8) and d18:1(8) LCBs).

In this chapter we examine the substrate specificity of a putative Δ8 LCB DES isolated from *Ricinus communis* (Castor bean) and propose that two distinct classes of Δ8 LCB DES exists. The first acts on fully saturated LCBs (d18:0 or t18:0) while the second strongly prefers d18:1(4) LCBs. We hypothesize that Δ4 LCB desaturation occurs prior to Δ8 desaturation and serves as a marker for GlcCer synthesis through a LOH2-like ceramide synthase.

6.2 RESULTS

6.2.1 IDENTIFICATION AND EXPRESSION OF A CASTOR BEAN Δ8 LCB DESATURASE

To determine the sphingolipid composition of castor bean, total LCB profiling by HPLC was conducted (Figure 6.1). The primary LCBs identified were t18:0, t18:1(8), and d18:2(4,8) demonstrating that the castor bean genome contains at least one Δ8 LCB DES. NCBI BLAST analysis returned two putative Δ8 LCB DES in the castor bean genome denoted putative fatty acid desaturase (hereby referred to as CbDES8-1) and desaturase/cytochrome b5 protein (hereby referred to as CbDES8-2). Expression of CbDES8-1 in the *Δsld1/sld2* double mutant produced little to no desaturated LCBs. This was contrasted with the *Δsld1/sld2* + At *SLD2* line which contained large amounts of both trihydroxy and dihydroxy desaturated LCBs (Representative total LCB profiles can be found in Figure 6.2 with total sphingolipid profiles found in Appendix E).

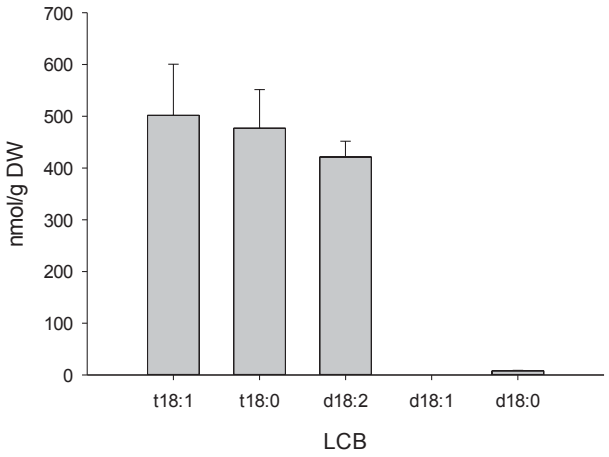

Figure 6.1: *Total LCB profile of mature castor bean leaves*. Mature leaves from castor bean were analyzed by HPLC. It was found that castor bean contains approximently equal amounts of t18:1, t18:0, and d18:2 LCB sphingolipids.

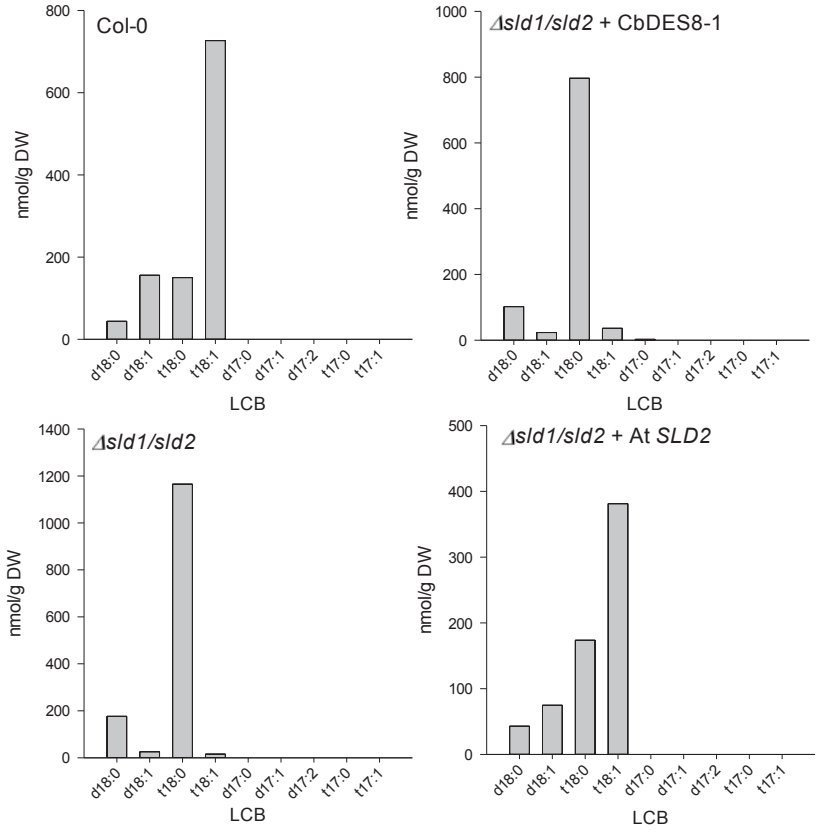

Figure 6.2 *Total LCB profiles from representative plants*. CbDES8-1 was not able to restore production of Δ8 desaturated LCBs in *Δsld1/sld2* double mutants of Arabidopsis.

6.2.2 PHYLOGENETIC ANALYSIS REVEALS DISTINCT EVOLUTIONARY Δ8 LCB DESATURASE BRANCHES

To investigate the possibility that CbDES8-1 belongs to a unique class of Δ8 LCB DESes, phylogenetic analysis was done using the amino acid sequence of confirmed and putative Δ8 LCB DESes (Figure 6.3) which found that Δ8 LCB DESes clustered into a many different branches. Since castor bean contains high levels of d18:2(4,8) LCBs and CbDES8-1 clustered with other plants enriched in d18:2(4,8) sphingolipids it was hypothesized that this branch of Δ8 LCB DESes requires the presence of a Δ4 double bond for activity.

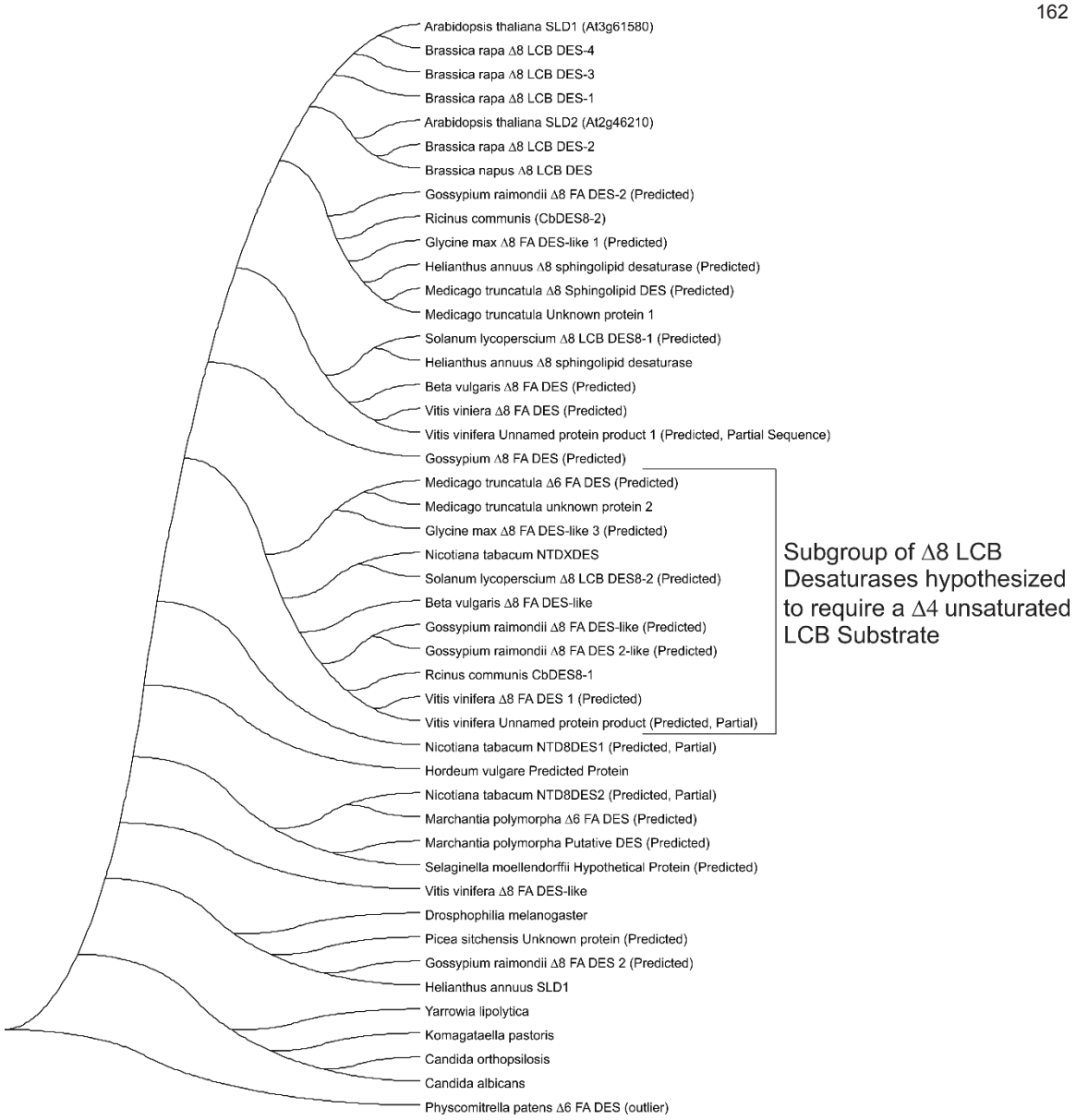

Figure 6.3: *Phylogenetic analysis of confirmed and putative Δ8 LCB DESes from plants and fungi*. Phylogenetic analysis of Δ8 LCB DESes was done using the neighbor-joining method. The bootstrap consensus tree inferred from 1000 replicates is representative of the evolution of Δ8 LCB DESes. All phylogenetic analysis was done using MEGA5 and the Physomitrella patens Δ6 fatty acid desaturase as an outlier. The percentage of replicate trees in which the associated taxa clustered together in the bootstrap test (1000 replicates) are shown next to the branches. The tree is drawn to scale, with branch lengths in the same units as those of the evolutionary distances used to infer the phylogenetic tree.

6.2.3 CASTOR BEAN Δ8 LCB DES REQUIRES A Δ4 DESATURATED LCB FOR ACTIVITY

In order to investigate the possibility of a Δ8 LCB desaturase family specific for Δ4 unsaturated LCBs, the Arabidopsis Δ8 LCB DES mutant (*Δsld1/sld2)* complemented with the CbDES8-1 was grown on LS media containing d17:0 or d17:1(4) LCBs. Complemented plants grown on d17:1(4) were found to contain large amounts of d17:2(4,8) LCBs, particularly in the GlcCer fraction. Representative total LCB and GlcCer profiles can be found in Figure 6.4 with complete sphingolipid profiles in Appendix E. The ceramide (Cer) and hydroxyceramide (hCer) profiles were found to contain large amounts of d17:1(4) sphingolipids but only small amounts of d17:2(4,8) sphingolipids. The glucoscylinositolphosphoceramide (GIPC) fraction contained little to no d17:1(4) or d17:2(4,8) sphingolipids. Complemented plants fed the d17:0 LCB were found to contain t17:0 sphingolipids but little to no d17:1(8) or t17:1(8) sphingolipids. Representative total LCB profiles can be found in Figure 6.5 with complete sphingolipid profiles in Appendix E. Non-complemented *Δsld1/sld2* plants contained no unsaturated sphingolipids (except for those fed d17:1(4) which was found primarily in GlcCers).

To verify that both d17:0 and t17:0 LCBs could be desaturated at the Δ8 position, *Δsld1/sld2* mutants complemented with *SLD2* were fed d17:0 and d17:1(4) LCBs. Similar profiles were found as described previously with exception of plants being fed d17:0 containing t17:1(8) LCBs in all class with large amounts in the GIPCs. Representative total LCB and GlcCer profiles can be found in Figure 6.4 and 6.5 with complete sphingolipid profiles in Appendix E.

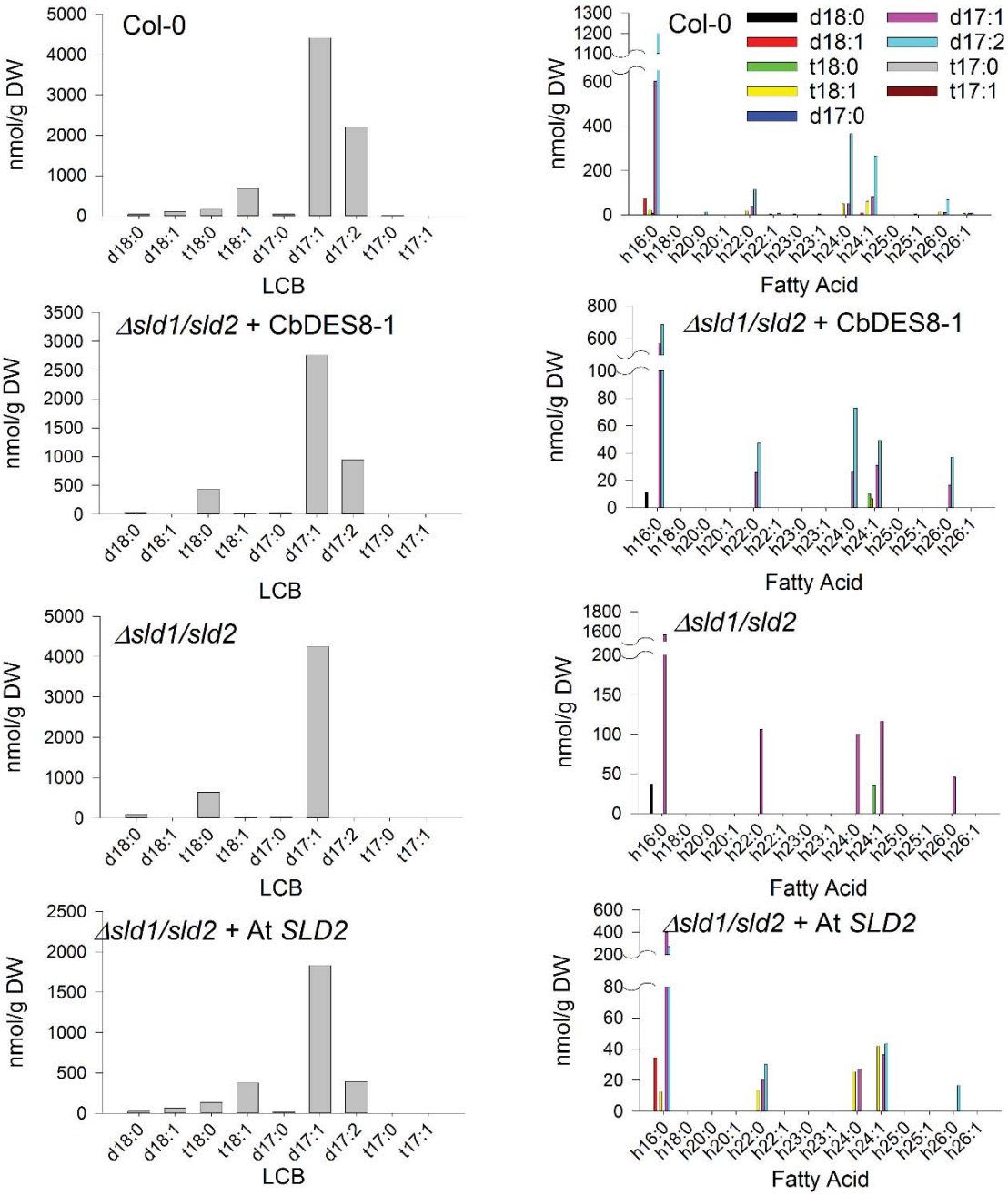

Figure 6.4: *Total LCB and GlcCer analysis of plants chemically complemented with d17:1(4) LCB.* Representative profiles of plants grown for 10 days on LS media containing the d17:1(4) LCB. Plants complemented with the CbDES8-1 were able to produce large amounts of d17:2(4,8) sphingolipids primarily found in the GlcCers.

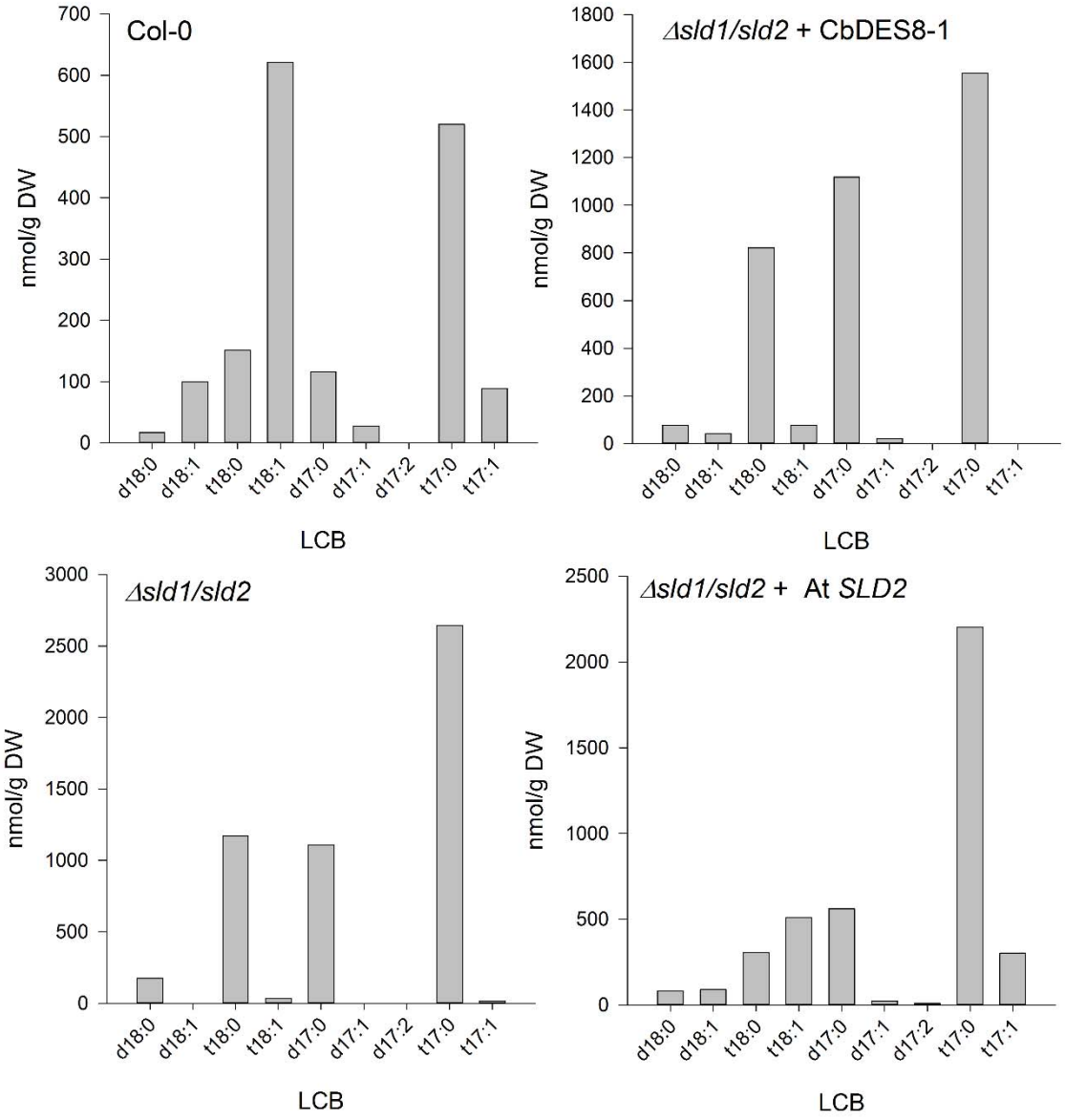

Figure 6.5: *Total LCB analysis of plants chemically complemented with d17:0 LCB.* Representative Total LCB profiles of plants grown for 10 days on LS media containing the d17:0 LCB. Plants complemented with the CbDES8-1 were unable to convert d17:0 to d17:1(8), however plants complemented with the Arabidopsis Δ8 LCB DES *SLD2* were able to produce both d17:1(8) and t17:1(8).

6.3 DISCUSSION

Sphingolipid LCB desaturation is an important step in sphingolipid synthesis. It is possible that these modifications serve to mark LCBs for synthesis into specific complex sphingolipids. Supporting this notion is the enrichment of certain LCBs in specific sphingolipid classes. For instance, the d18:2(4,8) LCB has previously been shown to be found almost exclusively in GlcCers with Arabidopsis Δ4 LCB DES knockouts containing significantly less GlcCers in pollen (Michaelson et al. 2009; Luttgeharm et al. 2015) (Chapter 5). Other plants, such as tobacco and tomato, also have elevated levels of GlcCers which are enriched in d18:2(4,8) LCBs implying that the enrichment of d18:2(4,8) in GlcCers is evolutionarily conserved (Markham et al. 2006). It is therefore unsurprising to find specialized Δ8 LCB DESes that require the presence of a Δ4 desaturation. The ability of CbDES8-1 to act on Δ4 desaturated LCBs and not fully saturated LCBs indicates that this enzyme is a part of a novel Δ8 LCB DES gene family that is responsible for targeting LCBs to GlcCers. The presence of a distinct evolutionary branch of Δ8 LCB DESes demonstrates that the specificity for Δ4 desaturated LCBs is a conserved in different organisms. The exact domains responsible for this selectivity have yet to be determined.

It is interesting to note that previous work with Arabidopsis ceramide synthase substrate specificity found that the Arabidopsis ceramide synthase LOH2 has the highest level of activity with d18:1(4) as a substrate but demonstrates little to no activity with d18:1(8). The other two ceramide synthase isoforms (LOH1 and LOH3) demonstrate low levels of activity with d18:1(4) and little to no activity with d18:1(8) (Chapter 3). Taken together these results indicate that the Δ4 LCB DES acts on the free LCB,

followed by incorporation into ceramide, and subsequent Δ8 desaturation. The d18:2(4,8) LCB ceramides are then preferentially synthesized into GlcCers as summarized in Figure 6.6. The presence of specialized Δ8 LCB DESes could act to increase the flux of LCBs to GlcCers.

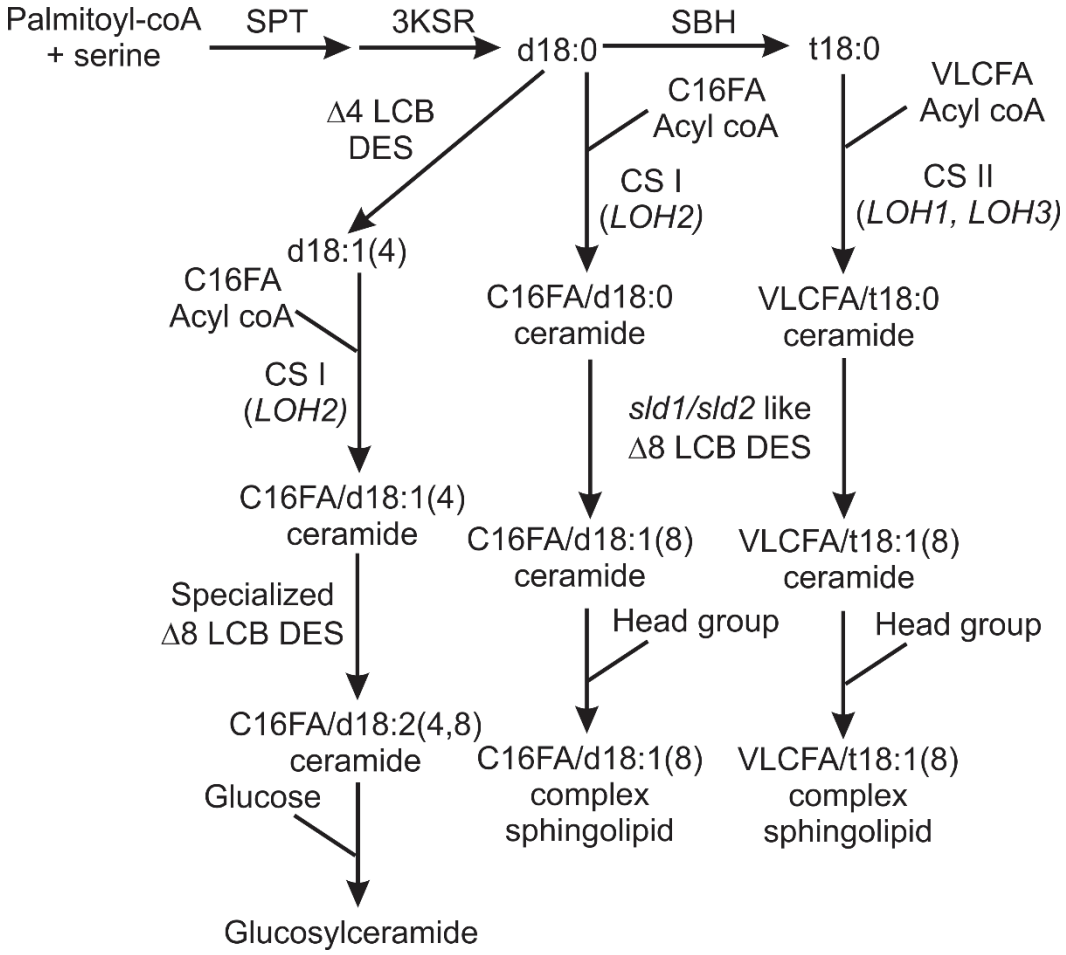

Figure 6.6: *Proposed pathway for the partitioning of LCBs into the GlcCer fraction by desaturation of the LCB through a specialized Δ8 LCB DES*. In this model the Δ4 desaturation is added to the free LCB and serves as a marker for conversion to ceramide by a LOH2-like ceramide synthase followed by desaturation by a specialized Δ8 LCB DES. This ceramide can then be readily incorporated into GlcCers.

GlcCers have been linked to cell differentiation and organogenesis (Msanne et al. 2015) in plants with this being a seemingly conserved function; for instance, dimorphous

yeast are unable to transition from a budding to filamentous yeast without GlcCers (Noble et al. 2010). In order to maintain proper GlcCer levels organisms may have developed specialized pathways, such as the one presented here, to shunt LCBs towards the synthesis of GlcCers. It is interesting to note that organisms, like Arabidopsis, contain GlcCers, albeit at a lower level, but seem to lack a specialized Δ8 LCB DES suggesting that Arabidopsis may have evolved some yet to be identified mechanism for targeting LCBs to GlcCers.

The findings presented here indicate that Δ8 LCB DESes have evolved into unique families. The Arabidopsis-like Δ8 LCB desaturase family prefers to act on fully saturated LCBs while a second family prefers to act on LCBs containing a Δ4 desaturation. By combining this with the previously published ceramide synthase enzyme specificity data we hypothesize that the Δ4 LCB DES acts on the free fully saturated LCB which is subsequently used to form ceramide through LOH2-like ceramide synthases. This ceramide can then be further desaturated by a specialized Δ8 LCB desaturase to form d18:2(4,8) LCB ceramides. The presence of the d18:2(4,8) LCB ultimately acts as a marker for GlcCer synthesis. This mechanism appears to be conserved throughout the plant kingdom with a few exceptions such as Arabidopsis. The evolutionary significance of these distinct GlcCer pathways has yet to be determined.

6.4 EXPERIMENTAL

6.4.1 PHYLOGENETIC ANALYSIS OF Δ8 LCB DES

Δ8 LCB DES sequences were identified by a NCBI BLAST search for different plant and fungal species using Arabidopsis Δ8 LCB DESes *SLD1* (At3g161580) and *SLD2* (At2g46210). Δ8 LCB DES identified are as follows: *Nicotiana tabacum NTDXDES* (tobacco, ABO31111), *NTD8DES1 and NTD8DES2* partial sequences were provided by Federico Garcia Maroto and sequences can be found in Appendix F; *Ricinus communis* (castor bean, AAD01240); *Drosophila melanogaster* (fly, NP_477154); *Brassica rapa* isoforms 1, 2, 3, and 4 (AEW24954, AEW24951, NP_001288997, AEW24593 respectively); *Brassica napus* (CAA11857); *Solanum lycopersicum* (Tomato) isoforms 1 and 2 (XP_004340093 and XP_004345093 respectively); *Glycine max* (soybean) Δ8 Fatty acid desaturase-like 1, Δ8 fatty acid desaturase-like 2, and Δ8 fatty acid desaturase-like 3 (XP_003517965, XP_003532059, XP_003550268 respectively); *Yarrowia lipolytica* (XP_504218); *Candida orthopsilosis* (XP_003867485); *Candida albicans* (XP_719958); *Komagataella pastoris* (XP_00248967); *Gossypium raimondii* Δ8 fatty acyid desaturase 2, Δ8 fatty acid desaturase like, Δ8 fatty acid desaturase 2-like, Δ8 fatty acid desaturase like and Δ8 fatty acid desaturase 2 (XP_82312438, XP_012446385, XP_012477302, XP 012437725, and XP_012490036 respectively); *Medicago truncatula* Δ8 sphingolipid desaturase, unknown protein 1, and unknown protein 2 (XP_003628379, AFK42352, and AFK34809 respectively); *Helianthus annuus* Δ8 sphingolipid desaturase and SLD1_HELAN (ADK91077 and Q43469 respectively); *Vitis vinifera* Δ8 fatty acid desaturase, Δ8 fatty acid desaturase 1, unnamed protein product 1, unnamed protein product 2, and Δ8 fatty

acid desaturase like (XP_002279227, XP_002279189, CBI40451, CBI20658, and XP_010656528 respectively); *Beta vulgaris* Δ8 fatty acid desaturase and Δ8 fatty acid desaturase like (XP_010669699 and XP_010669398 respectively); *Hordeum vulgare* predicted protein (BAK00580); *Marchantia polymorpha* putative desaturase and Δ6 fatty acid desaturase (AAT85664, AAT85661 respectively); *Selgainella moellendorffii* hypothetical protein (XP_002968817); *Marchantia polymorpha* Δ6 fatty acid desaturase (AAT85661). *Physcomitrella patens* Δ6 fatty acid desaturase (XP_001763930) was chosen as an outlier as previously described (Garcia-Maroto et al. 2007). MEGA5, using the neighbor-joining method (Tamura et al. 2011), was used for phylogenetic analysis of the aligned full-length Δ8 LCB DES sequences. All positions containing gaps and missing data were eliminated and the tree underwent the bootstrap test (1000 replicates).

6.4.2 ΔSLD1/SLD2 MUTANT BACKGROUND

The *Δsld1/sld2* mutant background was made as previously described (Chen et al. 2012).

6.4.3 OVEREXPRESSION OF SLD2 AND CASTOR BEAN Δ8 LCB DESES IN ARABIDOPSIS

CbDes8-1 was amplified from prepared cDNA (5'-TATAAGCTTAAAATGGCAGAAACAAAGAAGTACATTAC-3', 5'-TATGGATCCTATCATCCATGAGTATTAACAGCTTCC-3') and was cloned into pART7-AscI at the BamHI and HindIII cloning sites under the control of the CaMV 35S promoter. The promoter and gene were then cut from pART7-AscI at flanking AscI sites and cloned into the pB110 binary. The completed binary was transformed into the Arabidopsis *Δsld1/sld2* double mutant by Agrobacterium mediated floral dip (Strain

GV1301) (Clough and Bent 1998). Seeds were screened for the DS Red marker to identify transgenic seeds (Jach et al. 2001).

6.4.4 LCB FEEDING EXPERIMENTS

Plants were plated on Linsmaier and Skoog media containing 200 μM final concentration of d17:0 (Avanti 86065) or d17:1(4) (Avanti 860640) diluted from a 5 mM methanol stock solution and 0.2% w/v Tegeritol (diluted from 70% w/v Sigma NP40S). Control plates contained an equal volume of methanol in replace of LCB stocks. Seeds were surfaced sterilized in 1 mL of 1:1 bleach/water containing 0.2% Tween-20 for 10 min, washed 3x with 1 mL sterile water, and plated. Seed plates were incubated at 4°C for 48 hours then moved under grow lights with a 24 hour day (100 $\mu mol/m^{-2}/s^{-1}$). After 10 days seedlings were harvested, frozen with liquid nitrogen, and lyophilized overnight.

6.4.5 TOTAL LCB ANALYSIS

Total LCB analysis was performed as previously described (Markham et al. 2006) from mature castor bean leaves.

6.4.6 SPHINGOLIPIDOMIC ANALYSIS

Sphingolipids were extracted from 1 to 2 mg of lyophilized tissue using the lower phase of isopropanol/hexane/water (55:20:25 v/v/v) followed by 33% methylamine treatment described previously (Markham and Jaworski 2007). Samples were dissolved in tetrahydrofuran (THF)/methanol/water (2:1:2 v/v/v) containing 0.1% formic acid. Sphingolipids were analyzed using a Shimadzu Prominence UPLC coupled with a QTRAP4000 mass spectrometer (ABSciex) as previously described (Markham and Jaworski 2007). LCMS parameters and MRMs for C17 LCB sphingolipids can be found in Appendix G, all other parameters were the same as Markham et al (2007).

6.5 REFERENCES

Chen M, Markham JE, Cahoon EB (2012) Sphingolipid Delta8 unsaturation is important for glucosylceramide biosynthesis and low-temperature performance in Arabidopsis. Plant J 69 (5):769-781.

Chen M, Markham JE, Dietrich CR, Jaworski JG, Cahoon EB (2008) Sphingolipid long-chain base hydroxylation is important for growth and regulation of sphingolipid content and composition in Arabidopsis. Plant Cell 20 (7):1862-1878.

Clough SJ, Bent AF (1998) Floral dip: a simplified method for Agrobacterium-mediated transformation of Arabidopsis thaliana. Plant J 16 (6):735-743.

Garcia-Maroto F, Garrido-Cardenas JA, Michaelson LV, Napier JA, Alonso DL (2007) Cloning and molecular characterisation of a Delta8-sphingolipid-desaturase from Nicotiana tabacum closely related to Delta6-acyl-desaturases. Plant Mol Biol 64 (3):241-250.

Jach G, Binot E, Frings S, Luxa K, Schell J (2001) Use of red fluorescent protein from Discosoma sp (dsRED) as a reporter for plant gene expression. Plant J 28 (4):483-491.

Luttgeharm KD, Kimberlin AN, Cahoon RE, Cerny RL, Napier JA, Markham JE, Cahoon EB (2015) Sphingolipid metabolism is strikingly different between pollen and leaf in Arabidopsis as revealed by compositional and gene expression profiling. Phytochem.

Markham JE, Jaworski JG (2007) Rapid measurement of sphingolipids from Arabidopsis thaliana by reversed-phase high-performance liquid chromatography coupled to electrospray ionization tandem mass spectrometry. Rapid Commun Mass Spectrom 21 (7):1304-1314.

Markham JE, Li J, Cahoon EB, Jaworski JG (2006) Separation and identification of major plant sphingolipid classes from leaves. J Biol Chem 281 (32):22684-22694.

Michaelson LV, Zauner S, Markham JE, Haslam RP, Desikan R, Mugford S, Albrecht S, Warnecke D, Sperling P, Heinz E, Napier JA (2009) Functional characterization of a higher plant sphingolipid Delta4-desaturase: defining the role of sphingosine and sphingosine-1-phosphate in Arabidopsis. Plant Physiol 149 (1):487-498.

Msanne J, Chen M, Luttgeharm KD, Bradley AM, Mays ES, Paper JM, Boyle DL, Cahoon RE, Schrick K, Cahoon EB (2015) Glucosylceramide is Critical for Cell-Type Differentiation and Organogenesis, but not for Cell Viability in Arabidopsis. The Plant journal : for cell and molecular biology.

Noble SM, French S, Kohn LA, Chen V, Johnson AD (2010) Systematic screens of a Candida albicans homozygous deletion library decouple morphogenetic switching and pathogenicity. Nature genetics 42 (7):590-598.

Sperling P, Zahringer U, Heinz E (1998) A sphingolipid desaturase from higher plants. Identification of a new cytochrome b5 fusion protein. J Biol Chem 273 (44):28590-28596.

Tamura K, Peterson D, Peterson N, Stecher G, Nei M, Kumar S (2011) MEGA5: molecular evolutionary genetics analysis using maximum likelihood, evolutionary distance, and maximum parsimony methods. Molecular biology and evolution 28 (10):2731-2739.

CHAPTER 7

CONCLUSIONS AND FUTURE DIRECTIONS

7.1 CONCLUSIONS

The studies presented here have demonstrated that each of the three ceramide synthases found in *Arabidopsis thaliana* have distinct substrate preferences and susceptibilities to inhibition by FB_1. It was also shown that ceramide composition greatly influences plant growth/development and complex sphingolipid formation.

Through the use of *in vitro* assays (Chapter 3) it was determined that LOH1 and LOH3 have a strong preference for trihydroxy LCBs and VLCFAs with LOH2 preferring dihydroxy LCBs and C16 FAs. Previously, it was thought that LOH1 and LOH3 were functionally redundant, however the *in vitro* assay results indicate that each isoform may have a specific *in planta* function. Briefly, LOH1 showed essentially no activity with unsaturated LCB substrates while LOH3 showed moderate activity with t18:1(8), albeit lower than t18:0, indicating that LOH3 may be involved with recycling of LCB substrates from the breakdown of complex sphingolipids. LOH1 also demonstrated a high degree of specificity for C24 and C26 acyl-CoAs while LOH3 demonstrated moderate activity with C20-26 acyl-CoAs. LOH2 demonstrated high levels of activity with d18:1(4), d18:2(4,8), and d18:0 LCBs but not d18:1(8) which was surprising given the lack of d18:2(4,8) in Arabidopsis leaf tissue. The lack of activity with the d18:1(8) LCB indicates that the Δ8 LCB desaturase acts downstream of ceramide synthesis, while the high level of activity with d18:1(4) indicates that Δ4 desaturation occurs upstream of ceramide synthesis.

LCBs containing a Δ4 unsaturation seem to be targeted to the glucoscylceramides (GlcCer). This is especially evident in Arabidopsis pollen where d18:2(4,8) LCBs were found highly enriched in the GlcCers but not the GIPCs (Chapter 5). Upon knockout of

the Δ4 LCB DES, pollen GlcCer levels decreased by ~50%. The further identification of a specialized Δ8 LCB DES that requires Δ4 unsaturated substrates indicates that some organisms have evolved specialized pathways for GlcCer synthesis (Chapter 6). Despite the presence of a highly specific mechanism for targeting LCBs to GlcCer synthesis, the exact reason for the high levels found in pollen and plants such as tomato and soybean (Markham et al. 2006) is currently unknown, especially given that only low levels of GlcCer are required for viability (Chen et al. 2012). However it may have to do with GlcCers role in cell differentiation (Msanne et al. 2015).

In addition to substrate specificity each Arabidopsis ceramide synthase demonstrates a unique binding constant (K_i) in relation to FB_1. Previous reports have indicated that LOH1 and LOH3 are more susceptible to inhibition by FB_1 than LOH2 (Markham et al. 2011a), however the *in vitro* assays presented in Chapter 3 and the *in planta* overexpression data presented in Chapter 4 seem to indicate that LOH2 and LOH3 are both relatively resistant to FB_1 when compared to LOH1. The differential inhibition of LOH1 and LOH3 by FB_1 further supports the notion of unique functions for these seemingly redundant enzymes.

Overexpression of *LOH1*, *LOH2*, or *LOH3* in Arabidopsis were found to have a profound impact on plant growth (Chapter 4). *LOH2* overexpression resulted in a dwarf phenotype, upregulation of PCD related genes, and an increase in salicylic acid levels, whereas overexpression of *LOH1* or *LOH3* resulted in an increase in overall plant biomass. The changes in plant size can be attributed to changes in meristem activity with *LOH1* or *LOH3* overexpression demonstrating increased activity in root meristems and *LOH2* overexpression resulting in a decrease in root meristem activity. The increase in

cell division observed upon overexpression of *LOH1* and *LOH3* is likely due to VLCFA sphingolipids role in cell plate, or phragmoplast, formation during cytokinesis (Bach et al. 2011). The observed upregulation of PCD markers upon *LOH2* overexpression could be analogous to the apoptotic effects of C16 ceramides in mammalian cell culture (Novgorodov et al. 2011) or be the result of the shift away from VLCFA sphingolipids to C16 sphingolipids thus disrupting membrane dynamics.

Highly glycosylated GIPCs not found in leaf were also identified in Arabidopsis pollen (Chapter 5). Previously GIPCs with multiple sugar additions had been identified in Tobacco and Arabidopsis cell cultures, but not in specific plant tissues (Bure et al. 2011). It was found that pollen contains an additional hexose unit and up to three additional pentose units compared to the standard GIPC found in leaf. Due to lack of available standards it is currently not possible to quantitate these complex GIPCs. Additionally, the exact structure and function of these GIPCs is currently unknown.

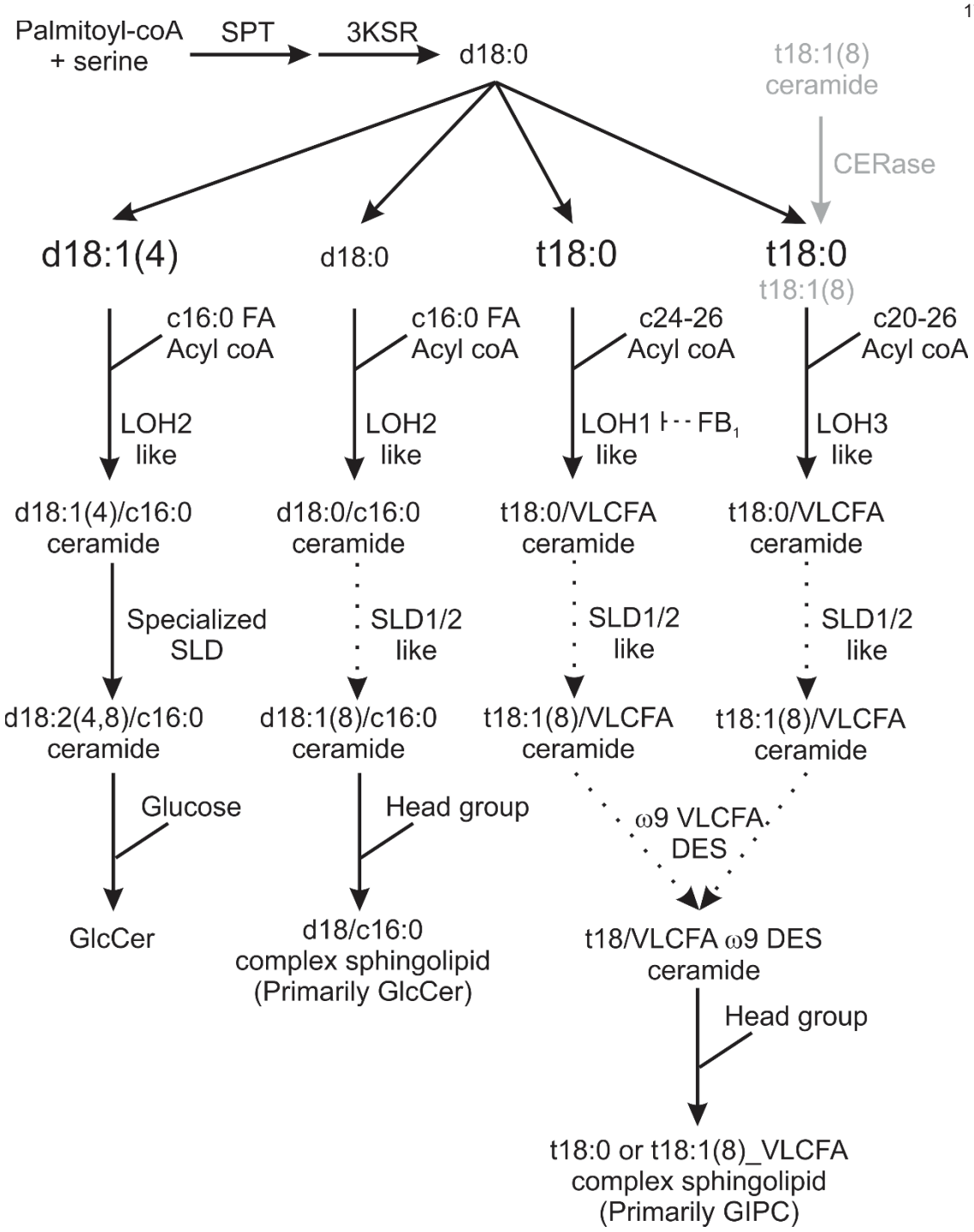

Figure 7.1 *Model of sphingolipid synthesis showing distinct pathways for complex sphingolipid synthesis*. Dotted lines represent possible, but not required enzymatic steps with LCBs coming from the degradation of complex sphingolipids in light grey.

The research presented in this dissertation and summarized above allows for a revised model of plant sphingolipid synthesis with four distinct pathways (Figure 7.1). The newly synthesized d18:0 LCB can follow one of three branches. First, it can be desaturated at the Δ4 position followed by synthesis to d18:1(4)_c16 ceramide through LOH2, with subsequent Δ8 desaturation to d18:2(4,8)_c16 ceramide and finally the addition of glucose to form GlcCer. Second the d18:0 LCB can be immediately used by LOH2 to form d18:0_c16:0 ceramide followed by Δ8 desaturation to form d18:1(8)_c16:0 ceramide which can be used for GlcCer or GIPC synthesis with a preference for GlcCer. Lastly, the d18:0 LCB can be hydroxylated to form t18:0. The t18:0 substrate can then be utilized by LOH1 to form a trihydroxy ceramide with a C24 or C26 FA or by LOH3 to form a trihydroxy ceramide with a C20-26 FA. These trihydroxy VLCFA ceramides can then undergo desaturation on the LCB and/or VLFCA, which can then be used in GIPC or GlcCer synthesis with a preference for GIPCs. Additionally, LOH1 is more susceptible to inhibition by FB_1 than either LOH2 or LOH3.

7.2 FUTURE RESEARCH PERSPECTIVES

7.2.1 STRUCTURAL DOMAINS RESPONSIBLE FOR SUBSTRATE SPECIFICITY

Previously it was thought that LOH1 and LOH3 were functionally redundant enzymes, however the results presented here clearly demonstrate that LOH1 and LOH3 are functionally unique. Since *LOH1* and *LOH3* are ~90% identical and *LOH2* is ~60% identical to both *LOH1* and *LOH3* the differences between these isoforms may provide clues as to the domains that control ceramide synthase substrate specificities and susceptibility to FB_1 (Markham et al. 2011a; Ternes et al. 2011). Chimeras of human ceramide synthases have identified domains that impart acyl-CoA specificities,

specifically the loop between the 5th and 6th predicted transmembrane domains, which influences both specificity and activity (Tidhar et al. 2012). Since LOH1 and LOH3 demonstrate vastly different properties in relation to FB_1 inhibition and have slightly different LCB/Acyl-CoA preferences, chimeras between these isoforms could reveal small domains responsible for these characteristics.

7.2.2 REGULATION OF CERAMIDE SYNTHESIS IN ARABIDOPSIS

While this dissertation provides evidence for distinct pathways to synthesize different complex sphingolipids many questions remain. The presence of ceramide synthases with specific substrate preferences combined with differential regulation of each ceramide synthase isoform would allow for a high degree of control over ceramide composition. To date very little is known about the regulation of ceramide synthases with only a few reports investigating ceramide synthase regulation in *Saccharomyces cerevisiae*. In yeast, ceramide synthase activity is dependent on a small activating subunit denoted *lip1* (Vallee and Riezman 2005). The mechanism by which *lip1* activates ceramide synthesis is currently unknown and no known sequence homologs exist in either mammalian or plant systems. It may be possible that plant ceramide synthases are reliant upon a similar, yet to be identified, functional homolog that serves as a regulator of plant ceramide synthases. In addition to *lip1*, yeast ceramide synthases are activated by direct phosphorylation from Casein Kinase 2 (Fresques et al. 2015) as well as activation by phosphorylation from Ypk2 in a TORC2 manner (Aronova et al. 2008). The TORC2/Ypk2 activation pathway is regulated by intracellular ROS levels. Sphingolipid depletion results in accumulation of ROS due to membrane stress which serves to activate the TORC2/Ypk2 pathway resulting in increased ceramide synthase

activity. Once sphingolipid levels have increased the membrane stress, and subsequent ROS production, is relieved thus providing a feedback mechanism for sphingolipid metabolism (Niles et al. 2014). Yeast ceramide synthases could also be regulated transcriptionally. The *LAC1* promoter contains a single PDRE site that is not found in the *LAG1* promoter indicating differential regulation by PDRE transcription factors (Kolaczkowski et al. 2004). Despite the presence of multiple regulatory pathways in yeast no studies have examined plant ceramide synthase regulation. With plants containing multiple ceramide synthase isoforms each with unique substrate specifies, differential regulation of each isoform is highly probable and the high degree of homology between the yeast and plant ceramide synthases (Markham et al. 2011a) leaves open the possibility that the yeast regulatory mechanism are conserved.

Human ceramide synthases have also been shown to be regulated by dimerization with the formation of homo- and hetero-dimers between different mammalian ceramide synthases changing the activity level (Laviad et al. 2012), however this has yet to be examined in Arabidopsis. Pull downs of the native plant ceramide synthases may provide insights into protein complex formation and phosphorylation status of plant ceramide synthases. Additionally, given the ~90% sequence similarity between *LOH1* and *LOH3* and their apparent differences in function, chimeras may be useful in determining if the few differences between *LOH1* and *LOH3* are regulatory domains

Arabidopsis ceramide synthase activity is also affected by the presence of different divalent cations. LOH1 and LOH3 are inhibited by Mg^{2+}, Cu^{2+}, Zn^{2+}, Mn^{2+}, and Ca^{2+} while LOH2 was activated by Mg^{2+}, Mn^{2+}, and Ca^{2+} with Cu^{2+} and Zn^{2+} acting as inhibitors. Previously calcium ions have been implicated in PCD signaling with C2

ceramide treatment inducing an increase in cytosolic Ca^{2+} and hydrogen peroxide which culminated in cell death (Townley et al. 2005). Interestingly, inhibition of Ca^{2+} release prevented cell death from occurring. With the apparent role of LOH2 and C16 ceramides in promoting PCD (Chapter 4) the cytosolic increase in Ca^{2+} may serve to inhibit VLCFA ceramide production (LOH1 and LOH3) while simultaneously promoting the synthesis of pro PCD C16 ceramides (LOH2). The increased ROS levels (in the form of hydrogen peroxide) could serve to activate ceramide synthases, particularly LOH2, in a manner similar to that observed in yeast (Niles et al. 2014).

7.2.3 *IN PLA*NTA FUNCTIONS OF LOH1, LOH2, AND LOH3

In planta LOH1 and LOH3 appear to be semi redundant with overexpression of either isoform resulting in larger plants, however they also are unique in both substrate specificity and susceptibility to FB_1 ultimately leaving the exact *in planta* functional differences between LOH1 and LOH3 unknown. Further studies examining *LOH1* or *LOH3* knockout/overexpression plants in different environmental conditions could reveal specific roles for *LOH1* and *LOH3*. Knockout of *LOH2* has previously been shown to have no effect on plant growth and development (Markham et al. 2011b), however overexpression results in a dwarf phenotype and upregulation of PCD-related genes (Chapter 4). These contrasting phenotypes leave open questions regarding the *in planta* function of LOH2 and C16 FA sphingolipids in general. One hypothesis is that C16 FA sphingolipids may be involved in PCD signaling. *LOH2* knockout plants show no phenotype in "ideal" conditions, however their susceptibility to pathogens has yet to be tested. LOH2 may also serve as a mechanism to shunt LCBs to GlcCer synthesis as demonstrated in Chapters 5 and 6. Given GlcCers role in cell differentiation and

organogenesis the production of GlcCer may be a critical step in plant development (Bach et al. 2011; Msanne et al. 2015). However since loss of this potential mechanism, through both knockout of the Δ4 LCB DES and *LOH2*, does not seem to have an effect on plant growth, the *in planta* function of LOH2 remains a mystery.

7.2.4 FUNCTION AND SYNTHESIS OF HIGHLY GLYCOSYLATED GIPCS

Currently both the function and the synthesis pathway of highly glycosylated GIPCs is unknown. The unique nature of the pollen sphingolipidome may make the pollen transcriptome an ideal starting point for identification of genes involved in GIPC synthesis. Because these species are not found in leaf, comparative transcriptome analysis could reveal currently uncharacterized glycosyltransferases unique to pollen. Examining the pollen morphology and sphingolipidome of potential glycosyltransferase knockouts could provide insights into both the synthesis and function of highly glycosylated sphingolipids.

7.3 CONCLUDING REMARKS

Overall this dissertation demonstrates the unique nature of and identifies possible *in planta* functions for each Arabidopsis ceramide synthase isoform, however questions remain as to the exact *in planta* function and regulation of each isoform. Additionally, highly glycosylated GIPCs not found in leaf were identified in pollen, though the exact amount, structure, and function of these complex GIPCs has yet to be elucidated. While our understanding of plant sphingolipids has greatly increased over the last decade the questions raised in this dissertation related to sphingolipid synthesis, regulation, and function underscores how enigmatic these unusual lipids remain over a hundred years after their discovery.

7.4 REFERENCES

Aronova S, Wedaman K, Aronov PA, Fontes K, Ramos K, Hammock BD, Powers T (2008) Regulation of ceramide biosynthesis by TOR complex 2. Cell Metab 7 (2):148-158.

Bach L, Gissot L, Marion J, Tellier F, Moreau P, Satiat-Jeunemaitre B, Palauqui JC, Napier JA, Faure JD (2011) Very-long-chain fatty acids are required for cell plate formation during cytokinesis in Arabidopsis thaliana. Journal of Cell Science 124 (19):3223-3234.

Bure C, Cacas JL, Wang F, Gaudin K, Domergue F, Mongrand S, Schmitter JM (2011) Fast screening of highly glycosylated plant sphingolipids by tandem mass spectrometry. Rapid Commun Mass Spectrom 25 (20):3131-3145.

Chen M, Markham JE, Cahoon EB (2012) Sphingolipid Delta8 unsaturation is important for glucosylceramide biosynthesis and low-temperature performance in Arabidopsis. The Plant journal : for cell and molecular biology 69 (5):769-781.

Fresques T, Niles B, Aronova S, Mogri H, Rakhshandehroo T, Powers T (2015) Regulation of Ceramide Synthase by Casein Kinase 2-dependent Phosphorylation in Saccharomyces cerevisiae. J Biol Chem 290 (3):1395-1403.

Kolaczkowski M, Kolaczkowska A, Gaigg B, Schneiter R, Moye-Rowley WS (2004) Differential regulation of ceramide synthase components LAC1 and LAG1 in Saccharomyces cerevisiae. Eukaryot Cell 3 (4):880-892.

Laviad EL, Kelly S, Merrill AH, Futerman AH (2012) Modulation of Ceramide Synthase Activity via Dimerization. J Biol Chem 287 (25):21025-21033.

Markham JE, Li J, Cahoon EB, Jaworski JG (2006) Separation and identification of major plant sphingolipid classes from leaves. J Biol Chem 281 (32):22684-22694.

Markham JE, Molino D, Gissot L, Bellec Y, Hematy K, Marion J, Belcram K, Palauqui JC, Satiat-Jeunemaitre B, Faure JD (2011a) Sphingolipids containing very-long-chain fatty acids define a secretory pathway for specific polar plasma membrane protein targeting in Arabidopsis. Plant Cell 23 (6):2362-2378.

Markham JE, Molino D, Gissot L, Bellec Y, Hematy K, Marion J, Belcram K, Palauqui JC, Satiat-Jeunemaitre B, Faure JD (2011b) Sphingolipids containing very-long-chain fatty acids define a secretory pathway for specific polar plasma membrane protein targeting in Arabidopsis. THE PLANT CELL 23 (6):2362-2378.

Msanne J, Chen M, Luttgeharm KD, Bradley AM, Mays ES, Paper JM, Boyle DL, Cahoon RE, Schrick K, Cahoon EB (2015) Glucosylceramide is Critical for Cell-Type Differentiation and Organogenesis, but not for Cell Viability in Arabidopsis. The Plant journal : for cell and molecular biology.

Niles BJ, Joslin AC, Fresques T, Powers T (2014) TOR Complex 2-Ypk1 Signaling Maintains Sphingolipid Homeostasis by Sensing and Regulating ROS Accumulation. Cell Reports 6 (3):541-552.

Novgorodov SA, Chudakova DA, Wheeler BW, Bielawski J, Kindy MS, Obeid LM, Gudz TI (2011) Developmentally regulated ceramide synthase 6 increases mitochondrial Ca2+ loading capacity and promotes apoptosis. J Biol Chem 286 (6):4644-4658.

Ternes P, Feussner K, Werner S, Lerche J, Iven T, Heilmann I, Riezman H, Feussner I (2011) Disruption of the ceramide synthase LOH1 causes spontaneous cell death in Arabidopsis thaliana. New Phytol 192 (4):841-854.

Tidhar R, Ben-Dor S, Wang E, Kelly S, Merrill AH, Futerman AH (2012) Acyl Chain Specificity of Ceramide Synthases Is Determined within a Region of 150 Residues in the Tram-Lag-CLN8 (TLC) Domain. J Biol Chem 287 (5):3197-3206.

Townley HE, McDonald K, Jenkins GI, Knight MR, Leaver CJ (2005) Ceramides induce programmed cell death in Arabidopsis cells in a calcium-dependent manner. Biol Chem 386 (2):161-166.

Vallee B, Riezman H (2005) Lip1p: a novel subunit of acyl-CoA ceramide synthase. Embo J 24 (4):730-741.

APPENDIX A

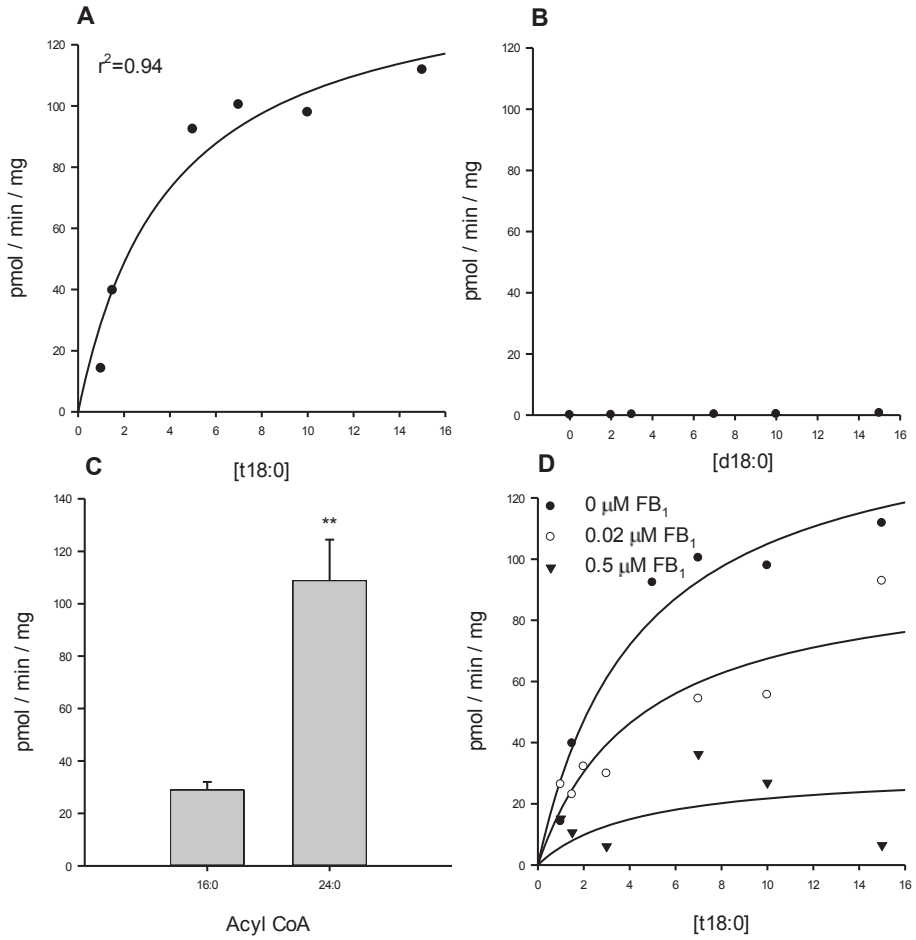

Enzymatic data for LOH1 overexpression Arabidopsis microsomes

(A) Plot of activity vs substrate concentration for t18:0 in assays containing 50µM 24:0 CoA, 10µM BSA, 10µg microsomal protein, and 0-15µM t18:0 LCB (V_{max}=146 ± 21, K_m=4.0 ± 1.6). Kinetic parameters were estimated by non-linear regression analysis using the Michaelis-Menten equation. **(B)** Plot of activity vs substrate concentration for d18:0 in assays containing 50µM acyl-CoA, 10µM BSA, 10µg microsomal protein and 0-15µM d18:0 LCB. No kinetic parameters were able to be extracted. **(C)** Comparison of activity between 16:0 and 24:0 CoAs. LOH1 preferred 24:0 CoA at a statistically significant (P=0.007) when compared to 16:0 CoA. **(D)** Fumonisin B1 inhibition studies using varying amounts of FB1, 10µg microsomal protein, 50µM 24:0 CoA, 10µM BSA, and 0-15µM t18:0 LCB. Kinetic parameters were estimated by non-linear regression analysis with the mixed-partial model of inhibition shown (V_{max}=151 ± 24, K_m=4.4 ± 1.9, K_i=0.027 ± 0.026, r^2=0.92).

APPENDIX B

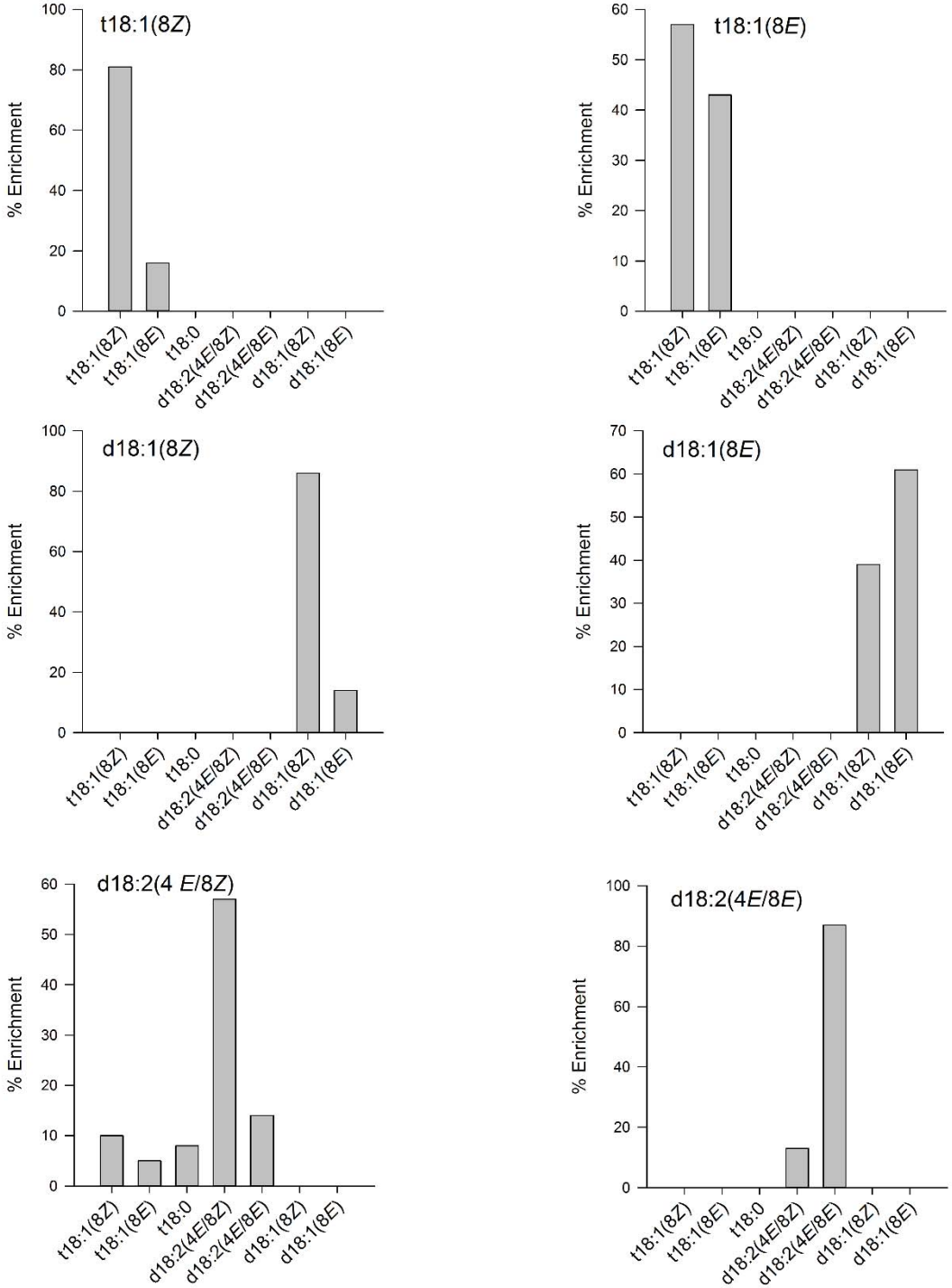

LCB composition of purified LCB fractions.

Composition of the different purified LCB fractions used to assess the LCB substrate specificity of Arabidopsis ceramide synthases. Composition expressed as mole percent.

APPENDIX C

MRM Parameters for yeast ceramide profiling

	[M+H]+			
Ceramide Backbone	**Exact mass**	**LCB fragment**	**DP**	**CE**
d18:1 c12:0	482.5	264.3	60	35
d18:0c16:0	540.536	284.3	39	46
d18:0c18:0	568.567	284.3	39	46
d18:0c20:0	596.598	284.3	39	46
d18:0 c22:0	624.6	284.3	39	48
d18:0 c24:0	652.7	284.3	39	48
d18:0 c26:0	680.7	284.3	43	48
d18:0 h16:0	556.531	284.3	95	46
d18:0 h18:0	584.562	284.3	95	46
d18:0 h 20:0	612.593	284.3	95	46
d18:0 h22:0	640.6	284.3	95	47
d18:0 h24:0	668.7	284.3	95	50
d18:0 h26:0	696.7	284.3	95	50
d18:0 dh16:0	572.526	284.3	100	49
d18:0 dh18:0	600.557	284.3	100	49
d18:0 dh20:0	628.588	284.3	100	49
d18:0 dh22:0	656.6	284.3	100	50
d18:0 dh24:0	684.7	284.3	100	50
d18:0 dh26:0	712.7	284.3	100	50
d20:0c16:0	568.568	312.3	100	49
d20:0c18:0	596.599	312.3	100	49
d20:0c20:0	624.63	312.3	100	49
d20:0 c22:0	652.7	312.3	100	50
d20:0 c24:0	680.7	312.3	100	50
d20:0 c26:0	708.7	312.3	100	50
d20:0 h16:0	584.563	312.3	100	49
d20:0 h18:0	612.594	312.3	100	49
d20:0 h 20:0	640.625	312.3	100	49
d20:0 h22:0	668.7	312.3	100	50
d20:0 h24:0	696.7	312.3	100	50
d20:0 h26:0	724.7	312.3	100	50
d20:0 dh16:0	600.558	312.3	100	49
d20:0 dh18:0	628.589	312.3	100	49
d20:0 dh20:0	656.62	312.3	100	49
d20:0 dh22:0	684.7	312.3	100	50
d20:0 dh24:0	712.7	312.3	100	50
d20:0 dh26:0	740.7	312.3	100	50

t18:0c16:0	556.531	300.3	100	41
t18:0c18:0	584.562	300.3	100	41
t18:0c20:0	612.593	300.3	100	41
t18:0 c22:0	640.6	300.3	100	42
t18:0 c24:0	668.7	300.3	100	43
t18:0 c26:0	696.7	300.3	100	44
t18:0 h16:0	572.526	300.3	100	43
t18:0 h18:0	600.557	300.3	100	43
t18:0 h 20:0	628.588	300.3	100	43
t18:0 h22:0	656.6	300.3	100	44
t18:0 h24:0	684.7	300.3	100	45
t18:0 h26:0	712.7	300.3	100	46
t18:0 dh16:0	588.521	300.3	100	45
t18:0 dh18:0	616.552	300.3	100	45
t18:0 dh20:0	644.583	300.3	100	45
t18:0 dh22:0	672.6	300.3	100	46
t18:0 dh24:0	700.6	300.3	100	47
t18:0 dh26:0	728.7	300.3	100	48
t20:0c16:0	584.563	328.3	100	49
t20:0c18:0	612.594	328.3	100	49
t20:0c20:0	640.625	328.3	100	49
t20:0 c22:0	668.7	328.3	100	50
t20:0 c24:0	696.7	328.3	100	50
t20:0 c26:0	724.7	328.3	100	50
t20:0 h16:0	600.558	328.3	100	49
t20:0 h18:0	628.589	328.3	100	49
t20:0 h 20:0	656.62	328.3	100	49
t20:0 h22:0	684.7	328.3	100	50
t20:0 h24:0	712.7	328.3	100	50
t20:0 h26:0	740.7	328.3	100	50
t20:0 dh16:0	616.553	328.3	100	49
t20:0 dh18:0	644.584	328.3	100	49
t20:0 dh20:0	672.615	328.3	100	49
t20:0 dh22:0	700.6	328.3	100	50
t20:0 dh24:0	728.7	328.3	100	50
t20:0 dh26:0	756.7	328.3	100	50

APPENDIX D

Primer Number	Oligonucleotide	Oligonucleotide Sequence	# of Cycles (if applicable)
1	LOH1(At3g25540)5' LOH1(At3g25540)3'	5'-ATATGAATTCAAAATGGGTCTCTTCGAATCGG-3' 5'-ATATTCTAGATTAATCCTCGTGTTCATCATCGC-3'	
2	LOH2(At3g19260)5' LOH2(At3g19260)3'	5’-CACCATGGAATCGGTAT CATCACGCGGCGGAGAC-3' 5’-CTAATCATCATCATCCTCTGAAT CGGATCTTATGTCT-3'	
3	LOH3(At1g13580)5' LOH3(At1g13580)3'	5'-ATATGAATTCAAAATG GGTTTGTTGGAATCGGTG-3' 5'-ATATTCTAGAGTCAGTCTTCGTGCTCATCTTCG-3'	
4	UBC(At5g25760)5' UBC(At5g25760)3'	5’-ATGCAGGCATCAAGAGCGCGACTGT-3’ 5’-CACCGCCTTCGTAAGGAGTCTCCGA-3’	30 cycles
5	PR-2(At3g57260)5' PR-2(At3g57260)3'	5’-AGCCTCACCACCAATGTTGATGAT-3’ 5’-GTTCTCGATGTTCTGCATTGCTTGT-3’	35 cycles
6	PRXc(At3g49120)5' PRXc(At3g49120)3'	5’-CAACATCGTCCACTTGGACAATCTT-3’ 5’-CCTGCCAAAGTGACAGATTGTTGAG-3’	30 cycles
7	SAG13(At2g29350)5' SAG13(At2g29350)3’	5’-GAAACTCAGCTTCAAGAACGCTTACGTG-3’ 5’-TCGCCCATTCGCAAGCTAAGTTT-3’	30 cycles
8	FMO(At1g19250)5’ FMO(At1g19250)3’	5’-CGTATTCGAAGCCTCGGATTCAGTC-3’ 5’-GGTATTCTTGGAACGTCGCCGTATT-3’	35 cycles
9	SAG12(At5g45890)5’ SAG12(At5g45890)3’	5’-TTGACTGGAGGAAGAAAGGAGCTGT-3’ 5’-CTTCAATTCCAACGCTAACCGGT-3’	35 cycles
10	PR-3(At3g12500)5’ PR-3(At3g12500)3’	5’-AACGGTCTATGCTGCAGCGAGTT-3’ 5’-GCGCTCGGTTCACAGTAGTCTGA-3’	30 cycles
11	ERD11(At1g02930)5' ERD11(At1g02930)3’	5’-ATGGCAGGAATCAAAGTTTTCGG-3’ 5’-CCTCTTCTTCTTCAACAACGGTTTTG-3’	25 cycles

Primers used amplification of LOH1, LOH2, and LOH3 cDNA and semi quantitative RT-PCR of hypersentive response related PCD genes

APPENDIX E

Predicted mass and observed mass for GIPC species detected by precussor scan.

GIPC (t18:1_24:1) ceramide backbone	Predicted Mass	Observed Mass	Δ amu
Hex(OH)-HexA-IPC	1260.7	1261.2	0.5
Pent-Hex(OH)-HexA-IPC	1392.7	1393	0.3
Hex-Hex(OH)-HexA-IPC	1422.7	1423	0.3
Pent-Hex-Hex(OH)-HexA-IPC	1554.7	1555.2	0.5
$(Pent)_2$-Hex-Hex(OH)-HexA-IPC	1686.7	1687	0.3
Hex(NAc)-HexA-IPC	1301.7	1302.2	0.5
Hex-Hex(NAc)-IPC	1463.8	1464.6	0.8
Pent-Hex-Hex(NAc)-IPC	1595.8	1596.4	0.6
$(Pent)_2$-Hex-Hex(NAc)-IPC	1727.9	1728.0	0.1
$(Pent)_3$-Hex-Hex(NAc)-IPC	1859.9	1860.4	0.5

Source parameters for each sphingolipid class. The source was equilibrated for 1 minute prior to running of samples. The mass spectrometer was operated in positive MRM mode for all analytes.

Analytes	**Curtain Gas (psi)**	**Gas 1 (psi)**	**Gas 2 (psi)**	**Spray voltage**	**Entrance potential (V)**	**Collision exit potential (V)**	**Source Temperature (°C)**
Ceramide	20	60	50	5000	10	14	550
Hydroxyceramide	10	40	50	5000	10	14	300
Glucosylceramide	20	60	50	5000	10	14	350
Hex-HexA-GIPC	20	60	50	5000	10	14	350
Free LCB	20	60	50	5000	10	17	400
Complex GIPC	20	60	50	5000	10	14	350

Sphingolipid species with MRM parameters

Hydroxy-Ceramides

Ceramide Backbone	[M+H]+ Exact mass	LCB fragment	Dwell time	DP	CE
d18:1 c12:0	482.457	264.269	9.08	60	35
t18:0 h16:0	572.525	300.29	12.54	100	36
t18:0 h18:0	600.556	300.29	12.54	100	38
t18:0 h20:0	628.588	300.29	12.54	100	38
t18:0 h20:1	626.572	300.29	12.54	100	44
t18:0 h22:0	656.619	300.29	12.54	100	45
t18:0 h22:1	654.603	300.29	12.54	100	45
t18:0 h23:0	670.634	300.29	12.54	100	45
t18:0 h23:1	668.619	300.29	12.54	100	45
t18:0 h24:0	684.65	300.29	12.54	100	45
t18:0 h24:1	682.634	300.29	12.54	100	45
t18:0 h25:0	698.666	300.29	12.54	100	45
t18:0 h25:1	696.65	300.29	12.54	100	45
t18:0 h26:0	712.681	300.29	12.54	100	46
t18:0 h26:1	710.666	300.29	12.54	100	45
t18:1 h16:0	570.509	298.274	12.54	100	36
t18:1 h18:0	598.541	298.274	12.54	100	36
t18:1 h20:0	626.572	298.274	12.54	100	38
t18:1 h20:1	624.556	298.274	12.54	100	38
t18:1 h22:0	654.603	298.274	12.54	100	43
t18:1 h22:1	652.588	298.274	12.54	100	43
t18:1 h23:0	668.619	298.274	12.54	100	44
t18:1 h23:1	666.603	298.274	12.54	100	44
t18:1 h24:0	682.634	298.274	12.54	100	45
t18:1 h24:1	680.619	298.274	12.54	100	45
t18:1 h25:0	696.65	298.274	12.54	100	45
t18:1 h25:1	694.634	298.274	12.54	100	45
t18:1 h26:0	710.666	298.274	12.54	100	45
t18:1 h26:1	708.65	298.274	12.54	100	45
d18:0 h16:0	556.53	266.284	12.54	80	43
d18:0 h18:0	584.561	266.284	12.54	80	46
d18:0 h20:0	612.593	266.284	12.54	90	48
d18:0 h20:1	610.577	266.284	12.54	88	49
d18:0 h22:0	640.624	266.284	12.54	95	47
d18:0 h22:1	638.608	266.284	12.54	85	44
d18:0 h23:0	654.64	266.284	12.54	93	48

d18:0 h23:1	652.624	266.284	12.54	90	46
d18:0 h24:0	668.655	266.284	12.54	92	50
d18:0 h24:1	666.64	266.284	12.54	81	50
d18:0 h25:0	682.671	266.284	12.54	96	50
d18:0 h25:1	680.655	266.284	12.54	86	50
d18:0 h26:0	696.687	266.284	12.54	98	50
d18:0 h26:1	694.671	266.284	12.54	88	52
d18:1 h16:0	554.514	264.269	12.54	62	37
d18:1 h18:0	582.546	264.269	12.54	62	41
d18:1 h20:0	610.577	264.269	12.54	68	42
d18:1 h20:1	608.561	264.269	12.54	56	43
d18:1 h22:0	638.608	264.269	12.54	68	47
d18:1 h22:1	636.593	264.269	12.54	65	45
d18:1 h23:0	652.624	264.269	12.54	70	46
d18:1 h23:1	650.608	264.269	12.54	67	45
d18:1 h24:0	666.64	264.269	12.54	75	45
d18:1 h24:1	664.624	264.269	12.54	69	45
d18:1 h25:0	680.655	264.269	12.54	79	46
d18:1 h25:1	678.64	264.269	12.54	72	46
d18:1 h26:0	694.671	264.269	12.54	83	48
d18:1 h26:1	692.655	264.269	12.54	78	49
d18:2 h16:0	552.499	262.253	12.54	70	40
d18:2 h18:0	580.53	262.253	12.54	70	40
d18:2 h20:0	608.561	262.253	12.54	70	42
d18:2 h20:1	606.546	262.253	12.54	70	41
d18:2 h22:0	636.593	262.253	12.54	70	44
d18:2 h22:1	634.577	262.253	12.54	70	43
d18:2 h23:0	650.608	262.253	12.54	70	47
h18:2 h23:2	648.593	262.253	12.54	70	45
d18:2 h24:0	664.624	262.253	12.54	70	50
d18:2 h24:1	662.608	262.253	12.54	70	49
d18:2 h25:0	678.64	262.253	12.54	70	51
d18:2 h25:1	676.624	262.253	12.54	70	50
d18:2 h26:0	692.655	262.253	12.54	70	52
d18:2 h26:1	690.64	262.253	12.54	70	51

Ceramides

Ceramide Backbone	Exact mass	[M+H]+ LCB fragment	Dwell time	DP	CE
d18:1 c12:0	482.457	264.269	12.54	60	35
t18:0 c16:0	556.53	300.29	12.54	100	35
t18:0 c18:0	584.561	300.29	12.54	100	35
t18:0 c20:0	612.593	300.29	12.54	100	37
t18:0 c20:1	610.577	300.29	12.54	100	37
t18:0 c22:0	640.624	300.29	12.54	100	43
t18:0 c22:1	638.608	300.29	12.54	100	43
t18:0 c23:0	654.639	300.29	12.54	100	43
t18:0 c23:1	652.624	300.29	12.54	100	43
t18:0 c24:0	668.655	300.29	12.54	100	43
t18:0 c24:1	666.639	300.29	12.54	100	43
t18:0 c25:0	682.671	300.29	12.54	100	43
t18:0 c25:1	680.655	300.29	12.54	100	43
t18:0 c26:0	696.686	300.29	12.54	100	43
t18:0 c26:1	694.671	300.29	12.54	100	43
t18:1 c16:0	554.514	298.274	12.54	100	38
t18:1 c18:0	582.546	298.274	12.54	100	38
t18:1 c20:0	610.577	298.274	12.54	100	40
t18:1 c20:1	608.561	298.274	12.54	100	40
t18:1 c22:0	638.608	298.274	12.54	100	42
t18:1 c22:1	636.593	298.274	12.54	100	42
t18:1 c23:0	652.624	298.274	12.54	100	42
t18:1 c23:1	650.608	298.274	12.54	100	42
t18:1 c24:0	666.639	298.274	12.54	100	42
t18:1 c24:1	664.624	298.274	12.54	100	44
t18:1 c25:0	680.655	298.274	12.54	100	44
t18:1 c25:1	678.639	298.274	12.54	100	44
t18:1 c26:0	694.671	298.274	12.54	100	44
t18:1 c26:1	692.655	298.274	12.54	100	44
d18:0 c16:0	540.535	266.284	12.54	40	42
d18:0 c18:0	568.566	266.284	12.54	40	43
d18:0 c20:0	596.598	266.284	12.54	42	43
d18:0 c20:1	594.582	266.284	12.54	40	48
d18:0 c22:0	624.629	266.284	12.54	39	48
d18:0 c22:1	622.613	266.284	12.54	40	48
d18:0 c23:0	638.645	266.284	12.54	40	48
d18:0 c23:1	636.629	266.284	12.54	40	48
d18:0 c24:0	652.66	266.284	12.54	39	44

d18:0 c24:1	650.645	266.284	12.54	37	43
d18:0 c25:0	666.676	266.284	12.54	40	45
d18:0 c25:1	664.66	266.284	12.54	40	45
d18:0 c26:0	680.692	266.284	12.54	43	48
d18:0 c26:1	678.676	266.284	12.54	46	48
d18:1 c16:0	538.519	264.269	12.54	40	39
d18:1 c18:0	566.551	264.269	12.54	38	39
d18:1 c20:0	594.582	264.269	12.54	44	39
d18:1 c20:1	592.566	264.269	12.54	42	42
d18:1 c22:0	622.613	264.269	12.54	44	46
d18:1 c22:1	620.598	264.269	12.54	39	44
d18:1 c23:0	636.629	264.269	12.54	40	46
d18:1 c23:1	634.613	264.269	12.54	40	44
d18:1 c24:0	650.645	264.269	12.54	38	49
d18:1 c24:1	648.629	264.269	12.54	42	43
d18:1 c25:0	664.66	264.269	12.54	42	44
d18:1 c25:1	662.645	264.269	12.54	42	44
d18:1 c26:0	678.676	264.269	12.54	38	46
d18:1 c26:1	676.66	264.269	12.54	46	48
d18:2 c16:0	536.504	262.253	12.54	50	40
d18:2 c18:0	564.535	262.253	12.54	50	40
d18:2 c20:0	592.566	262.253	12.54	50	42
d18:2 c20:1	590.551	262.253	12.54	50	41
d18:2 c22:0	620.598	262.253	12.54	50	44
d18:2 c22:1	618.582	262.253	12.54	50	43
d18:2 c23:0	634.613	262.253	12.54	50	46
c18:2 c23:2	632.598	262.253	12.54	50	46
d18:2 c24:0	648.629	262.253	12.54	50	50
d18:2 c24:1	646.613	262.253	12.54	50	49
d18:2 c25:0	662.645	262.253	12.54	50	50
d18:2 c25:1	660.629	262.253	12.54	50	51
d18:2 c26:0	676.66	262.253	12.54	50	52
d18:2 c26:1	674.645	262.253	12.54	50	51

2-hydroxy Glucosylceramides

Ceramide Backbone	[M+H]+ exact mass	Product mass	Dwell time	DP	CE
d18:1c12:0	644.51	264.269	12.54	90	50
t18:0h16:0	734.578	300.29	12.54	80	68
t18:0h18:0	762.609	300.29	12.54	80	68
t18:0h20:0	790.641	300.29	12.54	80	72
t18:0h20:1	788.625	300.29	12.54	80	75
t18:0h22:0	818.672	300.29	12.54	80	60
t18:0h22:1	816.656	300.29	12.54	80	63
t18:0h23:0	832.687	300.29	12.54	80	60
t18:0h23:1	830.672	300.29	12.54	80	63
t18:0h24:0	846.703	300.29	12.54	80	60
t18:0h24:1	844.687	300.29	12.54	80	65
t18:0h25:0	860.719	300.29	12.54	80	60
t18:0h25:1	858.703	300.29	12.54	80	65
t18:0h26:0	874.734	300.29	12.54	80	63
t18:0h26:1	872.719	300.29	12.54	80	65
t18:1h16:0	732.562	298.274	12.54	88	49
t18:1h18:0	760.594	298.274	12.54	70	54
t18:1h20:0	788.625	298.274	12.54	70	55
t18:1h20:1	786.609	298.274	12.54	75	60
t18:1h22:0	816.656	298.274	12.54	88	57
t18:1h22:1	814.641	298.274	12.54	75	60
t18:1h23:0	830.672	298.274	12.54	88	57
t18:1h23:1	828.656	298.274	12.54	75	60
t18:1h24:0	844.687	298.274	12.54	100	57
t18:1h24:1	842.672	298.274	12.54	100	59
t18:1h25:0	858.703	298.274	12.54	100	57
t18:1h25:1	856.687	298.274	12.54	100	59
t18:1h26:0	872.719	298.274	12.54	100	57
t18:1h26:1	870.703	298.274	12.54	100	62
d18:0h16:0	718.583	266.284	12.54	85	56
d18:0h18:0	746.614	266.284	12.54	85	80
d18:0h20:0	774.646	266.284	12.54	93	80
d18:0h20:1	772.63	266.284	12.54	93	75
d18:0h22:0	802.677	266.284	12.54	93	80
d18:0h22:1	800.661	266.284	12.54	93	75
d18:0h23:0	816.693	266.284	12.54	93	80
d18:0h23:1	814.677	266.284	12.54	93	75
d18:0h24:0	830.708	266.284	12.54	93	100

d18:0h24:1	828.693	266.284	12.54	100	95
d18:0h25:0	844.724	266.284	12.54	93	100
d18:0h25:1	842.708	266.284	12.54	100	95
d18:0h26:0	858.74	266.284	12.54	100	100
d18:0h26:1	856.724	266.284	12.54	100	95
d18:1h16:0	716.567	264.269	12.54	78	53
d18:1h18:0	744.599	264.269	12.54	80	56
d18:1h20:0	772.63	264.269	12.54	80	60
d18:1h20:1	770.614	264.269	12.54	80	58
d18:1h22:0	800.661	264.269	12.54	80	62
d18:1h22:1	798.646	264.269	12.54	80	66
d18:1h23:0	814.677	264.269	12.54	80	62
d18:1h23:1	812.661	264.269	12.54	80	66
d18:1h24:0	828.693	264.269	12.54	90	60
d18:1h24:1	826.677	264.269	12.54	95	63
d18:1h25:0	842.708	264.269	12.54	90	60
d18:1h25:1	840.693	264.269	12.54	95	63
d18:1h26:0	856.724	264.269	12.54	90	67
d18:1h26:1	854.708	264.269	12.54	85	63
d18:2h16:0	714.552	262.253	12.54	80	49
d18:2h18:0	742.583	262.253	12.54	95	49
d18:2h20:0	770.614	262.253	12.54	100	57
d18:2h20:1	768.599	262.253	12.54	63	57
d18:2h22:0	798.646	262.253	12.54	100	59
d18:2h22:1	796.63	262.253	12.54	63	59
d18:2h24:0	812.661	262.253	12.54	100	59
d18:2h24:1	810.646	262.253	12.54	63	59
d18:2h26:0	826.677	262.253	12.54	100	59
d18:2h26:1	824.661	262.253	12.54	65	59

LCB(P)s					
LCB	[M+H]+ exact mass	Product mass	Dwell time	DP	CE
d17:1	286.3	268.3	25	55	19
d18:0	302.3	284.3	25	75	21
d18:1	300.3	282.3	25	65	18
t18:0	318.3	300.4	25	70	21
t18:1	316.3	298.4	25	60	18
d18:2	298.3	280.3	25	60	18
3KS	300.4	270.3	25	78	28
d17:1P	366.2	250.3	25	60	23
d18:0P	382.3	266.3	25	65	19
d18:1P	380.3	264.3	25	60	25
d18:2-P	378.3	262.3	25	60	25
t18:0P	398.3	300.3	25	65	22
t18:1P	396.3	298.3	25	60	25

Headgroup structure	Hex-HexA-IPC				
	[M+H]+				
Ceramide backbone	Exact mass	Product mass	Dwell time	DP	CE
GM1	1546.9	366.3	22.03	145	50
t18:0h16:0	1152.628	554.514	22.03	145	60
t18:0h18:0	1180.614	582.5	22.03	145	60
t18:0h20:0	1208.714	610.6	22.03	145	60
t18:0h20:1/t18:1h20:0	1206.714	608.6	22.03	145	61
t18:0h22:0	1236.714	638.6	22.03	145	62.5
t18:0h22:1/t18:1h22:0/t18:0c23:0/d18:0h23:0	1234.714	636.6	22.03	145	61
t18:0h23:0	1250.714	652.6	22.03	145	62
t18:0h23:1/t18:1h23:0/t18:0c24:0/d18:0h24:0	1248.714	650.6	22.03	145	62
t18:0h24:0	1264.714	666.6	22.03	145	62.5
t18:0h24:1/t18:1h24:0/t18:0c25:0/d18:0h25:0	1262.714	664.6	22.03	145	62
t18:0h25:0	1278.814	680.7	22.03	145	62
t18:0h25:1/t18:1h25:0/t18:0c26:0/d18:0h26:0	1276.814	678.7	22.03	145	62
t18:0h26:0	1292.814	694.7	22.03	145	63
t18:0h26:1/t18:1h26:0	1290.814	692.7	22.03	145	63
t18:1h16:0	1150.614	552.5	22.03	145	56
t18:1h18:0	1178.614	580.5	22.03	145	58
t18:1h20:1	1204.714	606.6	22.03	145	60
t18:1h22:1/t18:0c23:1/t18:1c23:0/d18:0h23:1/d18:1h23:0	1232.714	634.6	22.03	145	60
t18:1h23:1/t18:0c24:1/t18:1c24:0/d18:0h24:1/d18:1h24:0	1246.714	648.6	22.03	145	61
t18:1h24:1/t18:0c25:1/t18:1c25:0/d18:0h25:1/d18:1h25:0	1260.714	662.6	22.03	145	63
t18:1h25:1/t18:0c26:1/t18:1c26:0/d18:0h26:1/d18:1h26:0	1274.714	676.6	22.03	145	64
t18:1h26:1	1288.814	690.7	22.03	145	65
t18:0c16:0/d18:0 h16:0	1136.614	538.5	22.03	145	57
t18:0c18:0/d18:0h18:0	1164.714	566.6	22.03	145	57
t18:0c20:0/d18:0h20:0	1192.714	594.6	22.03	145	57
t18:0c20:1/t18:1c20:0/d18:0h20:1/d18:1h20:0	1190.714	592.6	22.03	145	57
t18:0c22:0/d18:0h22:0	1220.714	622.6	22.03	145	58
t18:0c22:1/t18:1c22:0/d18:0h22:1/d18:1h22:0	1218.714	620.6	22.03	145	58
t18:1c18:0/d18:1h16:0	1134.614	536.5	22.03	145	57
t18:1c18:0/d18:1h18:0	1162.714	564.6	22.03	145	57
t18:1c20:1/d18:1h20:1	1188.714	590.6	22.03	145	57
t18:1c22:1/d18:1h22:1	1216.714	618.6	22.03	145	58
t18:1c23:1/d18:0h23:1	1230.714	632.6	22.03	145	60
t18:1c24:1/d18:1h24:1	1244.714	646.6	22.03	145	61
t18:1c25:1/d18:1h25:1	1258.714	660.6	22.03	145	62
t18:1c26:1/d18:1h26:1	1272.814	674.7	22.03	145	63

Headgroup structure	Hex-Hex-HexA-IPC				
	[M+H]+				
Cermide Backbone	Exact mass	Product mass	Dwell time	DP	CE
GM1	1546.9	366.3	22.03	145	50
t18:0h16:0	1314.68	554.514	22.03	145	60
t18:0h18:0	1342.666	582.5	22.03	145	60
t18:0h20:0	1370.766	610.6	22.03	145	60
t18:0h20:1/t18:1h20:0	1368.766	608.6	22.03	145	61
t18:0h22:0	1398.766	638.6	22.03	145	62.5
t18:0h22:1/t18:1h22:0/t18:0c23:0/d18:0h23:0	1396.766	636.6	22.03	145	61
t18:0h23:0	1412.766	652.6	22.03	145	62
t18:0h23:1/t18:1h23:0/t18:0c24:0/d18:0h24:0	1410.766	650.6	22.03	145	62
t18:0h24:0	1426.766	666.6	22.03	145	62.5
t18:0h24:1/t18:1h24:0/t18:0c25:0/d18:0h25:0	1424.766	664.6	22.03	145	62
t18:0h25:0	1440.866	680.7	22.03	145	62
t18:0h25:1/t18:1h25:0/t18:0c26:0/d18:0h26:0	1438.866	678.7	22.03	145	62
t18:0h26:0	1454.866	694.7	22.03	145	63
t18:0h26:1/t18:1h26:0	1452.866	692.7	22.03	145	63
t18:1h16:0	1312.666	552.5	22.03	145	56
t18:1h18:0	1340.666	580.5	22.03	145	58
t18:1h20:1	1366.766	606.6	22.03	145	60
t18:1h22:1/t18:0c23:1/t18:1c23:0/d18:0h23:1/d18:1h23:0	1394.766	634.6	22.03	145	60
t18:1h23:1/t18:0c24:1/t18:1c24:0/d18:0h24:1/d18:1h24:0	1408.766	648.6	22.03	145	61
t18:1h24:1/t18:0c25:1/t18:1c25:0/d18:0h25:1/d18:1h25:0	1422.766	662.6	22.03	145	63
t18:1h25:1/t18:0c26:1/t18:1c26:0/d18:0h26:1/d18:1h26:0	1436.766	676.6	22.03	145	64
t18:1h26:1	1450.866	690.7	22.03	145	65
t18:0c16:0/d18:0 h16:0	1298.666	538.5	22.03	145	57
t18:0c18:0/d18:0h18:0	1326.766	566.6	22.03	145	57
t18:0c20:0/d18:0h20:0	1354.766	594.6	22.03	145	57
t18:0c20:1/t18:1c20:0/d18:0h20:1/d18:1h20:0	1352.766	592.6	22.03	145	57
t18:0c22:0/d18:0h22:0	1382.766	622.6	22.03	145	58
t18:0c22:1/t18:1c22:0/d18:0h22:1/d18:1h22:0	1380.766	620.6	22.03	145	58
t18:1c18:0/d18:1h16:0	1296.666	536.5	22.03	145	57
t18:1c18:0/d18:1h18:0	1324.766	564.6	22.03	145	57
t18:1c20:1/d18:1h20:1	1350.766	590.6	22.03	145	57
t18:1c22:1/d18:1h22:1	1378.766	618.6	22.03	145	58
t18:1c23:1/d18:0h23:1	1392.766	632.6	22.03	145	60
t18:1c24:1/d18:1h24:1	1406.766	646.6	22.03	145	61
t18:1c25:1/d18:1h25:1	1420.766	660.6	22.03	145	62
t18:1c26:1/d18:1h26:1	1434.866	674.7	22.03	145	63

Headgroup structure	Hex(NAc)-HexA-IPC				
	[M+H]+				
Ceramide Backbone	Exact mass	Product mass	Dwell time	DP	CE
GM1	1546.9	366.3	22.03	135	50
t18:0h16:0	1193.655	554.514	22.03	135	45
t18:0h18:0	1221.641	582.5	22.03	135	45
t18:0h20:0	1249.741	610.6	22.03	135	45
t18:0h20:1/t18:1h20:0	1247.741	608.6	22.03	135	46
t18:0h22:0	1277.741	638.6	22.03	135	47.5
t18:0h22:1/t18:1h22:0/t18:0c23:0/d18:0h23:0	1275.741	636.6	22.03	135	46
t18:0h23:0	1291.741	652.6	22.03	135	47
t18:0h23:1/t18:1h23:0/t18:0c24:0/d18:0h24:0	1289.741	650.6	22.03	135	47
t18:0h24:0	1305.741	666.6	22.03	135	47.5
t18:0h24:1/t18:1h24:0/t18:0c25:0/d18:0h25:0	1303.741	664.6	22.03	135	47
t18:0h25:0	1319.841	680.7	22.03	135	47
t18:0h25:1/t18:1h25:0/t18:0c26:0/d18:0h26:0	1317.841	678.7	22.03	135	47
t18:0h26:0	1333.841	694.7	22.03	135	48
t18:0h26:1/t18:1h26:0	1331.841	692.7	22.03	135	48
t18:1h16:0	1191.641	552.5	22.03	135	41
t18:1h18:0	1219.641	580.5	22.03	135	43
t18:1h20:1	1245.741	606.6	22.03	135	45
t18:1h22:1/t18:0c23:1/t18:1c23:0/d18:0h23:1/d18:1h23:0	1273.741	634.6	22.03	135	45
t18:1h23:1/t18:0c24:1/t18:1c24:0/d18:0h24:1/d18:1h24:0	1287.741	648.6	22.03	135	46
t18:1h24:1/t18:0c25:1/t18:1c25:0/d18:0h25:1/d18:1h25:0	1301.741	662.6	22.03	135	48
t18:1h25:1/t18:0c26:1/t18:1c26:0/d18:0h26:1/d18:1h26:0	1315.741	676.6	22.03	135	49
t18:1h26:1	1329.841	690.7	22.03	135	50
t18:0c16:0/d18:0 h16:0	1177.641	538.5	22.03	135	42
t18:0c18:0/d18:0h18:0	1205.741	566.6	22.03	135	42
t18:0c20:0/d18:0h20:0	1233.741	594.6	22.03	135	42
t18:0c20:1/t18:1c20:0/d18:0h20:1/d18:1h20:0	1231.741	592.6	22.03	135	42
t18:0c22:0/d18:0h22:0	1261.741	622.6	22.03	135	43
t18:0c22:1/t18:1c22:0/d18:0h22:1/d18:1h22:0	1259.741	620.6	22.03	135	43
t18:1c18:0/d18:1h16:0	1175.641	536.5	22.03	135	42
t18:1c18:0/d18:1h18:0	1203.741	564.6	22.03	135	42
t18:1c20:1/d18:1h20:1	1229.741	590.6	22.03	135	42
t18:1c22:1/d18:1h22:1	1257.741	618.6	22.03	135	43
t18:1c23:1/d18:0h23:1	1271.741	632.6	22.03	135	45
t18:1c24:1/d18:1h24:1	1285.741	646.6	22.03	135	46
t18:1c25:1/d18:1h25:1	1299.741	660.6	22.03	135	47
t18:1c26:1/d18:1h26:1	1313.841	674.7	22.03	135	48

Headgroup structure	Hex-Hex(NAc)-HexA-IPC				
	[M+H]+				
Ceramide Backbone	Exact mass	Product mass	Dwell time	DP	CE
GM1	1546.9	366.3	22.03	135	50
t18:0h16:0	1355.707	554.514	22.03	135	45
t18:0h18:0	1383.693	582.5	22.03	135	45
t18:0h20:0	1411.793	610.6	22.03	135	45
t18:0h20:1/t18:1h20:0	1409.793	608.6	22.03	135	46
t18:0h22:0	1439.793	638.6	22.03	135	47.5
t18:0h22:1/t18:1h22:0/t18:0c23:0/d18:0h23:0	1437.793	636.6	22.03	135	46
t18:0h23:0	1453.793	652.6	22.03	135	47
t18:0h23:1/t18:1h23:0/t18:0c24:0/d18:0h24:0	1451.793	650.6	22.03	135	47
t18:0h24:0	1467.793	666.6	22.03	135	47.5
t18:0h24:1/t18:1h24:0/t18:0c25:0/d18:0h25:0	1465.793	664.6	22.03	135	47
t18:0h25:0	1481.893	680.7	22.03	135	47
t18:0h25:1/t18:1h25:0/t18:0c26:0/d18:0h26:0	1479.893	678.7	22.03	135	47
t18:0h26:0	1495.893	694.7	22.03	135	48
t18:0h26:1/t18:1h26:0	1493.893	692.7	22.03	135	48
t18:1h16:0	1353.693	552.5	22.03	135	41
t18:1h18:0	1381.693	580.5	22.03	135	43
t18:1h20:1	1407.793	606.6	22.03	135	45
t18:1h22:1/t18:0c23:1/t18:1c23:0/d18:0h23:1/d18:1h23:0	1435.793	634.6	22.03	135	45
t18:1h23:1/t18:0c24:1/t18:1c24:0/d18:0h24:1/d18:1h24:0	1449.793	648.6	22.03	135	46
t18:1h24:1/t18:0c25:1/t18:1c25:0/d18:0h25:1/d18:1h25:0	1463.793	662.6	22.03	135	48
t18:1h25:1/t18:0c26:1/t18:1c26:0/d18:0h26:1/d18:1h26:0	1477.793	676.6	22.03	135	49
t18:1h26:1	1491.893	690.7	22.03	135	50
t18:0c16:0/d18:0 h16:0	1339.693	538.5	22.03	135	42
t18:0c18:0/d18:0h18:0	1367.793	566.6	22.03	135	42
t18:0c20:0/d18:0h20:0	1395.793	594.6	22.03	135	42
t18:0c20:1/t18:1c20:0/d18:0h20:1/d18:1h20:0	1393.793	592.6	22.03	135	42
t18:0c22:0/d18:0h22:0	1423.793	622.6	22.03	135	43
t18:0c22:1/t18:1c22:0/d18:0h22:1/d18:1h22:0	1421.793	620.6	22.03	135	43
t18:1c18:0/d18:1h16:0	1337.693	536.5	22.03	135	42
t18:1c18:0/d18:1h18:0	1365.793	564.6	22.03	135	42
t18:1c20:1/d18:1h20:1	1391.793	590.6	22.03	135	42
t18:1c22:1/d18:1h22:1	1419.793	618.6	22.03	135	43
t18:1c23:1/d18:0h23:1	1433.793	632.6	22.03	135	45
t18:1c24:1/d18:1h24:1	1447.793	646.6	22.03	135	46
t18:1c25:1/d18:1h25:1	1461.793	660.6	22.03	135	47
t18:1c26:1/d18:1h26:1	1475.893	674.7	22.03	135	48

Headgroup structure	Pent-Hex-Hex(NAc)-HexA-IPC				
	[M+H]+				
Ceramide Backbone	Exact mass	Product mass	Dwell time	DP	CE
GM1	1546.9	366.3	22.03	140	50
t18:0h16:0	1487.749	554.514	22.03	140	48
t18:0h18:0	1515.735	582.5	22.03	140	48
t18:0h20:0	1543.835	610.6	22.03	140	48
t18:0h20:1/t18:1h20:0	1541.835	608.6	22.03	140	49
t18:0h22:0	1571.835	638.6	22.03	140	50.5
t18:0h22:1/t18:1h22:0/t18:0c23:0/d18:0h23:0	1569.835	636.6	22.03	140	49
t18:0h23:0	1585.835	652.6	22.03	140	50
t18:0h23:1/t18:1h23:0/t18:0c24:0/d18:0h24:0	1583.835	650.6	22.03	140	50
t18:0h24:0	1599.835	666.6	22.03	140	50.5
t18:0h24:1/t18:1h24:0/t18:0c25:0/d18:0h25:0	1597.835	664.6	22.03	140	50
t18:0h25:0	1613.935	680.7	22.03	140	50
t18:0h25:1/t18:1h25:0/t18:0c26:0/d18:0h26:0	1611.935	678.7	22.03	140	50
t18:0h26:0	1627.935	694.7	22.03	140	51
t18:0h26:1/t18:1h26:0	1625.935	692.7	22.03	140	51
t18:1h16:0	1485.735	552.5	22.03	140	44
t18:1h18:0	1513.735	580.5	22.03	140	46
t18:1h20:1	1539.835	606.6	22.03	140	48
t18:1h22:1/t18:0c23:1/t18:1c23:0/d18:0h23:1/d18:1h23:0	1567.835	634.6	22.03	140	48
t18:1h23:1/t18:0c24:1/t18:1c24:0/d18:0h24:1/d18:1h24:0	1581.835	648.6	22.03	140	49
t18:1h24:1/t18:0c25:1/t18:1c25:0/d18:0h25:1/d18:1h25:0	1595.835	662.6	22.03	140	51
t18:1h25:1/t18:0c26:1/t18:1c26:0/d18:0h26:1/d18:1h26:0	1609.835	676.6	22.03	140	52
t18:1h26:1	1623.935	690.7	22.03	140	53
t18:0c16:0/d18:0 h16:0	1471.735	538.5	22.03	140	45
t18:0c18:0/d18:0h18:0	1499.835	566.6	22.03	140	45
t18:0c20:0/d18:0h20:0	1527.835	594.6	22.03	140	45
t18:0c20:1/t18:1c20:0/d18:0h20:1/d18:1h20:0	1525.835	592.6	22.03	140	45
t18:0c22:0/d18:0h22:0	1555.835	622.6	22.03	140	46
t18:0c22:1/t18:1c22:0/d18:0h22:1/d18:1h22:0	1553.835	620.6	22.03	140	46
t18:1c18:0/d18:1h16:0	1469.735	536.5	22.03	140	45
t18:1c18:0/d18:1h18:0	1497.835	564.6	22.03	140	45
t18:1c20:1/d18:1h20:1	1523.835	590.6	22.03	140	45
t18:1c22:1/d18:1h22:1	1551.835	618.6	22.03	140	46
t18:1c23:1/d18:0h23:1	1565.835	632.6	22.03	140	48
t18:1c24:1/d18:1h24:1	1579.835	646.6	22.03	140	49
t18:1c25:1/d18:1h25:1	1593.835	660.6	22.03	140	50
t18:1c26:1/d18:1h26:1	1607.935	674.7	22.03	140	51

Headgroup structure	Pent-Pent-Hex-Hex(NAc)-HexA-IPC				
	[M+H]+				
Ceramide Backbone	Exact mass	Product mass	Dwell time	DP	CE
GM1	1546.9	366.3	22.03	145	50
t18:0h16:0	1619.791	554.514	22.03	145	51
t18:0h18:0	1647.777	582.5	22.03	145	51
t18:0h20:0	1675.877	610.6	22.03	145	51
t18:0h20:1/t18:1h20:0	1673.877	608.6	22.03	145	52
t18:0h22:0	1703.877	638.6	22.03	145	53.5
t18:0h22:1/t18:1h22:0/t18:0c23:0/d18:0h23:0	1701.877	636.6	22.03	145	52
t18:0h23:0	1717.877	652.6	22.03	145	53
t18:0h23:1/t18:1h23:0/t18:0c24:0/d18:0h24:0	1715.877	650.6	22.03	145	53
t18:0h24:0	1731.877	666.6	22.03	145	53.5
t18:0h24:1/t18:1h24:0/t18:0c25:0/d18:0h25:0	1729.877	664.6	22.03	145	53
t18:0h25:0	1745.977	680.7	22.03	145	53
t18:0h25:1/t18:1h25:0/t18:0c26:0/d18:0h26:0	1743.977	678.7	22.03	145	53
t18:0h26:0	1759.977	694.7	22.03	145	54
t18:0h26:1/t18:1h26:0	1757.977	692.7	22.03	145	54
t18:1h16:0	1617.777	552.5	22.03	145	47
t18:1h18:0	1645.777	580.5	22.03	145	49
t18:1h20:1	1671.877	606.6	22.03	145	51
t18:1h22:1/t18:0c23:1/t18:1c23:0/d18:0h23:1/d18:1h23:0	1699.877	634.6	22.03	145	51
t18:1h23:1/t18:0c24:1/t18:1c24:0/d18:0h24:1/d18:1h24:0	1713.877	648.6	22.03	145	52
t18:1h24:1/t18:0c25:1/t18:1c25:0/d18:0h25:1/d18:1h25:0	1727.877	662.6	22.03	145	54
t18:1h25:1/t18:0c26:1/t18:1c26:0/d18:0h26:1/d18:1h26:0	1741.877	676.6	22.03	145	55
t18:1h26:1	1755.977	690.7	22.03	145	56
t18:0c16:0/d18:0 h16:0	1603.777	538.5	22.03	145	48
t18:0c18:0/d18:0h18:0	1631.877	566.6	22.03	145	48
t18:0c20:0/d18:0h20:0	1659.877	594.6	22.03	145	48
t18:0c20:1/t18:1c20:0/d18:0h20:1/d18:1h20:0	1657.877	592.6	22.03	145	48
t18:0c22:0/d18:0h22:0	1687.877	622.6	22.03	145	49
t18:0c22:1/t18:1c22:0/d18:0h22:1/d18:1h22:0	1685.877	620.6	22.03	145	49
t18:1c18:0/d18:1h16:0	1601.777	536.5	22.03	145	48
t18:1c18:0/d18:1h18:0	1629.877	564.6	22.03	145	48
t18:1c20:1/d18:1h20:1	1655.877	590.6	22.03	145	48
t18:1c22:1/d18:1h22:1	1683.877	618.6	22.03	145	49
t18:1c23:1/d18:0h23:1	1697.877	632.6	22.03	145	51
t18:1c24:1/d18:1h24:1	1711.877	646.6	22.03	145	52
t18:1c25:1/d18:1h25:1	1725.877	660.6	22.03	145	53
t18:1c26:1/d18:1h26:1	1739.977	674.7	22.03	145	54

Headgroup structure	Pent-Pent-Pent-Hex-Hex(NAc)-HexA-IPC				
	[M+H]+				
Ceramide Backbone	exact mass	Product mass	Dwell time	DP	CE
GM1	1546.9	366.3	22.03	150	50
t18:0h16:0	1751.833	554.514	22.03	150	54
t18:0h18:0	1779.819	582.5	22.03	150	54
t18:0h20:0	1807.919	610.6	22.03	150	54
t18:0h20:1/t18:1h20:0	1805.919	608.6	22.03	150	55
t18:0h22:0	1835.919	638.6	22.03	150	56.5
t18:0h22:1/t18:1h22:0/t18:0c23:0/d18:0h23:0	1833.919	636.6	22.03	150	55
t18:0h23:0	1849.919	652.6	22.03	150	56
t18:0h23:1/t18:1h23:0/t18:0c24:0/d18:0h24:0	1847.919	650.6	22.03	150	56
t18:0h24:0	1863.919	666.6	22.03	150	56.5
t18:0h24:1/t18:1h24:0/t18:0c25:0/d18:0h25:0	1861.919	664.6	22.03	150	56
t18:0h25:0	1878.019	680.7	22.03	150	56
t18:0h25:1/t18:1h25:0/t18:0c26:0/d18:0h26:0	1876.019	678.7	22.03	150	56
t18:0h26:0	1892.019	694.7	22.03	150	57
t18:0h26:1/t18:1h26:0	1890.019	692.7	22.03	150	57
t18:1h16:0	1749.819	552.5	22.03	150	50
t18:1h18:0	1777.819	580.5	22.03	150	52
t18:1h20:1	1803.919	606.6	22.03	150	54
t18:1h22:1/t18:0c23:1/t18:1c23:0/d18:0h23:1/d18:1h23:0	1831.919	634.6	22.03	150	54
t18:1h23:1/t18:0c24:1/t18:1c24:0/d18:0h24:1/d18:1h24:0	1845.919	648.6	22.03	150	55
t18:1h24:1/t18:0c25:1/t18:1c25:0/d18:0h25:1/d18:1h25:0	1859.919	662.6	22.03	150	57
t18:1h25:1/t18:0c26:1/t18:1c26:0/d18:0h26:1/d18:1h26:0	1873.919	676.6	22.03	150	58
t18:1h26:1	1888.019	690.7	22.03	150	59
t18:0c16:0/d18:0 h16:0	1735.819	538.5	22.03	150	51
t18:0c18:0/d18:0h18:0	1763.919	566.6	22.03	150	51
t18:0c20:0/d18:0h20:0	1791.919	594.6	22.03	150	51
t18:0c20:1/t18:1c20:0/d18:0h20:1/d18:1h20:0	1789.919	592.6	22.03	150	51
t18:0c22:0/d18:0h22:0	1819.919	622.6	22.03	150	52
t18:0c22:1/t18:1c22:0/d18:0h22:1/d18:1h22:0	1817.919	620.6	22.03	150	52
t18:1c18:0/d18:1h16:0	1733.819	536.5	22.03	150	51
t18:1c18:0/d18:1h18:0	1761.919	564.6	22.03	150	51
t18:1c20:1/d18:1h20:1	1787.919	590.6	22.03	150	51
t18:1c22:1/d18:1h22:1	1815.919	618.6	22.03	150	52
t18:1c23:1/d18:0h23:1	1829.919	632.6	22.03	150	54
t18:1c24:1/d18:1h24:1	1843.919	646.6	22.03	150	55
t18:1c25:1/d18:1h25:1	1857.919	660.6	22.03	150	56
t18:1c26:1/d18:1h26:1	1872.019	674.7	22.03	150	57

Headgroup structure	Pent-Pent-Pent-Pent-Hex-Hex(NAc)-HexA-IPC				
	[M+H]+				
Ceramide Backbone	Exact mass	Product mass	Dwell time	DP	CE
GM1	1546.9	366.3	22.03	155	50
t18:0h16:0	1883.875	554.514	22.03	155	57
t18:0h18:0	1911.861	582.5	22.03	155	57
t18:0h20:0	1939.961	610.6	22.03	155	57
t18:0h20:1/t18:1h20:0	1937.961	608.6	22.03	155	58
t18:0h22:0	1967.961	638.6	22.03	155	59.5
t18:0h22:1/t18:1h22:0/t18:0c23:0/d18:0h23:0	1965.961	636.6	22.03	155	58
t18:0h23:0	1981.961	652.6	22.03	155	59
t18:0h23:1/t18:1h23:0/t18:0c24:0/d18:0h24:0	1979.961	650.6	22.03	155	59
t18:0h24:0	1995.961	666.6	22.03	155	59.5
t18:0h24:1/t18:1h24:0/t18:0c25:0/d18:0h25:0	1993.961	664.6	22.03	155	59
t18:0h25:0	2010.061	680.7	22.03	155	59
t18:0h25:1/t18:1h25:0/t18:0c26:0/d18:0h26:0	2008.061	678.7	22.03	155	59
t18:0h26:0	2024.061	694.7	22.03	155	60
t18:0h26:1/t18:1h26:0	2022.061	692.7	22.03	155	60
t18:1h16:0	1881.861	552.5	22.03	155	53
t18:1h18:0	1909.861	580.5	22.03	155	55
t18:1h20:1	1935.961	606.6	22.03	155	57
t18:1h22:1/t18:0c23:1/t18:1c23:0/d18:0h23:1/d18:1h23:0	1963.961	634.6	22.03	155	57
t18:1h23:1/t18:0c24:1/t18:1c24:0/d18:0h24:1/d18:1h24:0	1977.961	648.6	22.03	155	58
t18:1h24:1/t18:0c25:1/t18:1c25:0/d18:0h25:1/d18:1h25:0	1991.961	662.6	22.03	155	60
t18:1h25:1/t18:0c26:1/t18:1c26:0/d18:0h26:1/d18:1h26:0	2005.961	676.6	22.03	155	61
t18:1h26:1	2020.061	690.7	22.03	155	62
t18:0c16:0/d18:0 h16:0	1867.861	538.5	22.03	155	54
t18:0c18:0/d18:0h18:0	1895.961	566.6	22.03	155	54
t18:0c20:0/d18:0h20:0	1923.961	594.6	22.03	155	54
t18:0c20:1/t18:1c20:0/d18:0h20:1/d18:1h20:0	1921.961	592.6	22.03	155	54
t18:0c22:0/d18:0h22:0	1951.961	622.6	22.03	155	55
t18:0c22:1/t18:1c22:0/d18:0h22:1/d18:1h22:0	1949.961	620.6	22.03	155	55
t18:1c18:0/d18:1h16:0	1865.861	536.5	22.03	155	54
t18:1c18:0/d18:1h18:0	1893.961	564.6	22.03	155	54
t18:1c20:1/d18:1h20:1	1919.961	590.6	22.03	155	54
t18:1c22:1/d18:1h22:1	1947.961	618.6	22.03	155	55
t18:1c23:1/d18:0h23:1	1961.961	632.6	22.03	155	57
t18:1c24:1/d18:1h24:1	1975.961	646.6	22.03	155	58
t18:1c25:1/d18:1h25:1	1989.961	660.6	22.03	155	59
t18:1c26:1/d18:1h26:1	2004.061	674.7	22.03	155	60

APPENDIX F

Arabidopsis eFP Browser probe sets used for micro array data mining.

Gene Number	Gene Name	Probe Set
At5G19200	*TSC10a*	249947_at
AT3G06060	*TSC10b*	258467_at
AT3G25540	*LOH1*	257913_at
AT3G19260	*LOH2*	257038_at
AT1G13580	*LOH3*	256157_at
AT4G36480	*LCB1*	246213_at
AT5G23670	*LCB2a*	249799_at
At3g48780	*LCB2b*	252331_s_at
AT3G61580	*sld1*	251323_at
AT2G46210	*sld2*	266592_at
AT4G04930	*Δ4 DES*	255276_at
AT1G69640	*SBH1*	260421_at
At1g14290	*SBH2*	261492_at
AT2G19880	*GCS*	266703_at
AT3G54020	*IPCS1*	Not available
AT2G37940	*IPCS2*	266101_at
AT2G29525	*IPCS3*	Not available

APPENDIX G

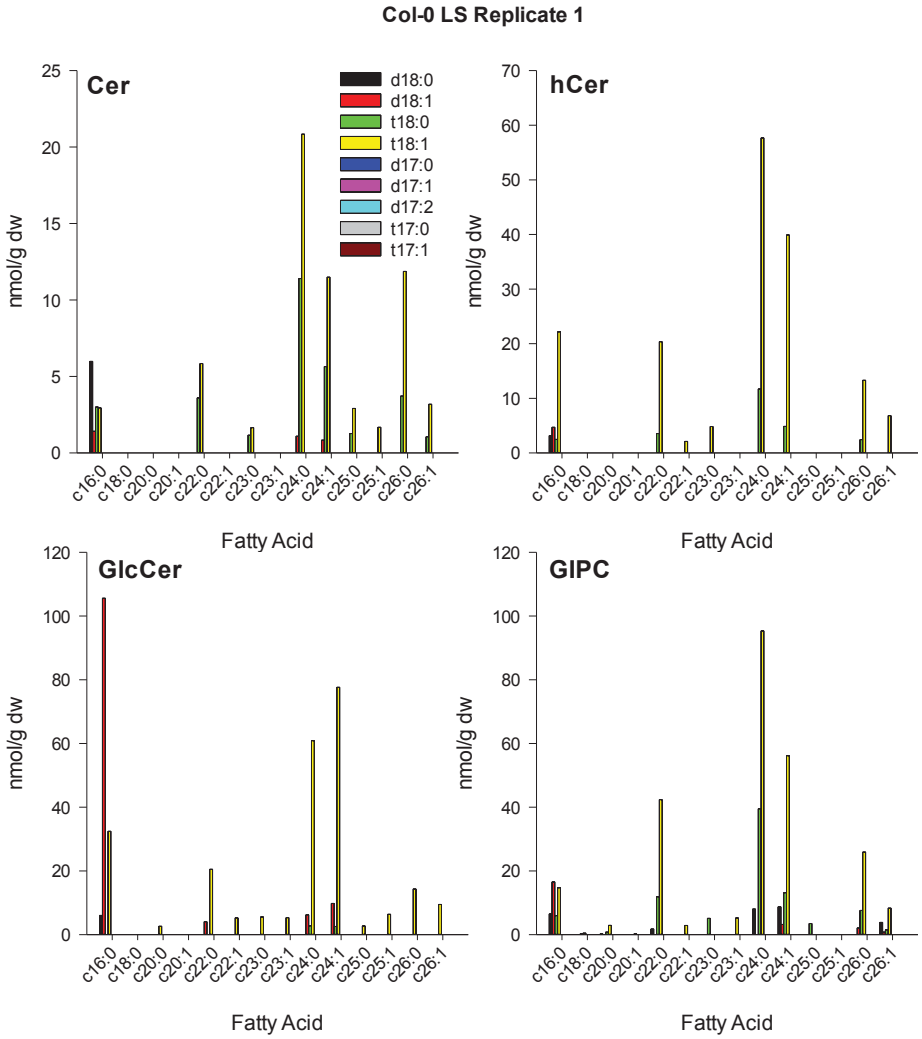
Col-0 LS Replicate 1
Cer
hCer
GlcCer
GIPC
d18:0
d18:1
t18:0
t18:1
d17:0
d17:1
d17:2
t17:0
t17:1
nmol/g dw
Fatty Acid
c16:0
c18:0
c20:0
c20:1
c22:0
c22:1
c23:0
c23:1
c24:0
c24:1
c25:0
c25:1
c26:0
c26:1

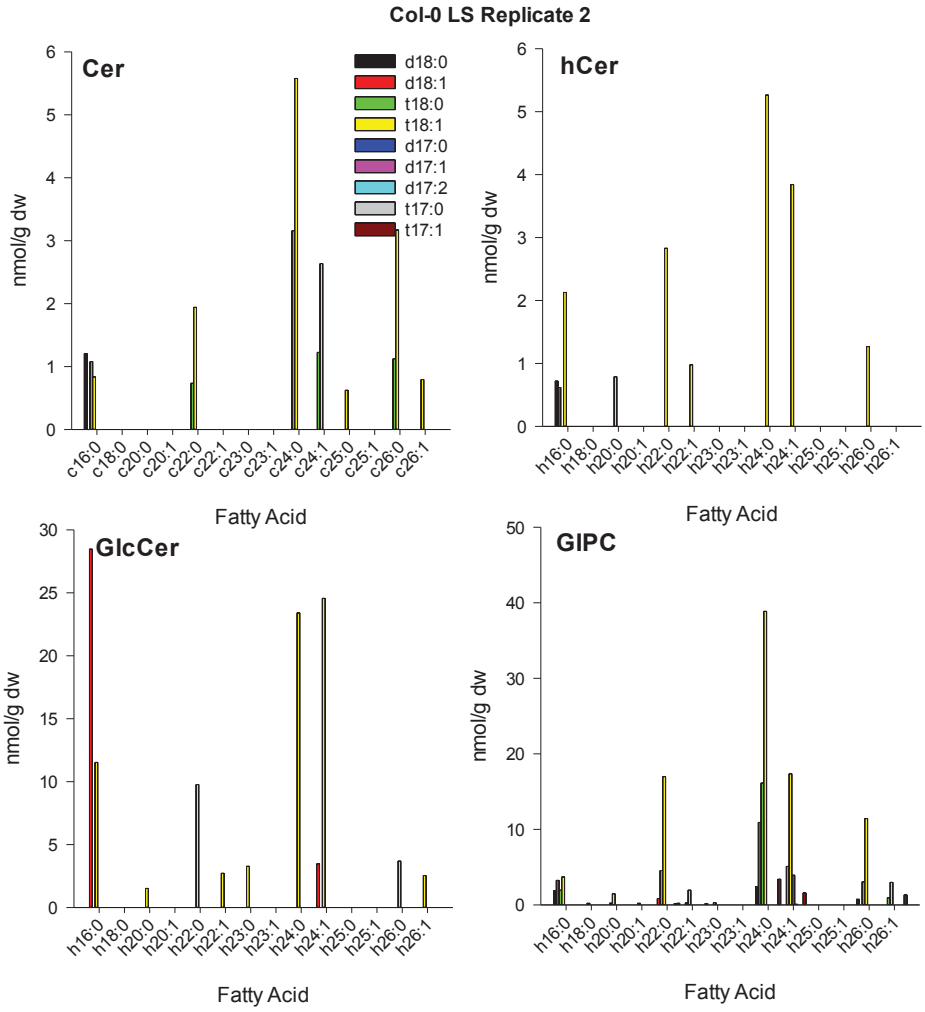
Col-0 LS Replicate 2
Cer
d18:0
d18:1
t18:0
t18:1
d17:0
d17:1
d17:2
t17:0
t17:1
nmol/g dw
Fatty Acid
c16:0
c18:0
c20:0
c20:1
c22:0
c22:1
c23:0
c23:1
c24:0
c24:1
c25:0
c25:1
c26:0
c26:1
hCer
h16:0
h18:0
h20:0
h20:1
h22:0
h22:1
h23:0
h23:1
h24:0
h24:1
h25:0
h25:1
h26:0
h26:1
GlcCer
GlPC

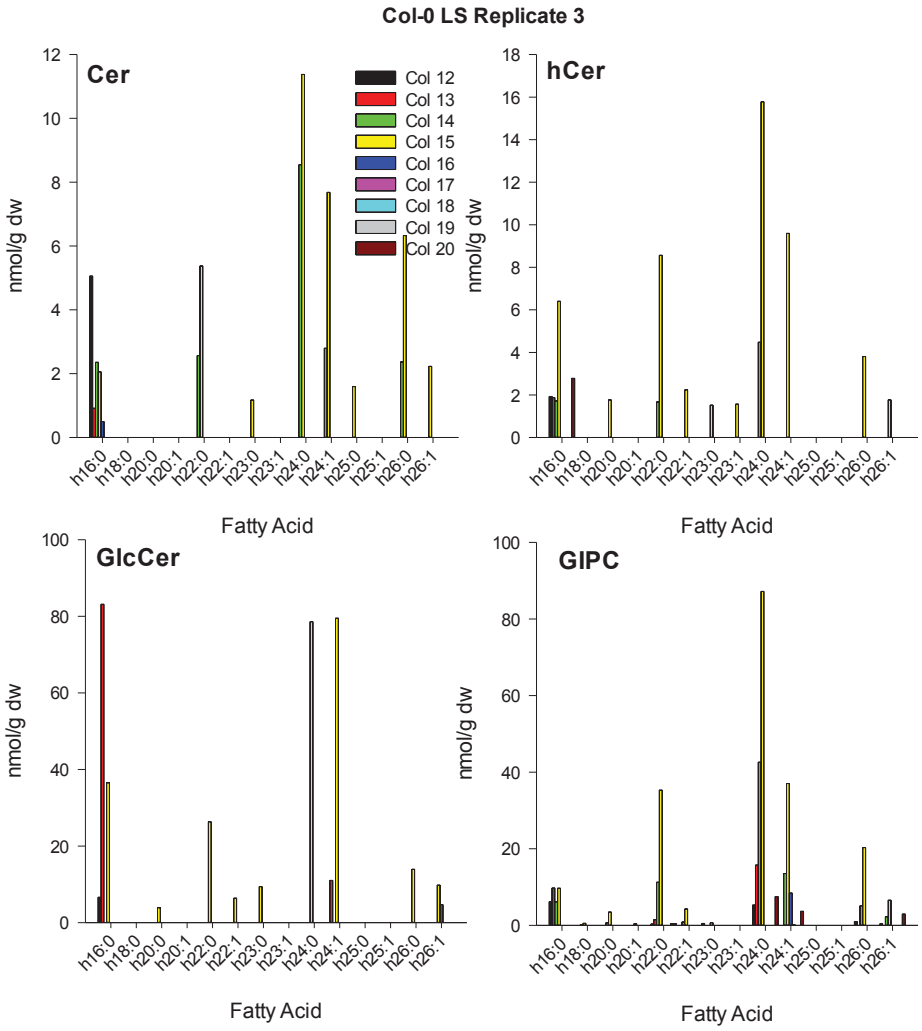
Col-0 LS Replicate 3
Cer
hCer
GlcCer
GIPC
Col 12
Col 13
Col 14
Col 15
Col 16
Col 17
Col 18
Col 19
Col 20
nmol/g dw
Fatty Acid
h16:0
h18:0
h20:0
h20:1
h22:0
h22:1
h23:0
h23:1
h24:0
h24:1
h25:0
h25:1
h26:0
h26:1

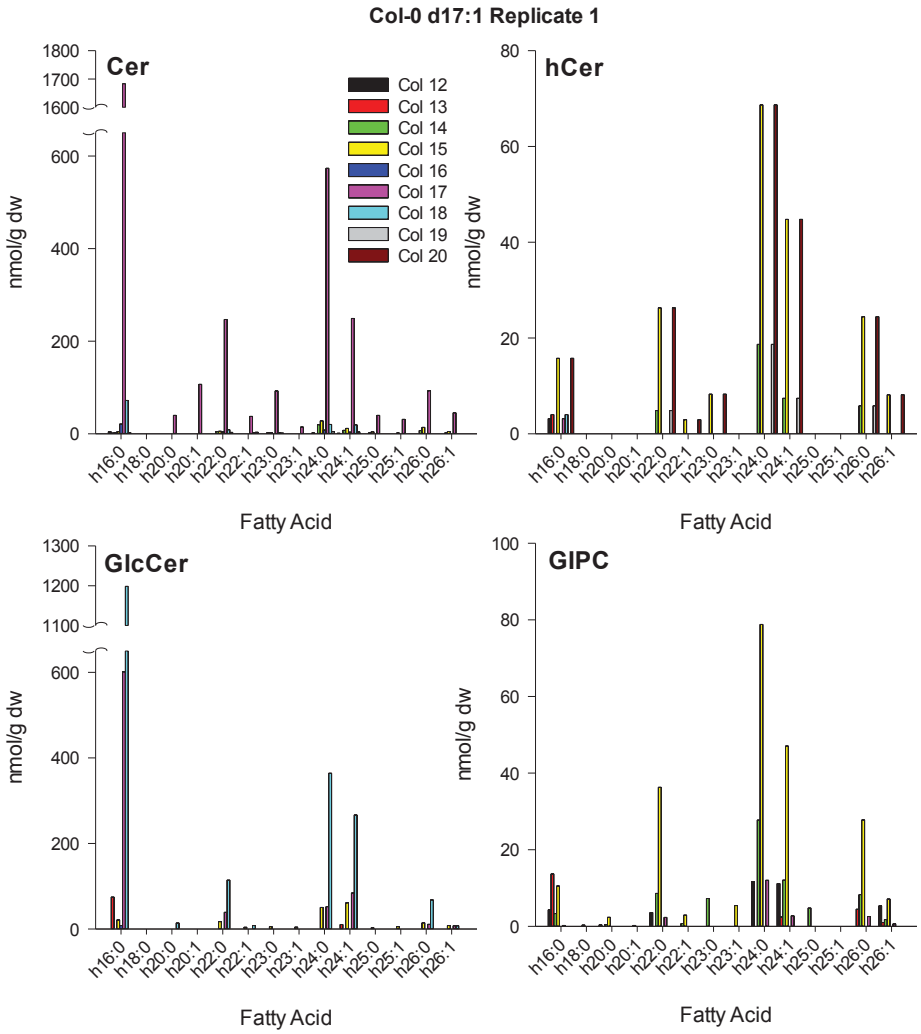
Col-0 d17:1 Replicate 1
Cer
hCer
GlcCer
GIPC
Col 12
Col 13
Col 14
Col 15
Col 16
Col 17
Col 18
Col 19
Col 20
nmol/g dw
Fatty Acid
h16:0
h18:0
h20:0
h20:1
h22:0
h22:1
h23:0
h23:1
h24:0
h24:1
h25:0
h25:1
h26:0
h26:1

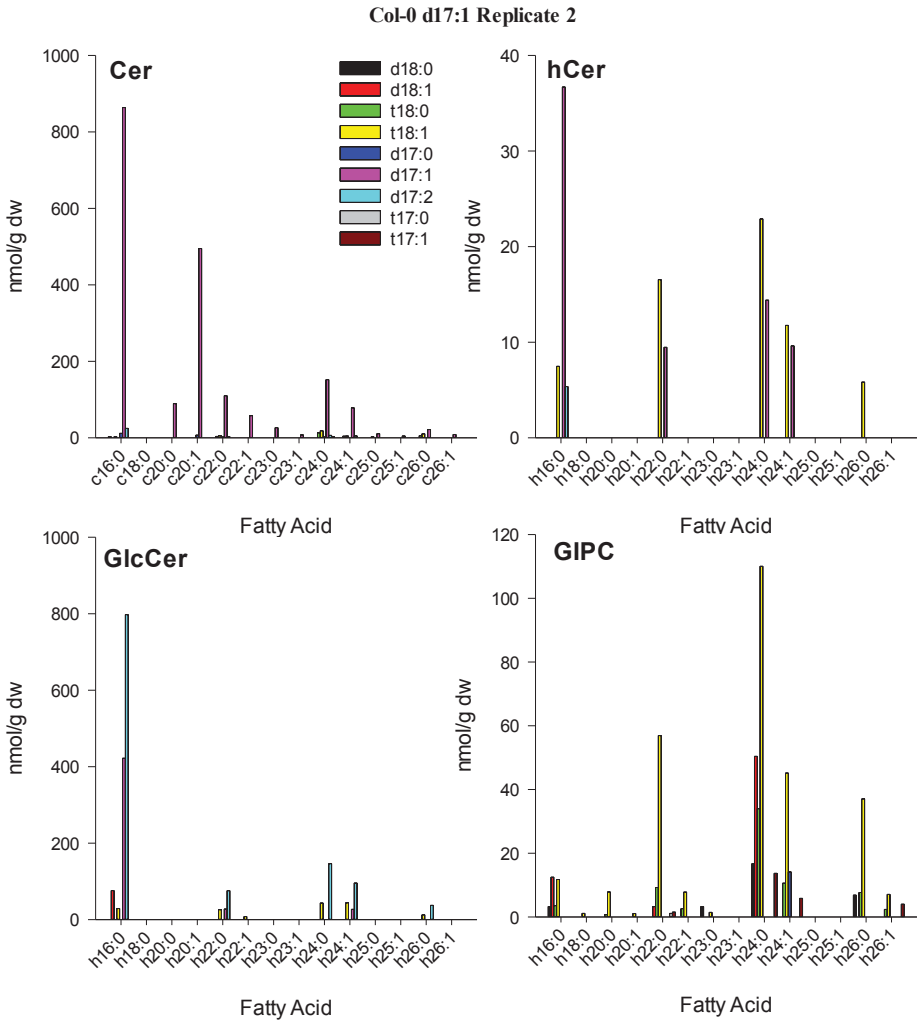
Col-0 d17:1 Replicate 2
Cer
d18:0
d18:1
t18:0
t18:1
d17:0
d17:1
d17:2
t17:0
t17:1
nmol/g dw
Fatty Acid
hCer
GlcCer
GIPC

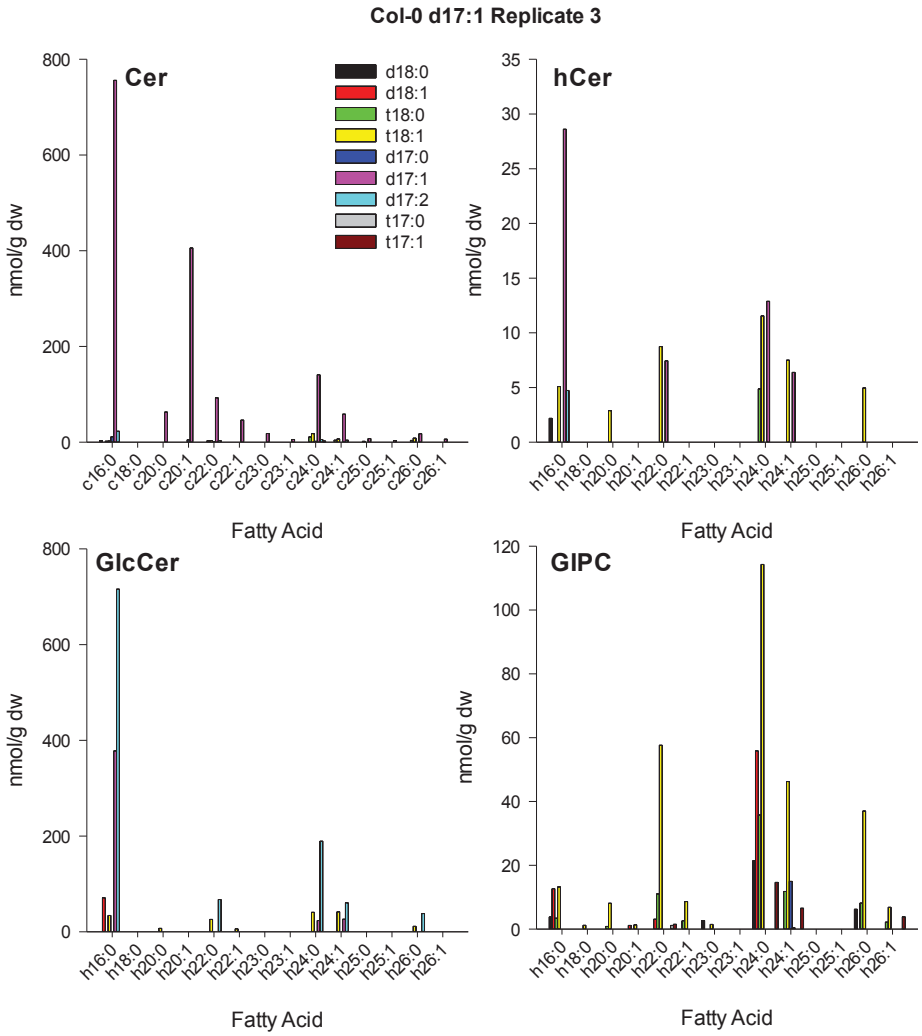
Col-0 d17:1 Replicate 3
Cer
d18:0
d18:1
t18:0
t18:1
d17:0
d17:1
d17:2
t17:0
t17:1
nmol/g dw
Fatty Acid
hCer
GlcCer
GIPC

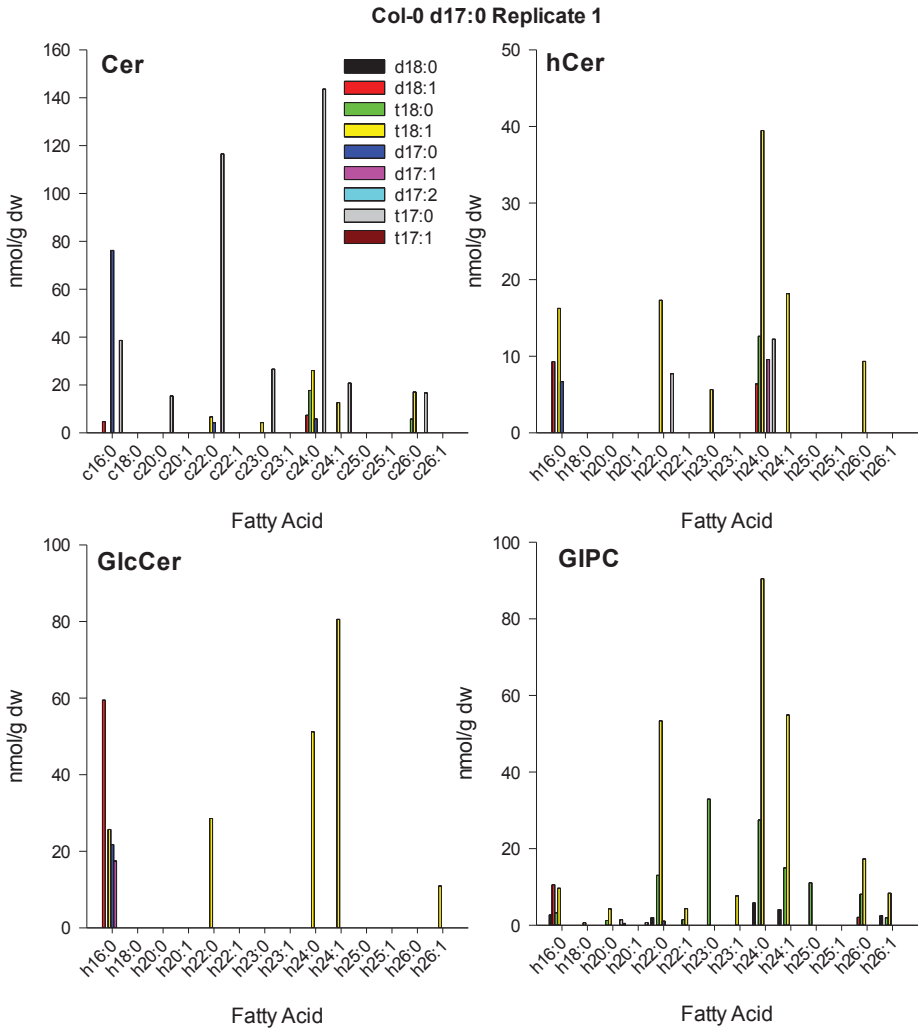
Col-0 d17:0 Replicate 1
Cer
d18:0
d18:1
t18:0
t18:1
d17:0
d17:1
d17:2
t17:0
t17:1
nmol/g dw
Fatty Acid
hCer
GlcCer
GIPC

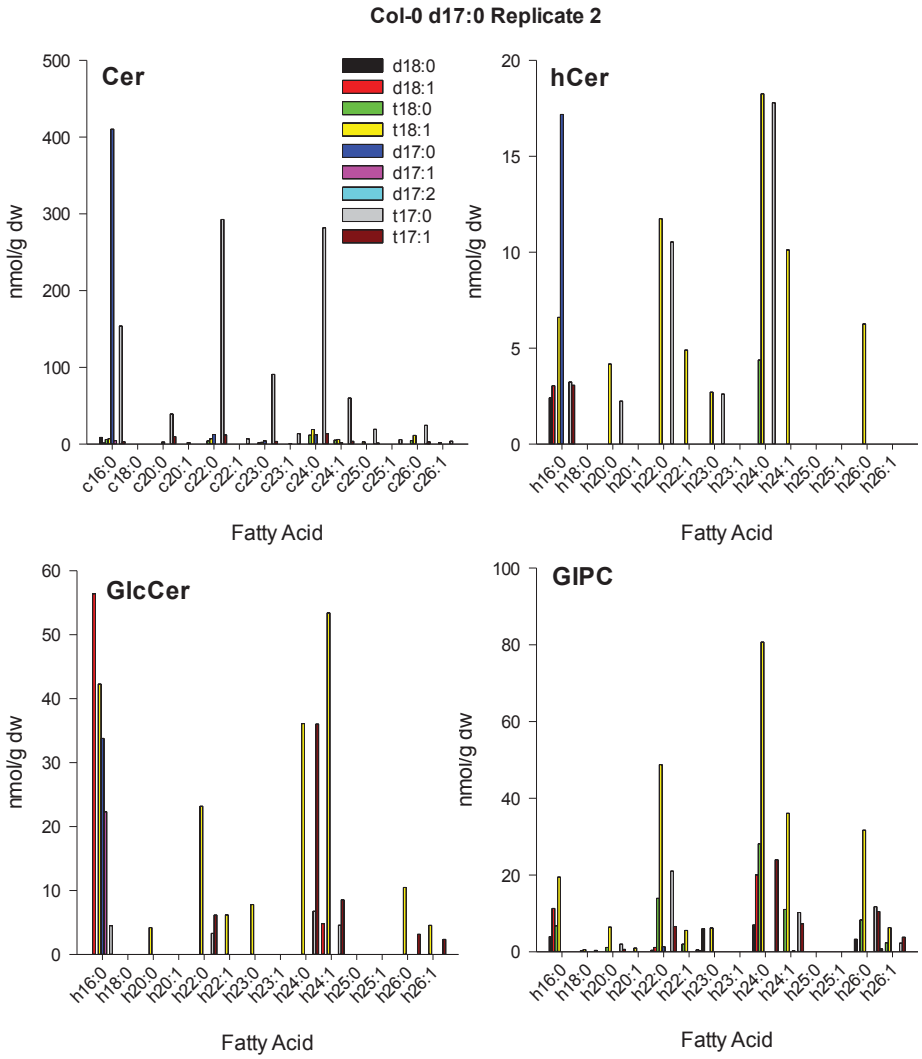
Col-0 d17:0 Replicate 2
Cer
d18:0
d18:1
t18:0
t18:1
d17:0
d17:1
d17:2
t17:0
t17:1
nmol/g dw
Fatty Acid
hCer
GlcCer
GIPC

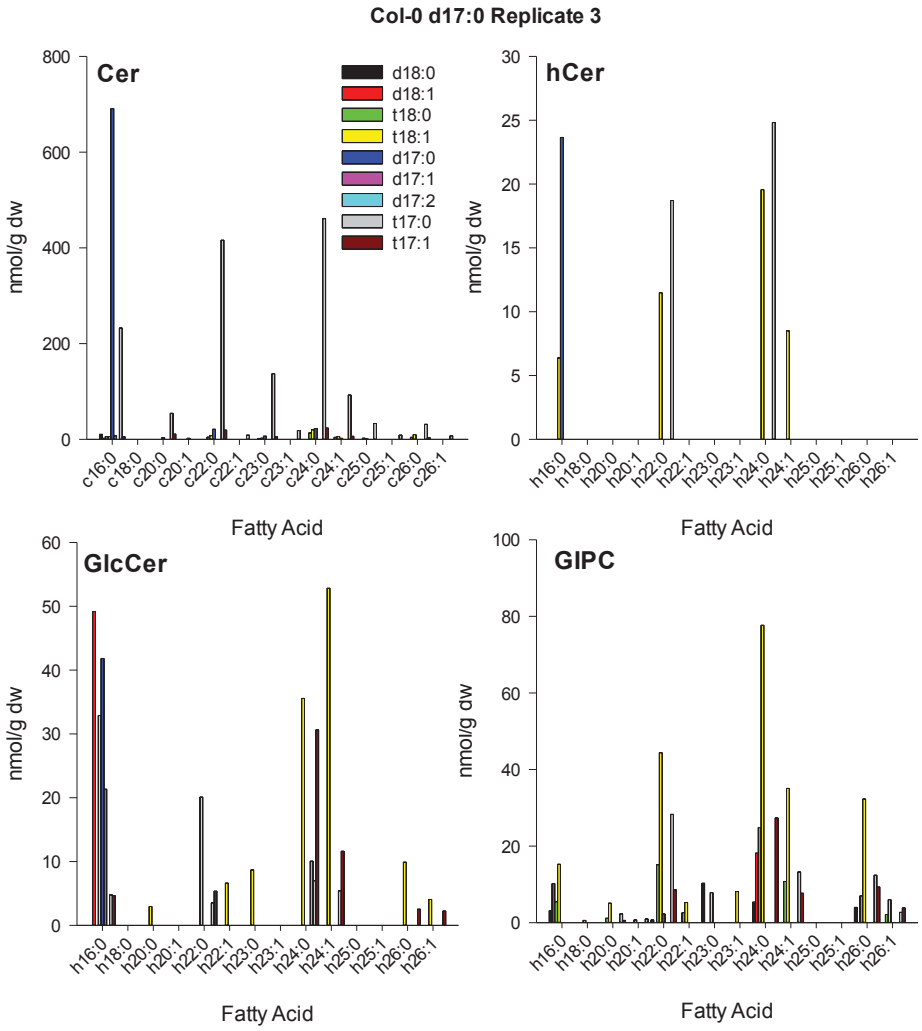
Col-0 d17:0 Replicate 3
Cer
d18:0
d18:1
t18:0
t18:1
d17:0
d17:1
d17:2
t17:0
t17:1
nmol/g dw
Fatty Acid
hCer
GlcCer
GIPC

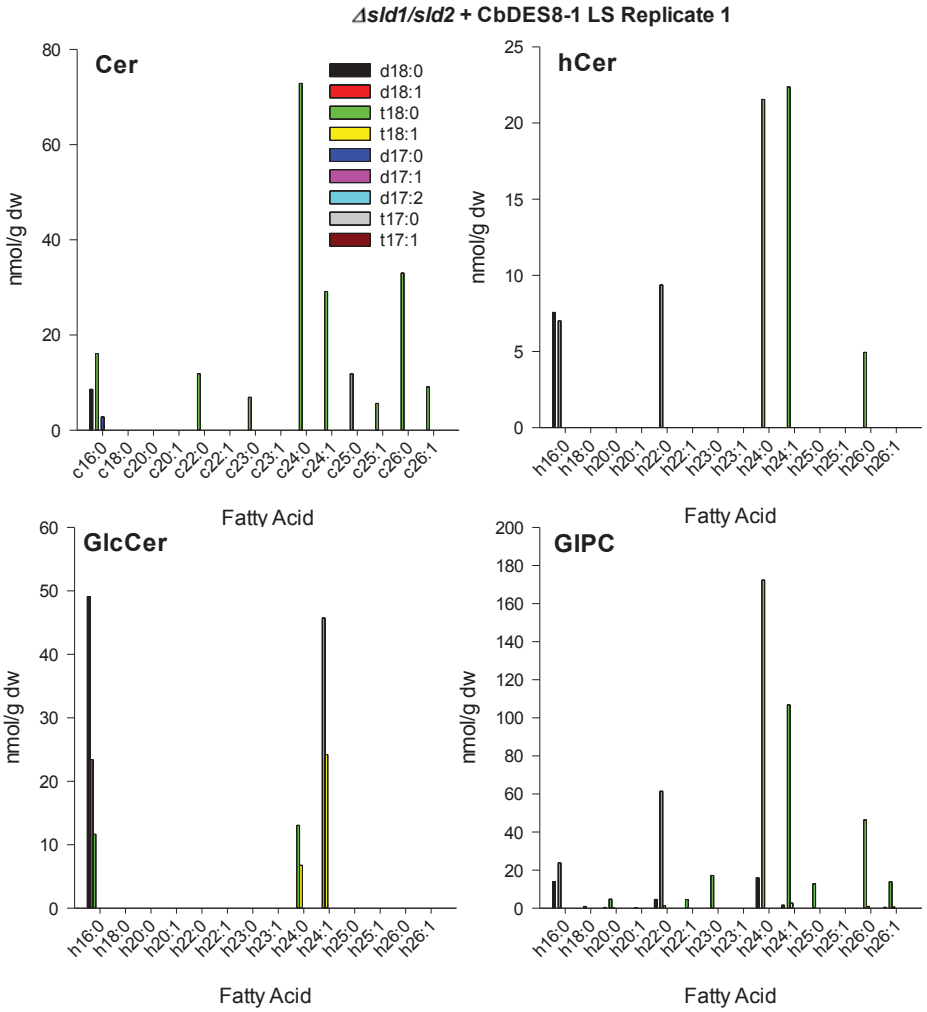
Δsld1/sld2 + CbDES8-1 LS Replicate 1
Cer
d18:0
d18:1
t18:0
t18:1
d17:0
d17:1
d17:2
t17:0
t17:1
nmol/g dw
Fatty Acid
hCer
GlcCer
GIPC

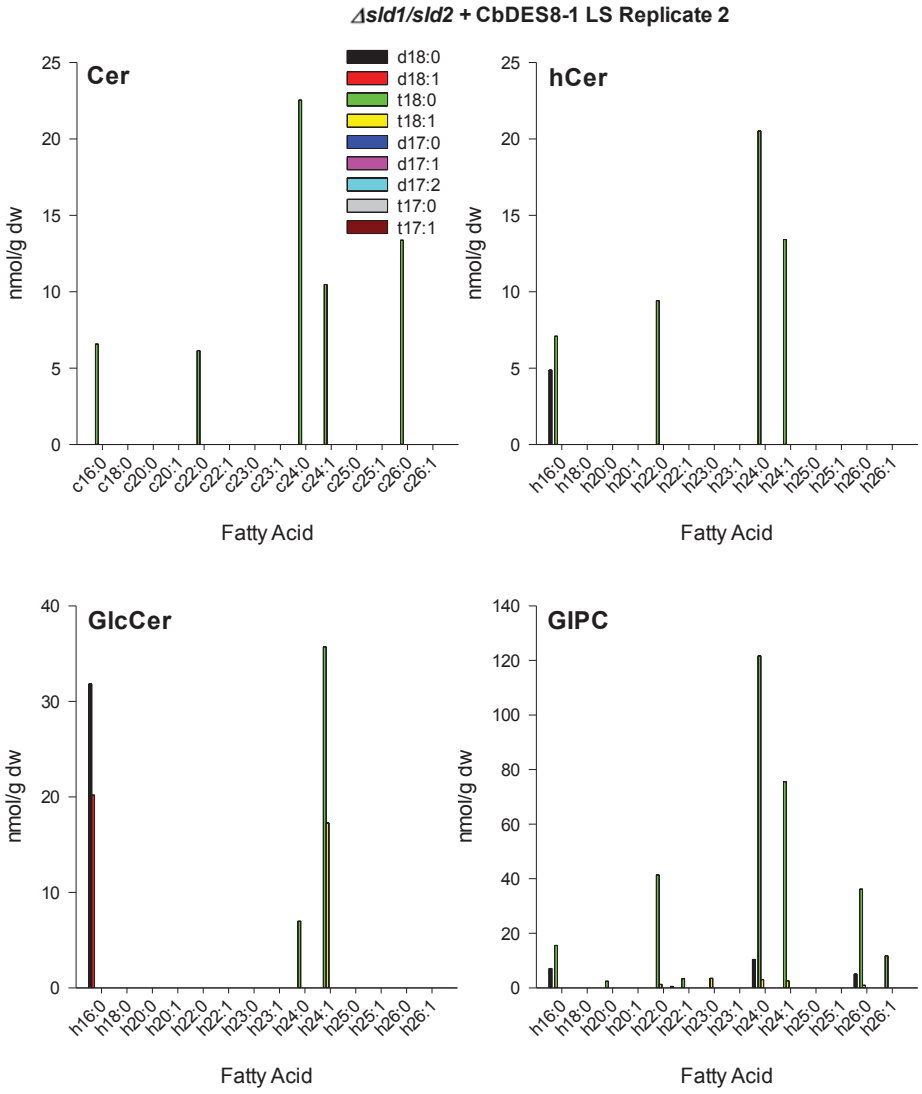
Δsld1/sld2 + CbDES8-1 LS Replicate 2
Cer
hCer
GlcCer
GIPC
nmol/g dw
Fatty Acid
d18:0
d18:1
t18:0
t18:1
d17:0
d17:1
d17:2
t17:0
t17:1
c16:0
c18:0
c20:0
c20:1
c22:0
c22:1
c23:0
c23:1
c24:0
c24:1
c25:0
c25:1
c26:0
c26:1
h16:0
h18:0
h20:0
h20:1
h22:0
h22:1
h23:0
h23:1
h24:0
h24:1
h25:0
h25:1
h26:0
h26:1

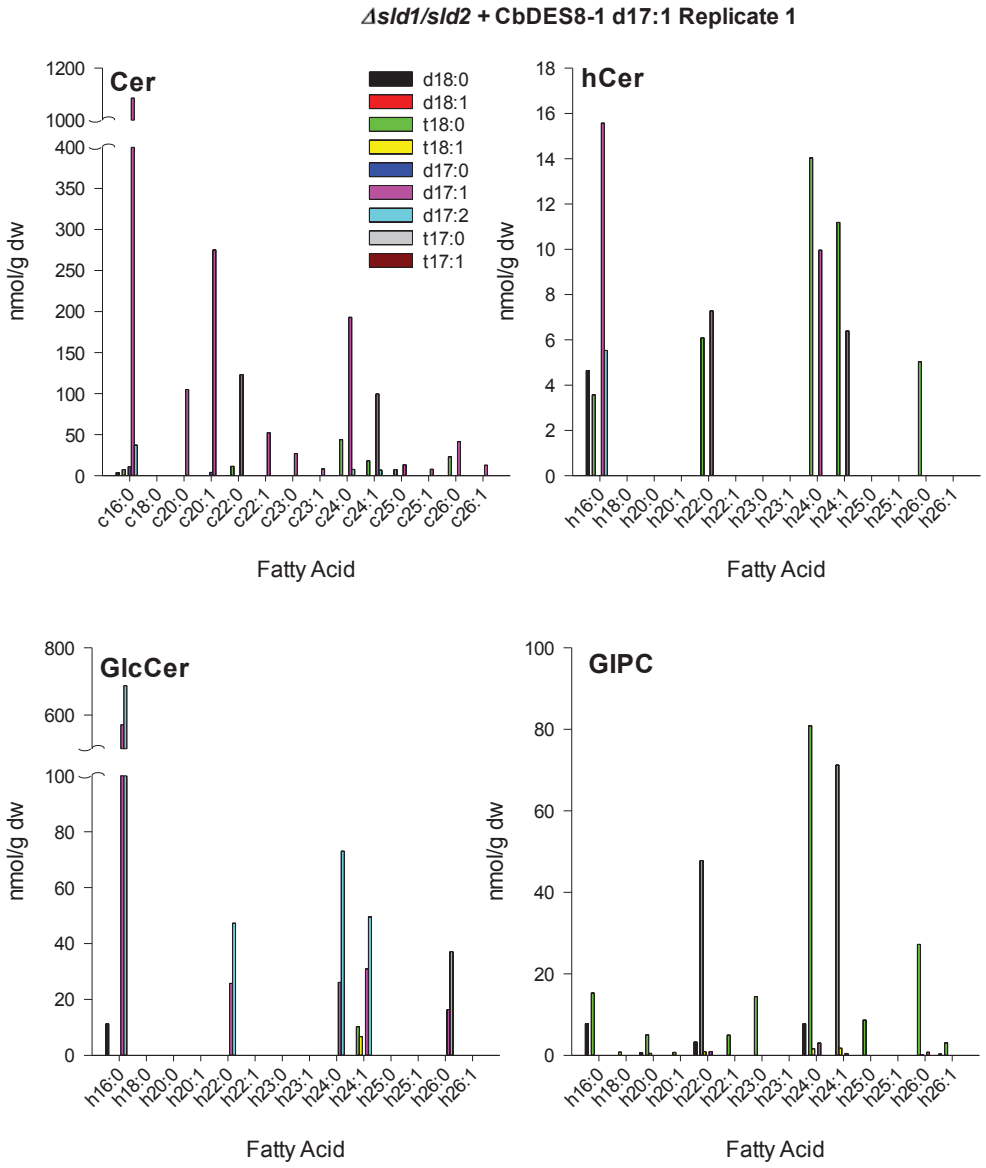
Δsld1/sld2 + CbDES8-1 d17:1 Replicate 1
Cer
hCer
GlcCer
GIPC
nmol/g dw
Fatty Acid
d18:0
d18:1
t18:0
t18:1
d17:0
d17:1
d17:2
t17:0
t17:1
c16:0 c18:0 c20:0 c20:1 c22:0 c22:1 c23:0 c23:1 c24:0 c24:1 c25:0 c25:1 c26:0 c26:1
h16:0 h18:0 h20:0 h20:1 h22:0 h22:1 h23:0 h23:1 h24:0 h24:1 h25:0 h25:1 h26:0 h26:1

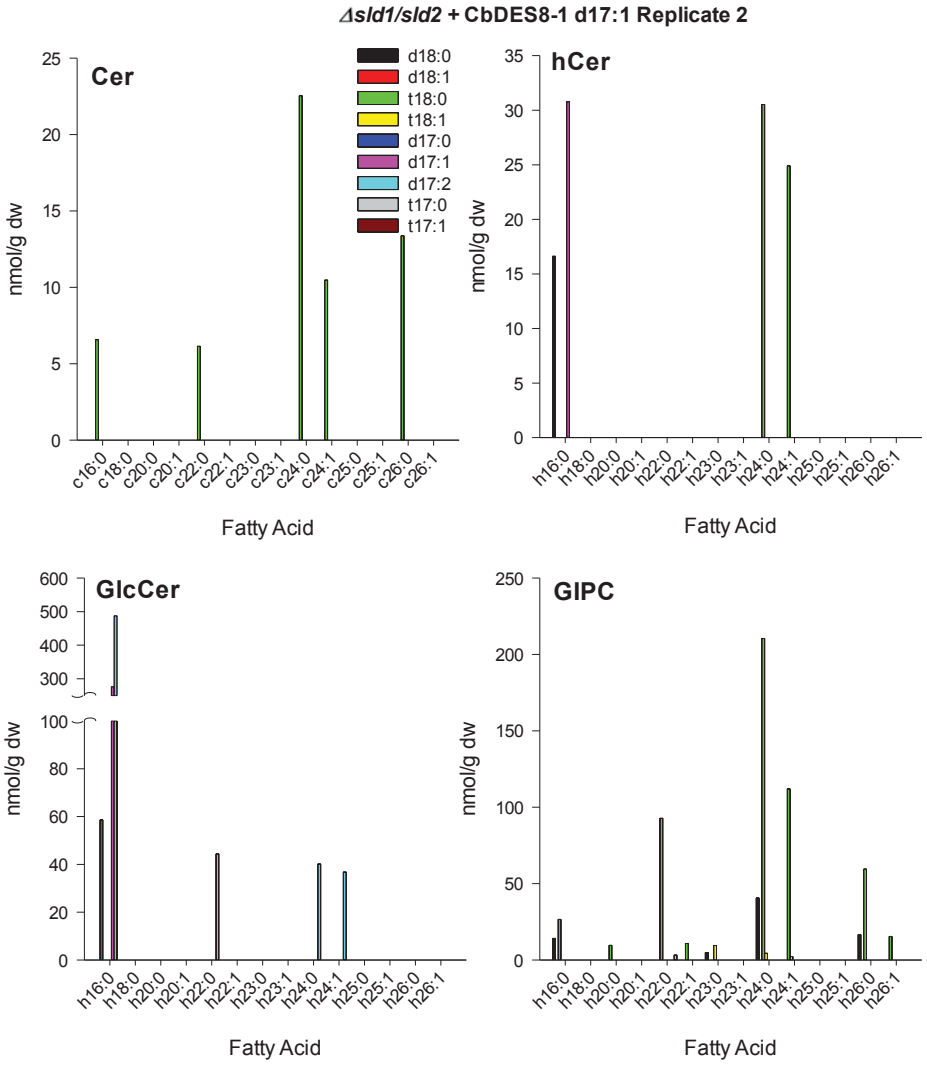
Δsld1/sld2 + CbDES8-1 d17:1 Replicate 2
Cer
hCer
GlcCer
GIPC
d18:0
d18:1
t18:0
t18:1
d17:0
d17:1
d17:2
t17:0
t17:1
nmol/g dw
Fatty Acid
c16:0
c18:0
c20:0
c20:1
c22:0
c22:1
c23:0
c23:1
c24:0
c24:1
c25:0
c25:1
c26:0
c26:1
h16:0
h18:0
h20:0
h20:1
h22:0
h22:1
h23:0
h23:1
h24:0
h24:1
h25:0
h25:1
h26:0
h26:1

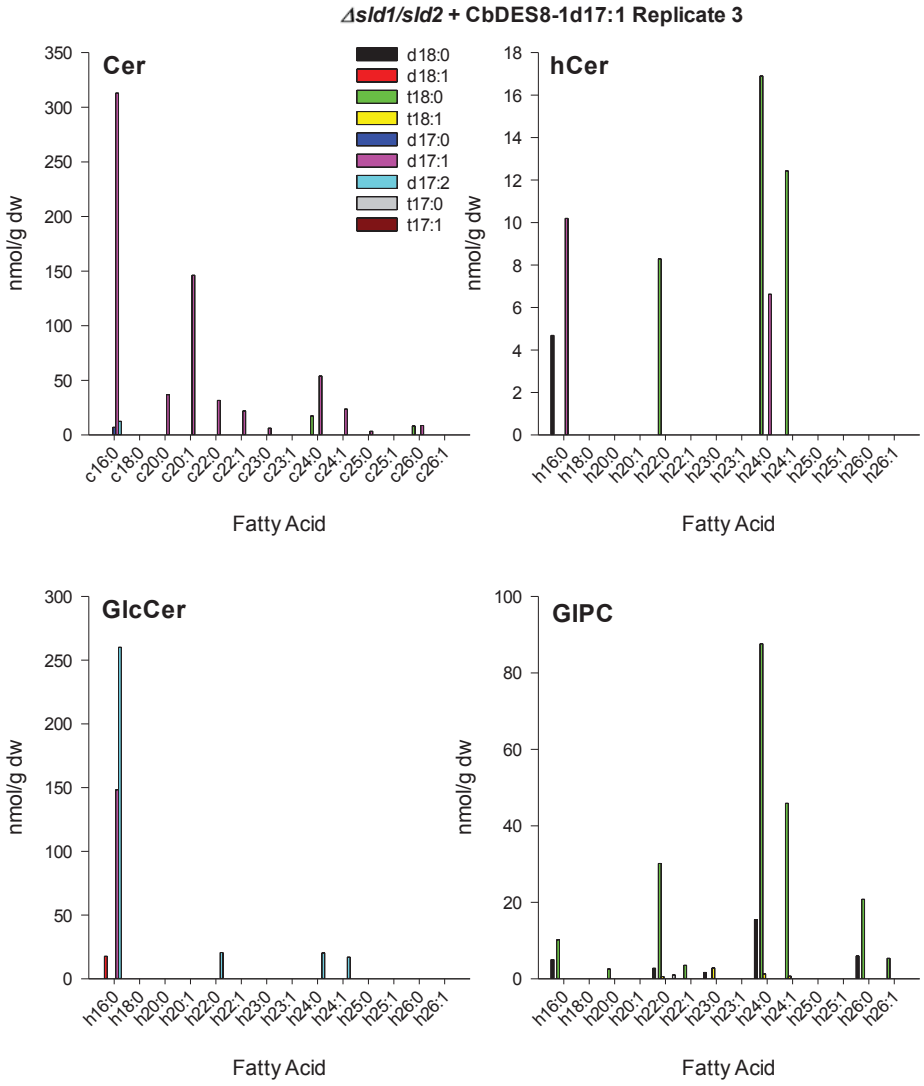
Δsld1/sld2 + CbDES8-1d17:1 Replicate 3
Cer
d18:0
d18:1
t18:0
t18:1
d17:0
d17:1
d17:2
t17:0
t17:1
nmol/g dw
Fatty Acid
c16:0
c18:0
c20:0
c20:1
c22:0
c22:1
c23:0
c23:1
c24:0
c24:1
c25:0
c25:1
c26:0
c26:1
hCer
h16:0
h18:0
h20:0
h20:1
h22:0
h22:1
h23:0
h23:1
h24:0
h24:1
h25:0
h25:1
h26:0
h26:1
GlcCer
GIPC

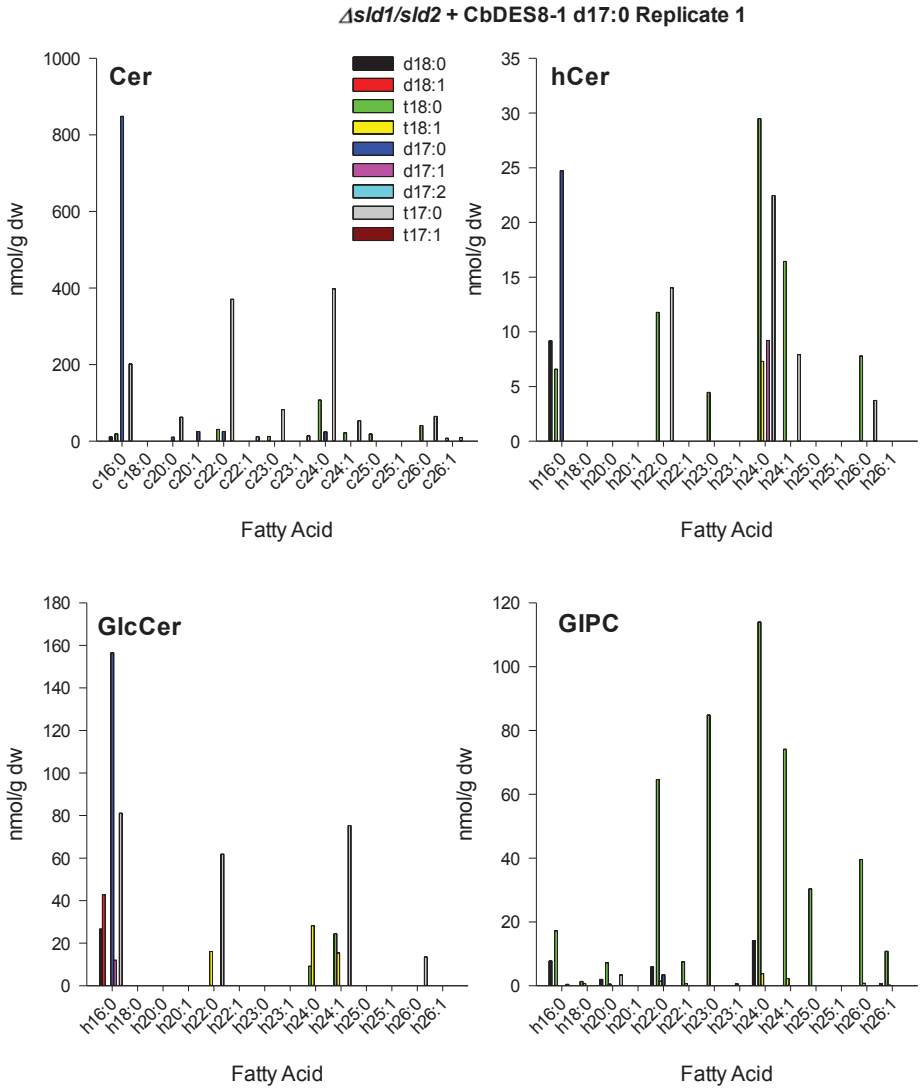
Δsld1/sld2 + CbDES8-1 d17:0 Replicate 1
Cer
d18:0
d18:1
t18:0
t18:1
d17:0
d17:1
d17:2
t17:0
t17:1
nmol/g dw
Fatty Acid
hCer
GlcCer
GIPC

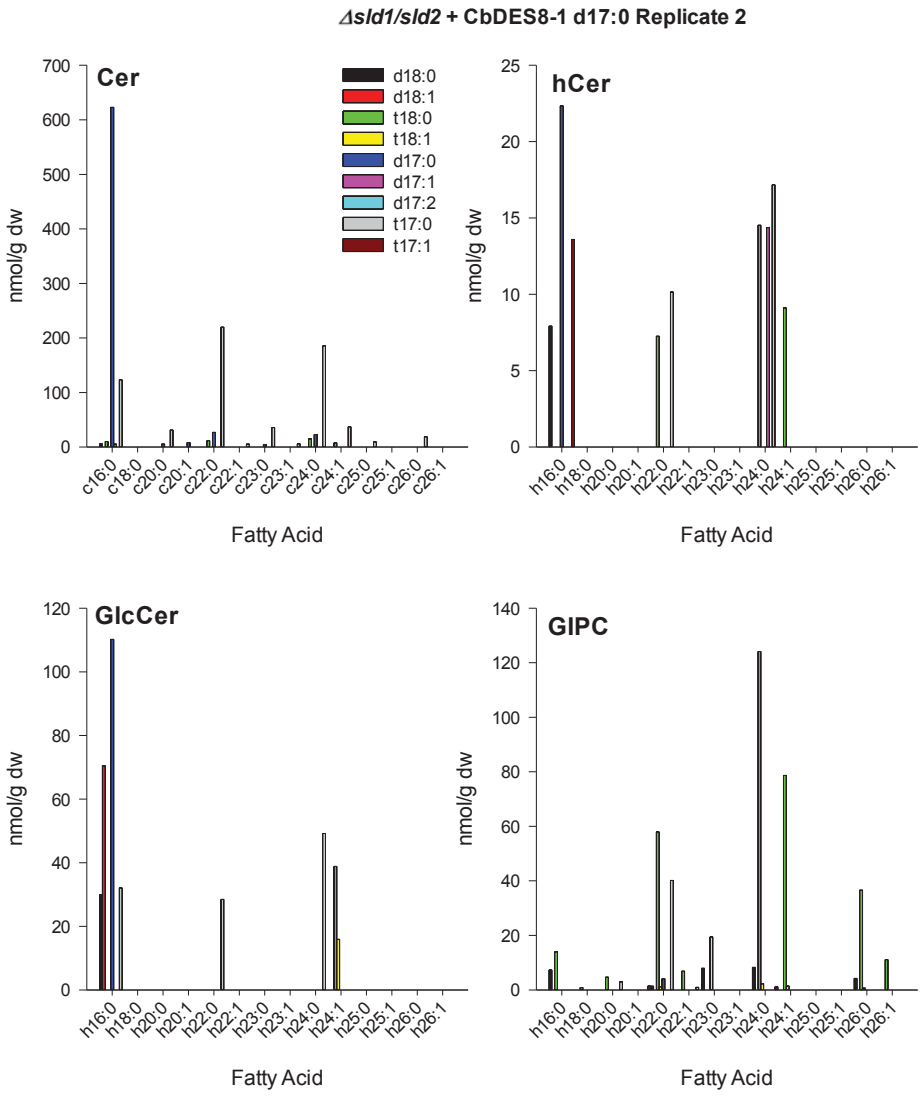
Δsld1/sld2 + CbDES8-1 d17:0 Replicate 2
Cer
d18:0
d18:1
t18:0
t18:1
d17:0
d17:1
d17:2
t17:0
t17:1
nmol/g dw
Fatty Acid
hCer
GlcCer
GIPC

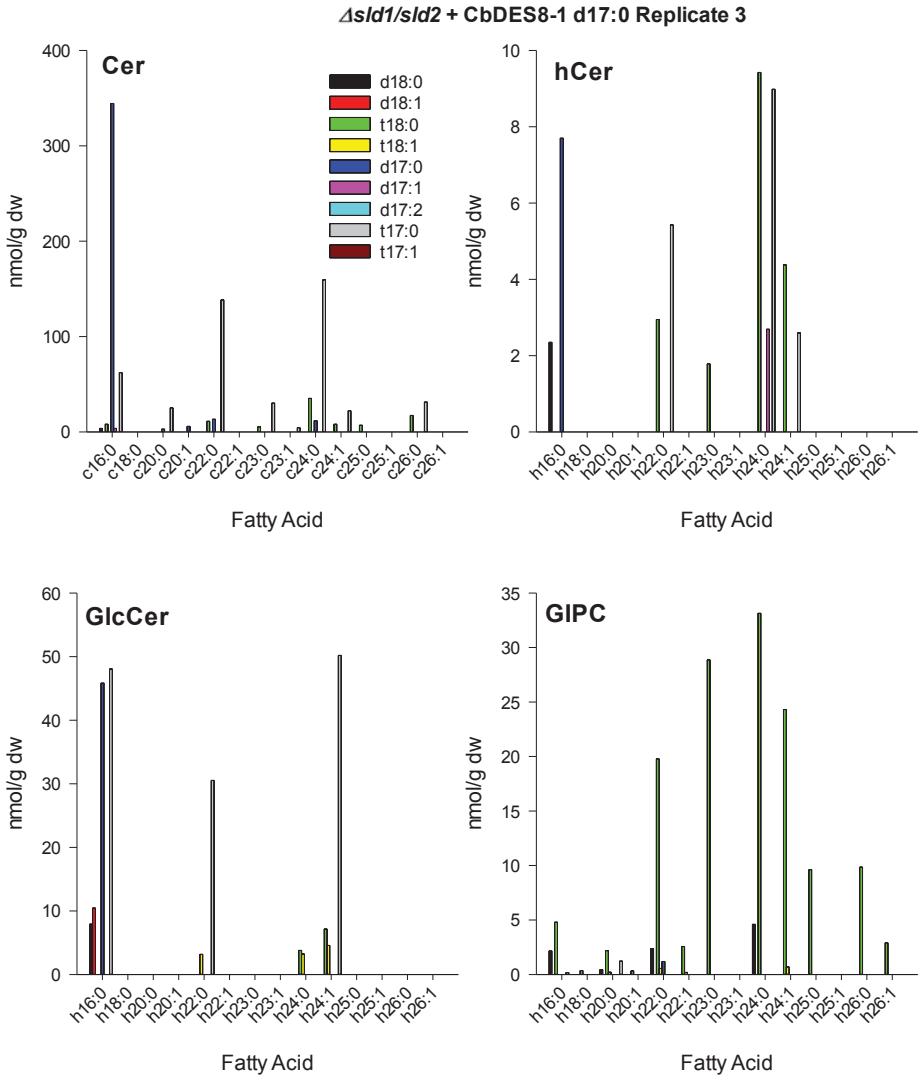
Δsld1/sld2 + CbDES8-1 d17:0 Replicate 3
Cer
d18:0
d18:1
t18:0
t18:1
d17:0
d17:1
d17:2
t17:0
t17:1
nmol/g dw
Fatty Acid
hCer
GlcCer
GIPC

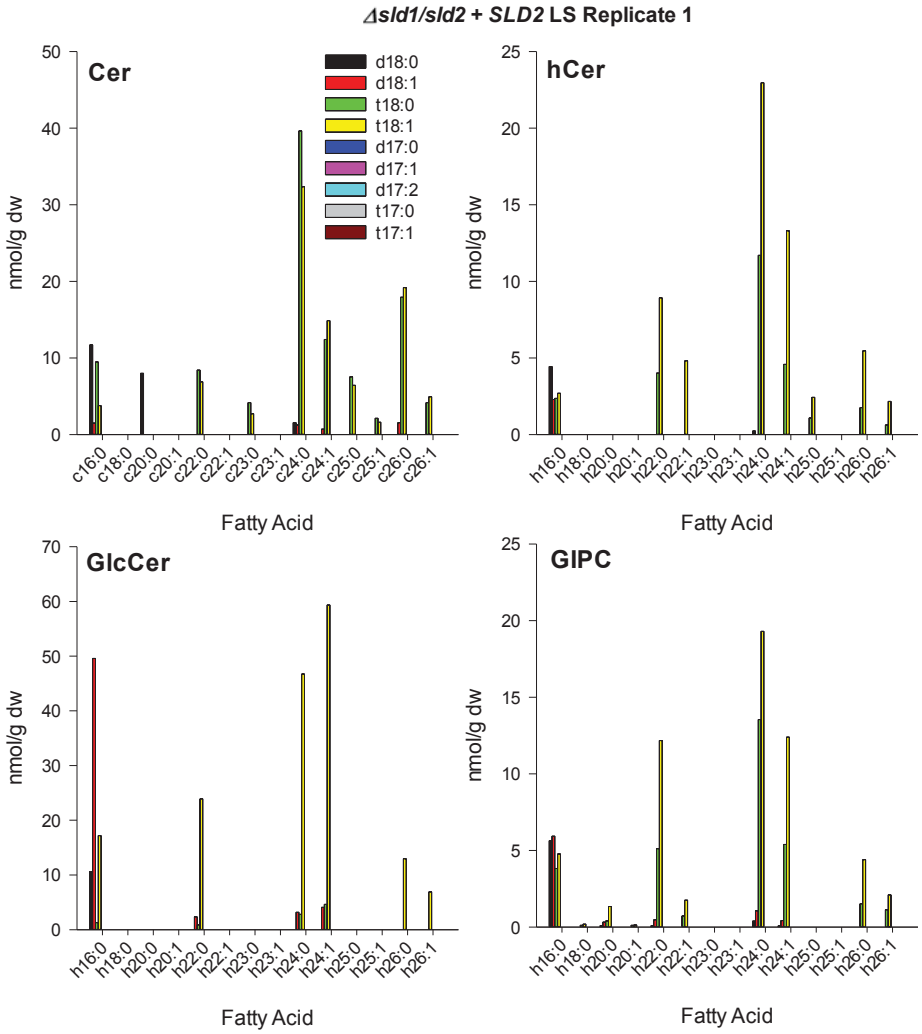
Δsld1/sld2 + SLD2 LS Replicate 1
Cer
d18:0
d18:1
t18:0
t18:1
d17:0
d17:1
d17:2
t17:0
t17:1
nmol/g dw
Fatty Acid
c16:0
c18:0
c20:0
c20:1
c22:0
c22:1
c23:0
c23:1
c24:0
c24:1
c25:0
c25:1
c26:0
c26:1
hCer
h16:0
h18:0
h20:0
h20:1
h22:0
h22:1
h23:0
h23:1
h24:0
h24:1
h25:0
h25:1
h26:0
h26:1
GlcCer
GIPC

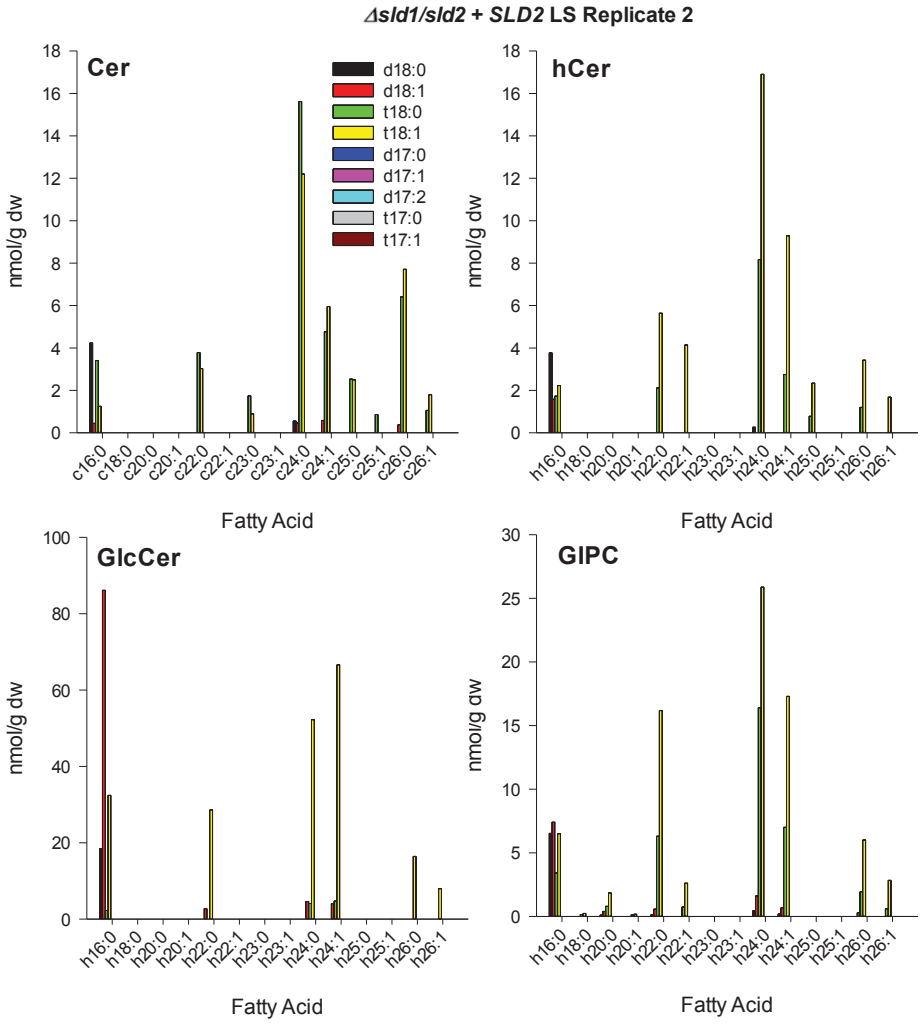
Δsld1/sld2 + SLD2 LS Replicate 2
Cer
d18:0
d18:1
t18:0
t18:1
d17:0
d17:1
d17:2
t17:0
t17:1
nmol/g dw
Fatty Acid
hCer
GlcCer
GIPC

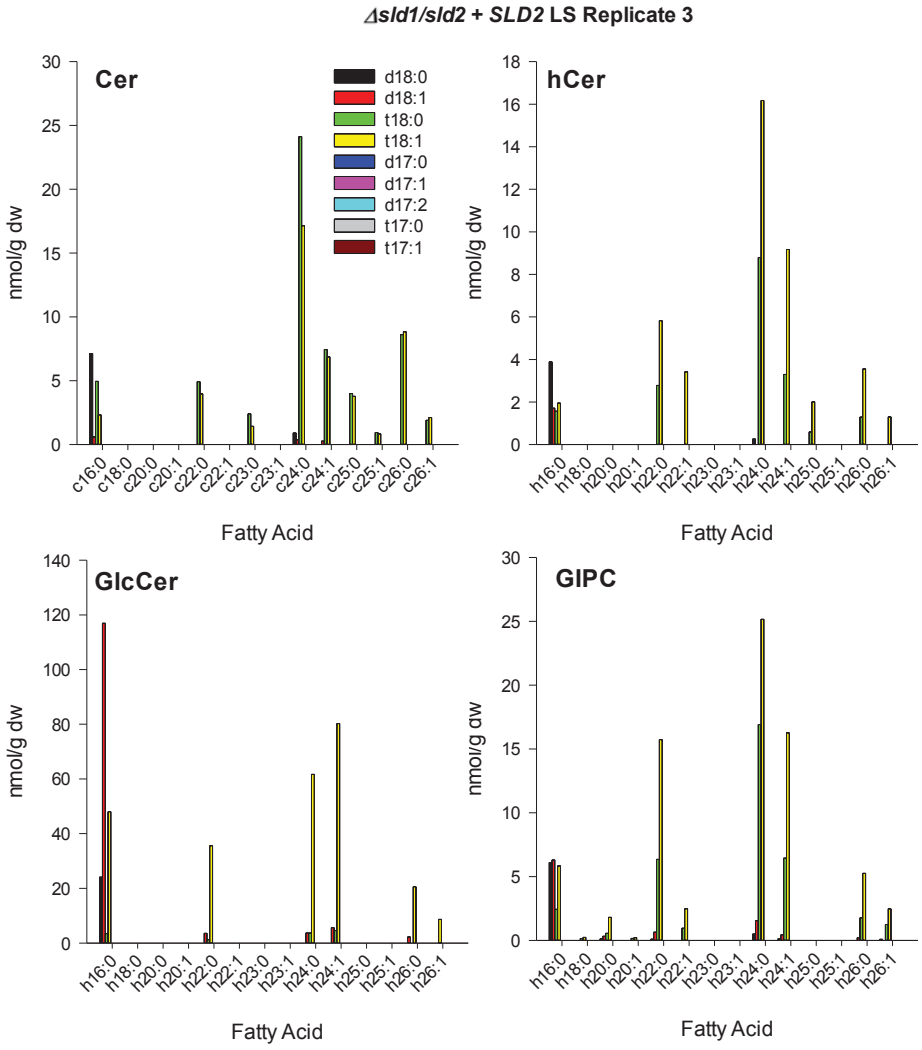
Δsld1/sld2 + SLD2 LS Replicate 3
Cer
d18:0
d18:1
t18:0
t18:1
d17:0
d17:1
d17:2
t17:0
t17:1
nmol/g dw
Fatty Acid
hCer
GlcCer
GIPC

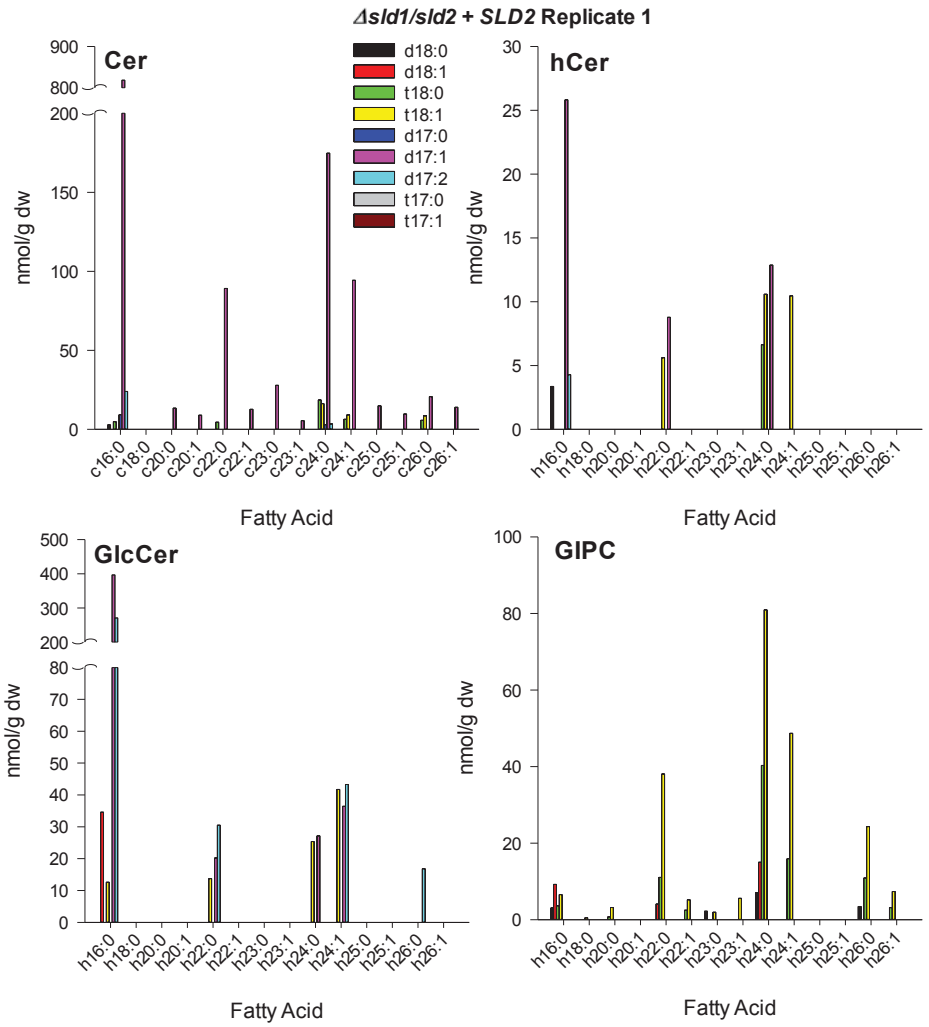
Δsld1/sld2 + SLD2 Replicate 1
Cer
hCer
GlcCer
GIPC
d18:0
d18:1
t18:0
t18:1
d17:0
d17:1
d17:2
t17:0
t17:1
nmol/g dw
Fatty Acid
c16:0 c18:0 c20:0 c20:1 c22:0 c22:1 c23:0 c23:1 c24:0 c24:1 c25:0 c25:1 c26:0 c26:1
h16:0 h18:0 h20:0 h20:1 h22:0 h22:1 h23:0 h23:1 h24:0 h24:1 h25:0 h25:1 h26:0 h26:1

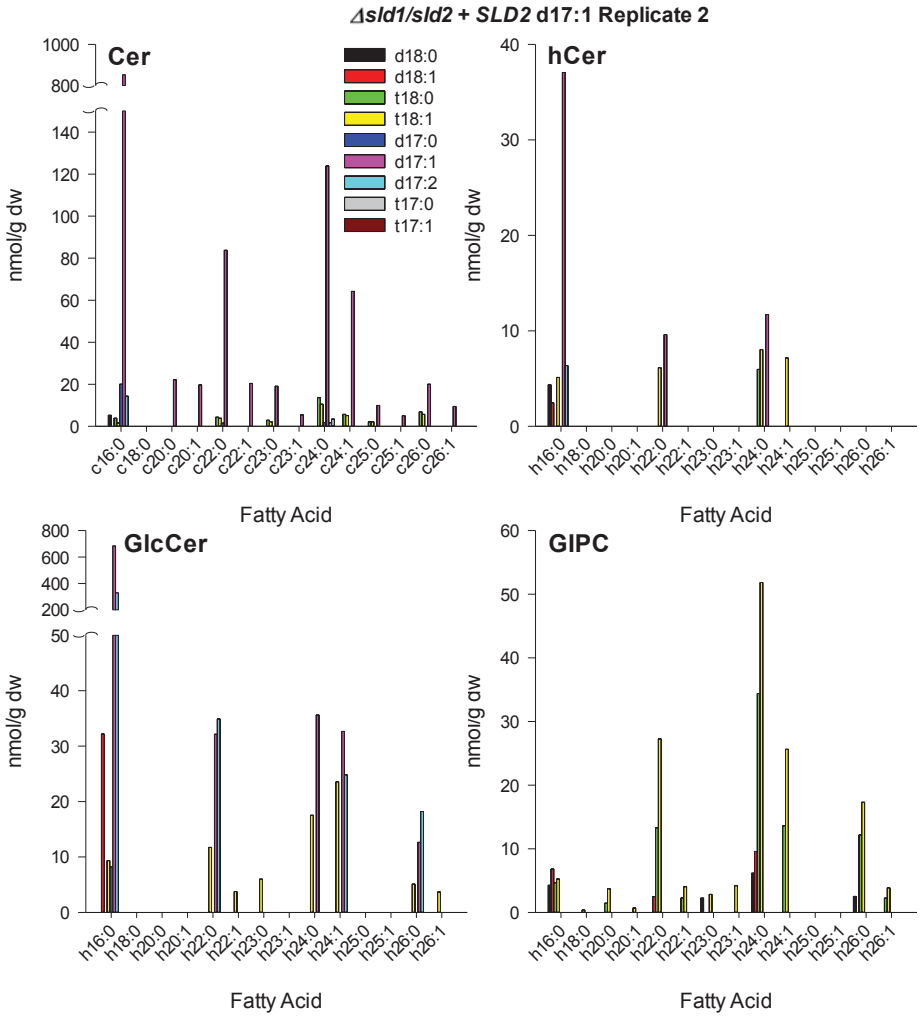
Δsld1/sld2 + SLD2 d17:1 Replicate 2
Cer
d18:0
d18:1
t18:0
t18:1
d17:0
d17:1
d17:2
t17:0
t17:1
nmol/g dw
Fatty Acid
hCer
GlcCer
GIPC

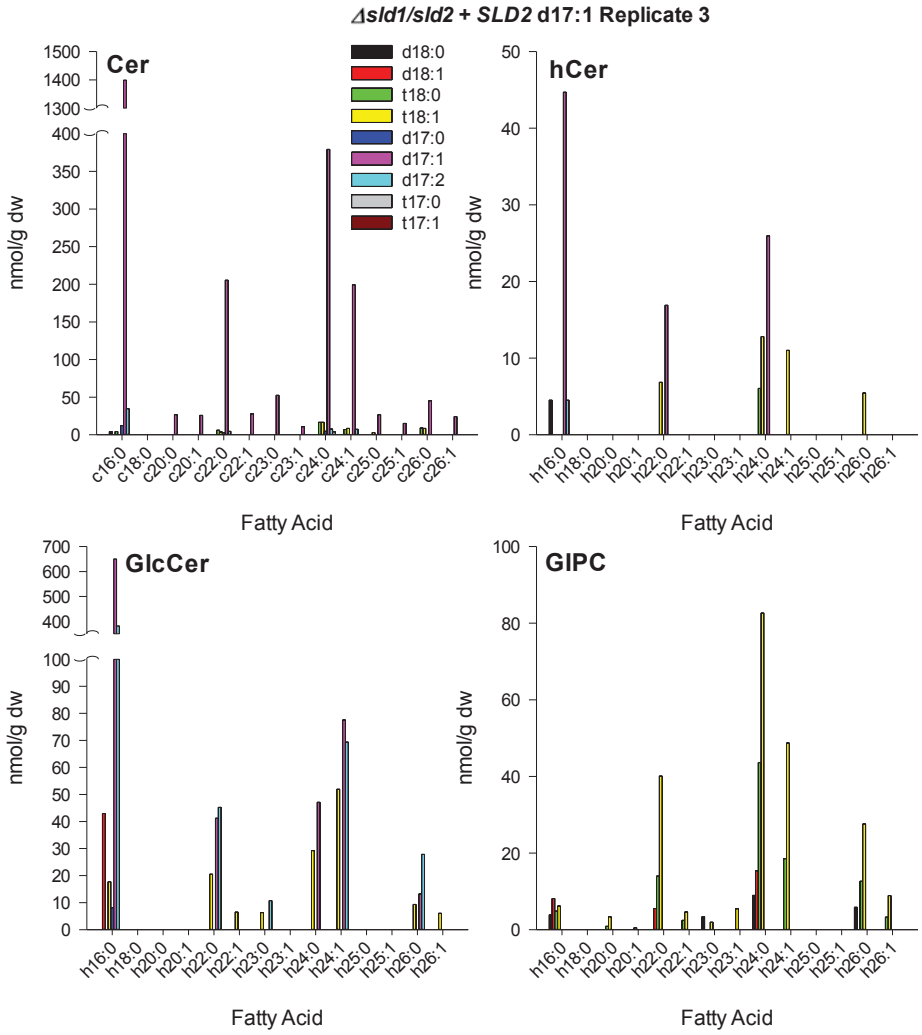
Δsld1/sld2 + SLD2 d17:1 Replicate 3
Cer
hCer
GlcCer
GIPC
d18:0
d18:1
t18:0
t18:1
d17:0
d17:1
d17:2
t17:0
t17:1
nmol/g dw
Fatty Acid
c16:0
c18:0
c20:0
c20:1
c22:0
c22:1
c23:0
c23:1
c24:0
c24:1
c25:0
c25:1
c26:0
c26:1
h16:0
h18:0
h20:0
h20:1
h22:0
h22:1
h23:0
h23:1
h24:0
h24:1
h25:0
h25:1
h26:0
h26:1

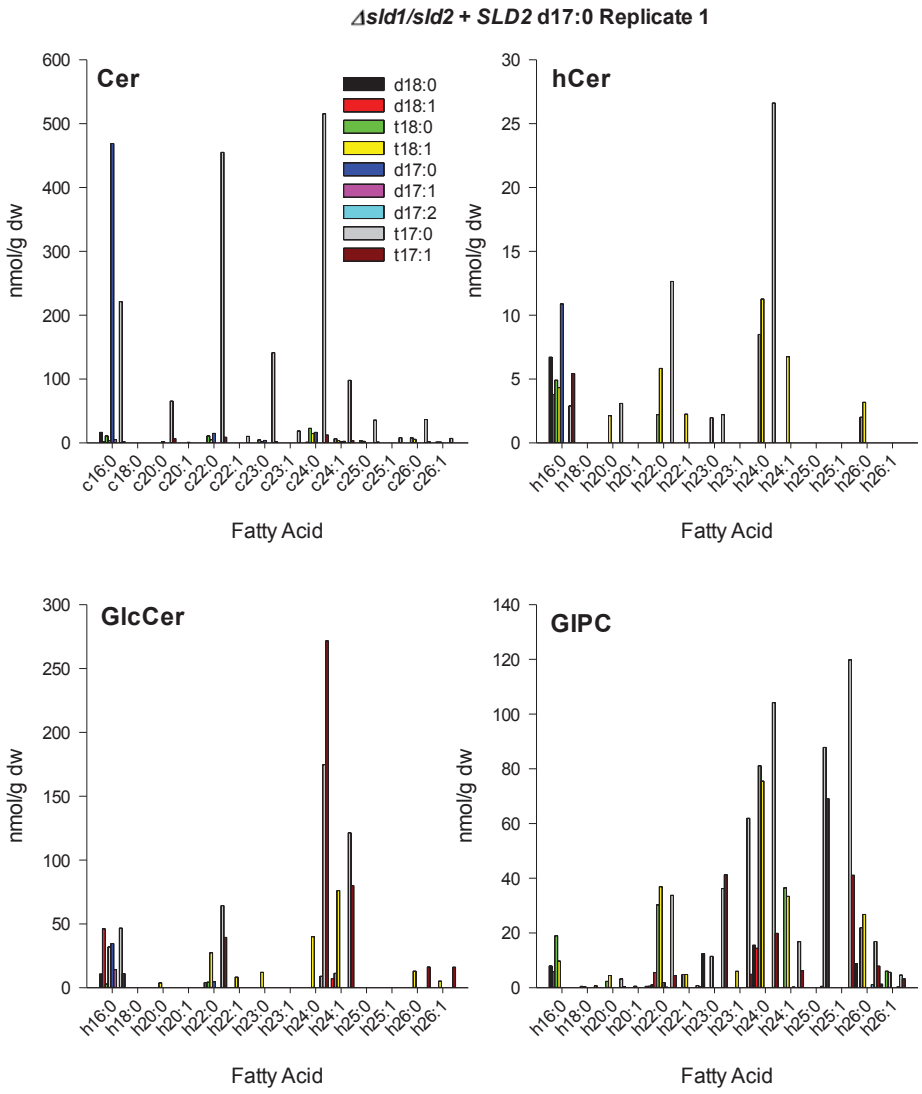
Δsld1/sld2 + SLD2 d17:0 Replicate 1
Cer
d18:0
d18:1
t18:0
t18:1
d17:0
d17:1
d17:2
t17:0
t17:1
nmol/g dw
Fatty Acid
hCer
GlcCer
GIPC

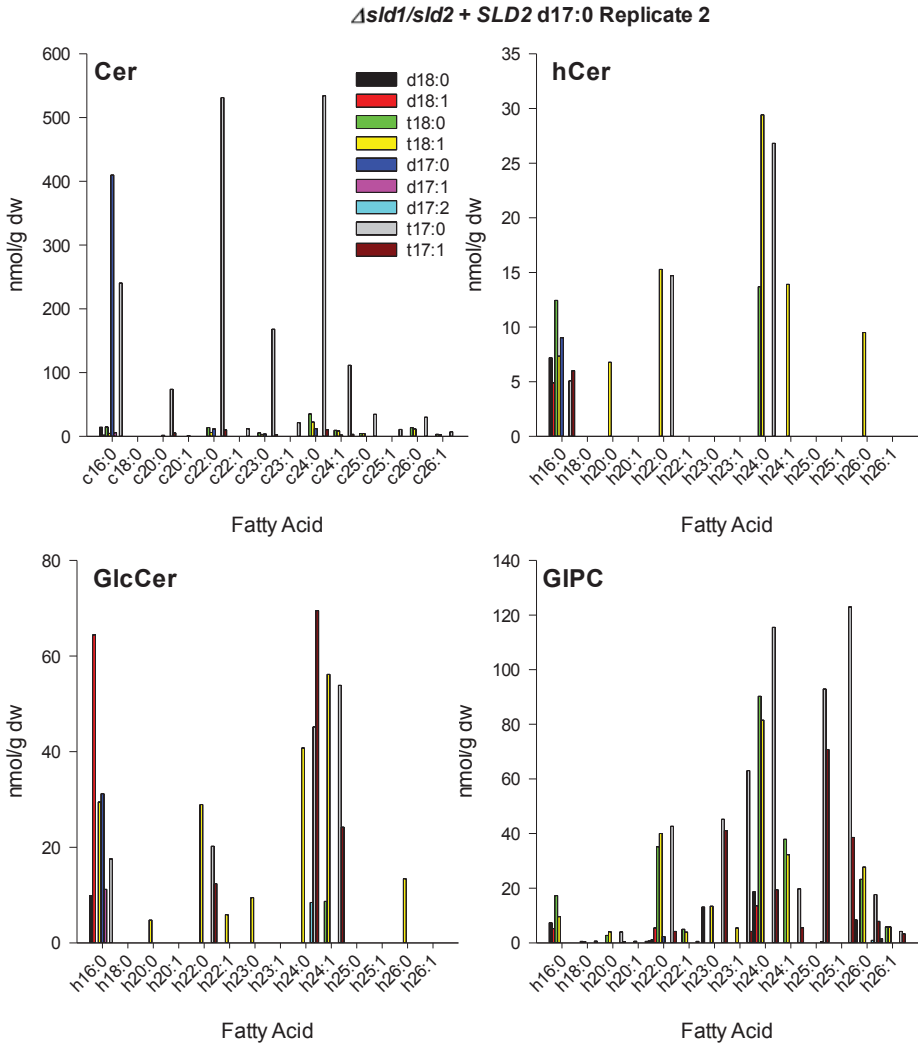
Δsld1/sld2 + SLD2 d17:0 Replicate 2
Cer
d18:0
d18:1
t18:0
t18:1
d17:0
d17:1
d17:2
t17:0
t17:1
nmol/g dw
Fatty Acid
hCer
GlcCer
GIPC

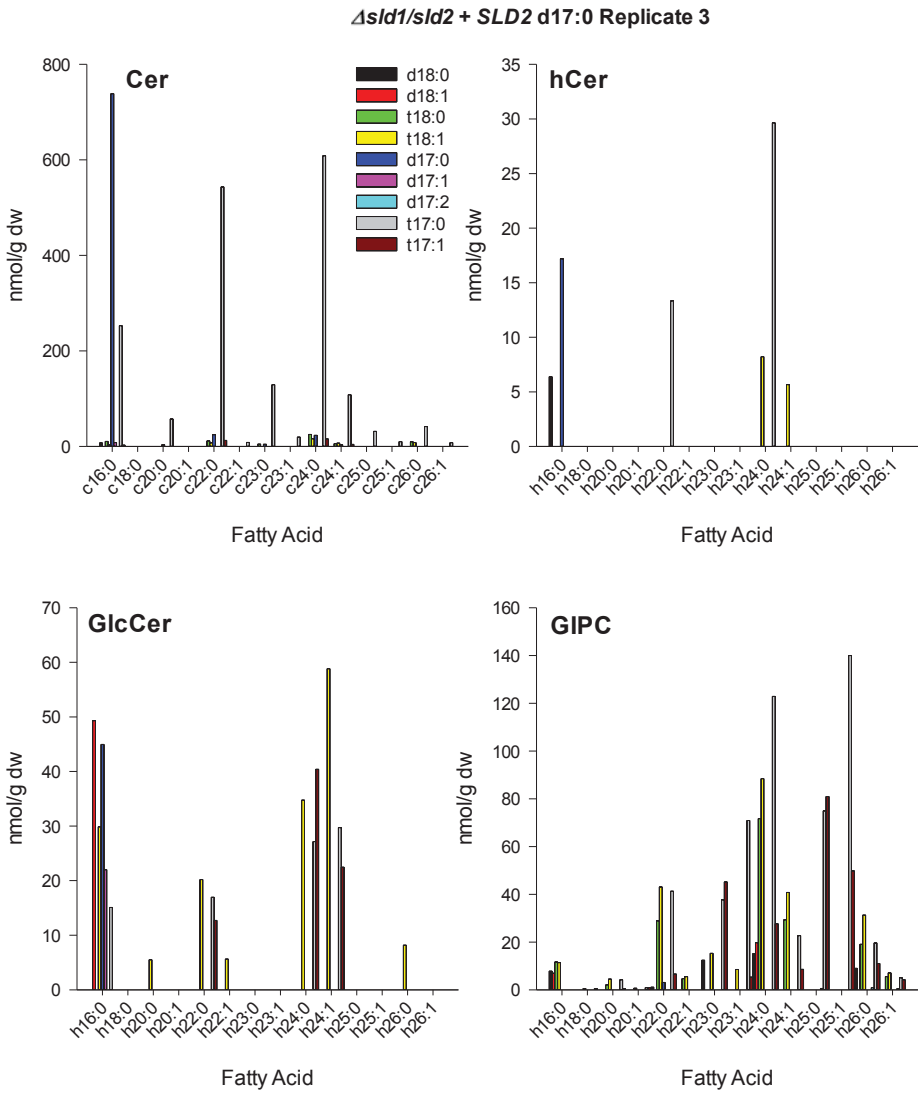
Δsld1/sld2 + SLD2 d17:0 Replicate 3
Cer
d18:0
d18:1
t18:0
t18:1
d17:0
d17:1
d17:2
t17:0
t17:1
nmol/g dw
Fatty Acid
hCer
GlcCer
GIPC

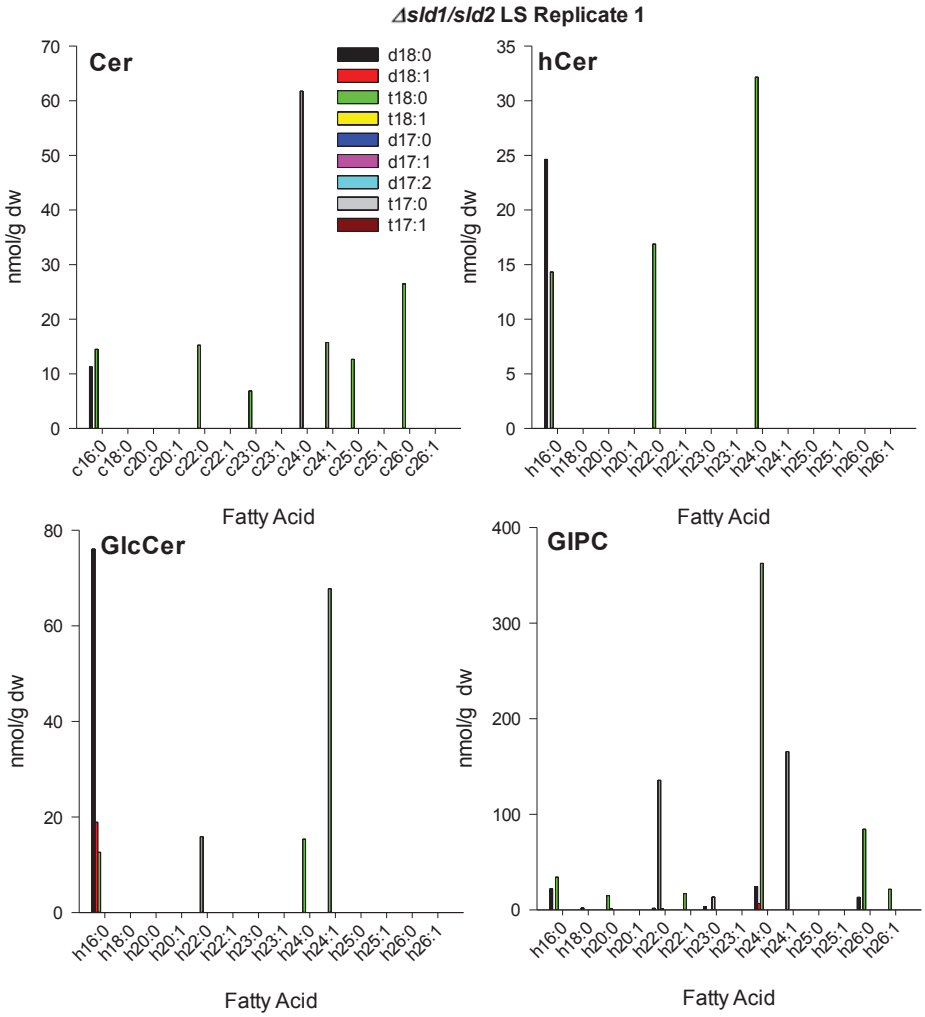
Δsld1/sld2 LS Replicate 1
Cer
d18:0
d18:1
t18:0
t18:1
d17:0
d17:1
d17:2
t17:0
t17:1
nmol/g dw
Fatty Acid
hCer
GlcCer
GIPC

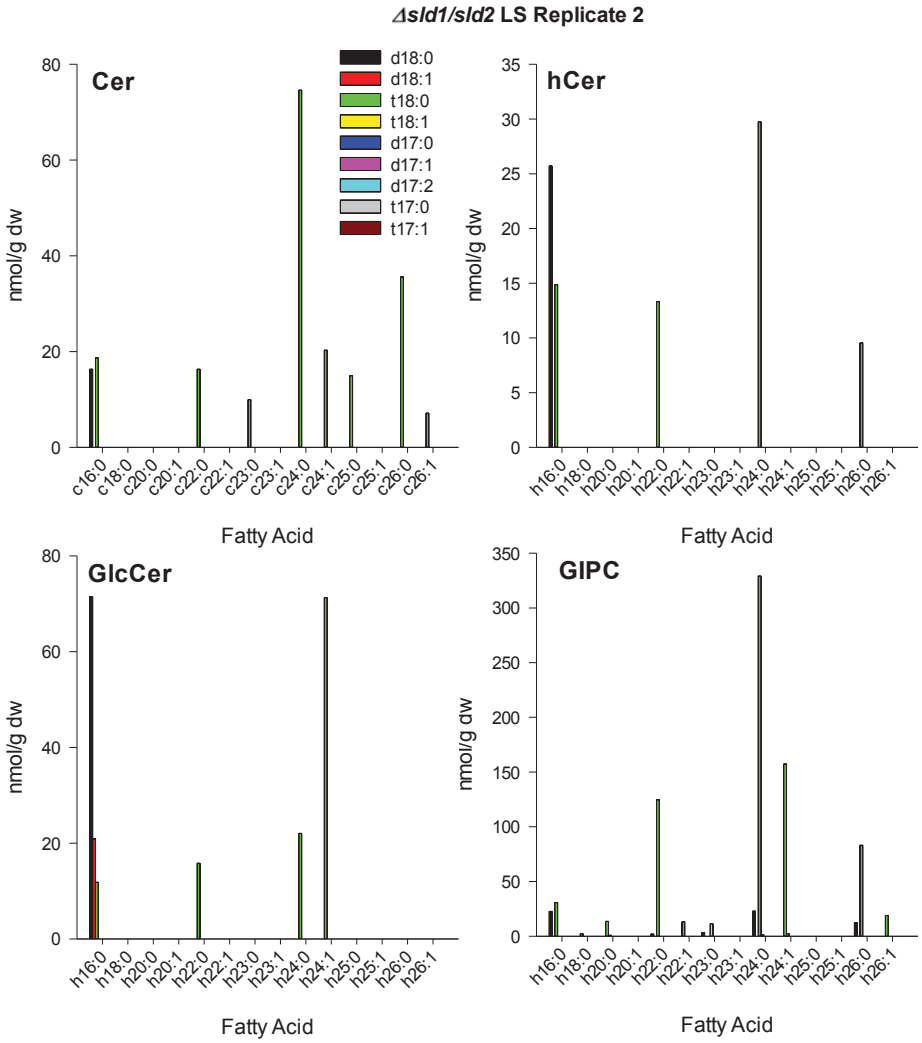
Δsld1/sld2 LS Replicate 2
Cer
hCer
GlcCer
GIPC
d18:0
d18:1
t18:0
t18:1
d17:0
d17:1
d17:2
t17:0
t17:1
nmol/g dw
Fatty Acid
c16:0
c18:0
c20:0
c20:1
c22:0
c22:1
c23:0
c23:1
c24:0
c24:1
c25:0
c25:1
c26:0
c26:1
h16:0
h18:0
h20:0
h20:1
h22:0
h22:1
h23:0
h23:1
h24:0
h24:1
h25:0
h25:1
h26:0
h26:1

***Δsld1/sld2* LS Replicate 3**

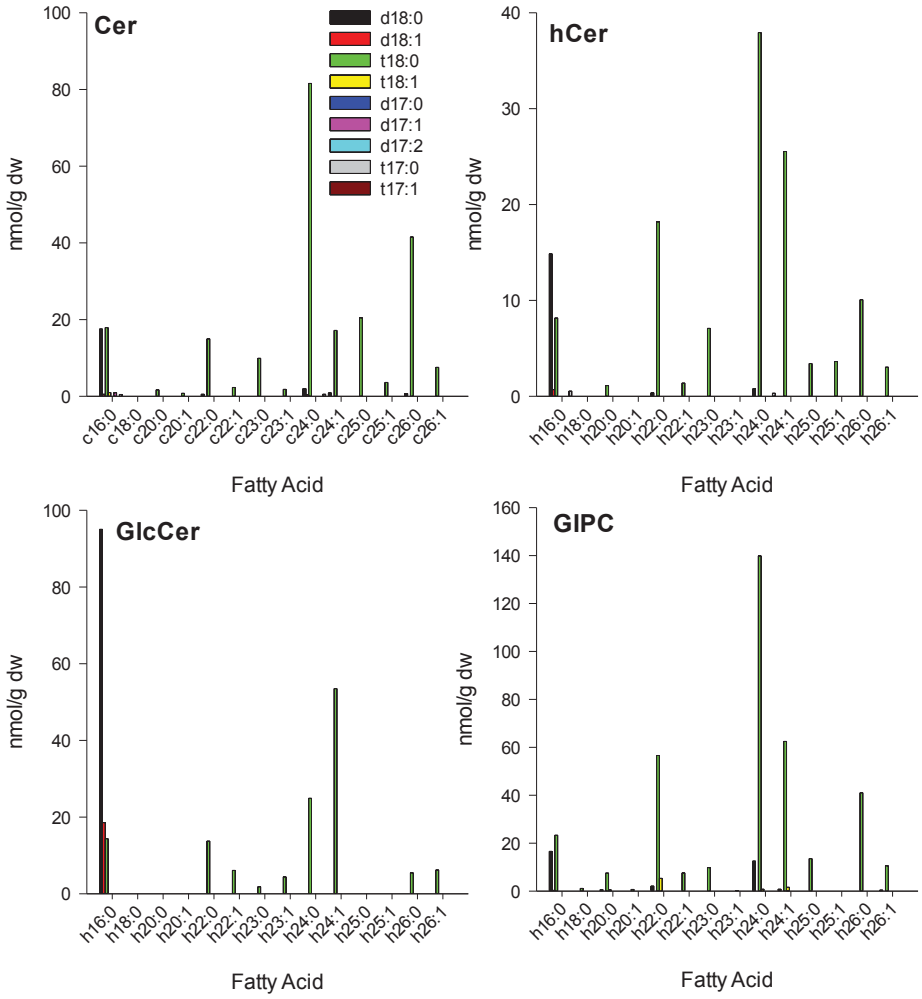

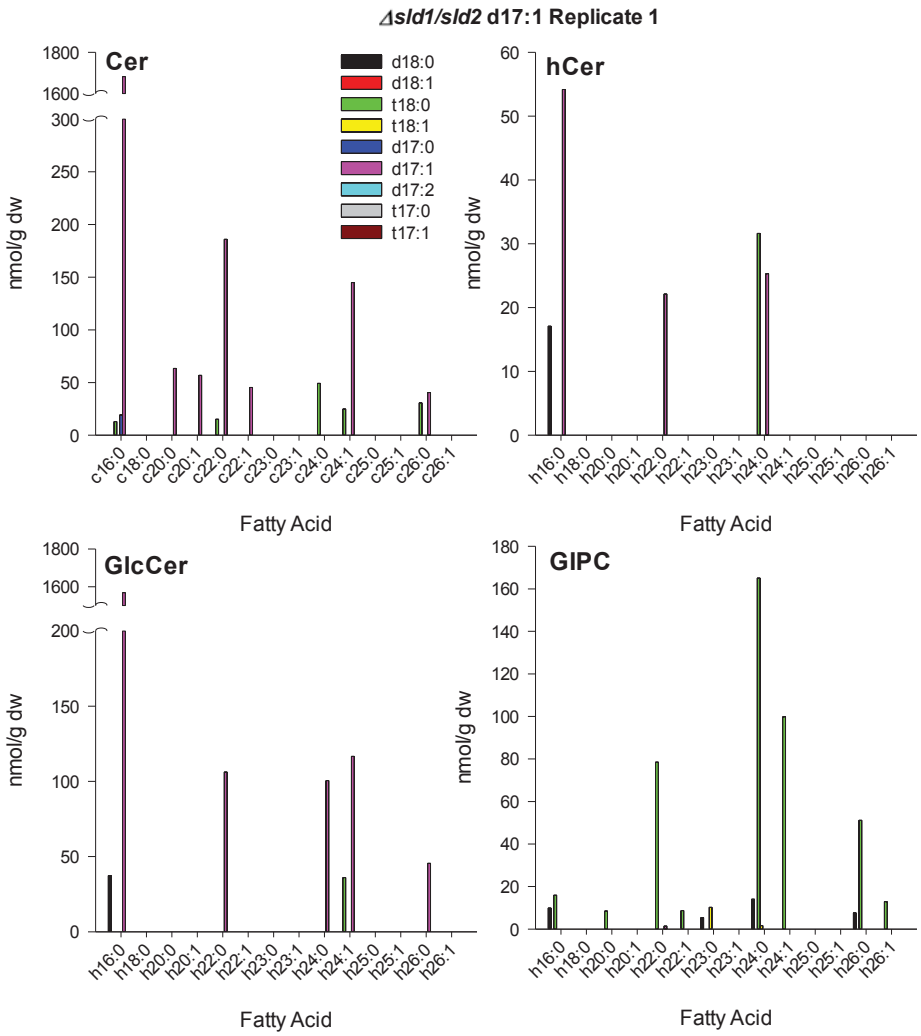
Δsld1/sld2 d17:1 Replicate 1
Cer
hCer
GlcCer
GlPC
d18:0
d18:1
t18:0
t18:1
d17:0
d17:1
d17:2
t17:0
t17:1
nmol/g dw
Fatty Acid
c16:0
c18:0
c20:0
c20:1
c22:0
c22:1
c23:0
c23:1
c24:0
c24:1
c25:0
c25:1
c26:0
c26:1
h16:0
h18:0
h20:0
h20:1
h22:0
h22:1
h23:0
h23:1
h24:0
h24:1
h25:0
h25:1
h26:0
h26:1

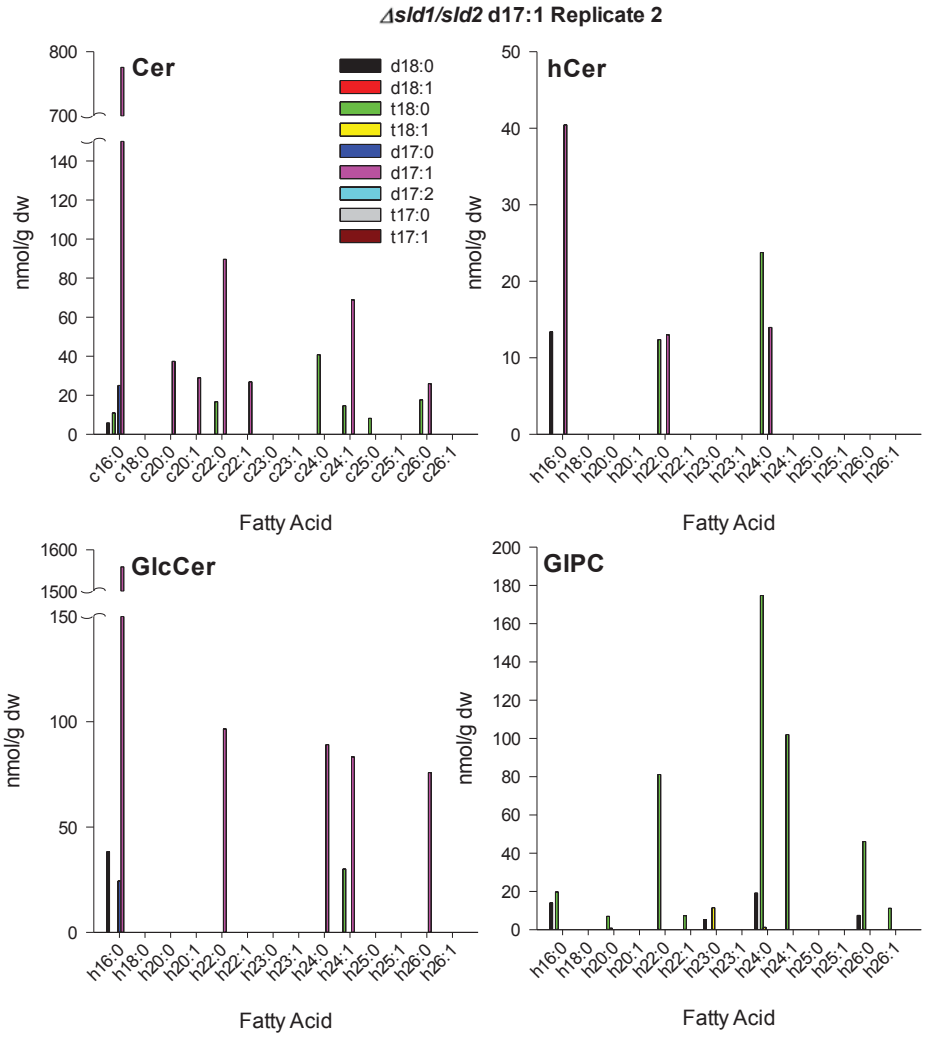
Δsld1/sld2 d17:1 Replicate 2
Cer
hCer
GlcCer
GIPC
d18:0
d18:1
t18:0
t18:1
d17:0
d17:1
d17:2
t17:0
t17:1
nmol/g dw
Fatty Acid
c16:0
c18:0
c20:0
c20:1
c22:0
c22:1
c23:0
c23:1
c24:0
c24:1
c25:0
c25:1
c26:0
c26:1
h16:0
h18:0
h20:0
h20:1
h22:0
h22:1
h23:0
h23:1
h24:0
h24:1
h25:0
h25:1
h26:0
h26:1

***Δsld1/sld2* d17:1 Replicate 3**

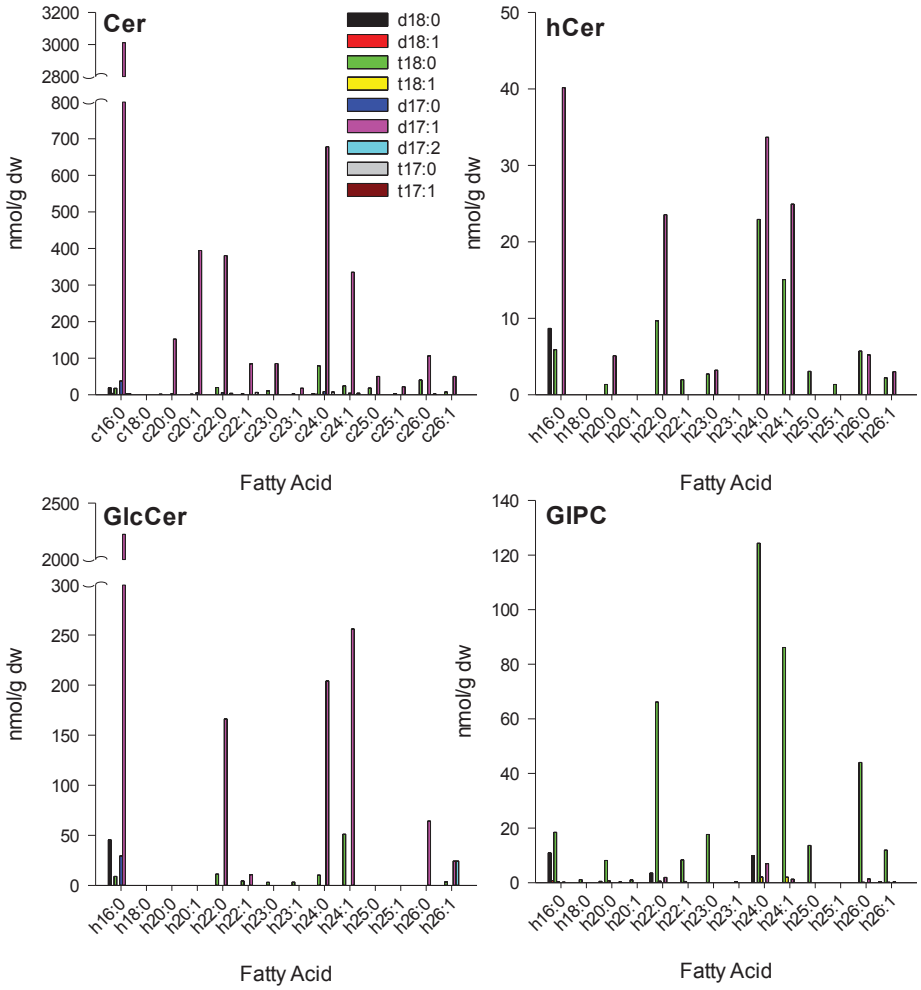

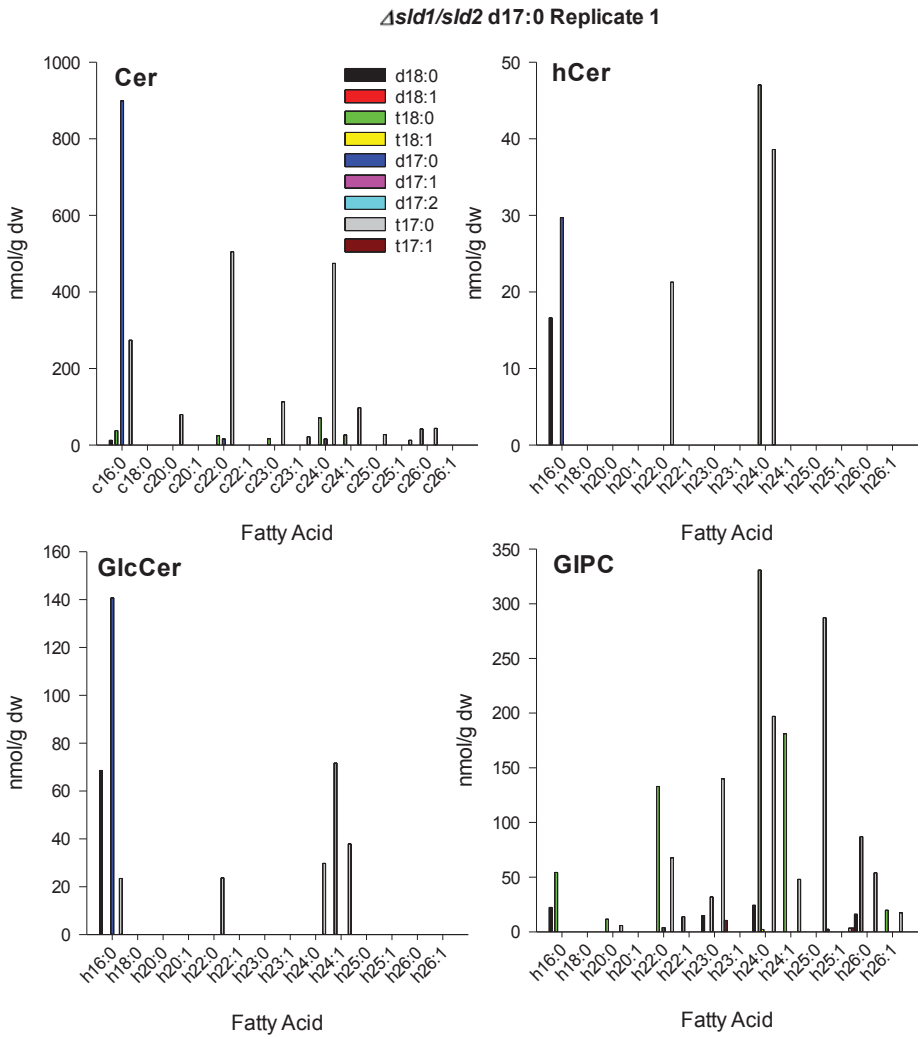
Δsld1/sld2 d17:0 Replicate 1
Cer
d18:0
d18:1
t18:0
t18:1
d17:0
d17:1
d17:2
t17:0
t17:1
nmol/g dw
Fatty Acid
hCer
GlcCer
GIPC

***Δsld1/sld2* d17:0 Replicate 2**

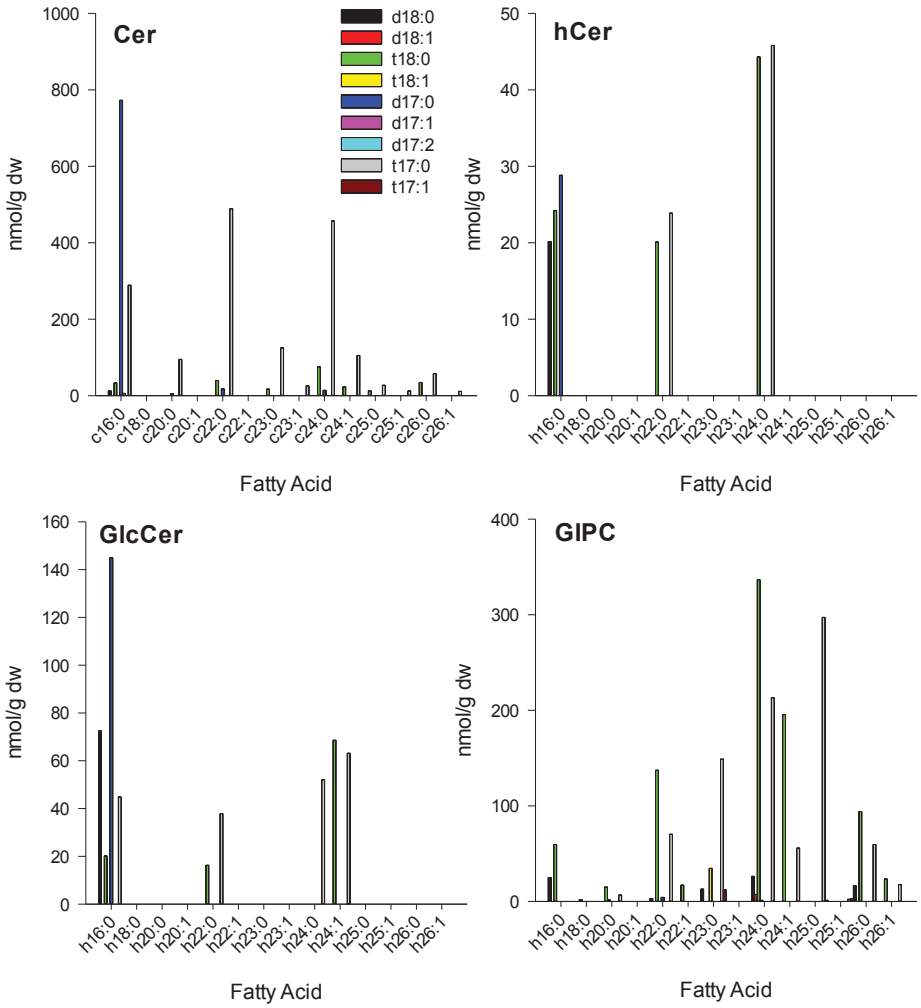

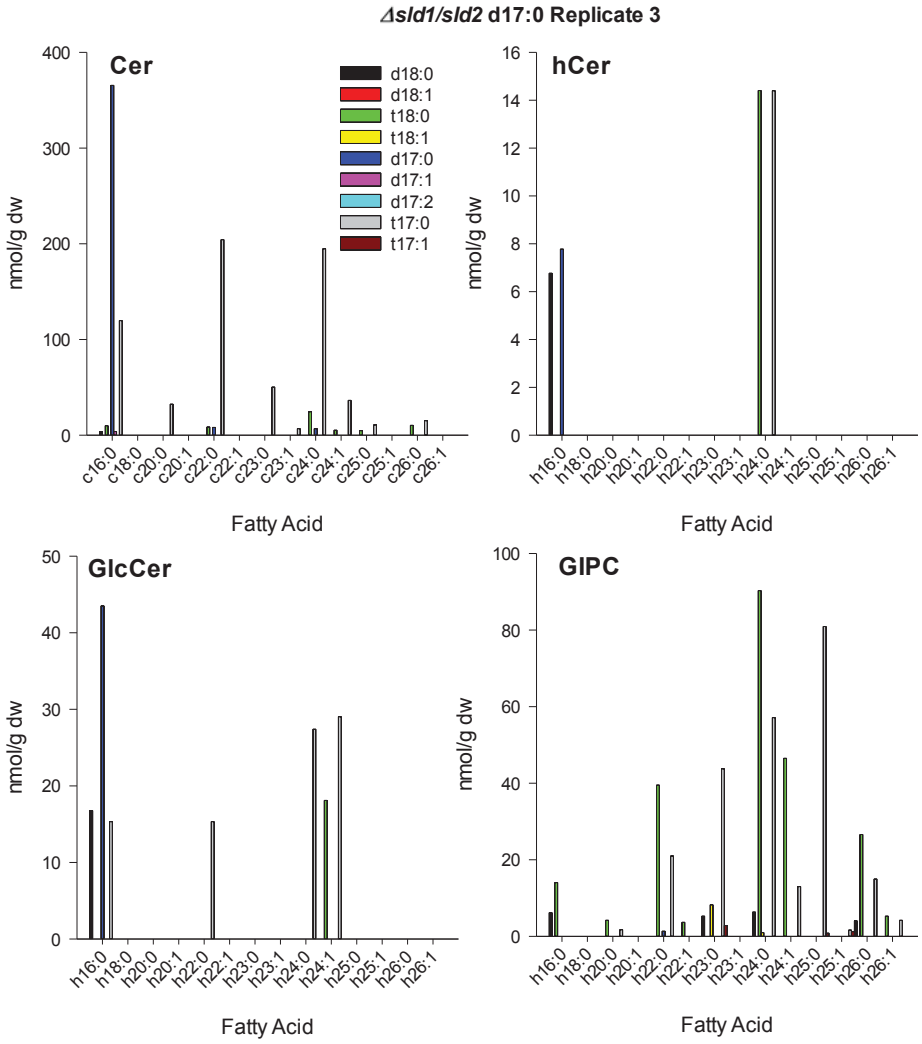
Δsld1/sld2 d17:0 Replicate 3
Cer
d18:0
d18:1
t18:0
t18:1
d17:0
d17:1
d17:2
t17:0
t17:1
nmol/g dw
Fatty Acid
hCer
GlcCer
GIPC

APPENDIX H

>NTD8DES1 (partial)

ISIGWWKWTHNAHHVACNSLDHDPDLQHLPVFAVSSTFFKSLNSYFYGRELTFD

SAKVFVSYQHFTYYPIMCVARVNLFVQTLLLLFSKRKVQDRFLNILGILVFWTWF

PLLVSTPNWTERVLFVLISFCVTSLQHIQFTLNHFAADVYVGQPEGNDWFEKQTG

GTIDIACSSWMDWFHGGA

>NTD8DES2 (partial)

ISIGWWKWTHNAHHVACNSLDYDPDLQHLPVFAVSSSLFKSLNSTFYGRELTFD

SLSKFFVSYQHFTFYPIVCVSRVNLFIQTLLLLFSRRKVTNRLRNILGIMVFWTWF

PLLSTLPNWTERVLFVLISFAVTGIQHVQFCLNHFAADVYVGQPKGNDWFEKQT

AGTIDIACSPRMDWFHGG

APPENDIX I

hydroxy-Ceramides

		[M+H]+		
Ceramide Backbone	**Exact mass**	**LCB fragment**	**DP**	**CE**
t17:0 h16:0	558.525	286.29	100	36
t17:0 h18:0	586.556	286.29	100	38
t17:0 h20:0	614.588	286.29	100	38
t17:0 h20:1	612.572	286.29	100	44
t17:0 h22:0	642.619	286.29	100	45
t17:0 h22:1	640.603	286.29	100	45
t17:0 h23:0	656.634	286.29	100	45
t17:0 h23:1	654.619	286.29	100	45
t17:0 h24:0	670.65	286.29	100	45
t17:0 h24:1	668.634	286.29	100	45
t17:0 h25:0	684.666	286.29	100	45
t17:0 h25:1	682.65	286.29	100	45
t17:0 h26:0	698.681	286.29	100	46
t17:0 h26:1	696.666	286.29	100	45
t17:1 h16:0	556.509	284.274	100	36
t17:1 h18:0	584.541	284.274	100	36
t17:1 h20:0	612.572	284.274	100	38
t17:1 h20:1	610.556	284.274	100	38
t17:1 h22:0	640.603	284.274	100	43
t17:1 h22:1	638.588	284.274	100	43
t17:1 h23:0	654.619	284.274	100	44
t17:1 h23:1	652.603	284.274	100	44
t17:1 h24:0	668.634	284.274	100	45
t17:1 h24:1	666.619	284.274	100	45
t17:1 h25:0	682.65	284.274	100	45
t17:1 h25:1	680.634	284.274	100	45
t17:1 h26:0	696.666	284.274	100	45
t17:1 h26:1	694.65	284.274	100	45
d17:0 h16:0	542.53	252.284	80	43
d17:0 h18:0	570.561	252.284	80	46
d17:0 h20:0	598.593	252.284	90	48
d17:0 h20:1	596.577	252.284	88	49
d17:0 h22:0	626.624	252.284	95	47
d17:0 h22:1	624.608	252.284	85	44
d17:0 h23:0	640.64	252.284	93	48
d17:0 h23:1	638.624	252.284	90	46
d17:0 h24:0	654.655	252.284	92	50
d17:0 h24:1	652.64	252.284	81	50
d17:0 h25:0	668.671	252.284	96	50

d17:0 h25:1	666.655	252.284	86	50
d17:0 h26:0	682.687	252.284	98	50
d17:0 h26:1	680.671	252.284	88	52
d17:1 h16:0	540.514	250.269	62	37
d17:1 h18:0	568.546	250.269	62	41
d17:1 h20:0	596.577	250.269	68	42
d17:1 h20:1	594.561	250.269	56	43
d17:1 h22:0	624.608	250.269	68	47
d17:1 h22:1	622.593	250.269	65	45
d17:1 h23:0	638.624	250.269	70	46
d17:1 h23:1	636.608	250.269	67	45
d17:1 h24:0	652.64	250.269	75	45
d17:1 h24:1	650.624	250.269	69	45
d17:1 h25:0	666.655	250.269	79	46
d17:1 h25:1	664.64	250.269	72	46
d17:1 h26:0	680.671	250.269	83	48
d17:1 h26:1	678.655	250.269	78	49
d17:2 h16:0	538.514	248.269	62	37
d17:2 h18:0	566.546	248.269	62	41
d17:2 h20:0	594.577	248.269	68	42
d17:2 h20:1	592.561	248.269	56	43
d17:2 h22:0	622.608	248.269	68	47
d17:2 h22:1	620.593	248.269	65	45
d17:2 h23:0	636.624	248.269	70	46
d17:2 h23:1	634.608	248.269	67	45
d17:2 h24:0	650.64	248.269	75	45
d17:2 h24:1	648.624	248.269	69	45
d17:2 h25:0	664.655	248.269	79	46
d17:2 h25:1	662.64	248.269	72	46
d17:2 h26:0	678.671	248.269	83	48
d17:2 h26:1	676.655	248.269	78	49

Ceramides

		[M+H]+		
Ceramide Backbone	**Exact mass**	**LCB fragment**	**DP**	**CE**
d17:0 c16:0	526.519	252.269	90	39
d17:0 c18:0	554.551	252.269	90	39
d17:0 c20:0	582.582	252.269	90	39
d17:0 c20:1	580.566	252.269	90	42
d17:0 c22:0	610.613	252.269	90	46
d17:0 c22:1	608.598	252.269	90	44
d17:0 c23:0	624.629	252.269	90	46

d17:0 c23:1	622.613	252.269	90	44
d17:0 c24:0	638.645	252.269	90	49
d17:0 c24:1	636.629	252.269	90	43
d17:0 c25:0	652.66	252.269	90	44
d17:0 c25:1	650.645	252.269	90	44
d17:0 c26:0	666.676	252.269	90	46
d17:0 c26:1	664.66	252.269	90	48
d17:1 c16:0	524.519	250.269	90	39
d17:1 c18:0	552.551	250.269	90	39
d17:1 c20:0	580.582	250.269	90	39
d17:1 c20:1	578.566	250.269	90	42
d17:1 c22:0	608.613	250.269	90	46
d17:1 c22:1	606.598	250.269	90	44
d17:1 c23:0	622.629	250.269	90	46
d17:1 c23:1	620.613	250.269	90	44
d17:1 c24:0	636.645	250.269	90	49
d17:1 c24:1	634.629	250.269	90	43
d17:1 c25:0	650.66	250.269	90	44
d17:1 c25:1	648.645	250.269	90	44
d17:1 c26:0	664.676	250.269	90	46
d17:1 c26:1	662.66	250.269	90	48
d17:2 c16:0	522.519	248.269	90	39
d17:2 c18:0	550.551	248.269	90	39
d17:2 c20:0	578.582	248.269	90	39
d17:2 c20:1	576.566	248.269	90	42
d17:2 c22:0	606.613	248.269	90	46
d17:2 c22:1	604.598	248.269	90	44
d17:2 c23:0	620.629	248.269	90	46
d17:2 c23:1	618.613	248.269	90	44
d17:2 c24:0	634.645	248.269	90	49
d17:2 c24:1	632.629	248.269	90	43
d17:2 c25:0	648.66	248.269	90	44
d17:2 c25:1	646.645	248.269	90	44
d17:2 c26:0	662.676	248.269	90	46
d17:2 c26:1	660.66	248.269	90	48
t17:0 c16:0	542.519	268.269	90	39
t17:0 c18:0	570.551	268.269	90	39
t17:0 c20:0	598.582	268.269	90	39
t17:0 c20:1	596.566	268.269	90	42
t17:0 c22:0	626.613	268.269	90	46
t17:0 c22:1	624.598	268.269	90	44
t17:0 c23:0	640.629	268.269	90	46
t17:0 c23:1	638.613	268.269	90	44

t17:0 c24:0	654.645	268.269	90	49
t17:0 c24:1	652.629	268.269	90	43
t17:0 c25:0	668.66	268.269	90	44
t17:0 c25:1	666.645	268.269	90	44
t17:0 c26:0	682.676	268.269	90	46
t17:0 c26:1	680.66	268.269	90	48
t17:1 c16:0	540.519	266.269	90	39
t17:1 c18:0	568.551	266.269	90	39
t17:1 c20:0	596.582	266.269	90	39
t17:1 c20:1	594.566	266.269	90	42
t17:1 c22:0	624.613	266.269	90	46
t17:1 c22:1	622.598	266.269	90	44
t17:1 c23:0	638.629	266.269	90	46
t17:1 c23:1	636.613	266.269	90	44
t17:1 c24:0	652.645	266.269	90	49
t17:1 c24:1	650.629	266.269	90	43
t17:1 c25:0	666.66	266.269	90	44
t17:1 c25:1	664.645	266.269	90	44
t17:1 c26:0	680.676	266.269	90	46
t17:1 c26:1	678.66	266.269	90	48

Glucosylceramide

[M+H]+

Ceramide Backbone	**Exact mass**	**LCB fragment**	**DP**	**CE**
d17:0h16:0	704.6	252.3	78	53
d17:0h18:0	732.6	252.3	80	56
d17:0h20:0	760.6	252.3	80	60
d17:0h20:1	758.6	252.3	80	58
d17:0h22:0	788.7	252.3	80	62
d17:0h22:1	786.6	252.3	80	66
d17:0h23:0	802.7	252.3	80	62
d17:0h23:1	800.6	252.3	80	66
d17:0h24:0	816.7	252.3	90	60
d17:0h24:1	814.7	252.3	95	63
d17:0h25:0	830.7	252.3	90	60
d17:0h25:1	828.7	252.3	95	63
d17:0h26:0	844.7	252.3	90	67
d17:0h26:1	842.7	252.3	85	63
d17:1h16:0	702.6	250.3	78	53
d17:1h18:0	730.6	250.3	80	56
d17:1h20:0	758.6	250.3	80	60
d17:1h20:1	756.6	250.3	80	58

d17:1h22:0	786.7	250.3	80	62
d17:1h22:1	784.6	250.3	80	66
d17:1h23:0	800.7	250.3	80	62
d17:1h23:1	798.6	250.3	80	66
d17:1h24:0	814.7	250.3	90	60
d17:1h24:1	812.7	250.3	95	63
d17:1h25:0	828.7	250.3	90	60
d17:1h25:1	826.7	250.3	95	63
d17:1h26:0	842.7	250.3	90	67
d17:1h26:1	840.7	250.3	85	63
d17:2h16:0	700.6	248.3	78	53
d17:2h18:0	728.6	248.3	80	56
d17:2h20:0	756.6	248.3	80	60
d17:2h20:1	754.6	248.3	80	58
d17:2h22:0	784.7	248.3	80	62
d17:2h22:1	782.6	248.3	80	66
d17:2h23:0	798.7	248.3	80	62
d17:2h23:1	796.6	248.3	80	66
d17:2h24:0	812.7	248.3	90	60
d17:2h24:1	810.7	248.3	95	63
d17:2h25:0	826.7	248.3	90	60
d17:2h25:1	824.7	248.3	95	63
d17:2h26:0	840.7	248.3	90	67
d17:2h26:1	838.7	248.3	85	63
t17:0h16:0	720.6	268.3	78	53
t17:0h18:0	748.6	268.3	80	56
t17:0h20:0	776.6	268.3	80	60
t17:0h20:1	774.6	268.3	80	58
t17:0h22:0	804.7	268.3	80	62
t17:0h22:1	802.6	268.3	80	66
t17:0h23:0	818.7	268.3	80	62
t17:0h23:1	816.6	268.3	80	66
t17:0h24:0	832.7	268.3	90	60
t17:0h24:1	830.7	268.3	95	63
t17:0h25:0	846.7	268.3	90	60
t17:0h25:1	844.7	268.3	95	63
t17:0h26:0	860.7	268.3	90	67
t17:0h26:1	858.7	268.3	85	63
t17:1h16:0	718.6	266.3	78	53
t17:1h18:0	746.6	266.3	80	56
t17:1h20:0	774.6	266.3	80	60
t17:1h20:1	772.6	266.3	80	58
t17:1h22:0	802.7	266.3	80	62

t17:1h22:1	800.6	266.3	80	66
t17:1h23:0	816.7	266.3	80	62
t17:1h23:1	814.6	266.3	80	66
t17:1h24:0	830.7	266.3	90	60
t17:1h24:1	828.7	266.3	95	63
t17:1h25:0	844.7	266.3	90	60
t17:1h25:1	842.7	266.3	95	63
t17:1h26:0	858.7	266.3	90	67
t17:1h26:1	856.7	266.3	85	63

Glucosylinositolphosphoceramide

		[M+H]+		
Ceramide Backbone	**Exact mass**	**LCB fragment**	**DP**	**CE**
d17:0h16:0	1112.6	514.5	145	57
d17:0h18:0	1150.7	552.6	145	57
d17:0h20:0	1178.7	580.6	145	57
d17:0h20:1	1176.7	578.6	145	57
d17:0h22:0	1206.7	608.6	145	58
d17:0h22:1	1204.7	606.6	145	58
d17:0h23:0	1220.7	622.6	145	60
d17:0h23:1	1218.7	620.6	145	60
d17:0h24:0	1234.7	636.6	145	61
d17:0h24:1	1232.7	634.6	145	61
d17:0h25:0	1248.7	650.6	145	63
d17:0h25:1	1246.8	648.6	145	62
d17:0h26:0	1262.7	664.6	145	64
d17:0h26:1	1260.8	662.7	145	63
d17:1h16:0	1110.6	512.5	145	57
d17:1h18:0	1148.7	550.6	145	57
d17:1h20:0	1176.7	578.6	145	57
d17:1h20:1	1174.7	576.6	145	57
d17:1h22:0	1204.7	606.6	145	58
d17:1h22:1	1202.7	604.6	145	58
d17:1h23:0	1218.7	620.6	145	60
d17:1h23:1	1216.7	618.6	145	60
d17:1h24:0	1232.7	634.6	145	61
d17:1h24:1	1230.7	632.6	145	61
d17:1h25:0	1246.7	648.6	145	63
d17:1h25:1	1244.8	646.6	145	62
d17:1h26:0	1260.7	662.6	145	64
d17:1h26:1	1258.8	660.7	145	63
d17:2h16:0	1108.6	510.5	145	57

d17:2h18:0	1146.7	548.6	145	57
d17:2h20:0	1174.7	576.6	145	57
d17:2h20:1	1172.7	574.6	145	57
d17:2h22:0	1202.7	604.6	145	58
d17:2h22:1	1200.7	602.6	145	58
d17:2h23:0	1216.7	618.6	145	60
d17:2h23:1	1214.7	616.6	145	60
d17:2h24:0	1230.7	632.6	145	61
d17:2h24:1	1228.7	630.6	145	61
d17:2h25:0	1244.7	646.6	145	63
d17:2h25:1	1242.8	644.6	145	62
d17:2h26:0	1258.7	660.6	145	64
d17:2h26:1	1256.8	658.7	145	63
t17:0h16:0	1128.6	530.5	145	57
t17:0h18:0	1166.7	568.6	145	57
t17:0h20:0	1194.7	596.6	145	57
t17:0h20:1	1192.7	594.6	145	57
t17:0h22:0	1222.7	624.6	145	58
t17:0h22:1	1220.7	622.6	145	58
t17:0h23:0	1236.7	638.6	145	60
t17:0h23:1	1234.7	636.6	145	60
t17:0h24:0	1250.7	652.6	145	61
t17:0h24:1	1248.7	650.6	145	61
t17:0h25:0	1264.7	666.6	145	63
t17:0h25:1	1262.8	664.6	145	62
t17:0h26:0	1278.7	680.6	145	64
t17:0h26:1	1276.8	678.7	145	63
t17:1h16:0	1126.6	528.5	145	57
t17:1h18:0	1164.7	566.6	145	57
t17:1h20:0	1192.7	594.6	145	57
t17:1h20:1	1190.7	592.6	145	57
t17:1h22:0	1220.7	622.6	145	58
t17:1h22:1	1218.7	620.6	145	58
t17:1h23:0	1234.7	636.6	145	60
t17:1h23:1	1232.7	634.6	145	60
t17:1h24:0	1248.7	650.6	145	61
t17:1h24:1	1246.7	648.6	145	61
t17:1h25:0	1262.7	664.6	145	63
t17:1h25:1	1260.8	662.6	145	62
t17:1h26:0	1276.7	678.6	145	64
t17:1h26:1	1274.8	676.7	145	63